306416596/

MIXING COHESIONLESS MATERIALS

by

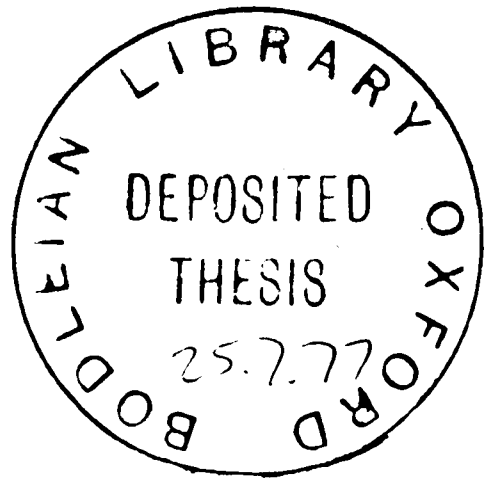
MICHAEL H. COOKE

BALLIOL COLLEGE

Thesis submitted for the degree of

Doctor of Philosophy at Oxford University,

September 1976.



ABSTRACT

When solid particles of different types are mixed together, a random distribution of the components is rarely produced and deterioration of the mixture can occur on subsequent handling. Among the microscopic processes responsible, one important mechanism for free-flowing materials is thought to be inter-particle percolation, the drainage of particles through the interstices between larger ones. If the larger particles are stationary this is called spontaneous percolation, whereas if it is produced by shear strain the term strain-induced percolation is used. Here a quantitative evaluation of both and some consequences are described.

A practical application of spontaneous percolation has been the design and construction of a new static mixer or distributor, consisting of rows of angle bars mounted horizontally in a vertical channel. Material fed to the top of a unit bounces off the bars and is distributed across the channel. Two mixers were built; one dispersed material in one lateral direction only and could be used for feeding material onto a belt or distributing seed from a moving vehicle. The other produced a two-dimensional dispersion and would be useful in distributing material flowing into hoppers or whenever a good mixture were required. Optimisation of the design was investigated using a computer program which simulated the motion of a spherical particle as it fell through such a mixer. Design data was deduced from the record of the position of the particle. The mixers were not suitable for use with fine materials.

Interpretation of experimental results from this equipment requires suitable statistical indices and two were developed here.

One related the variance of sample compositions to the number of particles fed to the mixer by assuming that the distributions of material were ordered. The second, using the correlation coefficient between samples, related the variance to the sample size in those situations where two orthogonal processes are in operation. Both techniques are generally applicable to fields other than that of powder mixing.

On the theoretical side, an existing model of spontaneous percolation for inelastic materials has been extended and improved. The original form did not account for the motion of a particle between collisions with bulk particles but this has now been included. An entirely new semi-empirical model for partly elastic materials has also been proposed. Both predict percolation velocities which agree with experimental data.

In order to extend earlier experimental studies on strain-induced percolation, a simple shear cell was modified by installing a hydraulic drive which enabled the cell to be driven at a constant speed. Advantages of the use of such a cell include the possibility of detecting a percolating particle on entry to and exit from the bed and the constant strain throughout the material. Reliable and accurate readings of residence times of percolating particles were recorded and percolation velocities and both lateral and axial diffusion coefficients were calculated. These were functions of the relative particle size and density, the material properties of the percolating particle and bed conditions such as strain rate and normal stress. Denser and softer particles percolated faster. Decreasing the diameter ratio between percolating and bulk particles from 0.67 to 0.27 caused a twenty-five fold increase in the percolation rate. The dependence of this rate on particle diameter was

interpreted using statistical mechanics. The percolation rate has been shown to reach a constant value as the strain rate increases, in contrast to the deductions drawn in earlier work by Scott, whose procedure has been proved to be unsound.

ACKNOWLEDGEMENTS

I would like to thank Dr. J. Bridgwater for his encouragement, guidance and advice throughout the supervision of this work and for his helpful suggestions during the preparation of this thesis. I am also indebted to Mr. R.A. Ducker who built and maintained the apparatus, Mr. G.N. Roger and the staff of the Engineering Laboratory Electronics Department and Dr. C.E. Phelps and the staff of the University Computing Centre.

This research has been sponsored by the Science Research Council and Thorn Lighting Ltd., to whom I am grateful for the award of an Industrial Studentship.

Thanks are due to my colleagues in the Department with whom the project was discussed and to Mrs Holloway for typing the thesis.

Finally, I should like to thank my wife for her encouragement and assistance.

CONTENTS

		Page
ABSTRACT		i
ACKNOWLEDGEMENTS		iv
CHAPTER 1	INTRODUCTION	1
CHAPTER 2	BACKGROUND	3
	2.1 Mixing mechanisms	5
	2.2 Segregation and percolation	7
	2.2.1 Free-flight segregation	7
	2.2.2 Interparticle percolation	8
	2.2.3 Large particle segregation	9
	2.2.4 Rolling segregation	9
	2.3 Importance of segregation	9
CHAPTER 3	SPONTANEOUS PERCOLATION	11
	3.1 Literature	11
	3.2 Axially dispersed plug flow	14
	3.3 Models of spontaneous percolation. Introduction	18
	3.4 Model I. Inelastic particles	19
	3.4.1 Model and percolation velocity	19
	3.4.2 Axial dispersion	27
	3.4.3 Radial dispersion	28
	3.5 Model II. Partly elastic particles	29
	3.6 Discussion and conclusion	32
CHAPTER 4	NEW MIXERS	35
	4.1 Introduction	35
	4.2 Design	37
	4.3 Theoretical background	39
	4.3.1 Introduction	39
	4.3.2 Performance tests	39
	4.3.3 Application of theory	43

		Page
	4.4 Three-dimensional mixer experiments	44
	4.5 Two-dimensional mixer experiments	47
	4.6 Comparison of the mixers	50
	4.7 Discussion and conclusions	51
CHAPTER 5	SIMULATION AND MODELLING OF MIXERS	54
	5.1 The computer program	54
	5.1.1 Introduction	54
	5.1.2 Program logic	55
	5.1.2.1 Initialisation	55
	5.1.2.2 Search routine	56
	5.1.2.3 Collisions with the bars	58
	5.1.2.4 Collisions with the sides	59
	5.1.2.5 Collisions with the bars-zero lateral velocity	60
	5.1.2.6 Velocities after collision	60
	5.1.2.7 Sliding	61
	5.1.2.8 Output	61
	5.1.3 Program development	62
	5.2 Results	65
	5.2.1 Data analysis	65
	5.2.1.1 Falling velocity	65
	5.2.1.2 Diffusion coefficients and Peclet numbers	66
	5.2.1.3 Other variables	67
	5.2.2 General considerations	68
	5.2.3 Different programs and reproducibility	69
	5.2.4 Coefficient of restitution	70
	5.2.5 Particle diameter	71
	5.2.6 Bar size	72
	5.2.7 Bar thickness	73
	5.2.8 Bar spacing (i)	73

		Page
	5.2.9 Bar spacing (ii)	74
	5.3 Modelling	74
	5.3.1 Limiting displacements	74
	5.3.2 Velocity of inelastic particles	77
	5.3.3 Partly elastic particles	80
	5.4 Summary	81
CHAPTER 6	STATISTICS OF SAMPLES	83
	6.1 Introduction	83
	6.2 Formulation	85
	6.2.1 Correlation coefficients	85
	6.2.2 Definition of distance between samples	87
	6.2.3 Models for the correlation coefficient	88
	6.3 Variance-sample size relationships	90
	6.4 Application to particular cases	93
	6.4.1 Method I	93
	6.4.2 Method II	96
	6.5 Discussion	96
	6.6 Conclusions	101
CHAPTER 7	STRAIN-INDUCED PERCOLATION. EQUIPMENT	103
	7.1 Introduction	103
	7.1.1 Previous work	103
	7.1.2 Variables affecting percolation	105
	7.2 Scott's equipment	108
	7.2.1 The cell	109
	7.2.2 The driving system	110
	7.2.3 The particle feeding and detection system	110
	7.2.4 Prevention of electrostatic charging	111
	7.3 Versions of the SSA used in this study	112
	7.3.1 The SSA Mk.IIIA	112

		Page
	7.3.2 The SSA Mk.V	113
	7.3.2.1 The driving system	113
	7.3.2.2 Safety precautions	115
	7.3.2.3 Particle detection	116
	7.3.2.4 The cell and framework	118
CHAPTER 8	STRAIN-INDUCED PERCOLATION. RESULTS AND DISCUSSION	119
	8.1 Introduction	119
	8.2 Experiments with the SSA Mk.IIIA	119
	8.2.1 Interpretation of results	119
	8.2.2 Experimental procedure	123
	8.2.3 Results and discussion	123
	8.3 Experiments with the SSA Mk.V	125
	8.3.1 Interpretation of results	125
	8.3.2 Experimental procedure	128
	8.3.3 Effect of particle properties	129
	8.3.3.1 Particle diameter ratio	129
	8.3.3.2 Particle density ratio	131
	8.3.3.3 Material properties	132
	8.3.4 Effect of bed variables	133
	8.3.4.1 Rate of strain	133
	8.3.4.2 Normal stress	136
	8.3.4.3 High bed heights	137
	8.3.4.4 Friction between the particles	137
	8.4 Theories of percolation	139
	8.5 Conclusions	142
CHAPTER 9	CONCLUSION	145
	9.1 Spontaneous percolation and its consequences	145
	9.2 Strain-induced percolation	146

APPENDIX I

APPENDIX II

APPENDIX III

NOTATION

REFERENCES

FIGURES

		After page
3.1	Comparison of exact and approximate solutions of axially dispersed plug flow equation, U = 0.5	17
3.2	Comparison of exact and approximate solutions of axially dispersed plug flow equation, U = 2.0	17
3.3	Comparison of exact and approximate solutions of axially dispersed plug flow equation, U = 5.0	17
3.4	Comparison of exact and approximate solutions of axially dispersed plug flow equation, U = 10.0	17
3.5	(i) Particle hitting a planar surface with zero coefficient of restitution. (ii) Distribution of impact angles	19
3.6	Resolution of V_f and V_o	19
3.7	Geometry of the lateral displacement of particles	28
3.8	Collision between a percolating particle and a bulk sphere	28
3.9	Relationship between dimensionless velocity and coefficient of restitution	33
4.1	Three-dimensional mixer. Original form with two glass sides	37
4.2	Three-dimensional mixer. Final form with four dural sides	37
4.3	Three-dimensional mixer. Dimensioned sketch	37
4.4	Three-dimensional mixer. Sample tray and collection box	38
4.5	Two-dimensional mixer, 2.3cm insert and sample tray	38
4.6	Two-dimensional mixer. Dimensioned sketch	38
4.7	Three-dimensional mixer. Observed and binomial frequency distributions	44
4.8	Two-dimensional mixer. σ^2/σ_R^2 vs. number of particles used	44
4.9	Three-dimensional mixer. Feedpoint and sample tray positions	45
4.10	Three-dimensional mixer. Typical distribution for a granular material	46
4.11	Three-dimensional mixer. Typical distribution for a fine material	47

		After page
4.12	Two-dimensional mixer. Q vs. flowrate	48
4.13	Two-dimensional mixer. $(N_1-\bar{N})/\sqrt{N/4}$ vs. angle at which mixer is mounted	49
4.14	Typical distributions	50
4.15	Iron filings flowing through the two-dimensional mixer	50
5.1	Concise program flowsheet	55
5.2	Bar layout in mixer including notation	56
5.3	Search routine; division of mixer into rectangles	56
5.4	Bar showing approximation to collision surface	58
5.5	Bar collision surface	58
5.6	Variation of particle height with time	65
5.7	Relationship between $\sigma^2(\Delta y)$ and time interval	66
5.8	Relationship between $\lvert\overline{S_{Jy}}\rvert^2$ and number of jumps	67
5.9	Relationship between $\sigma^2(\Delta r)$ and time interval	67
5.10	Distribution of times between collisions	68
5.11	Consistency of results. Effect on particle velocity	69
5.12	Consistency of results. Effect on root mean square lateral jump	69
5.13	Consistency of results. Effect on axial Peclet number	69
5.14	Consistency of results. Effect on radial Peclet number	69
5.15	Coefficient of restitution. Effect on particle velocity	70
5.16	Coefficient of restitution. Effect on root mean square lateral jump	70
5.17	Coefficient of restitution. Effect on axial Peclet number	70
5.18	Coefficient of restitution. Effect on radial Peclet number	70
5.19	Particle diameter. Effect on velocity	71
5.20	Particle diameter. Effect on root mean square lateral jump	71

		After page
5.21	Particle diameter. Effect on axial Peclet number	72
5.22	Particle diameter. Effect on radial Peclet number	72
5.23	Bar size. Effect on velocity	72
5.24	Bar size. Effect on root mean square lateral jump	72
5.25	Bar size. Effect on axial Peclet number	72
5.26	Bar size. Effect on radial Peclet number	72
5.27	Bar thickness. Effect on velocity	73
5.28	Bar thickness. Effect on root mean square lateral jump	73
5.29	Bar thickness. Effect on axial Peclet number	73
5.30	Bar thickness. Effect on radial Peclet number	73
5.31	Bar spacing (i). Effect on velocity	73
5.32	Bar spacing (i). Effect on root mean square lateral jump	73
5.33	Bar spacing (i). Effect on axial Peclet number	73
5.34	Bar spacing (i). Effect on radial Peclet number	73
5.35	Bar spacing (ii). Effect on velocity	74
5.36	Bar spacing (ii). Effect on root mean square lateral jump	74
5.37	Bar spacing (ii). Effect on axial Peclet number	74
5.38	Bar spacing (ii). Effect on radial Peclet number	74
5.39	Bar spacing (ii). Effect on axial diffusion coefficient	74
5.40	Bar spacing (ii). Effect on radial diffusion coefficient	74
5.41	Bar spacing (ii). Effect on D_r/u	74
5.42	Relationship between $\sigma^2(\Delta r)/S_y^2$ and $\Delta y/S_y$	75
5.43	Bounces on the side of the mixer	76
5.44	Relationship between $\lvert\overline{S_{Jr}}\rvert^2/S_y^2$ and number of jumps	76
5.45	Impact of a particle on a mixer bar	77
6.1	The number of pairs of unit samples in a 2x3 array	88
6.2	Correlogram for expt. B5 by Hall and Godfrey	89
6.3	Linear sample	90

		After page
6.4	Rectangular sample	91
6.5	Three-dimensional sample	92
6.6	Variance-sample size relationships for different shape samples	96
6.7	Variance-sample size relationships for square samples	97
6.8	Variance-sample size relationships for rectangular samples	97
6.9	Variance-sample size relationships. Vector and orthogonal measurement	98
6.10	Variance-sample size relationship for Hall and Godfrey's experiment B5 compared with equation 6.13	98
6.11	Correlograms derived from three-dimensional mixer experiments	98
7.1	Idealized horizontal failure zone	105
7.2	Close-up of the cell of the SSA Mk. IIA	108
7.3	The SSA Mk.IIA	108
7.4	Base of the SSA Mk.III	109
7.5	The SSA Mk.III showing rack and gear wheels	109
7.6	Close-up of the cell of the SSA Mk.V	111
7.7	Collection tray of the SSA Mk.IIIA	112
7.8	The SSA Mk.V	113
7.9	Hydraulics flowsheet. SSA Mk.V	114
7.10	The SSA Mk.V and electronic equipment	115
7.11	Collection tray of the SSA Mk.V	116
8.1	Experiment D33	121
8.2	Estimates of $D_z t_m$ at different bed heights. Species D	121
8.3	Estimates of $D_z t_m$ at different bed heights. Species E	121
8.4	Estimates of $D_x t_m$ at different bed heights; individual values. Species E	122
8.5	Estimates of $D_x t_m$ at different bed heights; mean values. Species E	122
8.6	Estimates of $D_z t_m$ at different normal loads. Species E	124

		After page
8.7	Estimates of $D_x t_m$ at different normal loads. Species E	124
8.8	Estimates of $D_z t_m$ at different strain rates. Species E	124
8.9	Estimates of $D_x t_m$ at different strain rates. Species E	124
8.10	Regression between mean residence strain and bed height. Species L	125
8.11	Regression between $D_z t_m$ and bed height. Species L	125
8.12	Regression between HPe_y/d_b and bed height. Species J	126
8.13	Dependence of percolation velocity on particle diameter ratio	129
8.14	Effect of particle diameter ratio on intercept in regression between mean residence strain and bed height	130
8.15	Dependence of dimensionless diffusion coefficient on particle diameter ratio	130
8.16	Dependence of axial Peclet number on particle diameter ratio	131
8.17	Relationship between mean residence strain and bed height. Species Q and R	132
8.18	Relationship between mean residence strain and strain rate. Species J	133
8.19	Traces showing the variation in bed height over a cycle	134
8.20	Relationship between $D_z t_m$ and strain rate. Species J	135
8.21	Relationship between HPe_y/d_b and strain rate. Species J	136
8.22	Relationship between mean residence strain and normal load, Species U and V	136
8.23	Relationship between $D_z t_m$ and normal load. Species U and V	136
8.24	Relationship between HPe_y/d_b and normal load. Species U	136
8.25	Relationship between mean residence strain and bed height at high bed heights. Species J	137
8.26	Plot of $(u/\dot{\gamma}d_b)^{-1}$ vs. $(d_p/d_b - 0.155)^2$	139
8.27	Plot of $\log_e (u/\dot{\gamma}d_b)$ vs. d_p/d_b	142

TABLES

		After page
3.1	Theoretical values predicted by model I and extrapolated experimental value of dimensionless percolation velocity	26
3.2	Theoretical and experimental values of Peclet numbers	28
4.1	Three-dimensional mixer experiments	44
4.2	Two-dimensional mixer. Relationship between σ^2/σ_R^2 and number of particles	44
4.3	Properties of materials	44
4.4	Mixtures (i)	47
4.5	Mixtures (ii)	47
4.6	Flowrate experiments	48
4.7	Two-dimensional mixer. Exhaustive tests	50
4.8	Two-dimensional mixer weighing experiments	50
4.9	Three-dimensional mixer. Experiments analysed in groups of 20 samples	51
5.1	Results of mixer simulation	64
7.1	Variables affecting percolation	107
8.1	Materials used in the experiments in the SSA Mk.IIIA	121
8.2	Experiments to measure lateral diffusion coefficients for different size particles (i) $D_z/\dot{\gamma}d_b^2$	123
8.3	Experiments to measure lateral diffusion coefficients for different size particles (ii) $D_x/\dot{\gamma}d_b^2$	123
8.4	Materials used in the experiments in the SSA Mk.V	125
8.5	SSA results, Mk.V	125

CHAPTER 1

INTRODUCTION

The mixing of dry cohesionless materials is a unit operation of considerable importance. Though it has been investigated by many workers, there are surprisingly few general theories. Industrial mixers operate both on the small scale as in pharmaceutical applications and on the large scale as in the blending of plastics or corn. The behaviour of mixtures of cohesionless materials is important in processes as diverse as segregation in preparing packed beds and the manufacture of washing powders.

A few mixing mechanisms have been suggested, among which interparticle percolation is probably the most important of the microscopic processes. It is the drainage of small particles through a bed of larger ones, under the influence of gravity alone if the particles are small enough, or else as a result of shear or vibration. These are termed spontaneous, strain-induced and vibration-induced percolation respectively.

It has been suggested that percolation is also an important cause of segregation, or demixing, in cohesionless materials. It has long been known that attempts to mix such materials for too long can lead to a decrease in the quality of the mixture. The vibration and shear during transportation of mixtures in sacks or bins can also affect the quality. Though such phenomena are clearly undesirable they have not been investigated rationally.

Some studies of spontaneously percolating systems have already been made and equipment to investigate strain-induced percolation has been built and tested. Motion due to vibration has been studied in connection with screening. Percolation in

surface layers in tumbling mixers and down the surfaces of heaps of material during pouring has also been examined. However these processes remain poorly understood.

The purpose of this thesis was to study thoroughly certain aspects of percolation. The particular objectives pursued were:

(i) The development of theories of spontaneous percolation which would account for the experimental data already available.

(ii) The development and evaluation of continuous mixers with no moving parts. The mechanism of mixing in the units is similar to the motion which occurs during spontaneous percolation.

(iii) A computer simulation of such mixers so that design data could be obtained.

(iv) Refinement of the apparatus used to study strain-induced percolation so that lateral diffusion in the system could be studied.

(v) The accumulation of accurate data on strain-induced percolation, together with the production of theories to explain the experimental results.

While evaluating the mixers it became necessary to survey the methods of characterizing distributions and mixtures. Statistical procedures which could be used to present information about mixtures were developed; they are of general interest and are reported here.

The studies on percolation revealed possible theoretical approaches which help to improve understanding of the subject. The experimental results have confirmed the value of the equipment and provide justification for the theories.

CHAPTER 2

BACKGROUND

Though the published work on the mixing of cohesionless materials is extensive, few fundamental studies have been made. In this chapter some of the more important work, particularly that dealing with mechanisms, will be discussed. Those papers which have direct bearing on specific topics are considered in more detail in the relevant chapters.

Much of the early work in the field was evaluated by Weidenbaum (1958) in a long review. The major part of his paper was concerned with the statistics of mixtures and the assessment of mixture quality. Generally mixing indices were arbitrary functions of the variance of the sample compositions and, as such, presented little information about the true state of the mixture. The rest of the review described tests on mixing devices, especially rotating drums. There are few references to mechanisms and rate studies only warrant a few pages. He was apparently unaware of the work on the variability of the ash content of coal which was reviewed by Bertholf (1955). In this context it had been suggested by Landry (1944) and Emery (1951) that a fundamental measure of the degree of mixing was the correlation coefficient between the compositions of neighbouring samples.

Since 1958 more attention has been paid to the behaviour of granular materials. In a report to the Institution of Chemical Engineers on powders, pastes and non-Newtonian fluids, Bourne (1964) saw two general difficulties which arise in mixing studies.

(i) The absence of a theoretical background to aid the deduction of further generalisations.

(ii) The absence of widely applicable criteria of mixing.

He recognised the danger, which has not been entirely avoided, of producing extensive data specific to the mixing equipment employed and useless in predicting the outcome of other experiments. Among his recommendations for further work was the suggestion that theoretical and experimental studies should be made on the flow and mixing of materials having simple rheological properties in simple geometries.

Fan et al. (1970) reviewed the literature from 1958 to 1969. They too considered mixing indices to be of importance and include a table listing over 30 which have been used by different investigators. The wide differences in the definitions reveals the uncertainty of the concepts used by earlier workers, and these indices are useless when comparing mixtures unless the number and size of samples are the same. They also record attempts to evaluate rate coefficients for mixing, generally based on a form of the diffusion equation. The use of stochastic modelling techniques as a means of avoiding the often difficult mathematical problems is reported. Cahn and Fuerstenau (1967), who simulated axial mixing in a simple horizontal cylinder, found that diffusion coefficients calculated from the simulation agreed well with the results of actual experiments. However this modelling is useless unless the underlying physical basis is correct. Fan et al. conclude that the only mechanism investigated in detail is that for mixing in a simple horizontal cylinder and it will be seen later that even this process is not well understood.

A recent thorough search through the literature (Cooke et al., 1976) revealed over 600 references on solids mixing. Because of the many applications, papers are scattered over a wide range of Journals. However, despite the interest shown in

the subject, little fundamental work was revealed.

2.1 Mixing mechanisms

In most solids mixing operations, mixing and segregation proceed simultaneously, and the mechanisms of material flow can be interpreted as causing one or the other. However convection is more likely to promote mixing while segregation is usually caused by percolation.

In 1954, Lacey suggested that there are three principal mixing mechanisms.

(i) Convective mixing; the transfer of groups of adjacent particles from one location in the mass to another.

(ii) Diffusive mixing; the distribution of particles over a freshly developed surface.

(iii) Shear mixing; the setting up of slipping planes within the mass.

Danckwerts (1953) divided all mixing problems into macro-mixing and micromixing. It would then be possible to identify convective mixing with the former and diffusive and shear mixing with the latter. Stephens (1976) supports this view, noting that a free surface can be considered as being related to a region where shear is taking place. Further refinement of these ideas is possible but this identifies the major mechanisms.

When a granular material is acted upon by forces, failure may occur and large groups of material move from one region to another. Between two groups of particles moving with respect to each other there is a thin layer known as a failure plane or zone. Within this small region, which is believed to be about ten particle diameters thick, a high velocity gradient exists and

under such circumstances shear mixing or percolation occurs.

A simple process of this type was considered by Weydanz (1960). In his model, mixing occurred by interchange of a small volume in one region of the mixture with a small volume in another. At the same time a volume of the heavier component from the upper region of the mixer exchanges with an equal amount of the other component in the lower region. The change in the standard deviation of sample compositions with time could be found from the model. More recently Bridgwater (1972) has considered a similar situation in which mixing by convection and inter-particle percolation are combined.

Diffusive mixing has been subjected to a number of studies; it appears to be an ideal method of analysing the mixing in a horizontal rotating drum. A typical case is that of Hogg et al. (1966) who replaced time in the diffusion equation by the number of revolutions and solved it for the case when the initial mixture is totally segregated. The theoretical functional relationship between the concentration and position in the mixture agreed closely with experimental results.

The limited application of this approach becomes clear when the behaviour of differently sized particles is considered, for then axial and radial segregation effects are operative. This was first reported by Oyama (1939). Donald and Roseman (1962) studied the phenomenon in more detail and noted the unexpected effect that radial bands are produced under some circumstances. This was ascribed to axial variations in the radial velocity. Subsequently Bridgwater et al. (1969a) offered an alternative explanation. Other recent work (Bridgwater, 1976) indicates that the phenomenon only occurs if electric charge on the particles is eliminated. This is clearly a field in which

further work is necessary.

Thus it appears that although diffusive mixing may be present in many situations, it is rarely likely to be the predominant effect and percolation is more likely to be important in deciding the quality of the final mix.

The diffusion equation has been applied by Otake et al. (1961) in a different situation, viz. to the movement of the bulk material in a stirred bed. Good agreement between the theoretically predicted and experimentally observed variances is claimed. However Bridgwater (1976) considers the fundamentals of the process and suggests that the consistency of the approach is merely fortuitous. Among the criticisms that can be levelled at the work is that the distance between the vessel wall and the impeller will affect the mixing and that it is known that the flow of particles over a moving blade depends on the particle size (Bridgwater et al., 1969b).

2.2 Segregation and percolation

Segregation can occur whenever a system contains particles with different properties such as size, density, shape and surface character. Scott (1974) distinguished four types of segregation and his divisions will be followed here.

2.2.1 Free-flight segregation

If particles of different sizes undergo free-flight with a horizontal velocity component, they experience different drag forces (Jenike, 1960) and land in different places. This can give rise to segregation in a rapidly rotating tumbling mixer (Valentin, 1965).

2.2.2 Interparticle percolation

Interparticle percolation occurs spontaneously when the different components of a mixture have very different particle sizes. Though of secondary industrial importance this has been considered by a number of workers. Strain-induced percolation has been studied in a vertical cylinder fitted with a rotating shaft to which pins were attached (Willemse, 1961), in a vertical failure zone adjacent to a wall (Campbell and Bridgwater, 1973) and in a reciprocating shear cell (Scott, 1974).

Vibration-induced percolation is important in screening. Rippie and co-workers published a series of papers (Olsen and Rippie, 1964; Rippie *et al.*, 1964; Faiman and Rippie, 1965; Rippie *et al.*, 1967) dealing with the relative magnitude of various effects. The work suggests that particle volume difference is the primary cause of segregation, with density and shape secondary causes. However, the applicability of the results to other systems is unlikely as the diameter of the cylinder used to study the phenomenon was only three times that of the largest sphere used and wall effects would therefore have been important. Other work includes that by Williams and Shields (1967) who studied segregation of fertilizer granules and Ahmad and Smalley (1973) who investigated the effects of vibration frequency and particle properties. Hudson *et al.* (1969) was concerned with segregation in deep beds on vibratory sieve screens. Recently Parsons (1976) has reported that segregation occurs during the tapping of fine powders (<30μm) and can lead to changes in the apparent mean particle size. In spite of the large amount of experimental data that now exists, there is no satisfactory theoretical framework to explain the phenomenon.

2.2.3 Large particle segregation

Brown (1939) reported that vibrating a granular mixture caused large particles to rise to the surface and Williams (1963) confirmed this for a mixture containing only one large particle. Scott (1974), in a limited range of experiments, investigated large particle motion during strain-induced percolation. He found that large particles initially in the middle of a failure zone did not move significantly whereas those at the top of the zone moved downwards. Recently Stephens (1976) performed experiments in an annular shear apparatus and found that large particles move towards the centre of a failure zone.

2.2.4 Rolling segregation

If particles roll down an inclined free surface of a material, then the larger ones will roll further (Brown, 1939). Williams (1963) and Matthée (1968) consider that this phenomenon is responsible for the central core of fines formed when a bunker is filled, and Matthée presents some theoretical considerations which relate the distance travelled by a particle down a plane to its radius. However Lawrence and Beddow (1969) reported that segregation during die filling was due to fines percolating down through the moving powder. The reasons for the difference in behaviour remain unresolved, though the mechanism may depend on the relative sizes of the different components.

2.3 Importance of segregation

The tendency for mixtures of cohesionless materials to segregate has important industrial consequences. It means that random mixtures of dissimilar materials are rarely found, which

is of particular importance in such processes as the preparation of tablets containing pharmaceuticals. Also what may have been a good mixture will change its state on handling. Other consequences may be found outside the field of mixing; ball mills and rotary kilns may suffer from segregation problems. Craven (1970) recognised that segregation could occur during preparation of a packed bed and modelled the changes in bed performance due to the irregular packing. Thus segregation can occur in nearly all processes which involve the use of granular materials.

CHAPTER 3

SPONTANEOUS PERCOLATION

3.1 Literature

Spontaneous percolation occurs in two situations. In one, percolating particles fall independently through a static array of larger ones. In the other there is interference between percolating particles.

Bridgwater et al. (1969a) investigated the former by dropping a small sphere through a random array of larger spheres packed in a cylindrical column. They modelled the motion of the small sphere by a random walk mechanism and introduced a radial diffusion coefficient D_r. Experimental results agreed with the model and were expressed in terms of a Peclet number Pe_r, the ratio of axial convection to radial diffusion, defined by

$$Pe_r = ud_b/D_r \qquad (3.1)$$

where u is the vertical velocity of the percolating particle and d_b is the diameter of a large sphere. The Peclet number was shown by dimensional analysis and physical considerations to be primarily a function of the coefficient of restitution between large and small particles, α. Pe_r decreased from about 11 at $\alpha = 0.2$ to about 6 at $\alpha = 0.9$. Values of α were determined by dropping the small particles onto either a large particle or a planar surface made from the same material as a large particle and measuring the height of rebound. The height of fall is not reported.

A problem which arises in this presentation is that the coefficient of restitution is a function of the relative velocity of the two spheres on impact. (See, for example, Bowden and

Tabor, 1950). Since the form of the plot of coefficient of restitution vs. impact velocity is known for some materials, a value of the coefficient for one height of fall or impact velocity may be sufficient to characterize the system. Thus it is suggested that in future, values of α should be measured for some typical impact velocity.

Later, Bridgwater and Ingram (1971) examined the distribution of residence times of the particles in a similar packed column and modelled the process by plug flow with axial dispersion. It was deduced that the axial Peclet number Pe_a was a function of the diameter ratio between the small and large spheres d_p/d_b and the coefficient of restitution α. Values of Pe_a lay between 6 and 9. They were calculated from the variance of the residence time distribution assuming that the system was unbounded. It will be shown later that this assumption, though strictly incorrect, is adequate when describing this system. The dimensionless percolation velocity, $u/\sqrt{gd_b}$, where g is the acceleration due to gravity, decreased from about 0.4 at $\alpha = 0.2$ to 0.2 at $\alpha = 0.9$. Higher values of d_p/d_b tended to give lower dimensionless velocities, though there was no clear relationship between the two.

Moore and Masliyah (1973) described a computer program which follows the path of a percolating particle through a two- or three-dimensional array of large spheres under the influence of a gravitational field. The results were reported by Masliyah and Bridgwater (1974), though only three different sets of numerical experiments are included, these being simulations of the two-dimensional case. The diameter of the bulk particles and hence the voidage was changed between runs though the distances between their centres remained constant. Successive lateral displacements were found to be independent enabling the lateral Peclet number to be

calculated. Vertical jumps were related to those up to four apart, though a limiting value of the vertical Peclet number, applicable at long times, could still be found from the diffusion equation. The lateral Peclet number increased from 2.7 to 5.2 and the vertical Peclet number increased from 4.7 to 10.0 as the bed voidage decreased from 0.381 to 0.255. The dimensionless percolation velocity remained approximately constant, changing from 0.252 to 0.233. These results are in reasonable agreement with the experimental data of Bridgwater et al. (1969a) and Bridgwater and Ingram (1971). Further supplementary experiments were also reported. The effect of percolating particle shape was investigated and ordered as well as random arrays of spheres were used.

An attempt to model the percolation process was made by Bridgwater and Scott (1974) who looked at the motion of a sphere as it fell through a series of surfaces. Their simpler models represented these surfaces as planes, but they later used spherical surfaces. Only the limiting case of zero coefficient of restitution was considered. There are two defects in the model; the particle comes to a rest each time it lands on a surface and only the motion of the particle when it is in contact with a surface is analysed. This leads to results for planar surfaces which are approximately correct if the surface length is replaced by the bulk particle diameter, and results for spherical surfaces which are too low.

In the second type of system in which spontaneous percolation occurs there is interference between the percolating particles. This can occur during flow from a hopper when the fines can pass through the interstices between the bulk particles. Shinohara et al. (1970) analysed the mechanism of segregation and blending of

a binary mixture of particles in this situation on the basis of a screen model. Results from an earlier paper (Shinohara et al., 1968) were incorporated in the model. Percolation rates were calculated and used to predict blending patterns in a hopper filled with small and large particles. Their experimental results agreed moderately well with the theory, which however included a number of empirical constants.

Later Shinohara et al. (1972) analysed the segregation produced when feeding a mixture of small and large particles to a V-shaped hopper. Predictive methods similar to those in the earlier paper indicated that fines would be confined to a V-shaped central zone that would be larger if the fraction of the small particles in the feed were increased, the length of flow surface increased and the feed rate increased. These predictions were supported by some experimental results. The theory is claimed to apply when the quantity of fines is insufficient to completely fill the spaces between the large particles and when $d_p/d_b<0.12$.

These papers by Shinohara and his co-workers indicate possible applications of results on spontaneous percolation, though the mechanisms may differ from those in the first system because of particle interference and they are therefore not related to the following work.

3.2 Axially dispersed plug flow

Before attempting to model spontaneous percolation, it is convenient to consider some of the methods used to analyse the results. Radial Peclet numbers may be calculated easily from the lateral distribution of particles if the system extends sufficiently far in the lateral directions. However calculation of axial Peclet numbers is not so simple.

Bridgwater and Ingram (1971) asserted that the variance of the residence time distribution can be used to determine the axial Peclet number Pe_a from

$$Pe_a = \frac{u\, d_b}{D_a} = \frac{2\, d_b\, t_m^2}{L\, \sigma_t^2} \qquad (3.2)$$

where D_a is the axial diffusion coefficient, t_m the mean residence time, L the height of the packing and σ_t^2 the variance of the residence time distribution.

In axial dispersion, material moves through the vessel with mean drift velocity u, while one-dimensional diffusion occurs in the axial (or y) direction. The general axially dispersed plug flow model as described by Levenspiel and Bischoff (1963) gives

$$\frac{\delta C}{\delta t} + u\, \frac{\delta C}{\delta y} = D_a\, \frac{\delta^2 C}{\delta y^2} \qquad (3.3)$$

where t is the time and C is the concentration. This may be changed to dimensionless form by making the following substitutions:

$$\theta = ut/L = t/t_m$$

$$Z = y/L$$

$$Pe_a = ud_b/D_a$$

$$c = C/C_o$$

where C_o is the mean concentration. $c(y,t)dy\, dt$ may be described as the probability of a percolating particle being between y and y + dy during the time interval t to t + dt. Equation 3.3 then becomes

$$\frac{\delta c}{\delta \theta} + \frac{\delta c}{\delta Z} = \frac{d_b}{LPe_a}\, \frac{\delta^2 c}{\delta Z^2} \qquad (3.4)$$

The simplest type of boundary conditions to use in solving

equation 3.4 are the "infinite pipe" conditions. If the vessel is infinite then

$$c = 0, \quad \theta = 0, \quad |Z| > 0$$

$$c = 0, \quad \theta > 0 \quad (Z-\theta) \rightarrow \pm\infty \tag{3.5}$$

$$\int_{-\infty}^{+\infty} c\,dZ = 1 \text{ for all } \theta$$

The solution to equation 3.4 is then (Levenspiel and Smith, 1957)

$$c = \frac{1}{2}\left[\frac{Pe_a L}{\pi\theta d_b}\right]^{\frac{1}{2}} \exp\left[\frac{-Pe_a L\,(Z-\theta)^2}{4\theta d_b}\right] \tag{3.6}$$

From this equation, the mean and variance of the dimensionless residence time are

$$\bar{\theta} = 1 + \frac{2d_b}{LPe_a} \tag{3.7}$$

$$\text{var}\,(\theta) = \frac{2d_b}{LPe_a} + 8\left[\frac{d_b}{LPe_a}\right]^2 \tag{3.8}$$

Van der Laan (1958) considered a more general system in which the bed was of finite length. The diffusion coefficients in the entry and exit sections were different from each other and from that in the bed. Laplace transforms were used in the solution and though the inverse transforms could not be found, the moments were calculated. Spontaneous percolation is most accurately modelled by assuming that the diffusion coefficient is zero outside the bed, which prevents diffusive motion carrying the particles above the top surface of the bed. Under these conditions the mean and variance found by Van der Laan reduce to

$$\bar{\theta} = 1 \tag{3.9}$$

$$\text{var}\ (\theta) = 2\left[\frac{d_b}{LPe_a}\right]^2\left[\frac{LPe_a}{d_b} - 1 + \exp\left(-\frac{LPe_a}{d_b}\right)\right] \quad (3.10)$$

As $Pe_aL/d_b \to \infty$, var $(\theta) \to 2d_b/LPe_a$ and thus Pe_a tends to the value given by equation 3.2. This can therefore be applied at high values of Pe_aL/d_b.

Solutions for this case have been presented by Yagi and Miyauchi (1953) and Brenner (1962), using a method that avoids Laplace transforms. They use the boundary conditions

$$\frac{\delta C}{\delta y} = 0 \text{ at } Z = 1 \text{ for all } t>0$$

$$uC - D_a\frac{\delta C}{\delta y} = uC_i \text{ at } Z = 0 \text{ for all } t>0$$

where C_i is the inlet concentration. For the case of a delta function input, Yagi and Miyauchi give, for Z = 1

$$c = 2\sum_{n=1}^{\infty}\mu_n\frac{(U\sin\mu_n+\mu_n\cos\mu_n)}{(U^2+2U+\mu_n^2)}\exp\left[U - \left(\frac{(U^2+\mu_n^2)\theta}{2U}\right)\right] \quad (3.11)$$

where $U = Pe_aL/2d_b$ and the μ_n are the positive roots, taken in order of increasing magnitude, of the transcendental equation

$$\cot\mu_n = (\mu_n/U - U/\mu_n)/2$$

Since the solution given by equation 3.11 converges slowly when U is large or t is small, Brenner also develops an asymptotic solution using Laplace transforms.

Equations 3.6 and 3.11 are compared for typical values of U at Z = 1 in figures 3.1-3.4. Values of c were calculated at intervals of θ of 0.05 and graphs plotted by computer.

In the experiments of Bridgwater and Ingram (1971), $LPe_a/d_b > 150$ and the difference in the Peclet numbers calculated from equations 3.2 and 3.10 is only of the order of 1%. However the accurate solution should be used for lower values of LPe_a/d_b.

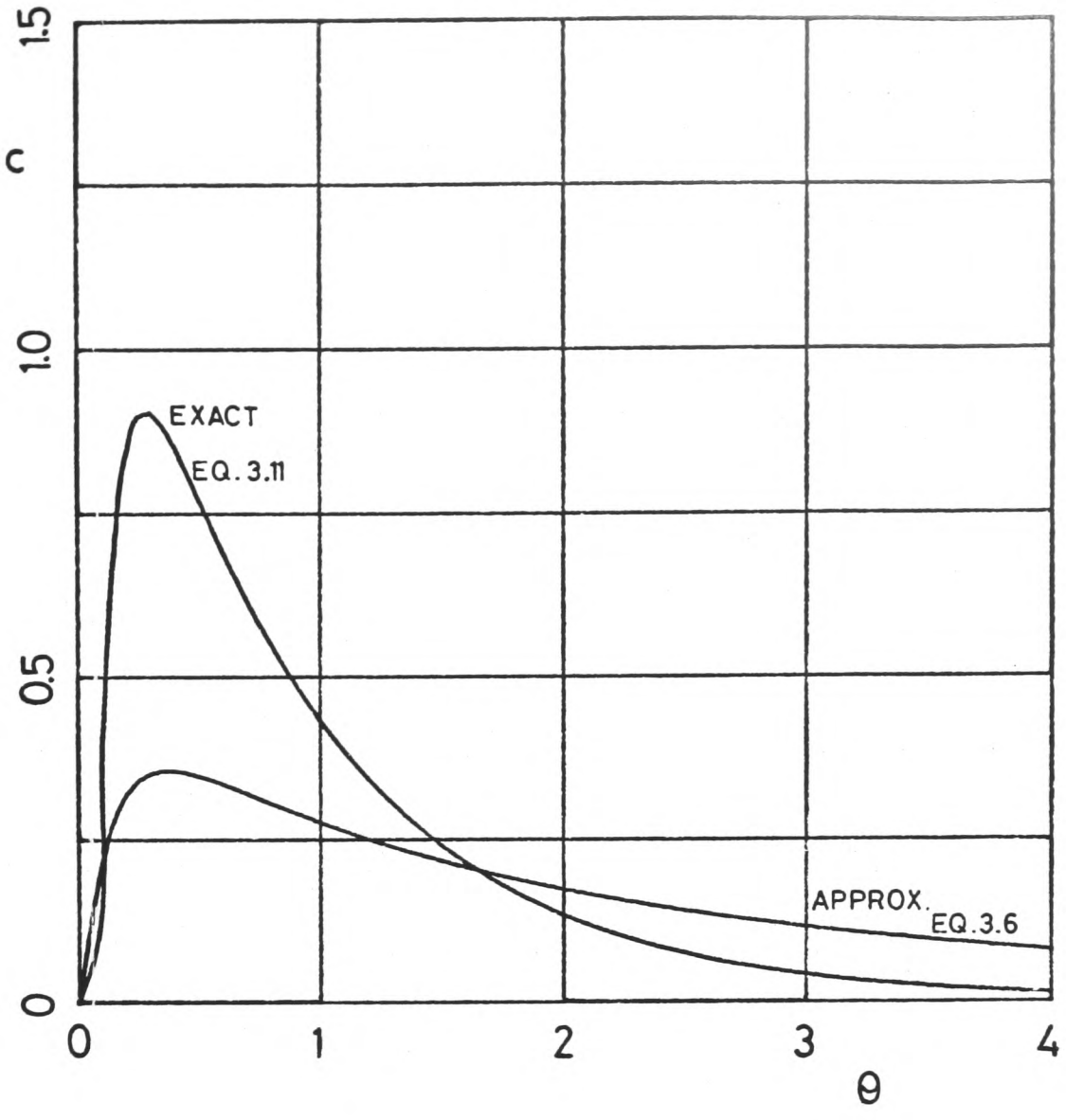


Figure 3.1 Comparison of exact and approximate solutions of the axially dispersed plug flow equation. U = 0.5.

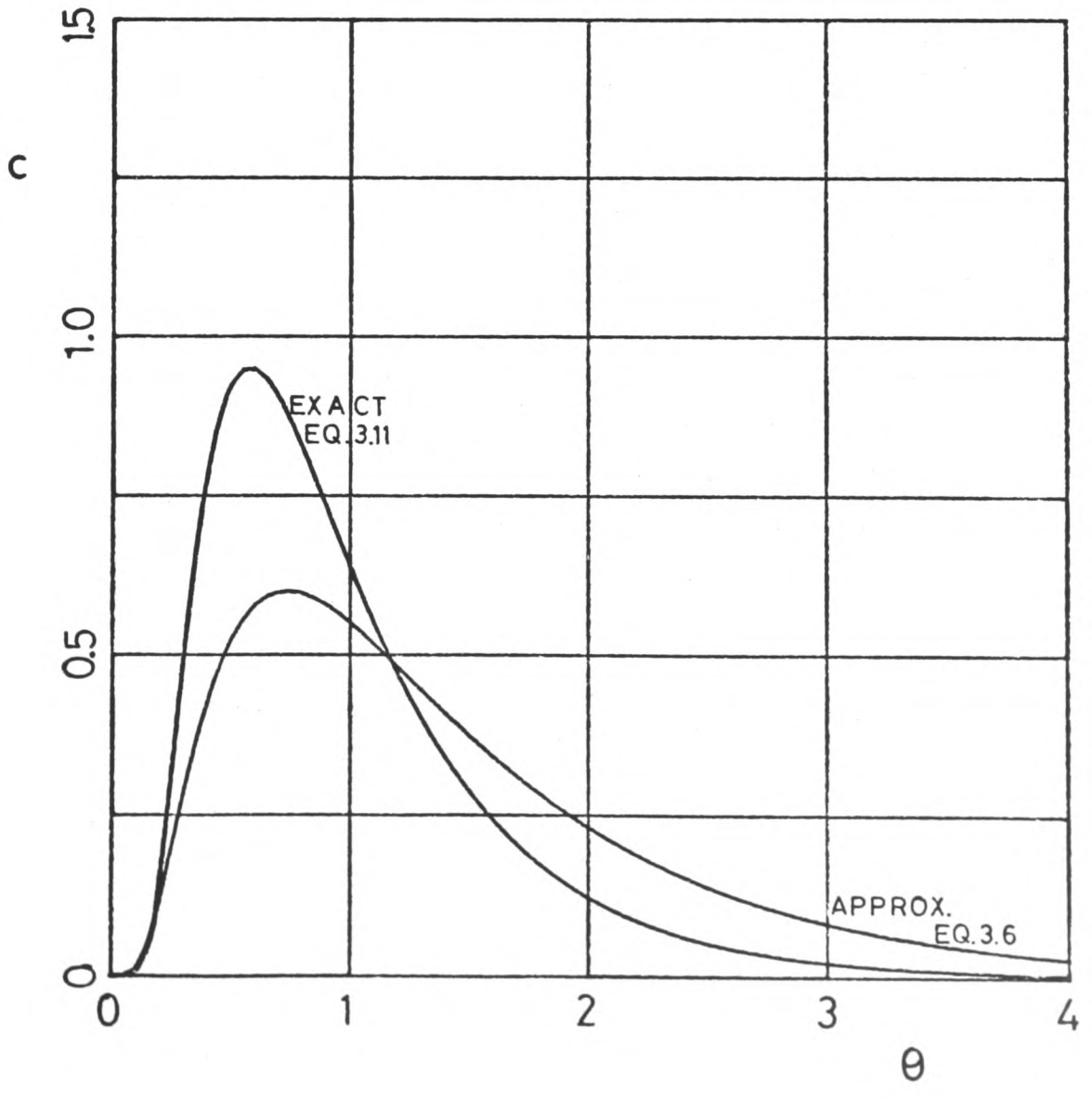


Figure 3.2 Comparison of exact and approximate solutions of the axially dispersed plug flow equation. U = 2.0.

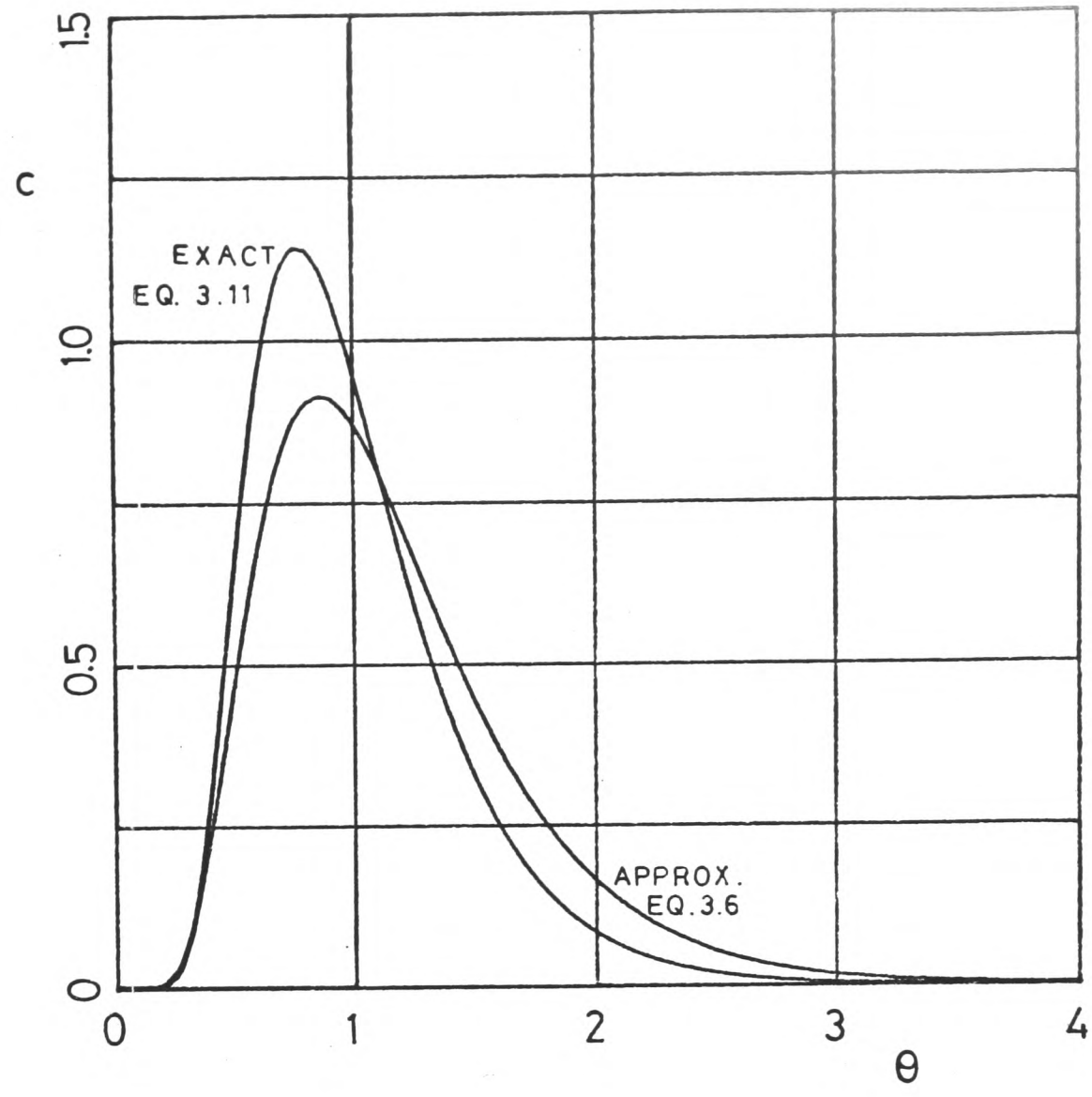


Figure 3.3 Comparison of exact and approximate solutions of the axially dispersed plug flow equation. U = 5.0.

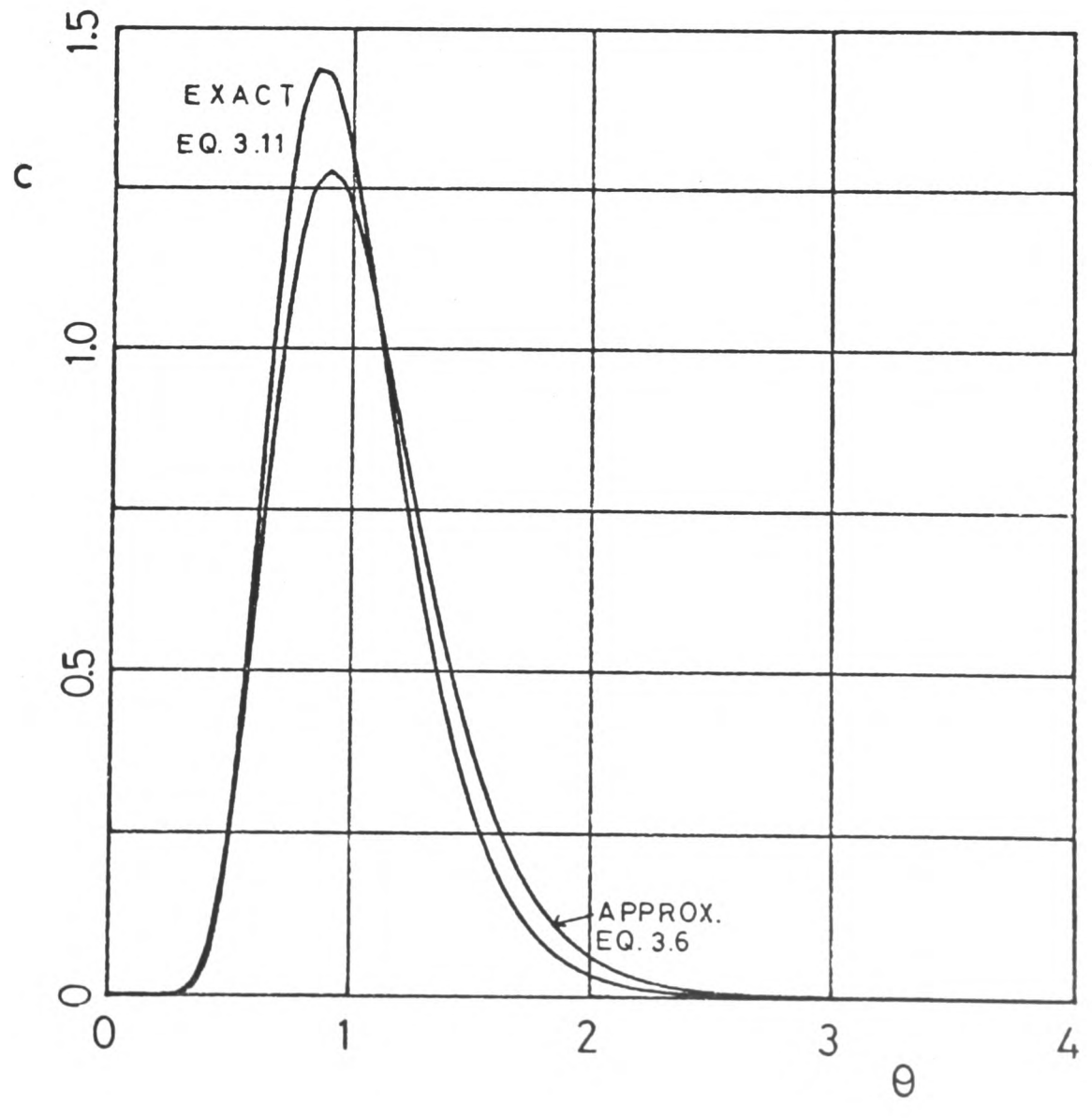


Figure 3.4 Comparison of exact and approximate solutions of the axially dispersed plug flow equation. U = 10.0.

3.3 Models of spontaneous percolation. Introduction

The only attempt to model spontaneous percolation has been by Bridgwater and Scott (1974) who looked at inelastic collisions. Even if only spherical particles are considered, it is unlikely that one theory could adequately cover the phenomenon. A qualitative change in the mechanism might be expected as the coefficient of restitution tends to zero and channelling effects might become important as the diameter ratio of the spheres approaches 0.155, the critical ratio above which spontaneous percolation is not possible (Bridgwater and Ingram, 1971). The problems become more complex with irregularly shaped particles, not least because the behaviour of the particle depends on its orientation on impact.

The theories of spontaneous percolation presented here assume that the motion of the percolating particle may be adequately described by the use of average quantities. These theories are based on attempts to understand the physical processes, assuming distributions for impact angles and velocities. Measurement of these distributions experimentally would be difficult and the simulation by Masliyah and Bridgwater (1974) considers only ordered two-dimensional arrays and neither the distributions of the interstitial velocities nor of the approach angles are reported. Thus the success of these theories depends to a large extent on the distributions assumed, though those chosen are thought to be physically realistic.

As noted in section 3.1, one defect with the model proposed by Bridgwater and Scott (1974) is that it takes no account of the motion of the particle while in flight and should therefore give percolation velocities that are too low. This is true of their spherical surface model. The first theory presented here seeks to

remedy this defect by considering interstitial velocities, though it remains restricted to wholly inelastic collisions, a limiting case of percolating particle behaviour. The second theory, based on an idea by Spink (1973), considers partly elastic collisions, where $0<\alpha<1$.

3.4 Model I. Inelastic particles

3.4.1 Model and percolation velocity

The model follows the motion of an inelastic spherical particle through an array of two-dimensional planar surfaces.

Consider a spherical particle landing on a plane and rolling along it. Since the coefficient of restitution is zero, energy is lost on collision. The particle is assumed to have no angular momentum before, or immediately after, the impact. The energy lost, E_{Li} is given by

$$E_{Li} = mV_f^2/2 - mV_a^2/2 \qquad (3.12)$$

where V_f is the velocity before impact and V_a the velocity immediately after impact. Momentum is conserved parallel to the plane and hence

$$mV_f\cos\theta_f = mV_a \qquad (3.13)$$

where θ_f is the impact angle (see figure 3.5). Eliminating V_a from equations 3.12 and 3.13

$$E_{Li} = \frac{mV_f^2(1-\cos^2\theta_f)}{2} = \frac{mV_f^2}{4}(1-\cos 2\theta_f) \qquad (3.14)$$

It will be assumed that the probability distribution of θ_f is proportional to $\cos(\pi/2-\beta-\theta_f)$ where β is the angle between the collision surface and the horizontal and $\pi-\beta>\theta_f>0$ (figure 3.5).

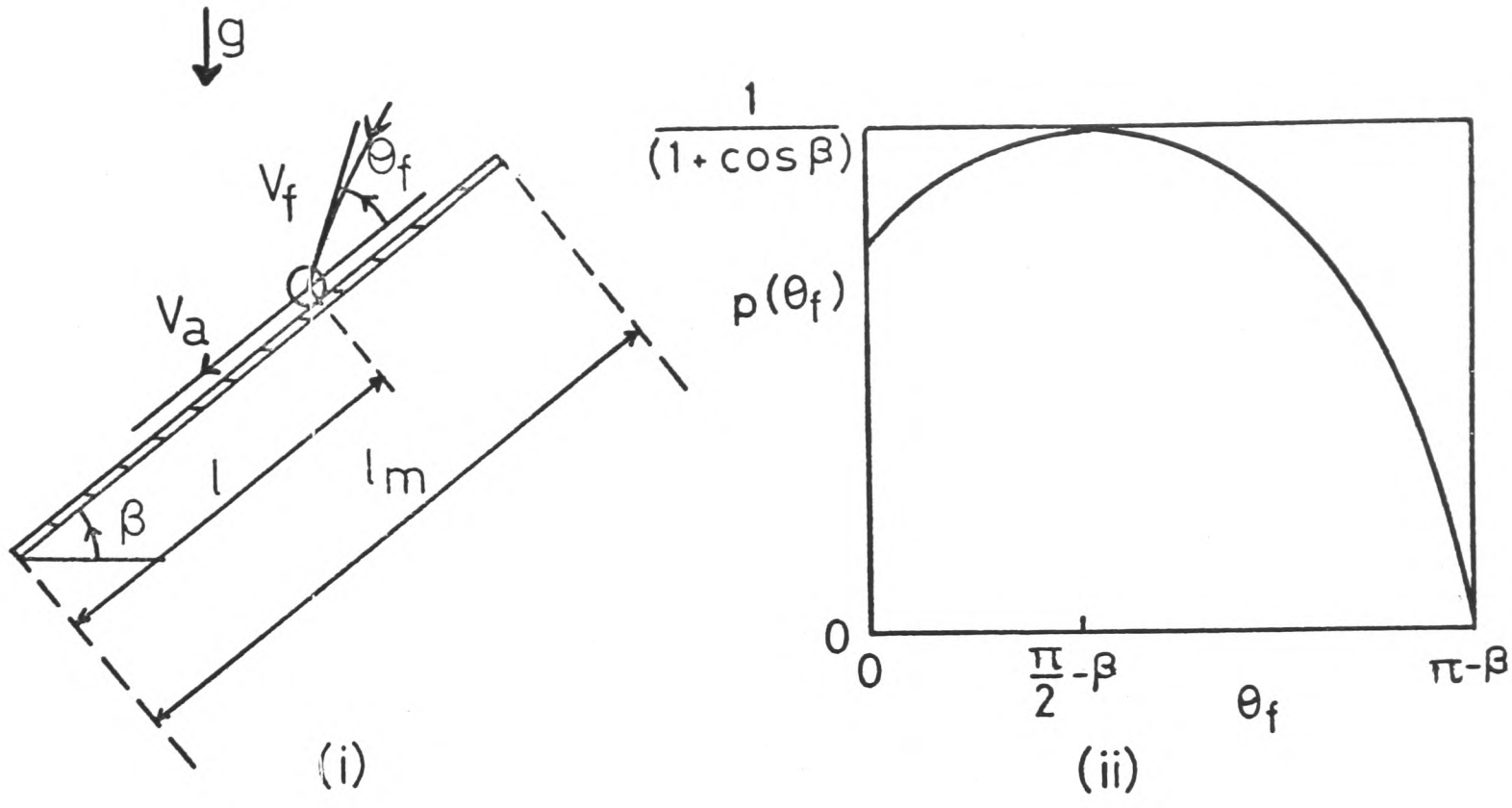


Figure 3.5 (i) Particle hitting a planar surface with zero coefficient of restitution. (ii) Distribution of impact angles θ_f.



Figure 3.6 Resolution of V_f and V_o into horizontal and vertical components.

This is a convenient choice which is probably approximately correct as particles are likely to be travelling at angles closer to the vertical than to the horizontal. Since the sum of the probabilities equals one,

$$\int_0^{\pi-\beta} K \cos(\pi/2-\beta-\theta_f)d\theta_f = 1$$

whence $K = 1/(1+\cos\beta)$. Then the average energy loss E_L is given by

$$E_L = \int_0^{\pi-\beta} \frac{mV_f^2}{4} \frac{(1-\cos 2\theta_f)(\cos(\pi/2-\beta-\theta_f))}{(1+\cos\beta)} d\theta_f \qquad (3.15)$$

$$= \frac{mV_f^2}{6}(1+\cos\beta)$$

Other hypotheses about the distribution of θ_f are possible, though that chosen is both simple and physically realistic.

The motion of the particle after it has hit the plane is considered next. There will probably be a short period during which skidding occurs,after which it will roll. In this analysis only rolling is included. The angular momentum of the particle has been neglected; since this might have been in either direction, the net effect after averaging will be small. After hitting the plane, the particle will roll upwards if $\theta_f > \pi/2$. If this occurs, two events are possible.

(i) The particle rolls up the plane, stops, and rolls down again.

(ii) The particle rolls off the top of the plane.

If (i) occurs, the net effect will be that the velocity of the particle after impact is reversed in direction and the time spent by the particle on the plane increased. It will be shown later that the probability of (ii) occurring is small and thus it

need not be considered further. In the analysis of the motion of the particle after impact it can therefore be assumed that V_a is down the plane.

If, after the particle has rolled a distance l down the plane, its translational velocity is V and angular velocity is ω

$$mgl\sin\beta + \frac{mV_a^2}{2} = \frac{mV^2}{2} + \frac{I\omega^2}{2} \qquad (3.16)$$

where I is the moment of inertia of the particle. For a sphere of uniform density $I = md_p^2/10$, $V = d_p\omega/2$ and hence

$$mgl\sin\beta + \frac{mV_a^2}{2} = \frac{7mV^2}{10} \qquad (3.17)$$

Substituting for V_a^2 from equation 3.12, averaging over θ_f and substituting for E_L from equation 3.15,

$$V^2 = \frac{5}{14}\left[4gl\sin\beta + \frac{2V_f^2}{3}(2 - \cos\beta)\right] \qquad (3.18)$$

The interstitial motion can be described by simple equations. The velocity of the particle as it leaves the plane can be resolved into V_H horizontally and V_1 downwards. V_f can be resolved into V_H' horizontally and V_2 downwards (see Figure 3.6). Then

$$V_H' = V_f \cos(\beta+\theta_f) \qquad (3.19)$$

$$V_2 = V_f \sin(\beta+\theta_f) \qquad (3.20)$$

$$V_1 = V_o \sin\beta \qquad (3.21)$$

$$V_H = V_o \cos\beta \qquad (3.22)$$

where V_o is the velocity of the particle as it leaves the plane. Expressions for the mean square velocities averaged over β are required. Hence, if V_{oa} is the value of V_o averaged over different surface lengths,

$$\overline{V_1^2} = \overline{(V_{oa}\sin\beta)^2} \tag{3.23}$$

$$\overline{V_H^2} = \overline{(V_{oa}\cos\beta)^2} \tag{3.24}$$

where the bar signifies averaging over β.

As in the work by Bridgwater and Scott (1974), it is assumed that the distribution of β is such that the probability of the inclination being between β and $\beta + d\beta$ is $\sin\beta\, d\beta$ where $0<\beta<\pi/2$, and that the surface lengths are randomly distributed between 0 and l_m, i,e. the fraction of surfaces with length l to $l + dl$ is dl/l_m where l_m is the maximum plane length. Then V_{oa}^2 can be found from equation 3.18,

$$V_{oa}^2 = \int_0^{l_m} V^2 dl/l_m$$

$$= \frac{5}{14}\left[2gl_m\sin\beta + \frac{2V_f^2}{3}(2-\cos\beta)\right] \tag{3.25}$$

assuming V_f^2 is not a function of l. If V_f^2 is independent of β, from equation 3.23,

$$\overline{V_1^2} = \int_0^{\pi/2} V_{oa}^2 \sin^2\beta . \sin\beta d\beta$$

$$= \frac{5}{14}\left[\frac{3\pi g l_m}{8} + \frac{13V_f^2}{18}\right] \tag{3.26}$$

and similarly for $\overline{V_H^2}$ from equation 3.24,

$$\overline{V_H^2} = \int_0^{\pi/2} V_{oa}^2 \cos^2\beta . \sin\beta d\beta$$

$$= \frac{5}{14}\left[\frac{\pi g l_m}{8} + \frac{5V_f^2}{18}\right] \tag{3.27}$$

The mean vertical distance travelled on a plane $\bar{l}$ is given by

$$\bar{l} = \int_0^{\pi/2}\int_0^{l_m} l\sin\beta . \frac{dl}{l_m} \sin\beta d\beta = \pi l_m/8 \tag{3.28}$$

The mean vertical distance travelled in flight $\bar{h}$ is given by

$$\bar{h} = \frac{\overline{V_2^2 - V_1^2}}{2g} \tag{3.29}$$

Two different assumptions about $\bar{h}$ will be used. These will be distinguished as hypotheses H_1 and H_2, namely

$$H_1 \qquad \bar{h} = l_m/2 \tag{3.30}$$

$$H_2 \qquad \bar{h} = \int_0^{\pi/2} \int_0^{l_m} (l_m - l\sin\beta)\frac{dl}{l_m} \sin\beta d\beta$$

$$= l_m(1-\pi/8) \tag{3.31}$$

H_1 makes $\bar{h}$ equal to half the maximum surface length; H_2 results in the distances travelled in flight and on a plane having similar distributions such that $\bar{l} + \bar{h} = l_m$.

The mean percolation velocity u is the ratio of the mean vertical distance travelled to the time taken to travel that distance. Thus

$$u = \frac{\bar{h} + \bar{l}}{\bar{t} + \bar{t}'} \tag{3.32}$$

where $\bar{t}$ is the mean time that a particle spends on a plane and $\bar{t}'$ is the mean time spent in flight, as motion on a plane and motion in flight occur alternately. $\bar{t}'$ can be found from

$$\overline{V_2 - V_1} = g\bar{t}' \tag{3.33}$$

To apply this equation it will be assumed that $\overline{V_2 - V_1} = \sqrt{\overline{V_2^2}} - \sqrt{\overline{V_1^2}}$.

The model as described includes one redundant piece of information as the distribution of θ_f is defined by the other equations. Some assumption as to the form of this distribution was necessary before progress was possible and this is probably the weakest part of the model. Its effect can be minimised by combining equations 3.19 and 3.20 to give

$$V_f^2 = \overline{V_2^2} + \overline{V_H'^2} \tag{3.34}$$

Since there is no change in the horizontal velocity while the particle is in flight, $\overline{V_H'^2} = \overline{V_H^2}$.

$\bar{t}$ can be found from equation 3.18. Substituting dl/dt for V,

$$\left(\frac{dl}{dt}\right)^2 = \frac{5}{14}\left[4gl\sin\beta + \frac{2V_f^2(2-\cos\beta)}{3}\right] \qquad (3.35)$$

assuming that V_a is down the plane. Integrating equation 3.35,

$$t_p = \frac{\sqrt{7/10}}{g\sin\beta}\left[\left(\frac{2V_f}{3}^2(2-\cos\beta) + 4gl\sin\beta\right)^{\frac{1}{2}} - \left(\frac{2V_f}{3}^2(2-\cos\beta)\right)^{\frac{1}{2}}\right] \qquad (3.36)$$

where t_p is the time spent by the particle on a plane of length l. Averaging over l and β gives

$$\frac{\sqrt{7/10}}{g}\int_0^{\pi/2}\left[\frac{\left(2V_f^2(2-\cos\beta)/3 + 4gl_m\sin\beta\right)^{3/2} - \left(2V_f^2(2-\cos\beta)/3\right)^{3/2}}{6gl_m\sin\beta} - \left(2V_f^2(2-\cos\beta)/3\right)^{\frac{1}{2}}\right]d\beta \qquad (3.37)$$

To this must be added the mean time taken by the particle to roll up the plane and back to the impact point multiplied by the probability that this occurs. The probability can be found from the θ_f distribution. From equation 3.13,

$$V_a^2 = V_f^2\cos^2\theta_f \qquad (3.38)$$

Since the direction of motion is upwards,

$$\frac{mV_a}{2}^2 = \frac{7mV^2}{10} + mgl\sin\beta \qquad (3.39)$$

Substituting V = dl/dt and integrating, the time taken for a particle to roll to a halt a distance l_u up the plane is given by

$$\frac{2\sqrt{7/10}}{g\sin\beta}\left[\left(\frac{V_a}{2}^2\right)^{\frac{1}{2}} - \left(\frac{V_a}{2}^2 - gl_u\sin\beta\right)^{\frac{1}{2}}\right]$$

Since energy is conserved, $V_a^2 = 2gl_u\sin\beta$ and t_{ui}, the time taken for the particle to roll up the plane and back to the collision point is given by

$$t_{ui} = \frac{\sqrt{2}}{g\sin\beta}\sqrt{\frac{7V_a^2}{10}} \qquad (3.40)$$

V_a will be up the plane if $\pi/2<\theta_f<\pi-\beta$. Substituting in equation 3.40 from equation 3.38, t_u the average of t_{ui} over θ_f is given by

$$t_u = \pm \frac{2}{g\sin\beta}\left(\frac{7V_f^2}{5}\right)^{\frac{1}{2}} \int_{\pi/2}^{\pi-\beta} \frac{\cos\theta_f.\cos(\pi/2-\beta-\theta_f)}{1+\cos\beta}\, d\theta_f$$

$$= \pm \frac{1}{2g}\sqrt{\frac{7V_f^2}{5}} \cdot \frac{(\pi/2-\beta-\cot\beta)}{(1+\cos\beta)} \qquad (3.41)$$

Averaging over β,

$$\overline{t_u} = \pm \frac{1}{2g}\sqrt{\frac{7}{5}V_f^2} \int_0^{\pi/2} \frac{(\pi/2-\beta-\cot\beta)\sin\beta}{(1+\cos\beta)}\, d\beta$$

$$= 0.1332\sqrt{\frac{V_f^2}{g}} \qquad (3.42)$$

The mean distance travelled by those particles which begin to roll upwards, $\bar{l}_u$, indicates whether it is reasonable to disregard the possibility of a particle rolling over the top of a plane. From equation 3.39, $l_u = V_a^2/2g\sin\beta$. Substituting for V_a^2 from equation 3.38 and averaging over values of θ_f and β,

$$\bar{l}_u = \frac{V_f^2}{6g} \int_0^{\pi/2} \frac{(1-\sin\beta)^2}{(1+\cos\beta)}\, d\beta$$

$$= V_f^2(\pi-4\log_e 2)/12g \qquad (3.43)$$

whence

$$\frac{\bar{l}_u}{l_m} = 0.03075\,\frac{V_f^2}{gl_m} \qquad (3.44)$$

The value of V_f^2/gl_m can be found from equations 3.26-7, 29-31, 34, which give

$$H_1 \qquad \frac{V_f^2}{gl_m} = \frac{28 + 5\pi}{18} = 2.43 \tag{3.45}$$

$$H_2 \qquad \frac{V_f^2}{gl_m} = \frac{28 - \pi}{9} = 2.76 \tag{3.46}$$

Thus, from equation 3.44, $\bar{l}_u/l_m = 0.08$, indicating that the probability of a particle rolling over the top of a plane is small.

If the bulk particles are spherical, an approximate relationship between their diameter d_b and l_m can be found by considering motion on a spherical surface. The maximum path length will occur if the percolating particle lands on top of a bulk particle with near zero lateral velocity. The particle will leave the surface at the point where the force due to gravity, resolved in a radial direction, is equal to the centrifugal force, that is:

$$mg\cos\phi_o = \frac{2m}{d_p+d_b}\left(\frac{d_p+d_b}{2}\frac{d\phi}{dt}\right)^2 \tag{3.47}$$

where ϕ is the local surface slope, and ϕ_o the slope at the point where the particle leaves the surface. Equating the loss in potential energy and the gain in kinetic energy,

$$\left(\frac{d_p+d_b}{2}\frac{d\phi}{dt}\right)^2 = \frac{5g(d_p+d_b)(1-\cos\phi)}{7} \tag{3.48}$$

Combining equations 3.47 and 3.48, $\cos\phi_o = 10/17$, and the maximum distance travelled by the particle on the sphere is $0.471d_b$.

The dimensionless velocities and times can now be calculated by solving equations 3.26-34, 37, 42 and eliminating $\overline{V_H^2}$, $\overline{V_1^2}$, $\overline{V_2^2}$, V_f^2, l_m, $\bar{l}$, $\bar{h}$, $\bar{t}$, $\bar{t}'$, $\bar{t}_u$ and u in turn. Equations 3.37 and 3.42 required numerical calculation on a desk computer. A library routine employing Gaussian quadrature was used. The results are reported in Table3.1.

	H_1	H_2
$\bar{h}/d_b$	0.235	0.286
$\sqrt{V_f^2}/gd_b$	1.069	1.141
$\sqrt{\overline{V_1^2}}/gd_b$	0.702	0.731
$\sqrt{\overline{V_2^2}}/gd_b$	0.982	1.052
$\sqrt{V_H^2}/gd_b$	0.424	0.442
$\bar{t}'\sqrt{g/d_b}$	0.280	0.321
$\bar{t}\sqrt{g/d_b}$	0.604	0.579
$\bar{t}_u\sqrt{g/d_b}$	0.152	0.173
$u/\sqrt{gd_b}$	0.406	0.439
$u/\sqrt{gd_b}$(E)	~0.45	

Table 3.1: Theoretical values predicted by Model I and extrapolated experimental value of dimensionless percolation velocity.

E Extrapolation to $\alpha = 0$ from experimental results of Bridgwater and Ingram (1971)

3.4.2 Axial dispersion

The numerical experiments of Masliyah and Bridgwater (1974) show that the axial dispersion in spontaneously percolating systems obeys the diffusion equation. From Einstein's (1926) equation for one-dimensional diffusion,

$$\text{var}(y)_t = 2D_a t \tag{3.49}$$

where $\text{var}(y)_t$ is the variance of axial displacements from the mean movement at time t. Since $u = y_m/t$ where y_m is the mean axial displacement,

$$Pe_a = ud_b/D_a = 2y_m d_b/\text{var}(y)_t \tag{3.50}$$

It is impossible to evaluate $\text{var}(y)_t$ directly and simplifying assumptions must be made. The easiest method is to calculate the variance of the displacements after the particle has rolled down S surfaces, $\text{var}(y)_s$. If the on-surface and free-flight sections are assumed to be independent, the variances can be calculated separately and then added together.

For the motion on the planar surfaces,

$$\begin{aligned}\text{var}(y)_s &= S\left[(y^2)_m - y_m^2\right] \\ &= S\int_0^{\pi/2}\int_0^{l_m} l^2\sin^3\beta\,\frac{dl}{l_m}\,d\beta - S\left[\frac{l_m\pi}{8}\right]^2 \\ &= S\,l_m^2\left[\frac{2}{9} - \frac{\pi^2}{64}\right]\end{aligned} \tag{3.51}$$

If hypothesis H_1 is used, the distribution of h, the vertical free-flight distance is not defined, though $\bar{h} = l_m/2$. A possible distribution is $p(h) = \frac{\pi}{2}\sin(h\pi/l_m)$ where $0 \leq h \leq l_m$. Then,

$$\begin{aligned}\text{var}(y)_s &= S\int_0^{l_m} h^2 p(h)\frac{dh}{l_m} - \frac{Sl_m^2}{4} \\ &= (\pi^2-8)Sl_m^2/4\pi^2\end{aligned} \tag{3.52}$$

If H_2 is used, the distribution of lengths is the same as that for the part of the motion on the surface and thus $var(y)_s$ is given by equation 3.51.

The mean axial displacement y_m equals Sl_m $(0.5+\pi/8)$ (H_1) or Sl_m (H_2). Pe_a can be calculated from equations 3.50-52 after substituting $0.471d_p$ for l_m. The values are in Table 3.2.

3.4.3 Radial dispersion

On-surface and free flight parts of the motion are again separated and $var(x)_s$ replaces $var(x)_t$. The former can be calculated using the method of Bridgwater and Scott (1974). Co-ordinates x, y and z are defined in figure 3.7. The motion of the sphere is at an angle β to the horizontal and its projection on a horizontal plane makes an angle ν $(0<\nu<2\pi)$ with the x co-ordinate axis. Whilst on the plane, the particle moves a distance $l\cos\beta\cos\nu$ in the x direction. Since the average distance moved in the x direction is zero, the variance of x displacements is given by

$$var(x)_s = \int_{\nu=0}^{2\pi} \int_{\beta=0}^{\pi/2} \int_{l=0}^{l_m} Sl^2\cos^2\beta\cos^2\nu \frac{dl}{l_m}\sin\beta d\beta\frac{d\nu}{2\pi}$$

$$= Sl_m^2/18 \qquad (3.53)$$

The variance of z displacements is also $Sl_m^2/18$ and hence the variance of on-surface displacements $var(\lambda_s)$ is $Sl_m^2/9$.

The preceding theory has not produced any information about the distribution of horizontal displacements during free flight. Two different assumptions, P_1 and P_2 will be considered.

(i) P_1. The variance is assumed to be the same as that due to motion on the surfaces, i.e. $Sl_m^2/9$.

	H_1	H_2
ul_m/D_a	15.4	14.7
ul_m/D_a (B/S)	$31.4 \geq ul_m/D_a \geq 11.6$	
ud_b/D_a (E)	~9	
ul_m/D_r (P_1)	16.1	18.0
ul_m/D_r (P_2)	19.1	18.2
ul_m/D_r (B/S)	$18.0 \geq ul_m/D_r \geq 9.4$	
ud_b/D_r (E)	~13	

Table 3.2: Theoretical and experimental values of Peclet numbers.

B/S Models of Bridgwater and Scott (1974)

E Extrapolation to $\alpha = 0$ from experimental results (Bridgwater and Ingram, 1971).

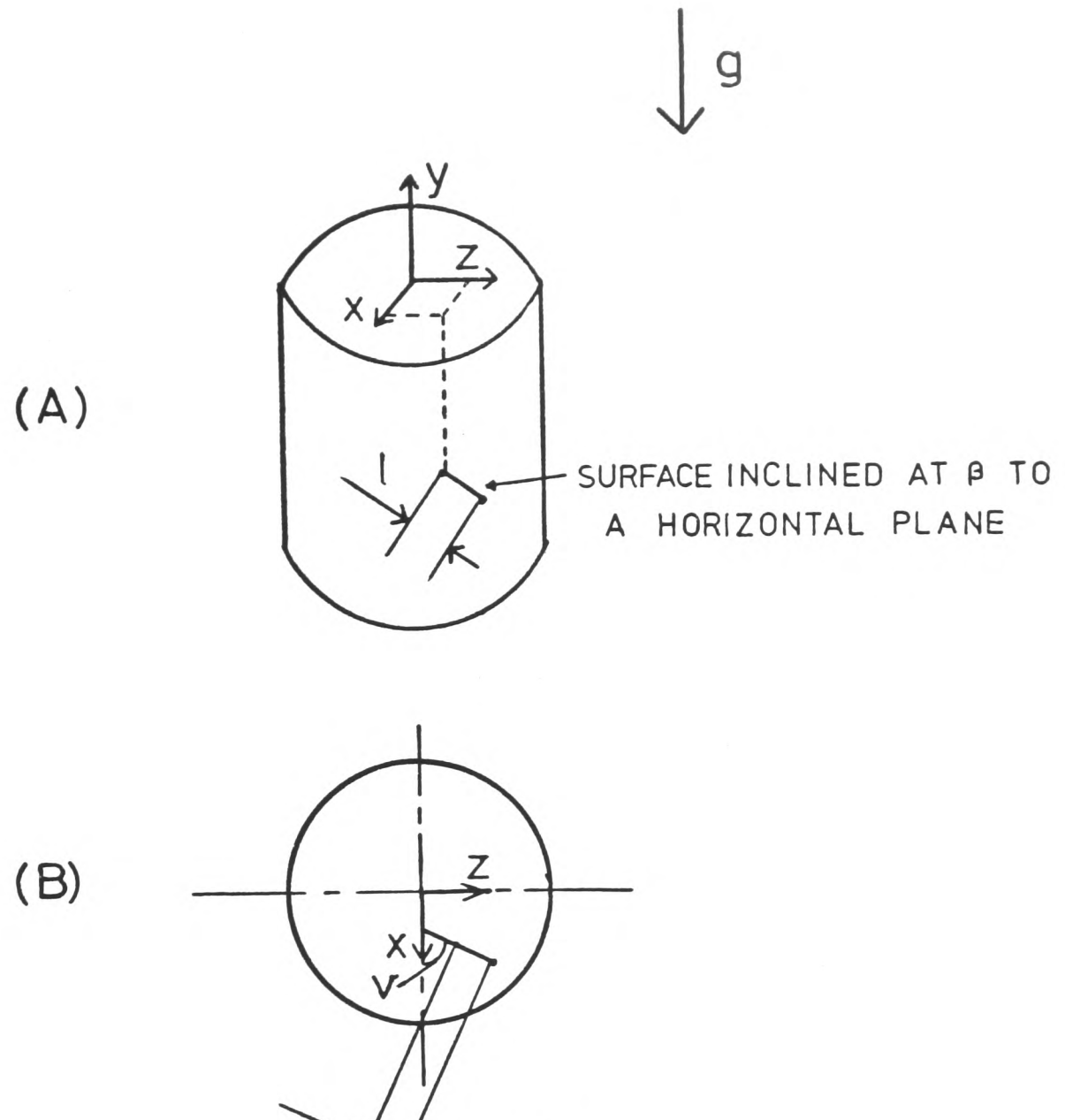


Figure 3.7 Geometry of the lateral displacement of particles.
(A) General view
(B) Projection onto a horizontal plane

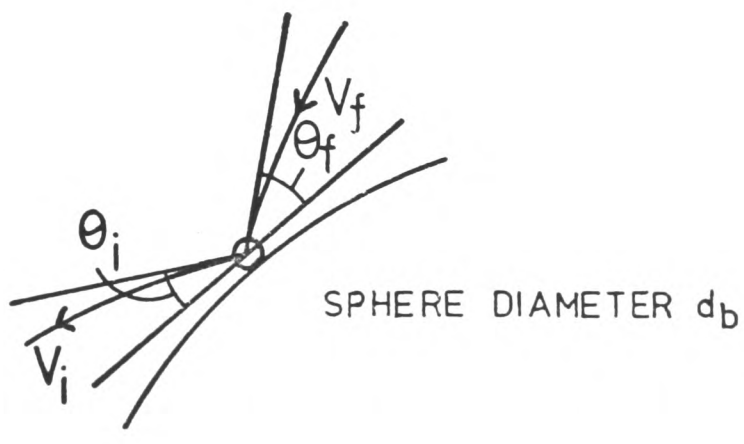


Figure 3.8 Collision between a percolating particle and a bulk sphere.

(ii) P_2. Alternatively a convenient distribution of x is $p(x) = \left(\frac{\pi}{2}\right)\left(\sin \frac{\pi x}{2x_m}\right)$ where $0 \leqslant x \leqslant 2x_m$ and x_m is the mean displacement. Then the variance of the displacements in the x direction equals

$$S \int_0^{2x_m} \frac{\pi x^2}{2} \sin \frac{\pi x}{2x_m} dx = S x_m^2 (2 - 8/\pi^2)$$

If the distribution of displacements in the z direction is the same then the total variance is twice this. x_m can be found from the values of $\bar{V}_H$ and $\bar{t}'$ in Table 1 and equals 0.119db (H_1) or $0.142d_b$ (H_2).

The total variance of horizontal displacements $var(\lambda_H)$ equals $4D_r t$. The radial Peclet number $Pe_r = ud_b/D_r = 4y_m d_b/var(\lambda_H)$ and the values are shown in Table 2.

3.5 Model II. Partly elastic particles

A similar approach can be applied to partly elastic collisions. A percolating particle of mass m, diameter d_p and velocity V_f collides with a spherical surface and rebounds with velocity V_i. A plane can be drawn through the two trajectories (though it does not necessarily pass through the centre of the bulk sphere) as in figure 3.8. The particle approach path is at an angle θ_f to the tangent to the sphere at the point of impact and the corresponding angle of rebound is θ_i.

The average loss of kinetic energy on collision equals the average gain during flight, i.e.

$$\frac{1}{2}.m\ (\overline{V_f^2 - V_i^2}) = mg\overline{\Delta y} \qquad (3.54)$$

where $\overline{\Delta y}$ is the mean vertical distance between collisions. Momentum is conserved parallel to the tangent at the point of impact.

$$mV_f\cos\theta_f = mV_i\cos\theta_i \tag{3.55}$$

If the coefficient of restitution is α, assumed for simplicity to be constant,

$$mV_f\sin\theta_f = \alpha mV_i\sin\theta_i \tag{3.56}$$

whence from equations 3.55 and 3.56

$$V_i^2 = V_f^2\,(1 - (1 - \alpha^2)\sin^2\theta_f) \tag{3.57}$$

In the absence of gravity, the mean velocity downwards would be zero, and therefore

$$u \simeq g\,T/2 \tag{3.58}$$

where u is the percolation velocity and T is the mean time interval between collisions. Since $u = \overline{\Delta y}/T$, from equations 3.54 and 3.58,

$$\overline{V_f^2 - V_i^2} = g^2T^2 \tag{3.59}$$

If V_f is not a function of θ_f, then from equations 3.57 and 3.59

$$\overline{V_f^2} = \frac{g^2T^2}{(1-\alpha^2)\overline{\sin^2\theta_f}} \tag{3.60}$$

and

$$\overline{V_i^2} = g^2T^2\left[\frac{1 - (1 -\alpha^2)\overline{\sin^2\theta_f}}{(1-\alpha^2)\overline{\sin^2\theta_f}}\right] \tag{3.61}$$

One more equation is required to describe the motion of the particle. A possibility is to introduce the mean free path of the particle λ, which is approximately equal to $T\,\bar{V}$, where $\bar{V}$ is the mean interstitial velocity of the particle, but estimation of λ is difficult. The only data comes from the simulation by Masliyah and Bridgwater. Experimental void fractions for a random array of spheres are about 0.37. In the corresponding numerical experiment the mean square lateral jump was $0.0846b^2$ where b is

the distance between sphere centres. If in three dimensions the mean square jump in the orthogonal lateral direction were the same, then these can be added to the mean square vertical jump reported by Masliyah and Bridgwater to give a value $0.186b^2$ for λ. In this experiment the ratio of the effective bulk particle diameter to b was 0.826, whence $\lambda = 0.52\ (d_b - d_p)$.

If $\bar{V}$ is approximated by $(\sqrt{\overline{V_1^2}} + \sqrt{\overline{V_2^2}})/2$, then, from equations 3.60 and 3.61,

$$\bar{V} = 0.5gT \left[\frac{1 + \sqrt{1 - (1-\alpha^2)\overline{\sin^2\theta_f}}}{\sqrt{(1-\alpha^2)\overline{\sin^2\theta_f}}} \right]$$

Since $\bar{V} = 0.52\ (d_b - d_p)/T$ and $u = gT/2$

$$u = 0.5 \left[\frac{1.04g(d_b - d_p)\ \sqrt{(1-\alpha^2)\overline{\sin^2\theta_f}}}{1 + \sqrt{1 - (1-\alpha^2)\overline{\sin^2\theta_f}}} \right]^{\frac{1}{2}} \qquad (3.62)$$

The distribution of impact angles on a sphere has been discussed by Bridgwater and Scott (1974). The probability that the angle of approach is θ_f may be assumed to be equal to the fractional area, projected onto a horizontal plane, of surface having inclination between $(\pi/2 - \theta_f)$ and $(\pi/2 - \theta_f + d\theta_f)$ to the vertical. This is exact if the particle were moving vertically downwards and if there were no local ordering of paths. It may be shown that $p(\theta_f) = \sin 2\theta_f$ and the average value of $\sin^2\theta_f$ is therefore

$$\int_0^{\pi/2} \sin^2\theta_f \sin 2\theta_f\, d\theta_f = 0.5$$

Substituting in equation 3.62, the dimensionless percolation velocity is given by

$$\frac{u}{\sqrt{g(d_b-d_p)}} = \left[\frac{0.26\ \sqrt{(1-\alpha^2)/2}}{1+\sqrt{(1+\alpha^2)/2}}\right]^{\frac{1}{2}} \qquad (3.63)$$

3.6 Discussion and conclusion

The first topic considered in this chapter was the solution of the axially dispersed plug flow equation with boundary conditions which are relevant to percolation through a packed bed. The correct solution, that due to Yagi and Miyauchi, has been identified and it has been shown that an approximate solution using simple boundary conditions leads to acceptable results when high values of LPe_a/d_b occur. The exact solution will be employed in the study of strain-induced percolation in Chapter 8. Consideration of different boundary conditions was unnecessary in the models.

The major part of the chapter is the presentation of two models of spontaneous percolation. The first is an extension of the work of Bridgwater and Scott from which it differs in that the interstitial motion of the particle is also considered. A better estimate of the percolation velocity would therefore be expected from it and this is found to be the case. The values of $u/\sqrt{gd_b}$ predicted by the theory, 0.41 (H_1) and 0.44 (H_2), compare favourably with the experimental evidence which, when extrapolated to zero coefficient of restitution predicts a value between 0.4 and 0.5. Bridgwater and Scott found values $0.29 < u/\sqrt{gl_m} < 0.50$ for their planar surface model and 0.15 for the spherical surface model, results which, if l_m is replaced by $0.471d_b$, are low. The model presented here therefore successfully replaces the earlier one, and also provides estimates of the interstitial velocity.

It has not been possible to apply the concept to three dimensions or to spherical surfaces. In the latter case the integrations are connected in such a way that even numerical integration would be difficult. It was considered that the model probably represented a sufficient level of sophistication as it stood.

Axial and radial Peclet numbers are compared in Table 3.2. The values derived here are generally about the same as those of the earlier model, though both indicate less diffusion than the extrapolated experimental results if l_m is replaced by $0.471d_b$. This lack of agreement may be due to a defect in the model; coupling between the on-surface and in-flight parts of the motion almost certainly occurs. It may also be a real effect not shown by the experimental results which do not include values of α less than 0.19. Some evidence of high axial Peclet numbers at low coefficients of restitution in a related system is to be found in the numerical experiments reported in Chapter 5.

The second model can be subjected to more stringent tests. Equation 3.63 is compared with the experimental data in figure 3.9. If the coefficient of restitution were equal to 1, the particle would not lose any energy on collision and the percolation velocity would be zero. This is correctly predicted by the theoretical curve. The experimental points are on average about 15-20% above the values predicted by the theory. This may in part be due to inadequate determination of the coefficients of restitution, though the agreement is good considering the assumptions made in the model. Thus if λ were $0.69\ (d_b-d_p)$, the predicted values would be 15% greater.

Both approaches to spontaneous percolation presented here

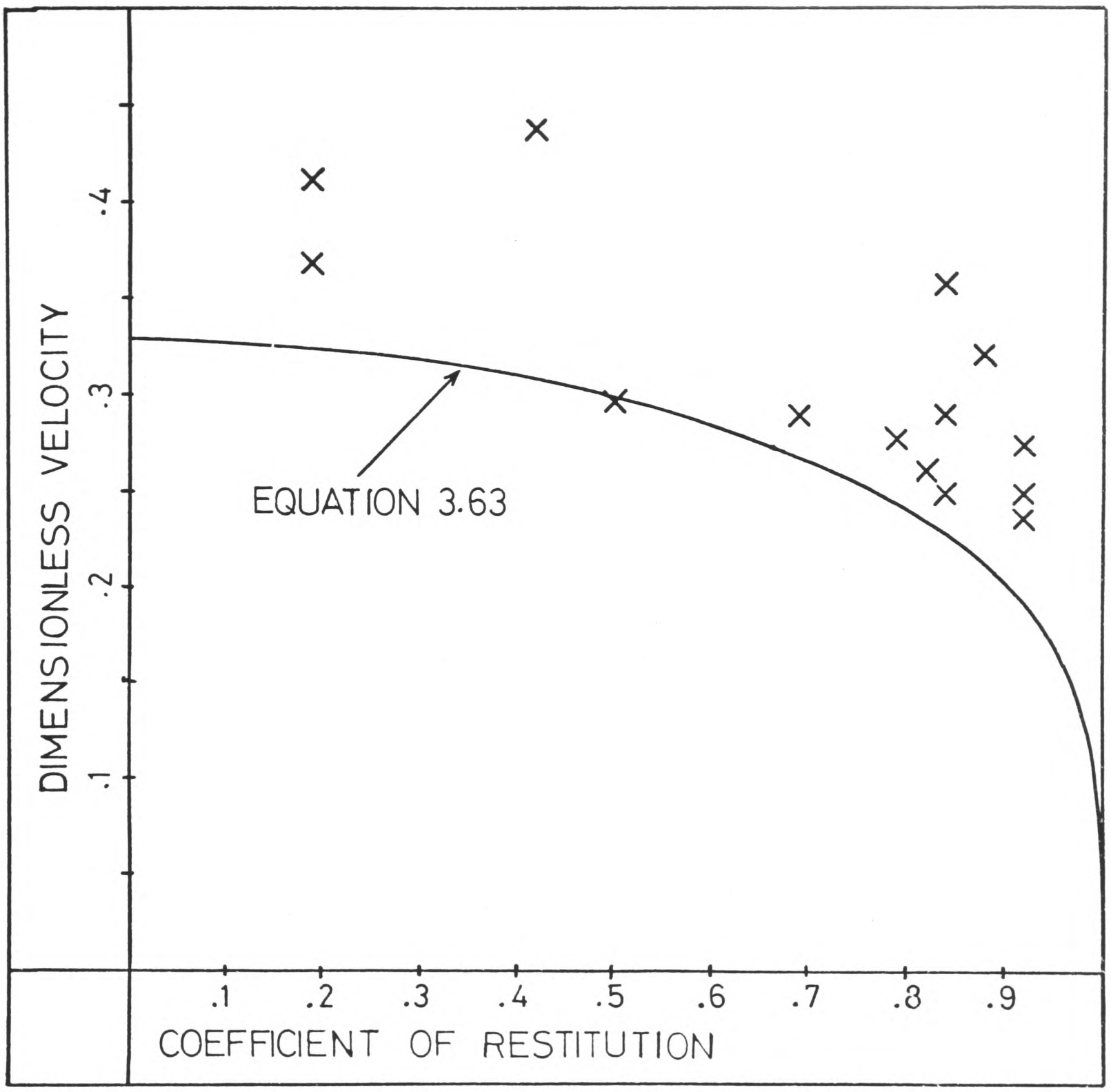


Figure 3.9 Relationship between dimensionless velocity $u/\sqrt{g(d_b-d_p)}$ and coefficient of restitution α.

× Experimental results of Bridgwater and others (1969a, 1971).

have therefore predicted values which agree well with the experimental data and show how understanding of the phenomenon may be gained.

CHAPTER 4

NEW MIXERS

4.1 Introduction

It has been noted that the mixing of cohesionless materials, especially those with very different properties, is more difficult than might at first be supposed. A random mixture is rarely achieved, and the mixture quality can easily deteriorate during discharge of the mixer and subsequent handling of the material. Thus there is, in some situations, a need for an in-line mixer which can produce mixtures of such materials close to where they are required. An idea for a new design of mixer, which it was hoped would be applicable in such circumstances, arose from the preceding work on spontaneous percolation.

Since the lateral distribution produced by percolation through a randomly packed bed of spherical particles satisfies the diffusion equation, a uniform rain of material should be produced if the bed were high enough, and if wall effects such as channelling near the sides of the container were absent. The rate of lateral movement, which has been characterized by a Peclet number, has been shown (Bridgwater et al., 1969a) to be a function of the coefficient of restitution between percolating and bulk particles. Experiments have shown that less dispersion occurs with materials with low coefficients of restitution, the lowest and highest Peclet numbers recorded differing by a factor of two. Even though different materials would be expected to disperse at different rates a uniform distribution should be obtained from a sufficiently high bed.

A packed bed is not very practicable for prolonged industrial

operation as there is a risk of blockage, and hence it was decided to examine the feasibility of a mixer which uses layers of horizontally mounted angle strip. Tubes were not used because of the possibility of hold-up of material on top of them, a potential drawback if food or biochemical materials were being used. Whilst the cost of a unit is never likely to be great, 90^{o}-angle strip is particularly inexpensive and easy to purchase or fabricate.

Two prototype units were built, each with one size of disperser bar. In practice there should be no difficulty in first producing a coarse dispersion with large bars and then progressively refining it with layers of smaller bars. The bar size would depend to a certain extent on the level of scrutiny at which the mixture was required to be well-mixed. One mixer is hereafter termed a three-dimensional mixer in that it is of square cross-section and particles falling through it move in two lateral directions. The other is called a two-dimensional mixer and allows particles to move in one horizontal direction only.

The vertical spacing of the bars in the mixers was decided more or less arbitrarily, though some trials were performed with a small disperser of variable geometry. The three-dimensional mixer was designed to be of commercial size and to handle a throughput of about 5 ton hr^{-1} (1.4 kg s^{-1}). The two-dimensional mixer was considerably smaller and more suitable for laboratory trials.

The aim of the investigation was to ascertain whether the geometry chosen was adequate, to determine the range of materials for which such mixers or distributors are suited and to evaluate the mixture quality produced.

4.2 Design

The three-dimensional mixer was constructed first. No obvious design method presented itself but the following approach offered some guidance.

An estimate of the vertical particle velocity in the system was found from the work of Masliyah and Bridgwater (1974) who, in their simulation of spontaneous percolation, found that $u/\sqrt{gb}$ is about 0.25 where b is the centre to centre sphere spacing. This value, which was used in the design, was for a coefficient of restitution of 0.8 and was relatively insensitive to changes in the voidage. A typical particle diameter was taken as about 2mm and the gap between pieces of angle about ten times this to prevent blocking should the flow be channelled abnormally. Thus gaps were about 2 cm wide and a bar width about twice this used. Hence if b is taken as the horizontal bar spacing in this system, b = 6 cm and as $u/\sqrt{gb} = 0.25$, the velocity u is about 0.2 ms^{-1}.

For a material density of 1,500 $kg.m.^{-3}$, the number of particles passing through a horizontal section per second $n_p = 1.4/((4\pi/3) \times 10^{-9} \times 1500) = 2.2 \times 10^5\ s^{-1}$. n_p also equals $(1-\varepsilon)Au/V_p$ where $(1-\varepsilon)$ is the volume fraction of solids, A is the cross-sectional area of the mixer and V_p the volume of a single particle. Hence $(1-\varepsilon)A = 4.6 \times 10^{-3}\ m^2$. The free area between the bars is approximately A/3. Particles must have sufficient room to bounce about between bars and thus it was decided that the voidage should be about 0.9 between the bars so as to prevent too much inter-particle interference. Then $(1-\varepsilon)$ is 0.033, A is 0.14 m^2, and 0.4 m was chosen as the length of one side of the mixer. This method is approximate though was later partly justified by a computer simulation of the mixer (Chapter 5).

The three-dimensional mixer is shown in figures 4.1-4.3.

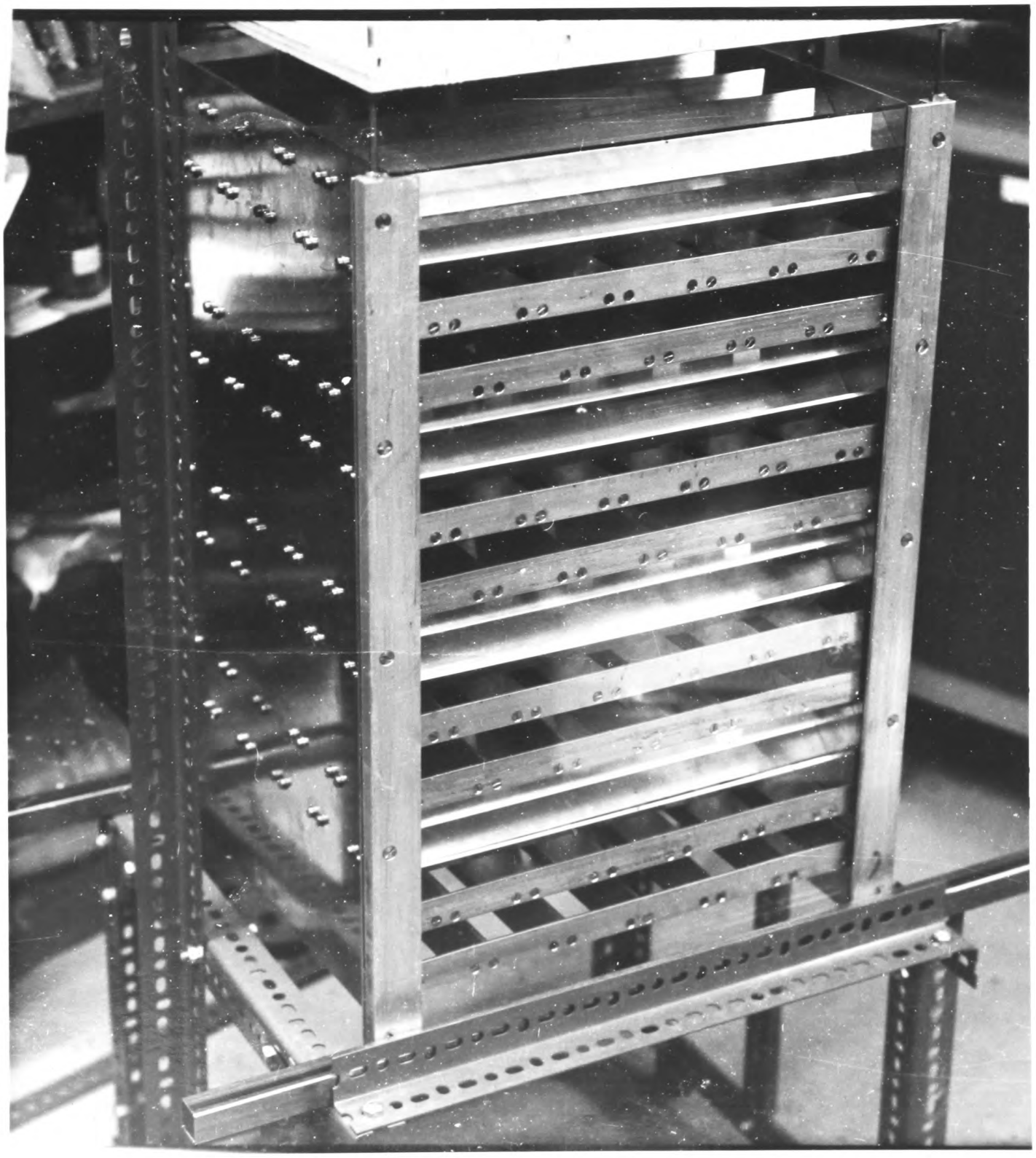


Figure 4.1: Three-dimensional mixer. Original form with two glass sides.

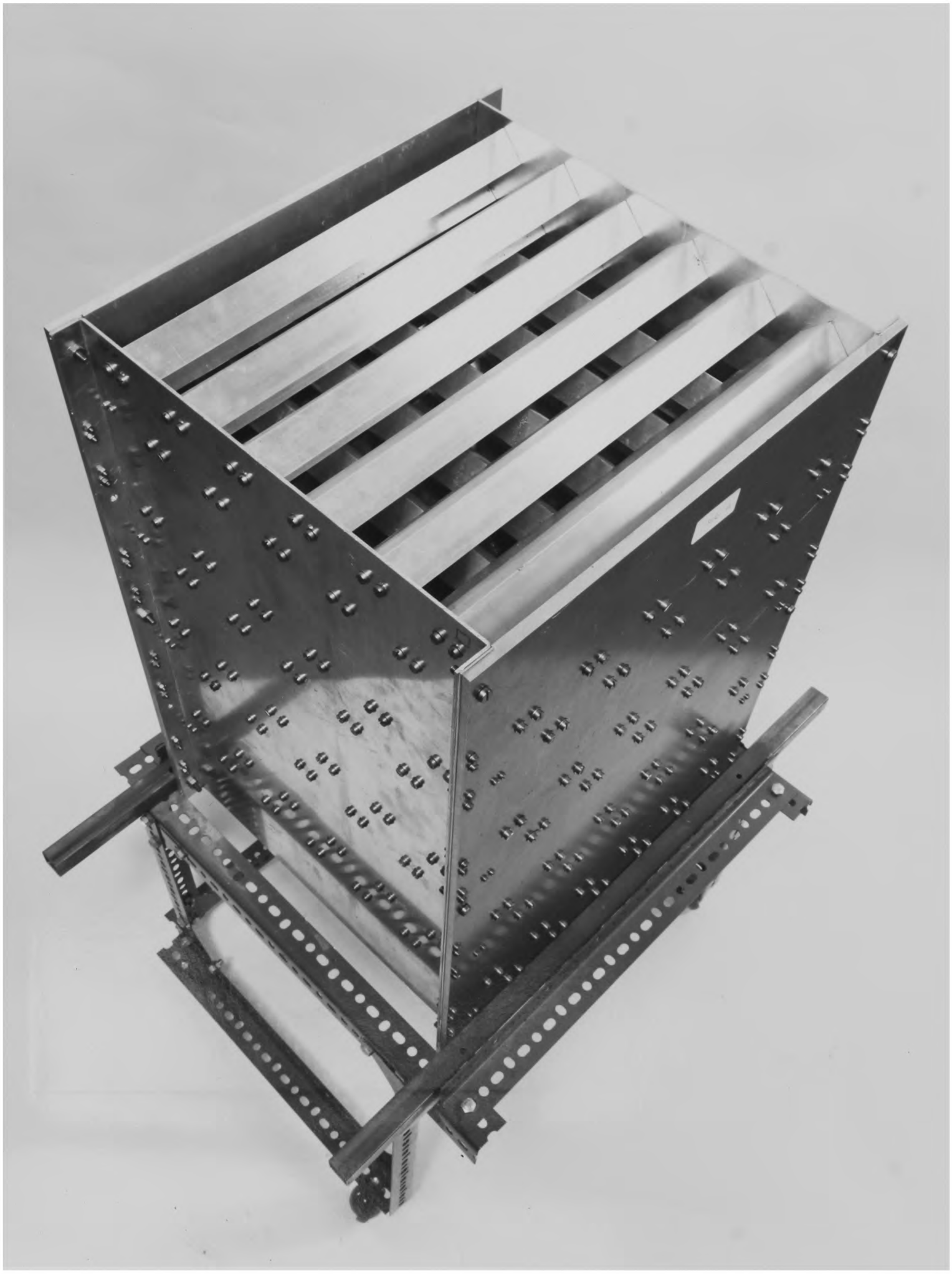


Figure 4.2: Three-dimensional mixer. Final form with four dural sides.

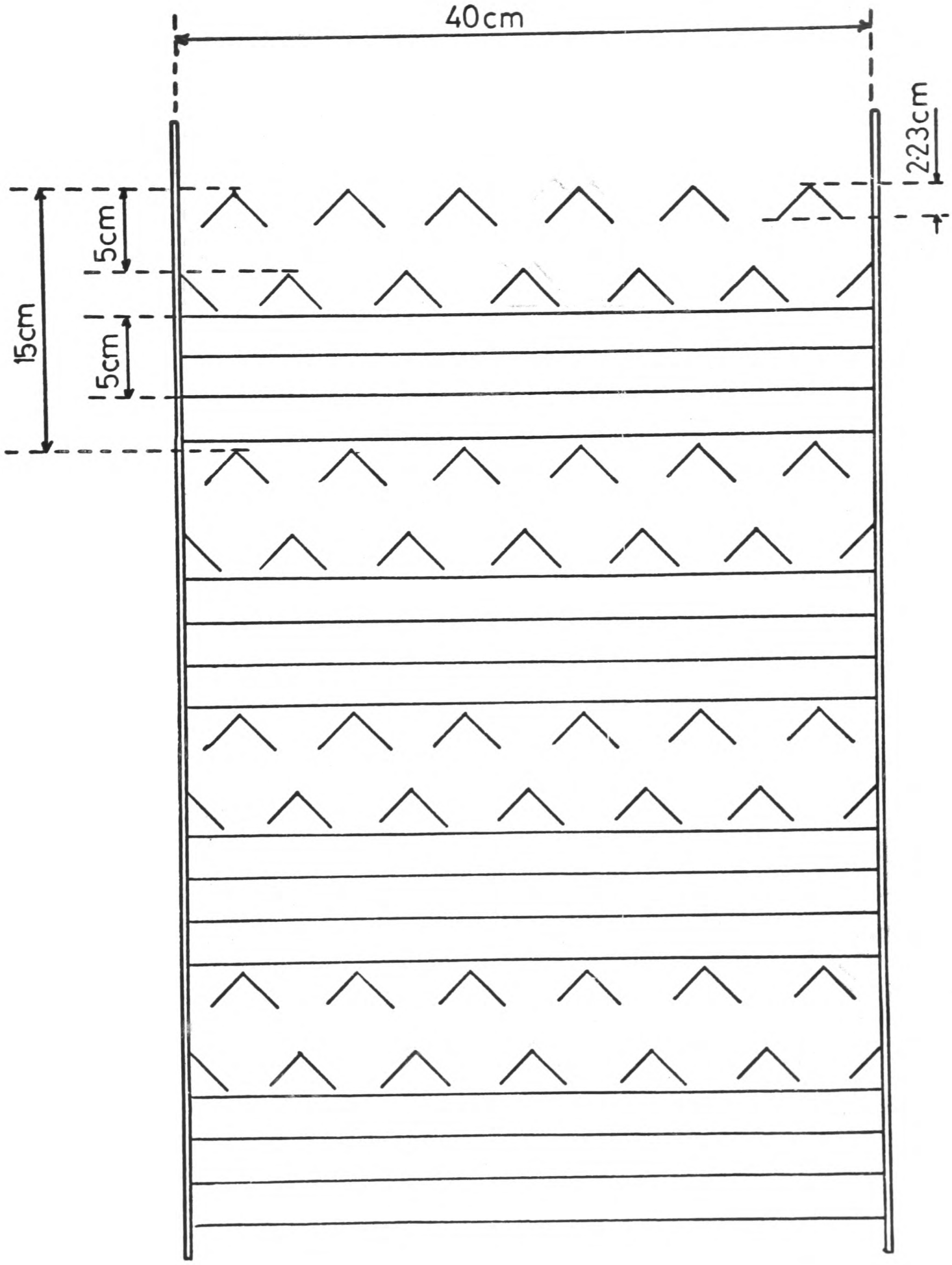


Figure 4.3: Three-dimensional mixer. Dimensioned sketch.

The original construction was from dural with two glass sides opposite each other so that flow patterns could be observed (figure 4.1). However experiments showed that the glass and metal walls produced different effects and the glass sides were later replaced with dural ones (figure 4.2). The mixer was fitted with sixteen rows of disperser bars made from 40 cm lengths of 1¼" angle fixed in pairs at right angles to each other (figure 4.3). For the purpose of evaluating the mixer, material was fed from a small hopper fitted with a valve which allowed the flow rate to be controlled. The hopper output pipe had a circular cross-section and fitted into a sheet of wood on top of the mixer. Holes were drilled in the wood in different places, allowing the use of different feed positions. A sample tray divided into 400 divisions, each 2 cm by 2 cm (figure 4.4) could be placed at different positions below the mixer to collect material. In each experiment a small amount of material was passed through the mixer and the numbers of particles in each division of the sample tray counted. Later provision was made for insertion of a wire mesh below the mixer to determine whether this would improve the mixing action.

The two-dimensional mixer was constructed from perspex so that particle motion inside the mixer could be followed. The sides were 20 cm long and were held 2 cm apart (figure 4.5). The bars, which were made of dural, were half the size of those in the larger mixer, 2 cm in length and were stuck in place. The vertical spacing was slightly different as it was no longer constrained by the need to fit bars in orthogonal directions. The layout is shown in figure 4.6. Methods of feeding material to the mixer and collecting samples were similar to those used with the large mixer. The sample tray had 20 divisions each 1 cm by 2 cm.

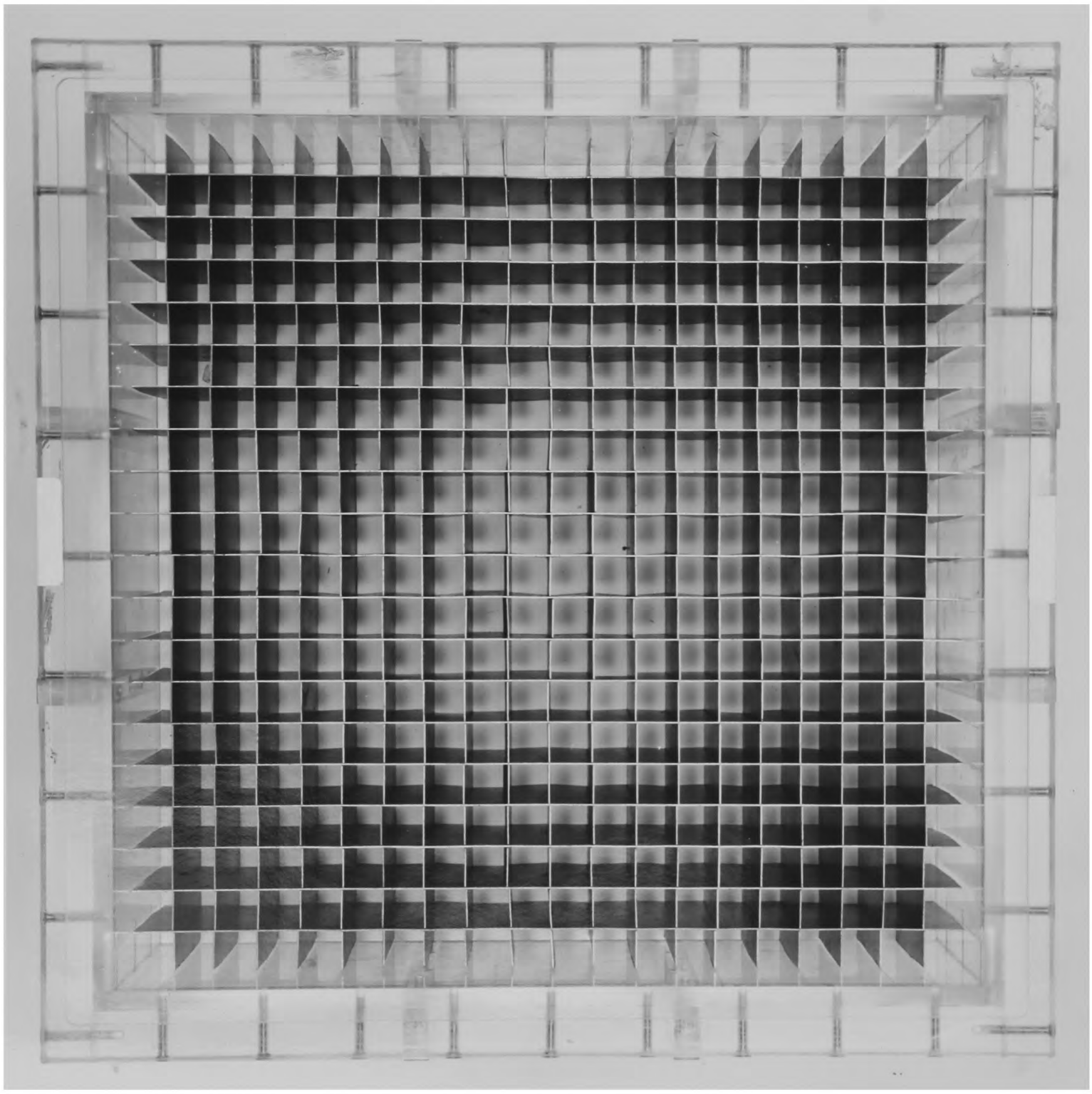


Figure 4.4: Three-dimensional mixer. Sample tray and collection box.

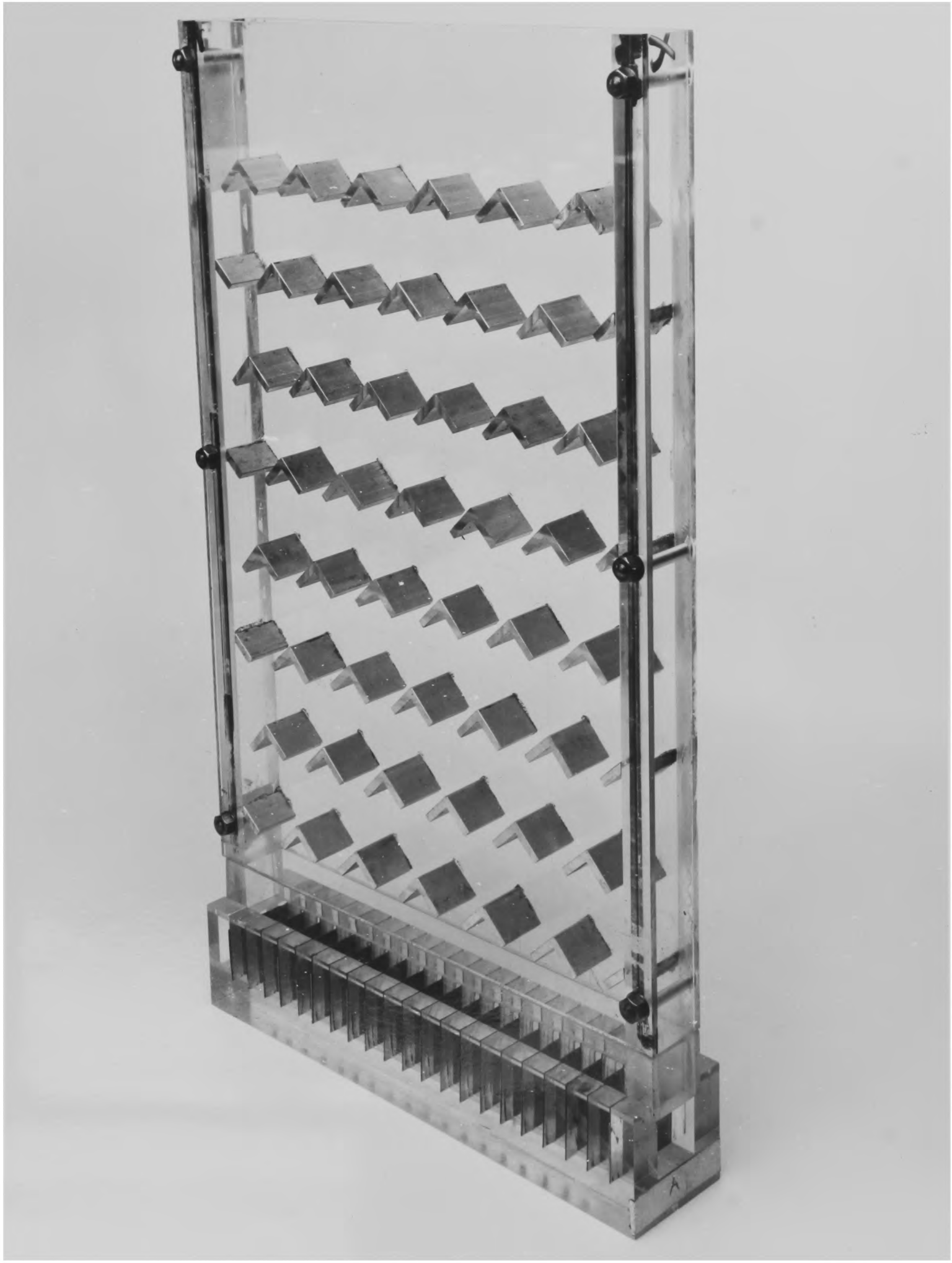


Figure 4.5: Two-dimensional mixer, 2.3cm insert and sample tray.

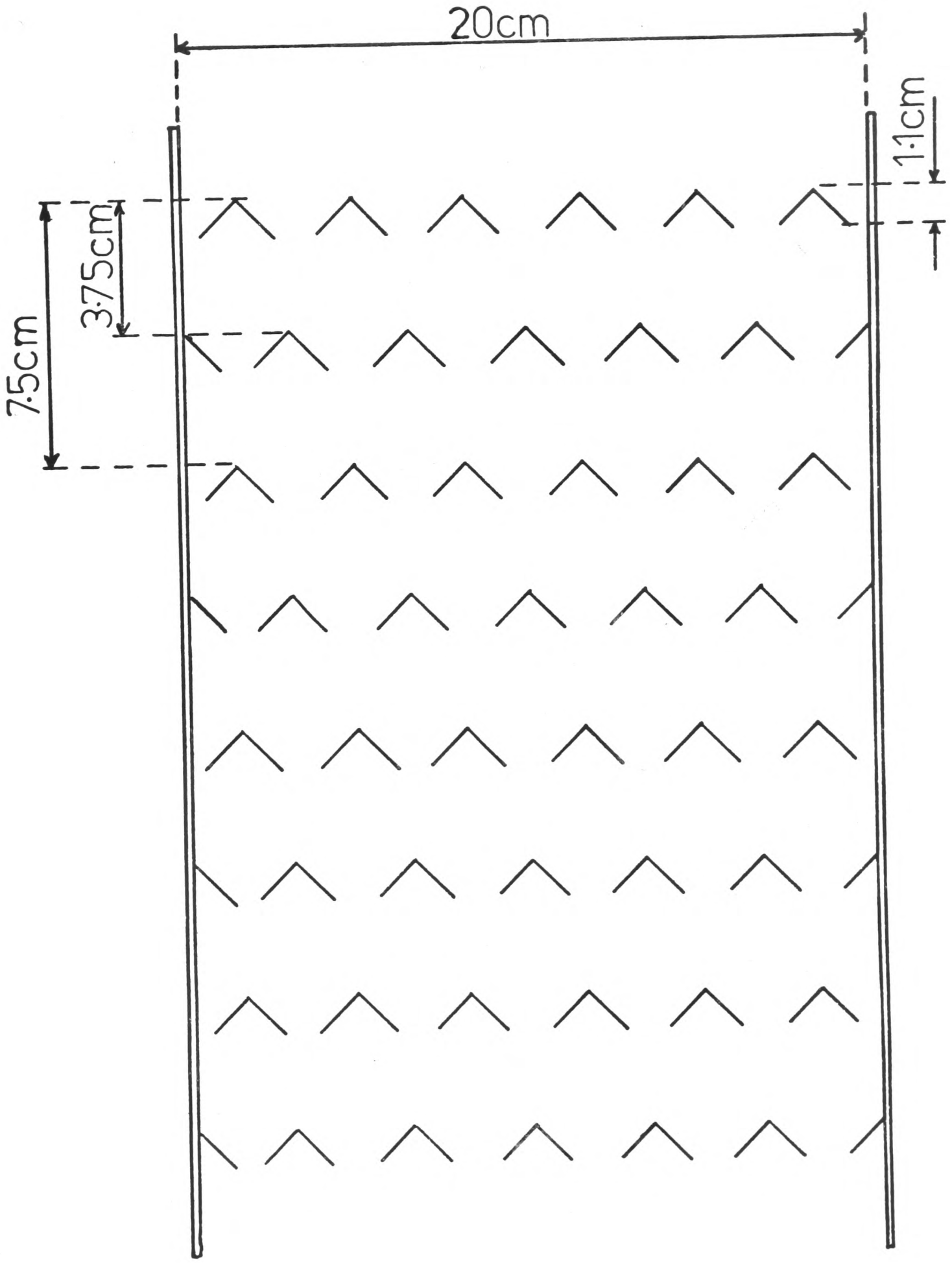


Figure 4.6: Two-dimensional mixer. Dimensioned sketch.

4.3 Theoretical background

4.3.1 Introduction

Many different indices have been used to evaluate the performance of mixers (Fan et al., 1970). Some statistical measure of the performance of the equipment had to be selected before extensive quantitative experiments were begun. Though the equipment was designed to mix different materials together, it was considered that it would be better to test the distributions produced by feeding one material at a time. There would then be no problems in the analysis due to variations in the numbers of particles in each sample (Clements, 1969). Instead these variations would be the basis for testing mixer performance. If it could then be shown that the simultaneous feeding of two materials did not affect the distributions, this would allow accumulation of data on the behaviour of individual materials rather than on particular mixtures.

4.3.2 Performance tests

The first test that could be applied is one in which it is assumed that the distributions produced when a single material is fed to the mixer are of a certain type and checking whether this is so. Tests for randomness are conducted in this manner. Since the best that could be expected from equipment of this type is a random distribution, this was considered first.

Two tests were applied to determine whether or not distributions were random. The simplest and easiest is the 'F' test, a comparison of the variance of the distribution with that of a random distribution. The variance of the distribution σ^2 is defined as $\sum_i (x_i-\bar{x})^2$ where x_i is the number of particles in

division i and $\bar{x}$ is the mean number of particles in a division. If N particles are dropped through the mixer, the probability $p(x_t)$ that x_t of them will fall into any one division of the sample tray, if the process were random, is given by

$$p(x_t) = \frac{N!}{(N-x_t)!x_t!} \left(\frac{1}{D_s}\right)^{x_t} \left(1 - \frac{1}{D_s}\right)^{N-x_t} \qquad (4.1)$$

where D_s is the number of divisions in the sample tray. This is a binomial distribution with mean N/D_s and variance $N(1-1/D_s)/D_s$ (see, for example, Belz, 1973). The ratio $\sigma^2/\{N(1-1/D_s)/D_s\}$ is then a measure of the randomness of the distribution. Statistical 'F' tables give the confidence limits for accepting or rejecting the hypothesis that the distribution is random as a function of the number of degrees of freedom, (D_s-1) in this case. A value of F equal to one indicates a random distribution.

A second, more rigorous approach, is the use of the χ^2-test which compares one distribution with another. In its application here, the actual distribution is tested against the binomial distribution. The value of χ^2 is given by $\sum \frac{(O-E)^2}{E}$ where O is the frequency of observation of a given number of particles in one sample tray division and E is the expected frequency. χ^2 tables give the probability that the distribution is random as a function of the number of degrees of freedom, which is equal to the number of categories compared less three, since the total frequencies, the variances and the means of the two distributions are made equal. When applying the test, the class frequency should exceed four and when classes containing less than five observations occur, they are combined (Guttman and Wilkes, 1965). More than about thirty-five observations are necessary to apply the test (Harnby, 1972), more than are provided by the two-dimensional mixer.

If it is found that a distribution is not random, other

methods of assessment can be applied. One method that has recently found favour (Kristensen, 1976) is the calculation of a correlation coefficient between different pairs of samples. This method allows for the dependence of the composition of a sample on the compositions of the samples near it. The concept was investigated, but after considering the physical significance of the approach, it was decided not to apply it in this case. The method should be employed if the probability that a given value of x_t will occur in any division i is materially affected by the values of x_t in neighbouring divisions, especially i-1, i+1. There was no evidence to suggest that the distributions under investigation were of this type; the approach using correlation is considered in Chapter 6.

Another type of distribution is one which is ordered, where the probability of finding a given value of x_t in any sample is a function of the sample position. Williams (1970) applied this concept to a mixture and a similar approach can be used when considering distributions.

Allow N particles to pass through the mixer. Let the probability that a particle will fall into division i of the D_s divisions of the sample tray be P_i $(1<i<D_s)$. The probability $P_{i,M}$ that division i will contain M particles is

$$P_{i,M} = \binom{N}{M} P_i^M (1-P_i)^{N-M} \qquad (4.2)$$

Let the mean number of particles in a division be $\bar{M}$ $(= N/D_s)$. In division i, M may take any value between 0 and N. All of these contribute to the square of deviations from the mean δ_x^2, which is then given by:

$$\delta_x^2 = \sum_{M=0}^{N} P_{i,M} (M-\bar{M})^2$$

Substituting from equation 4.2,

$$\delta_x^2 = \sum_{M=0}^{N} \binom{N}{M} P_i^M (1-P_i)^{N-M} (M-\bar{M})^2 \qquad (4.3)$$

Now,

$$\delta_x^2 = \sum_{M=0}^{N} \binom{N}{M} P_i^M (1-P_i)^{N-M} M^2 - 2 \sum_{M=0}^{N} \binom{N}{M} P_i^M (1-P_i)^{N-M} M\bar{M}$$

$$+ \sum_{M=0}^{N} \binom{N}{M} P_i^M (1-P_i)^{N-M} \bar{M}^2 \qquad (4.4)$$

The summation in the third term of this equation equals $\bar{M}^2$. Then

$$\delta_x^2 = \sum_{M=0}^{N} \frac{N!}{(N-M)!M!} P_i^M (1-P_i)^{N-M} M\{(M-1)+1\}$$

$$-2\bar{M} \sum_{M=0}^{N} \frac{N!}{(N-M)!M!} P_i^M (1-P_i)^{N-M} M + \bar{M}^2$$

Rearranging,

$$\delta_x^2 = N(N-1) P_i^2 \sum_{M=2}^{N} \frac{(N-2)!}{(N-M)!(M-2)!} P_i^{M-2} (1-P_i)^{N-M}$$

$$+ NP_i \sum_{M=1}^{N} \frac{(N-1)!}{(N-M)!(M-1)!} P_i^{M-1} (1-P_i)^{N-M}$$

$$- 2\bar{M} NP_i \sum_{M=1}^{N} \frac{(N-1)!}{(N-M)!(M-1)!} P_i^{M-1} (1-P_i)^{N-M} + \bar{M}^2$$

In this form it can be seen that the summations are equal to one.

Hence

$$\delta_x^2 = N(N-1)P_i^2 + NP_i - 2\bar{M} NP_i + \bar{M}^2 \qquad (4.5)$$

or since $\bar{M} = N/D_s$,

$$\delta_x^2 = N^2(P_i - 1/D_s)^2 + NP_i(1 - P_i) \qquad (4.6)$$

The variance of the contents of the divisions σ^2 is therefore

$$\frac{1}{D_s} \sum_{i=1}^{D_s} \left[N^2(P_i - 1/D_s)^2 + NP_i(1-P_i) \right]$$

Let $\sigma^2 = L_1N^2 + L_2N$ where $L_1 = \left[\sum_{i=1}^{D_s} (P_i - 1/D_s)^2 \right]/D_s$ and $L_2 = \left[\sum_{i=1}^{D_s} P_i(1-P_i) \right]/D_s$. If only one particle were passed through the mixer, N = 1 and

$$L_1 + L_2 = \frac{1}{D_s} \sum_{i=1}^{D_s} (1/D_s^2 - 2P_i/D_s + P_i)$$

$$= \frac{1}{D_s} (1 - \frac{1}{D_s})$$

Defining this as σ_s^2

$$\sigma^2 = L_1N^2 + (\sigma_s^2 - L_1)N \qquad (4.7)$$

The variance of a binomial distribution σ_R^2 equals $N\sigma_s^2$ and hence

$$\frac{\sigma^2}{\sigma_R^2} = \frac{L_1N}{\sigma_s^2} + \frac{\sigma_s^2 - L_1}{\sigma_s^2}$$

$$= 1 + \frac{L_1}{\sigma_s^2} (N-1) \qquad (4.8)$$

This is true whatever the values of P_i. The index used here is $Q = 1 - L_1/\sigma_s^2$, since for a random distribution where $L_1 = 0$, $Q = 1$ and for a totally segregated distribution $L_1 = \sigma_s^2$ and $Q = 0$.

4.3.3 Application of theory

The action of the mixer depends upon the instability in the distributive mechanism and so a very small difference in particle position at the top of the mixer leads to a large difference at the bottom. Thus experiments which involve relatively few particles need to be repeated to obtain a mean value of the variance. Owing to the time necessary to accumulate large quantities of information with the three-dimensional mixer, most of the experiments were done with the two-dimensional mixer.

Values of σ^2/σ_R^2 were calculated for each experiment. Most of the values from the three-dimensional mixer were in the range 1-2. Experiment 6 in Table 4.1 gave the lowest value, namely 1.07. Statistical 'F' tables show that this does not prevent the distribution from being random and it was examined with the χ^2-test. The observed and binomial distributions are compared in Figure 4.7. The value of χ^2 was calculated and it was deduced that the probability that the distributions were the same was 0.08. Since, in this, the most favourable experiment, the probability that the distribution was random was so low, it was decided that other methods of testing the distributions should be used.

Some correlation coefficients were calculated at this point but the approach was subsequently abandoned as described previously.

The theory of the latter part of section 4.3.2 was then applied by testing equation 4.8. Twelve experiments were performed (Table 4.2) with each of 50, 100, 200 and 400 particles of one material (3/32" dia. steel balls) and the mean value of σ^2/σ_R^2 for each group plotted against N in Figure 4.8. This gave a straight line indicating that equation 4.8 applies and that the distributions could be satisfactorily characterized by the index Q. This index was therefore used throughout.

4.4 Three-dimensional mixer experiments

The results of the sixteen quantitative experiments done are shown in Table 4.1. Details of the materials used are in Table 4.3. The number of particles in each division of the sample tray was counted with the aid of a torch. Difficulty was encountered if there were too many particles in a division and this limited the number of particles that could be used in an

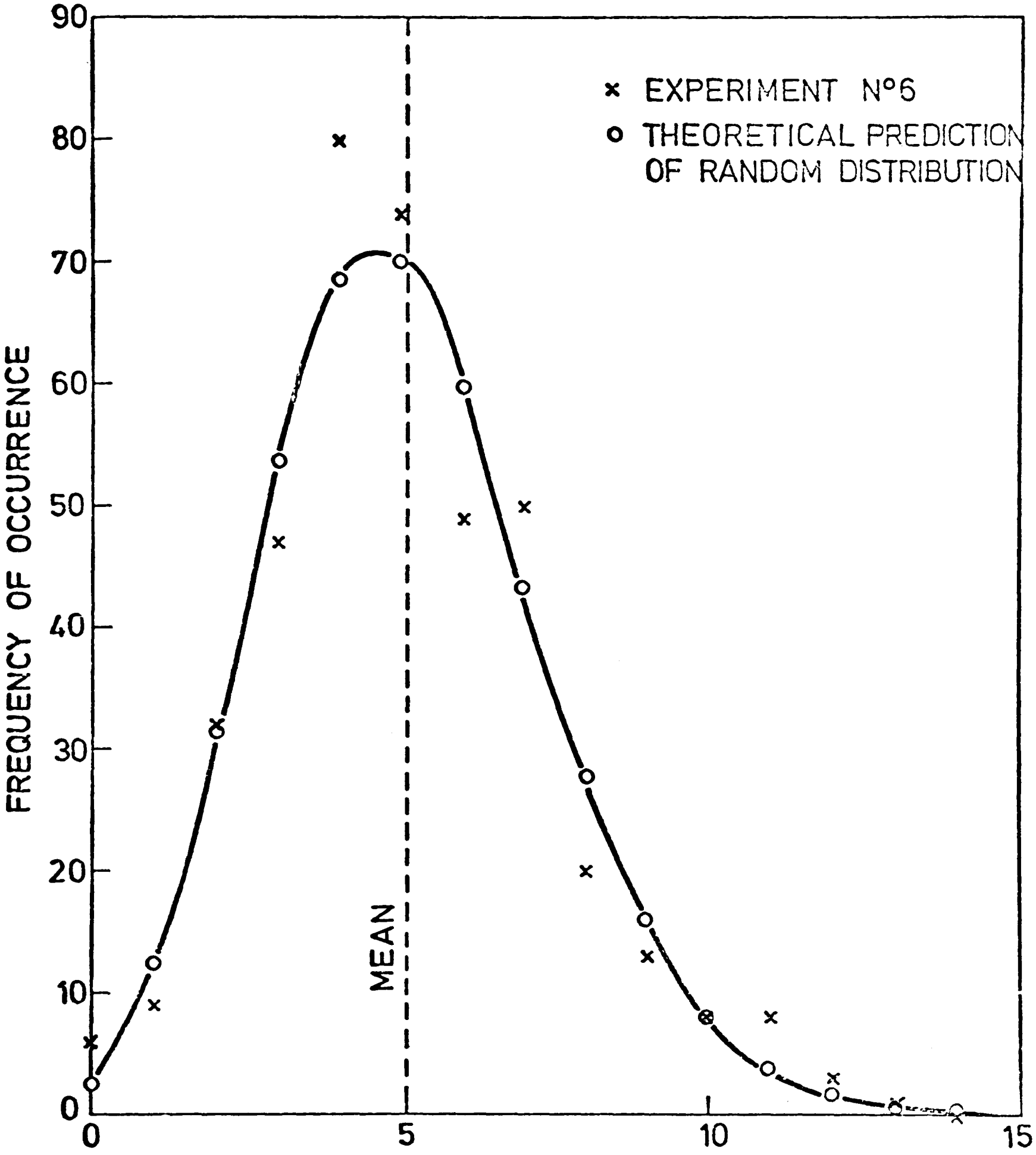


FIGURE 4.7

THREE-DIMENSIONAL MIXER-

EXPERIMENT N° 6 - OBSERVED AND BINOMIAL FREQUENCY DISTRIBUTIONS.

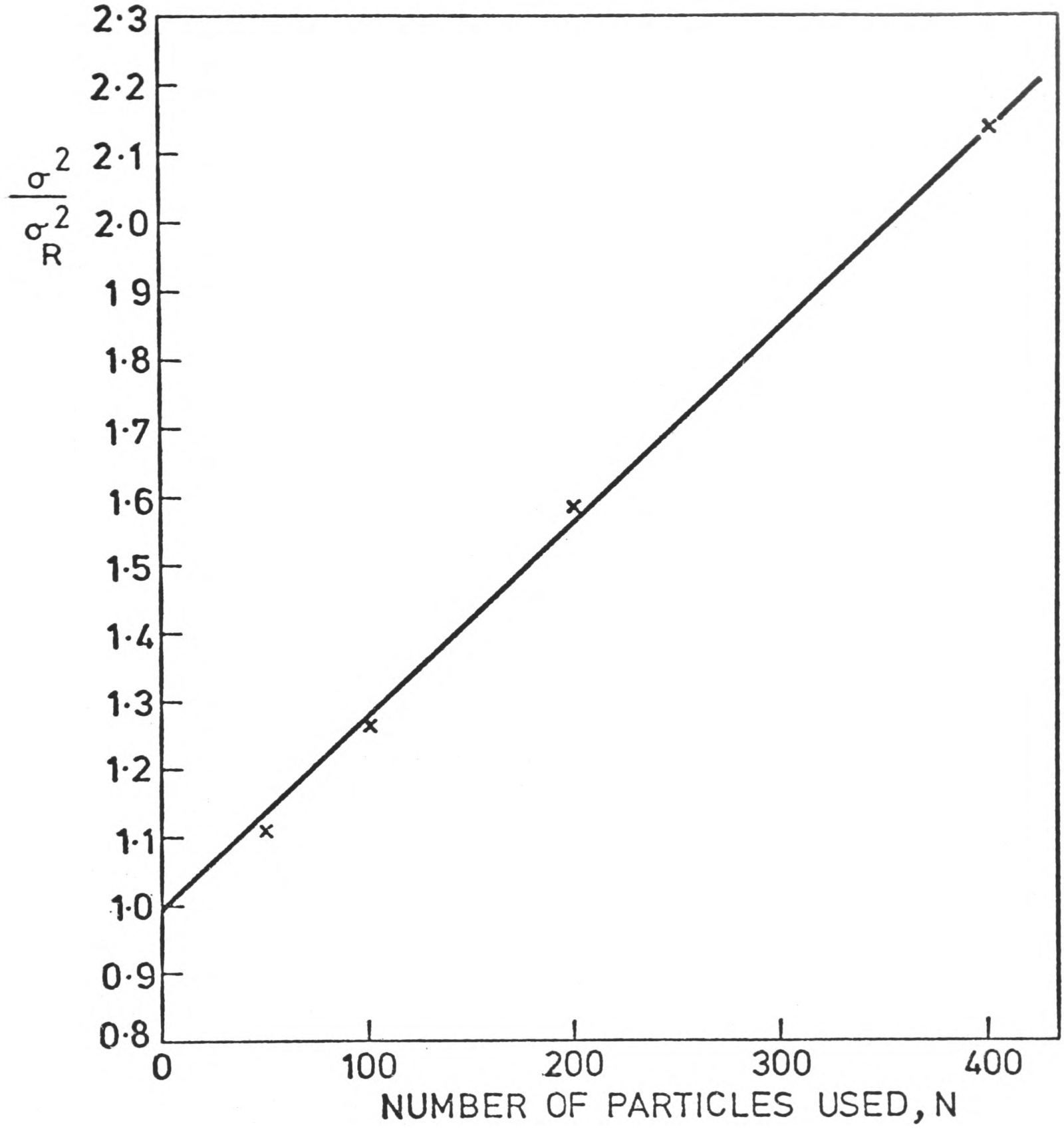


Figure 4.8: Two-dimensional mixer. σ^2/σ_R^2 vs. number of particles used. Data from Table 4.2.

Table 4.1: Three-dimensional mixer experiments

Experiment Number	Material	Sample Tray Position*	Feed Point Position	Number of Particles Used	$\frac{\sigma^2}{\sigma_R^2}$	Q
1	3.5mm dia. ballotini	1	1	3342	1.91	0.99973
2	2mm dia. lead shot	1	1	4024	4.42	0.99915
3	Barley	1	1	2440	1.55	0.99977
4	3.5mm dia. ballotini	4	1	3127	1.49	0.99984
5	2mm dia. lead shot	4	1	4023	3.29	0.99943
6	1mm dia. ballotini	4	1	2042	1.07	0.99997
7	2mm dia. ballotini	4	1	2926	1.18	0.99994
8	3.5mm dia. ballotini	3	1	3088	1.46	0.99985
9	2mm dia. ballotini	4	1	3088	1.43	0.99986
10	2mm dia. ballotini	4	3	2966	1.26	0.99991
11	2mm dia. ballotini	4	1	2943	1.21	0.99993
12	2mm dia. ballotini	4	2	2967	1.30	0.99990
13	3/32" dia. steel balls	2**	1	4263	1.45	0.99990
14	3/32" dia. steel balls	2	1	3836	1.59	0.99985
15	2mm dia. lead shot	2**	1	3975	2.03	0.99974
16	2mm dia. lead shot	2	1	4001	3.16	0.99946

* see Figure 4.9 ** wire mesh ($\frac{1}{4}$" centres, 1/16" thick)

Table 4.2: Two-dimensional mixer. Relationship between σ^2/σ_R^2 and number of particles

Material	Feedpoint (distance from edge of mixer) (cm)	Height of insert between mixer & sample tray (cm)	Number of experiments	Number of particles in each experiment	Mean value of σ^2/σ_R^2	Q
3/32" dia. steel balls	10.00	2.3	12	50	1.11	0.9978 ± 0.0012
"	10.00	2.3	12	100	1.27	0.9973 ± 0.0011
"	10.00	2.3	12	200	1.58	0.9971 ± 0.0006
"	10.00	2.3	12	400	2.14	0.9971 ± 0.0004

Table 4.3: Properties of materials

Material	Nominal Diameter	Mean Particle weight (mg)	Mean size (mm) (spherical unless otherwise stated)	Density ($kg\ m^{-3}.10^3$)
Ballotini	0.5mm	0.2	0.50 dia.	2.97
Ballotini	0.75mm	1.0	0.85 dia.	2.97
Ballotini	1.0 mm	1.9	1.06 dia.	2.97
Ballotini	2.0 mm	13.7	2.06 dia.	2.97
Ballotini	3.5 mm	69.7	3.55 dia.	2.97
Precision glass balls	1.5 mm	4.5	1.50 dia.	2.55
Steel balls	1/16 in	16.3	1.59 dia.	7.68
Steel balls	3/32 in	54.8	2.38 dia.	7.68
Steel balls	1/8 in	130.0	3.18 dia.	7.68
Lead shot	2mm	48.1	2.01 dia.	11.37
Acrylic resin	1/8 in	18.4	3.09 dia.	1.19
Polyester chip	-	22.9	Platelets, 1.8 thick	1.33
Celon chip	-	10.5	Cylindrical, 2.2 dia., 2.8 long	1.15
Barley	-	31.6	Typically 2.75 max. dia., 8-12 long	1.18
Mustard seed	-	7.9	2.3 dia.	1.17
Canary seed	-	8.7	Typically 1.5 max. dia., 4 long	1.22
Iron filings	-	-	sieved <0.125μm	7.87

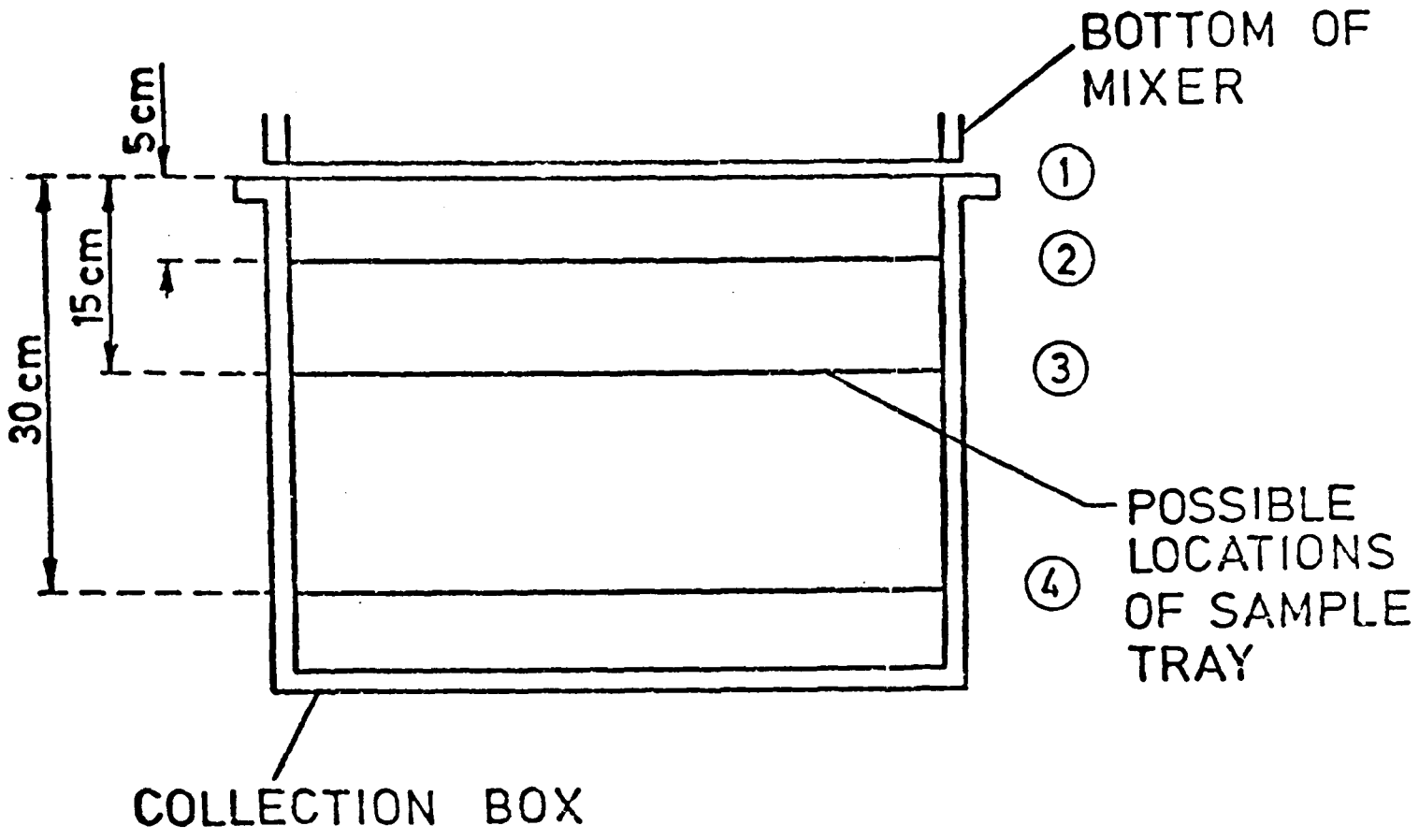
experiment to about 4,000. The following points were considered.

(i) Reproducibility

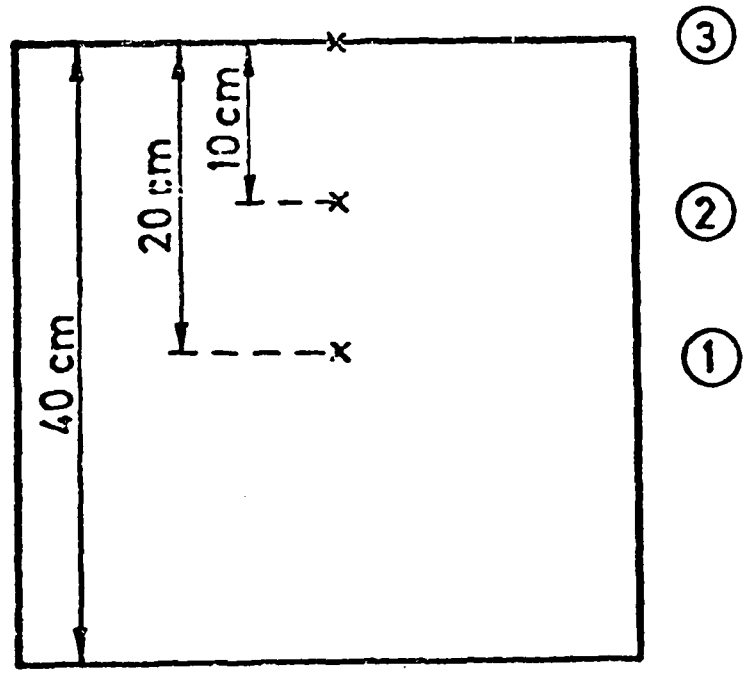
Experiments 7, 9 and 11 were done with the same material under identical conditions. The mean value of Q was 0.99991 with a maximum deviation of 0.00005. This and non-quantitative experiments indicated that approximately the same results were obtained if experiments were repeated.

(ii) Sample tray position

Experiments were done with the sample tray in four different positions. If the tray were too close to the bottom of the mixer (position 1 in Figure 4.9) a shadow pattern was produced by the bottom layer of disperser bars. Conversely if the tray were too far away from the mixer, material accumulated around the edges of the collection box leaving the centre depleted. This was particularly noticeable when using lead shot. The magnitude of these effects was slightly different in each of the orthogonal directions; the former was most marked when caused by the bottom pair of bars. Some quantitative evidence is provided by the experiments with lead shot, numbers 2, 5 and 16. If the samples are divided into three portions by cuts in one direction, the cuts being such as to make the centre portion twice the size of each of the outer portions, then 50% of the particles should be in the centre. In experiment 5, where the sample tray was a long way from the mixer this was only 35% whereas in experiment 16 it was 43%. The presence of a shadow pattern below the bottom pair of bars in experiment 2 can be shown by dividing the sample into 20 line samples, each 20 units long in the direction of these bars. Values of Q based on these 20 samples can then be calculated. For experiment 2 it was 0.987



SAMPLE TRAY POSITIONS



FEED POINT POSITIONS

FIGURE 4.9

THREE-DIMENSIONAL MIXER - FEEDPOINT & SAMPLE TRAY POSITIONS.

whereas for experiment 16 it was 0.996.

(iii) Wire mesh

The effect of inserting a single piece of wire mesh between the mixer and sample tray was investigated in experiments 13 and 15. The distributions produced were better than the controls, numbers 14 and 16, the improvement being greater with lead shot than with steel balls.

(iv) Feed point

Experiments with off-centre feeding were performed with 2mm dia. ballotini. No change in Q resulted, values of 0.99990 and 0.99991 (experiments 10 and 12) being recorded for off-centre feeds, compared with the mean of the controls 0.99991 (experiments 7, 9 and 11).

(v) Granular materials

Only a restricted range of materials was tested in the three-dimensional mixer. In all experiments it was found that the average number of particles in a division was slightly higher nearer the edges of the sample. The materials used gave roughly comparable results with the exception of lead shot which did not produce very good distributions, possibly because of its low coefficient of restitution. A photograph of a typical distribution (polyester chips), with the sample tray removed, is shown in Figure 4.10.

(vi) Fine materials

Some experiments were performed with considerably finer materials - ballotini, sands and iron filings with particle sizes in the range 50-200μm. A photograph of a typical distribution is

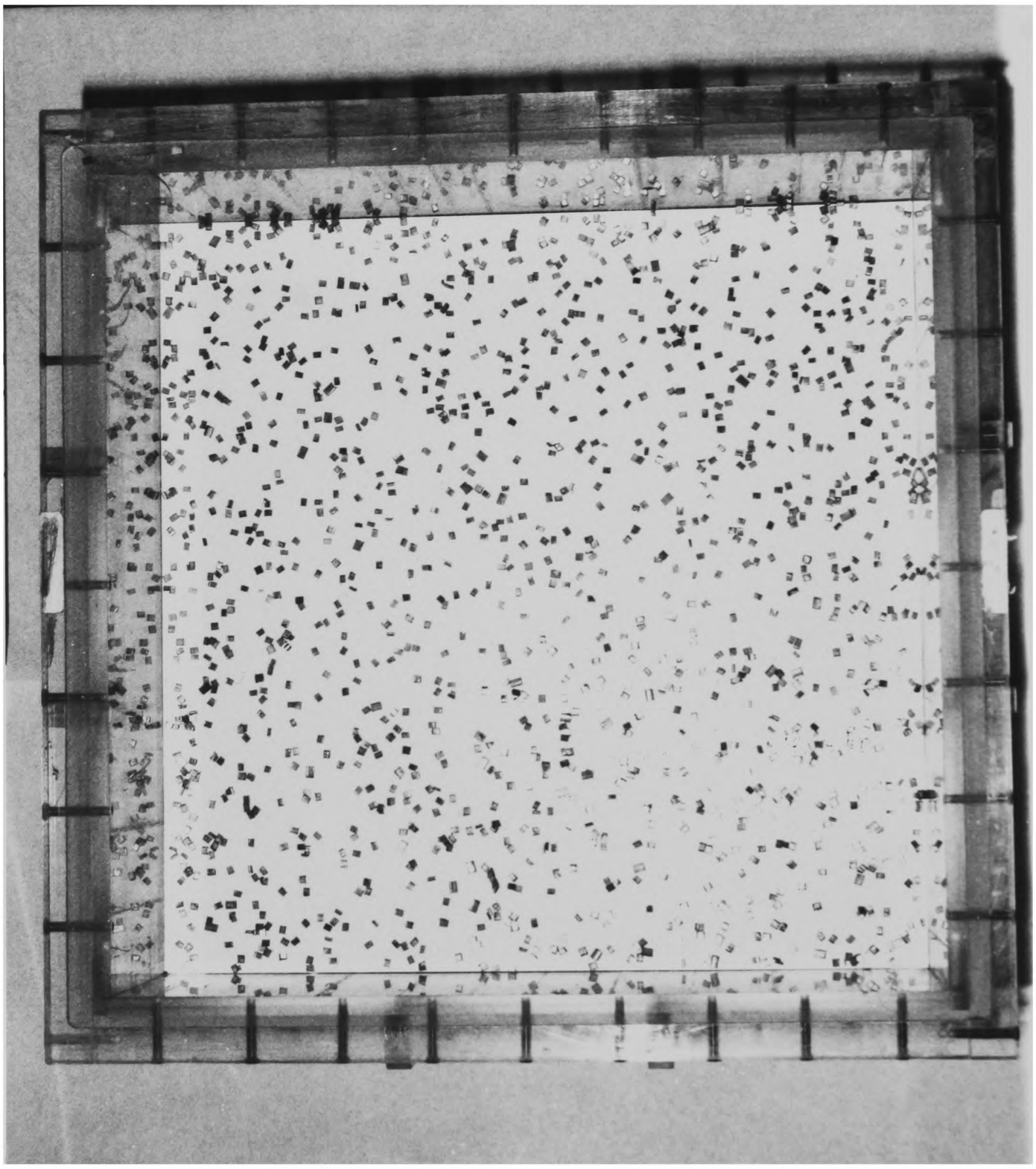


Figure 4.10: Three-dimensional mixer. Typical distribution for a granular material; polyester chips.

shown in Figure 4.11. These materials 'flowed' rather than 'bounced' through the mixer in well-defined streams. This is in agreement with the work of Darton (1976) who found similar results when passing 100μm alumina through an array of rods. He noticed that the dispersion along the rods was random and constructed an array in which successive sets of rods were mounted at an angle of 45° to each other. This apparently produced a good dispersion, though numerical analysis was not attempted.

4.5 Two-dimensional mixer experiments

Results are shown in Tables 4.4-4.8 and details of the materials used are in Table 4.3. The points considered were:

(i) Mixtures

Two series of experiments were performed with different pairs of materials to ascertain whether there was any difference between feeding materials together or separately. The first series was a short one, using mixtures of barley and mustard seed, and steel balls and polyester chip. Two pairs of experiments were done with each mixture; in one of the pair the materials were fed together and in the other they were fed separately. The results (Table 4.4) were inconclusive though it appeared that any difference was small. Subsequently a second series was done involving six experiments with each of three mixtures. These involved steel balls with lead shot, polyester chip or ballotini. The results were compared with those obtained for the materials alone and are tabulated in Table 4.5. In two cases values of Q differ by more than the standard errors. These are the experiments with polyester chip and the last one with steel balls. In both of

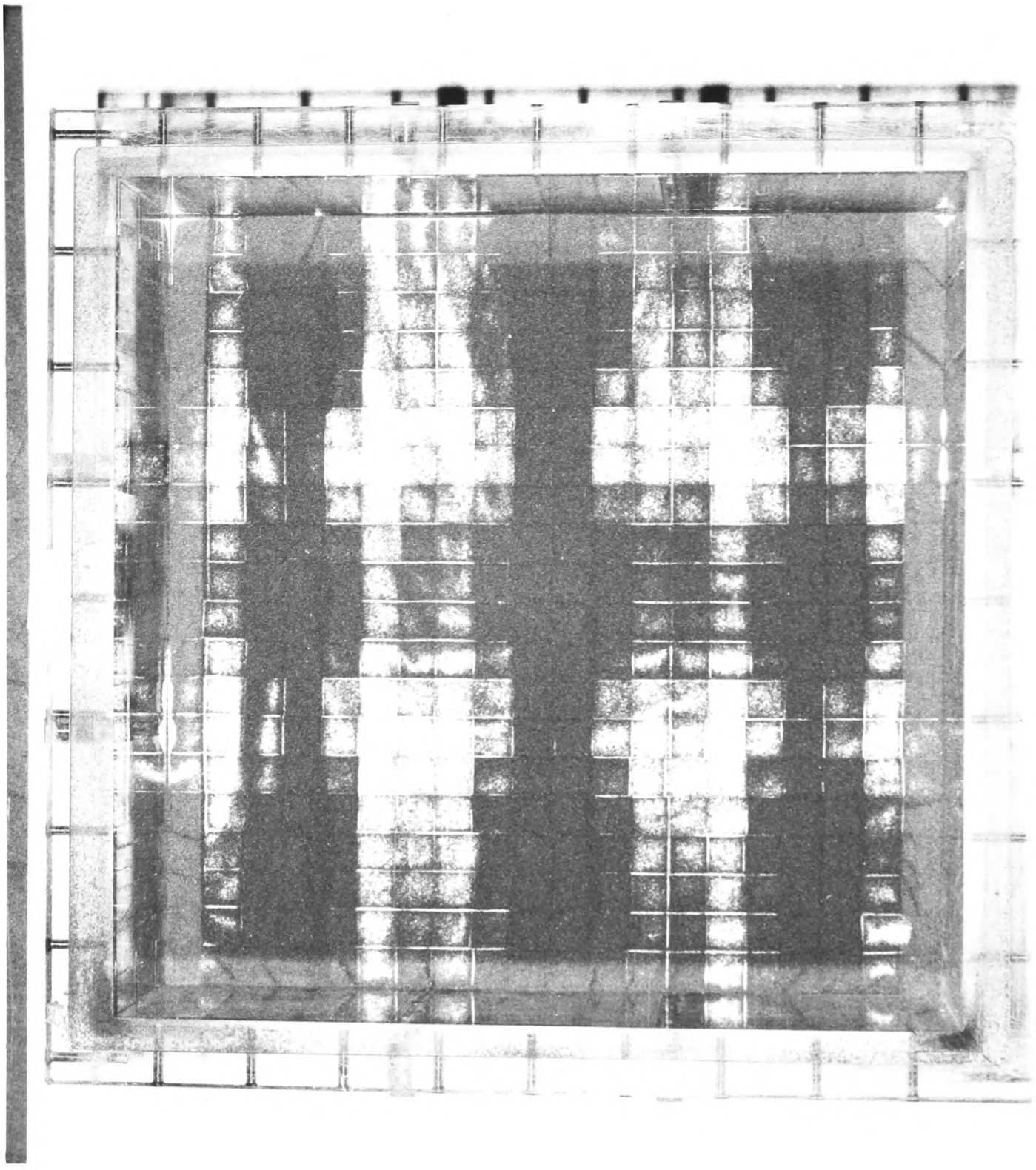


Figure 4.11: Three-dimensional mixer. Typical distribution for a fine material; iron filings.

Table 4.4: Mixtures (i)

	Material	Alone (A) or Mixed (M)	σ^2/σ_R^2	Q
1	Barley	M	1.37	0.9983
	Barley	A	1.11	0.9995
	Mustard seed	M	2.10	0.9976
	Mustard seed	A	1.95	0.9980
2	3/32" dia. steel balls	M	1.97	0.9980
	3/32" dia. steel balls	A	1.26	0.9992
	Polyester chip	M	0.83	1.0011
	Polyester chip	A	1.31	0.9981

Feedpoint: central

Insert: 2.3cm

No. of experiments on which values of Q are based: 2

Table 4.5: Mixtures (ii)

Material	σ^2/σ_R^2 mixture	Q mixture	Standard error x 10^4	Q alone	Standard error x 10^4
3/32" dia. steel balls	1.73	0.9981	8	0.9976	8
2mm dia. lead shot	1.20	0.9994	4	0.9994	3
3/32" dia. steel balls	1.47	0.9988	4	0.9976	8
polyester chip	1.22	0.9992	4	0.9971	10
3/32" dia. steel balls	1.44	0.9989	2	0.9976	8
2mm dia. ballotini	1.66	0.9983	4	0.9987	5

Feedpoint: central

Insert: 2.3 cm

No. of experiments on which values of Q are based: 6

Values of Q for each material alone taken from Table 4.7.

these cases the better dispersion was produced when the material was part of a mixture and thus it appears that there is no deterioration in the quality of the distribution if materials are fed together rather than separately.

(ii) Flowrates

It was impossible to investigate the effect of flowrate on the distributions in the three-dimensional mixer because the quantities of materials available were small. Initially a limited range of experiments was done with the two-dimensional mixer in which the distributions produced were subjectively classified as good, fair or poor (Table 4.6). For flowrates less than some critical value, the effect of a change in flowrate seemed small.

Later an accurate balance became available, and twelve experiments were done in which the time taken for 80g of 2mm dia. ballotini to be fed to the mixer was measured with a stop-watch. The quantity of material in each of the sample tray divisions was weighed and the number of particles in each estimated from the average weight of one particle (Table 4.3). Values of Q were then calculated and are plotted as a function of the flowrate in Figure 4.12, which confirms the initial impressions. For flowrates below about 35g/s Q is constant at about 0.9991, but distributions deteriorate increasingly rapidly with an increase in flowrate above this value. This value is comparable with that obtained from the experiments in which particles were counted, 0.9987 ± 0.0005.

Visual observation indicated that above this critical flow-rate interparticle collisions became numerous and at very high flowrates the behaviour was similar to that of fine particles

Table 4.6: Flowrate experiments

Material	Flowrate (g s^{-1})	Subjective evaluation of distribution
2mm dia. ballotini	< 40	good
2mm dia. ballotini	60	fair
2mm dia. ballotini	110	poor
3/32" dia. steel balls	<110	good
3/32" dia. steel balls	160	fair
3/32" dia. steel balls	330	poor

Feedpoint: central

Insert: 2.3cm

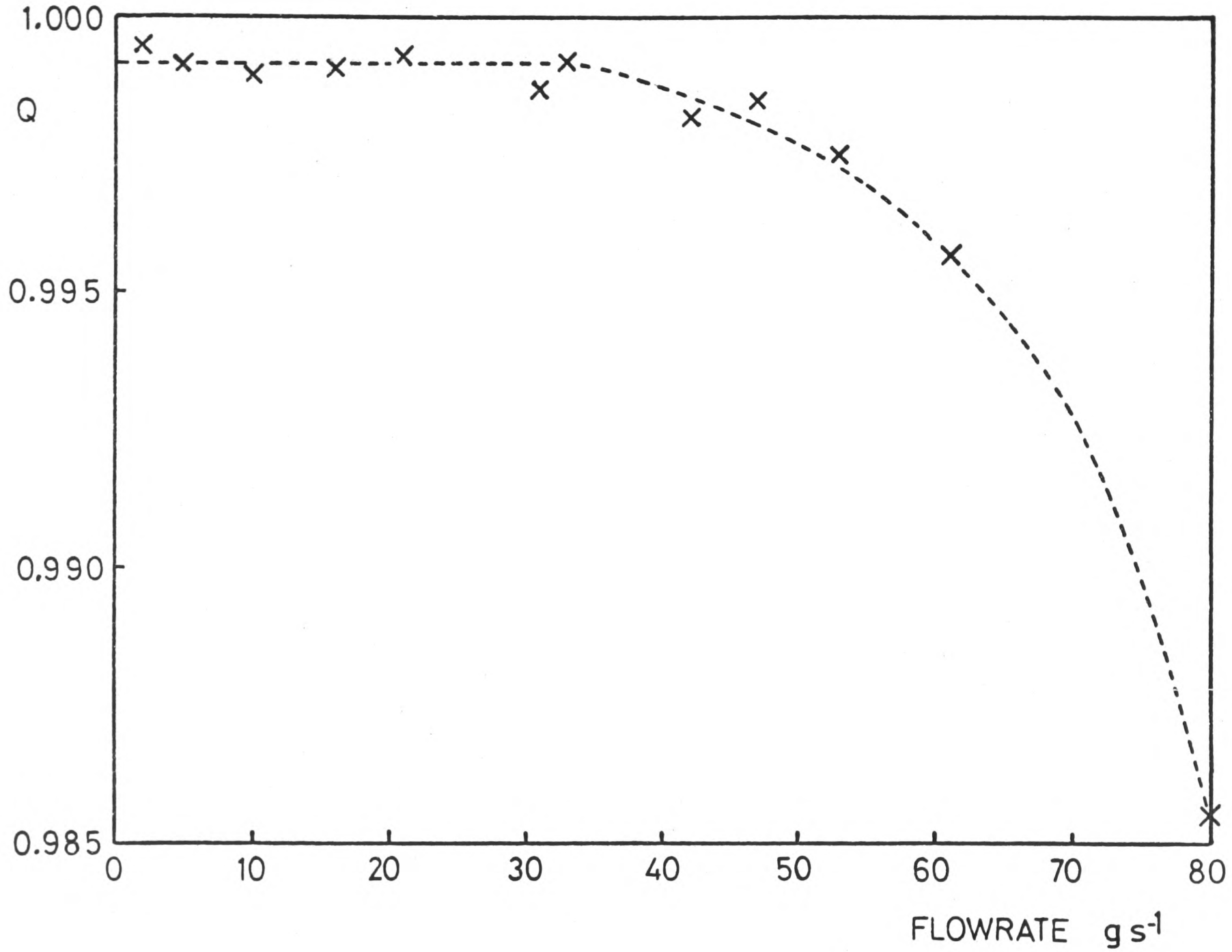


Figure 4.12 Two-dimensional mixer. Q vs. flowrate; 2 mm dia. ballotini.

(section (vi)). This confirms the importance of the concept of a 'critical voidage' in the design procedure. A flow of 35g s^{-1} in the small mixer corresponds to 1.4kg s^{-1} in the three-dimensional mixer which has a cross-sectional area forty times as great.

(iii) Mixer alignment

Experiments were performed to check how the quality of distributions deteriorate as the angle at which the mixer is mounted is increased. Five different angles were used and four experiments were done at each angle. The data was evaluated by comparing the number of particles in one half of the sample N_1, with the mean of the numbers in each half $\bar{N}$. If the mixer were level, the difference between the two would be distributed binomially with zero mean and variance N/4 where N is the number of particles fed to the mixer. If N is large the distribution is approximately normal and the quantity $(N_1-\bar{N})/\sqrt{N/4}$ can be used as an index to measure the effect of mounting the mixer at an angle. N_1 was chosen as the number of particles in the lower half of the sample. The confidence limits for a one-tailed test on the distribution of $(N_1-\bar{N})/\sqrt{N/4}$ indicate that a value equal to 1.65 corresponds to a 5% probability that the distribution is normal (Guttman and Wilkes, 1965). $(N_1-\bar{N})/\sqrt{N/4}$ is plotted against the angle of the mixer to the horizontal in Figure 4.13. The relationship appears linear though the difference is below the confidence limit for angles less than about 2^{o} from the horizontal.

(iv) Distance between mixer and sample tray

The effect of changes in the distance between the bottom of the mixer and the sample tray was similar to that described in 4.4 section (ii). Three different sizes of insert were used and

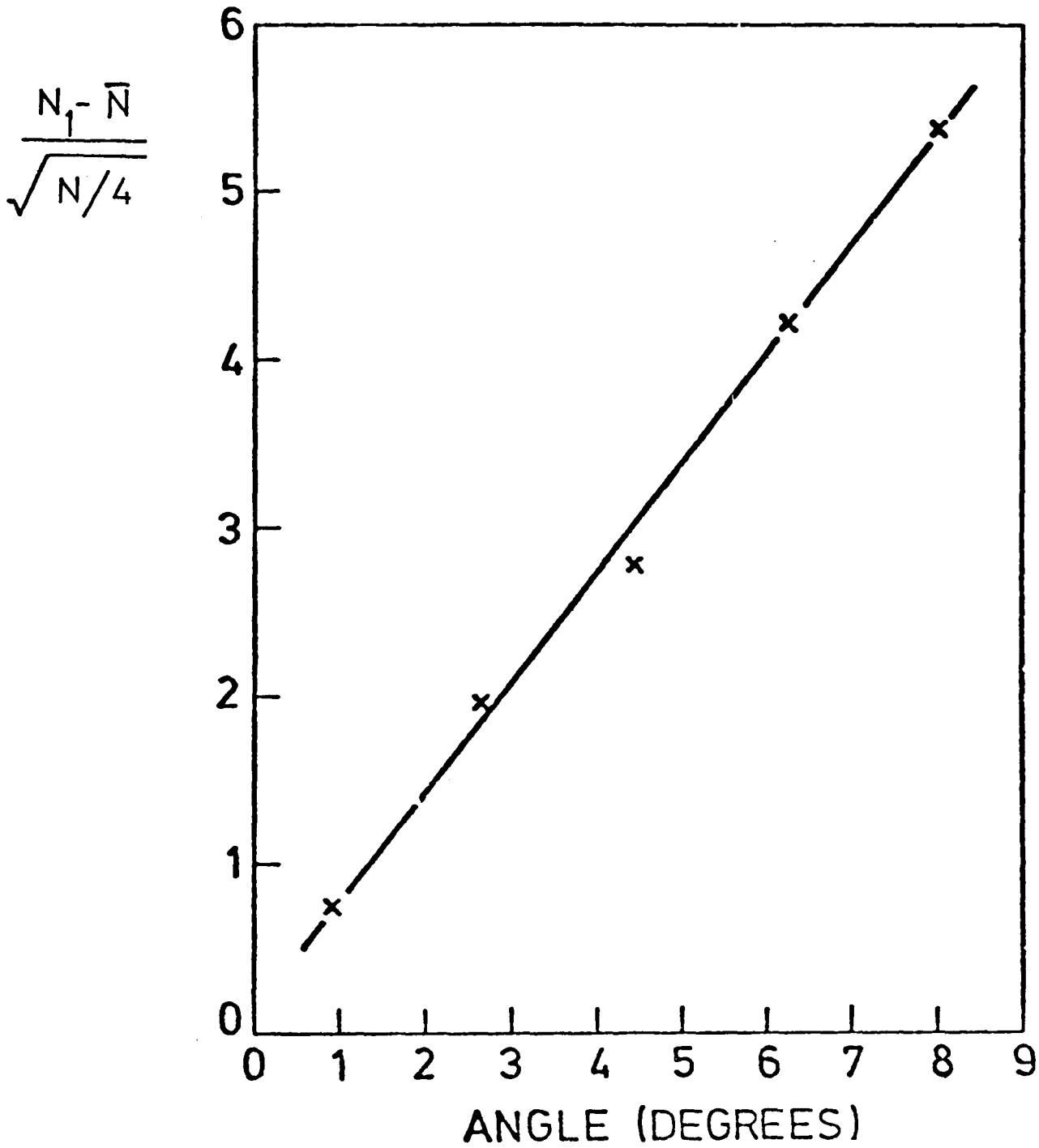


Figure 4.13: Two-dimensional mixer. $(N_1-\bar{N})/\sqrt{N/4}$ vs. angle at which mixer is mounted.

the optimum appeared to be 2.3 cm.

(v) Granular materials

A wide range of materials was tested by counting the numbers of particles in each division of the sample tray. All the materials used gave similar values of Q (Table 4.7). Because of the small quantities involved, flowrates could not be measured, though they were well below the critical values. Two experiments with materials with smaller particle sizes were done by weighing the amount in each sample tray division and then converting the weight to a number using the average particle weight (Table 4.8). The results indicate that the mixer is useful over a range of particle sizes from 0.5 to over 3mm dia. Two typical distributions are shown in Figure 4.14.

(vi) Fine materials

Results were similar to those reported in 4.4 section (vi). A photograph of iron filings flowing through the mixer is shown in Figure 4.15. Experiments at different flowrates showed that even when material was fed to the mixer at such a rate as to greatly reduce the amount of inter-particle interference similar distributions were obtained. Most of the particles in these experiments rolled rather than bounced down the bars, and the poor distributions may be due to low coefficients of restitution.

4.6 Comparison of the mixers

Direct comparison of values of Q achieved in the two mixers is not possible because of the different numbers of samples. It appeared that similar materials behaved similarly in both pieces of equipment. It might have been expected that the smaller mixer could cope better with smaller particles though no quantitative

Table 4.7: Two-dimensional mixer. Exhaustive tests

Material	Feedpoint (distance from edge of mixer) (cm)	Height of insert between mixer and sample tray (cm)	Number of Experiments	Mean value of σ^2/σ_R^2	Q
2mm dia. ballotini	10.00	0.0	4	1.77	0.9980 ± 0.0017
2mm dia. lead shot	"	"	4	2.01	0.9976 ± 0.0011
Barley	"	"	4	1.47	0.9955 ± 0.0013
Polyester chip	"	"	4	1.86	0.9949 ± 0.0015
2mm dia. ballotini	"	2.3	12	1.53	0.9987 ± 0.0005
1.5 mm dia. ballotini	"	"	6	2.39	0.9977 ± 0.0004
1mm dia. ballotini	"	"	"	2.07	0.9985 ± 0.0005
1/8" dia. acrylic resin	"	"	"	1.49	0.9984 ± 0.0006
2mm dia. lead shot	"	"	"	1.27	0.9994 ± 0.0003
1/16" dia. steel balls	"	"	"	1.76	0.9985 ± 0.0004
3/32" dia. steel balls	"	"	"	1.75	0.9976 ± 0.0008
1/8" dia. steel balls	"	"	"	1.30	0.9983 ± 0.0008
Celon chip	"	"	"	1.20	0.9992 ± 0.0006
Polyester chip	"	"	"	1.44	0.9971 ± 0.0010
Barley	"	"	"	0.99	1.0001 ± 0.0013
Mustard seed	"	"	"	1.64	0.9980 ± 0.0006
Plain canary seed	"	"	"	1.27	0.9985 ± 0.0006

Table 4.7 (continued)

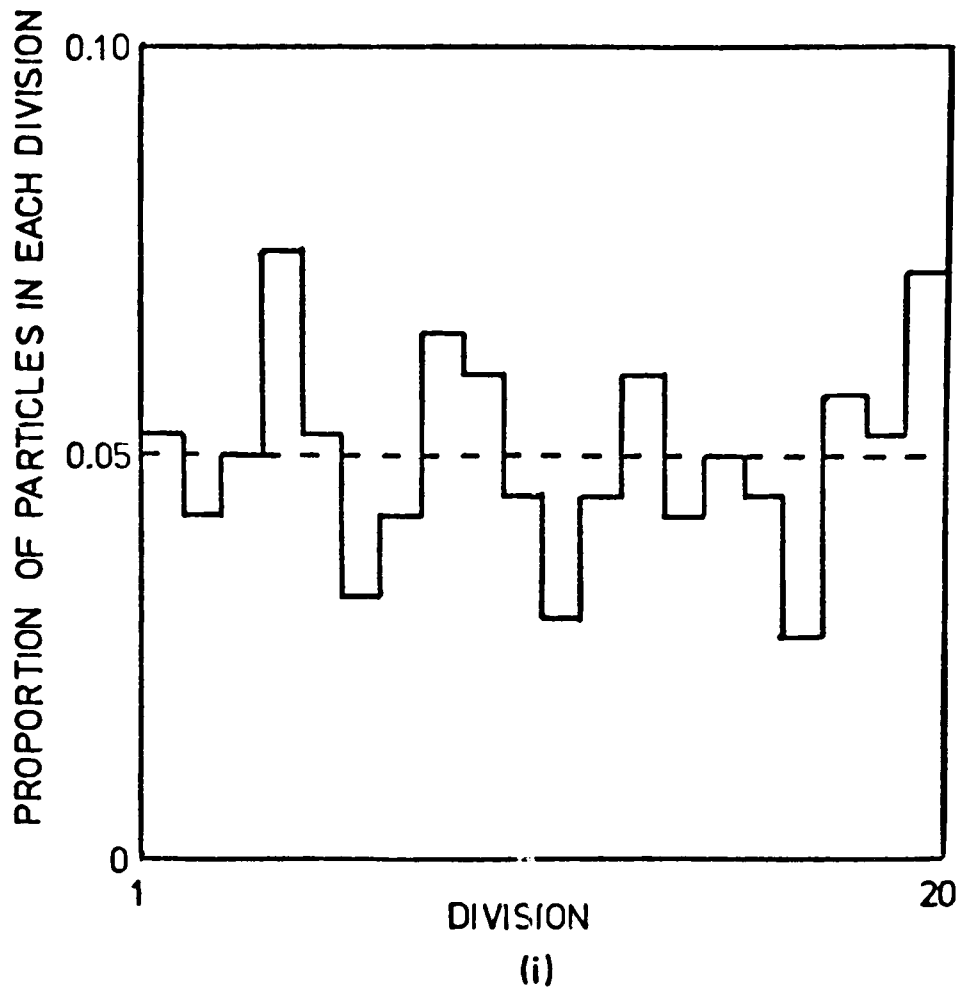
Material	Feedpoint (distance from edge of mixer) (cm)	Height of insert between mixer and sample tray (cm)	Number of Experiments	Mean value of σ^2/σ_R^2	Q
2mm dia. ballotini	"	4.7	4	2.44	0.9968 ± 0.0005
2mm dia. lead shot	"	"	"	1.31	0.9993 ± 0.0003
Barley	"	"	"	1.33	0.9975 ± 0.0013
Polyester chip	"	"	"	1.24	0.9987 ± 0.0008
2mm dia. ballotini	"	7.2	"	3.50	0.9938 ± 0.0009
2mm dia. lead shot	"	"	"	1.10	0.9998 ± 0.0007
Barley	"	"	"	1.32	0.9974 ± 0.0013
Polyester chip	"	"	"	1.65	0.9968 ± 0.0013
1mm dia. ballotini	"	"	2	2.61	0.9965 ± 0.0009
0.5mm dia. ballotini	"	"	"	2.12	0.9970 ± 0.0008
Celon chip	"	"	4	1.68	0.9973 ± 0.0010
2mm dia. ballotini	1.67	"	2	4.19	0.9921 ± 0.0026
1mm dia. ballotini	5.00	"	"	4.53	0.9934 ± 0.0006
2mm dia. ballotini	"	"	"	5.61	0.9885 ± 0.0003
Barley	"	"	"	1.47	0.9963 ± 0.0009
Celon chip	"	"	"	2.53	0.9939 ± 0.0012

Table 4.8: Two-dimensional mixer weighing experiments

Material	No. of particles used	F	Q
0.5mm dia. ballotini	294,700	353	0.9988
0.75mm dia. ballotini	99,100	111	0.9989

Feedpoint: central

Insert: 2.3cm



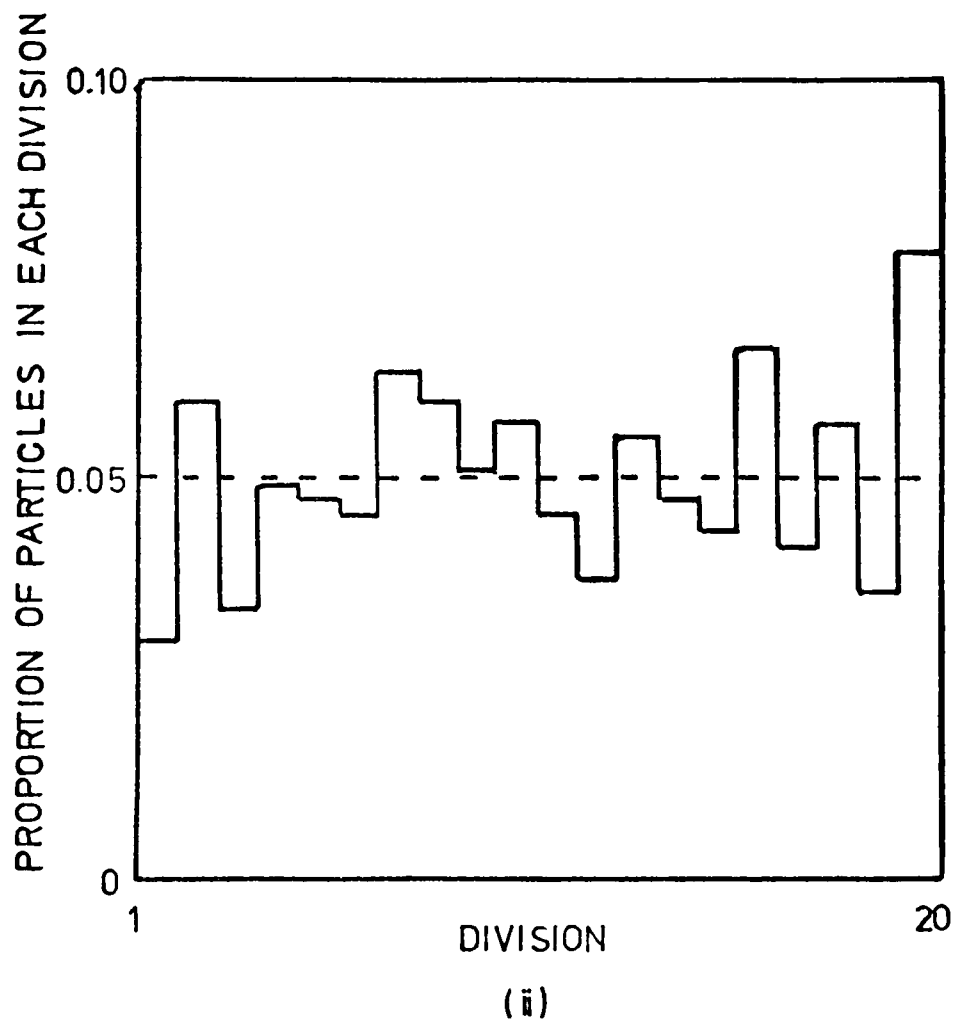


Figure 4.14: Typical distributions.

(i) 2mm dia. ballotini, central feed, 2.3cm insert.
(ii) 1/16 in. dia. steel balls, central feed, 2.3cm insert.

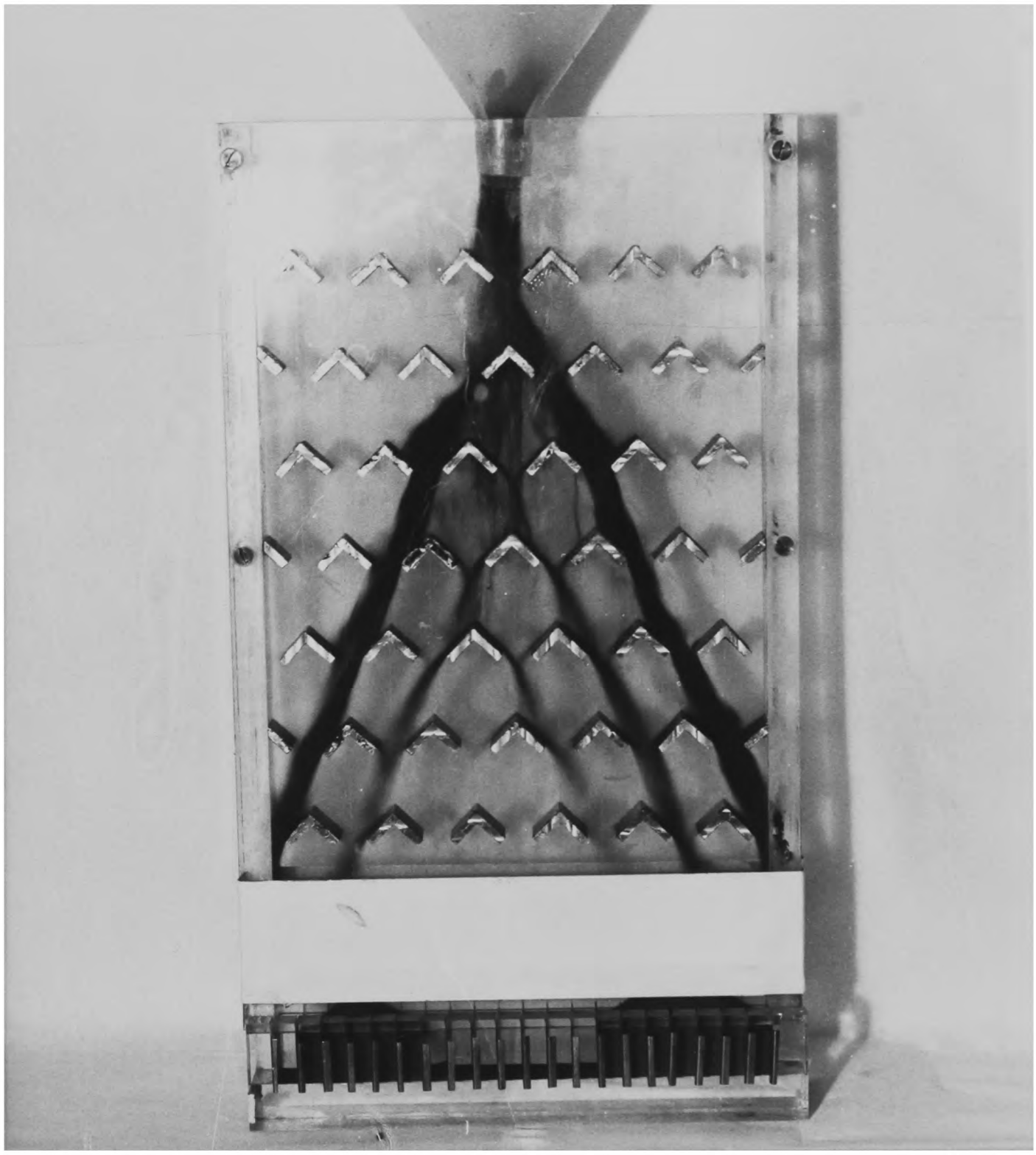


Figure 4.15: Iron filings flowing through the two-dimensional mixer.

experiments were done with particles smaller than 1mm dia. in the three-dimensional mixer because of the difficulty in counting small particles in the sample tray.

Numerical comparison of results is possible if the procedure outlined in 4.4 section (ii) is followed. Twenty line samples, each twenty units long can be produced and results can be calculated for the two orthogonal directions. The means of the two values of Q produced, Q_a, are shown in Table 4.9. It appears that ballotini is distributed slightly better by the three-dimensional mixer and lead shot better by the two-dimensional mixer. Barley and steel balls give similar results in both units.

4.7 Discussion and conclusions

Harwood et al. (1975) have recently described and assessed the performance of seven continuous mixers, one of which, the Kenics mixer, has no moving parts. This mixer has been subjected to detailed studies by Fan and co-workers (Fan et al., 1971; Chen et al., 1972; Chen et al., 1973; Lai and Fan, 1975). It consists of a number of helices with 180^{o} twists inserted into a cylindrical tube. A dense stream of solid particles entering the tube is split into two by the first helix. The streams recombine at the bottom of the helix and are split again by the second one. Successive helices are arranged so that the streams flowing through any helix are composed of approximately one-half of each of the two streams which left the one above. Comparison with the mixers described here is impossible as Fan only investigated axial mixing. However, subjective evaluation of the results presented by Fan et al. (1971) indicates that the helical mixer is not very efficient. This is probably because the low voidage in the system prevents much particle motion. The

Table 4.9: Three-dimensional mixer. Experiments analysed in groups of 20 samples

Experiment Number	Material	Sample Tray position*	Feed Point Position	Q_a
1	3.5mm dia. ballotini	1	1	0.9975
2	2mm dia. lead shot	1	1	0.9914
3	Barley	1	1	0.9977
4	3.5mm dia. ballotini	4	1	0.9991
5	2mm dia. lead shot	4	1	0.9944
6	1mm dia. ballotini	4	1	0.9995
7	2mm dia. ballotini	4	1	0.9992
8	3.5mm dia. ballotini	3	1	0.9987
9	2mm dia. ballotini	4	1	0.9992
10	2mm dia. ballotini	4	3	0.9995
11	2mm dia. ballotini	4	1	0.9996
12	2mm dia. ballotini	4	2	0.9991
13	3/32" dia. steel balls	2**	1	0.9991
14	3/32" dia. steel balls	2	1	0.9983
15	2mm dia. lead shot	2**	1	0.9977
16	2mm dia. lead shot	2	1	0.9953

* See Figure 4.9. **wire mesh ($\frac{1}{4}$" centres, 1/16" thick)

quality of the final mix is likely to be controlled by segregation which would make the creation of a random mixture impossible. The mixers studied here are not subject to these constraints.

The experiments have shown that both the two- and three-dimensional mixers produce reasonably good though not random distributions of materials, which have particle sizes in the range 0.5-3.5mm dia. Though experiments on the two-dimensional mixer were much more extensive and thorough, both pieces of equipment produce similar results. It has also been shown that use of the index Q is a useful method for analysing such equipment. One advantage of these mixers is that if the flowrates are below the critical values, the distributive mechanisms for different materials are independent, and materials can be tested individually.

The action of fine materials in the equipment has been tested and there is apparently a change in mechanism when the particle diameter falls below a value between 0.125 and 0.5mm. This may be related to coefficients of restitution. The three-dimensional mixer could cope with its design flowrate with ballotini though possibly not with a lighter material. This suggests that the critical voidage used in the design procedure should be about 0.95. It appears that there is an optimum removal point from below the mixers though the effect is not always marked.

The slight depletion of the centre of the distributions produced by the three-dimensional mixer suggests that material bouncing on the sides of the mixer is not returning to the centre. This could probably be rectified by fitting slightly larger bars at the walls of the mixer. Since the lead shot experiments gave considerably more depletion than the others, this effect is probably related to the coefficient of restitution. The effect was not noticed in the experiments with the two-dimensional mixer.

Possible applications of these devices include:

(i) Mixing or blending granular materials metered into the device through separate openings, e.g. plastic granules or grain.

(ii) Feeding mixtures of the type mentioned above to storage hoppers; the uniform distribution will avoid formation of a conical heap where segregation may occur (Mitchell, 1938). The device must then be the same size as the hopper.

(iii) The two-dimensional distributor could be used for depositing a layer of particles onto a moving conveyor belt or behind a moving body, e.g. distributing fertilizer or gravel.

The performance of the equipment could be improved if necessary by:

(i) Making the mixer higher. Estimates of the optimum height of such equipment will be considered in the next chapter.

(ii) Adjusting the size and orientation of the half-bars at the walls.

(iii) Insertion of one or more layers of wire mesh below the mixer.

(iv) Providing layers of successively smaller bars to even out an initially coarse distribution.

In summary, these mixers are particularly useful for the on-site mixing or distribution of segregating, cohesionless powders, materials which cannot easily be mixed in conventional equipment.

CHAPTER 5

SIMULATION AND MODELLING OF MIXERS

5.1 The computer program

5.1.1 Introduction

The units described in the previous chapter have been shown to be capable of mixing and distributing cohesionless material. It would have been difficult to construct a mixer with different sets of bars and provision for mounting them in various positions and so a computer program was written to simulate the motion of a single spherical particle passing through a mixer. Design data, it was hoped, could be obtained from the results.

Moore and Masliyah (1973) had already reported a program to study percolation. They define a regular array of spheres in three-dimensional Cartesian space. A small sphere is released into this array from a given point and with given initial velocity. It undergoes constant acceleration in one direction, with the result that its path is parabolic. Upon impact with a sphere or container wall, its velocity is changed such that the tangential velocity remains the same and the normal velocity is changed in sign and reduced by a factor α, the coefficient of restitution. Results from the program have been published by Masliyah and Bridgwater (1974).

There are two major differences between the problems of simulating the mixer and spontaneous percolation.

(i) The objectives are different. Spontaneous percolation was investigated in an infinite medium and percolation velocities

and diffusion coefficients calculated. The aim in simulating the mixer was to produce design information on the optimum bar layout and mixer height. Though data on particle velocities are valuable in evaluating a transient response, they are generally of secondary importance.

(ii) The detailed calculations are different. In spontaneous percolation, Moore and Masliyah had to solve an equation representing the intersection of a parabola with a sphere, i.e. a quartic equation. This they achieved by searching the particle path for possible collisions and, having found the relevant one, solving the equation iteratively to the desired accuracy. With the mixer it is only necessary to solve for the intersection of a parabola with a plane, if collisions on the corners of bars are simplified. The ensuing quadratic equation may be solved by formula to machine accuracy, using considerably less computer time.

Thus an entirely new program was written as described in the following sections.

5.1.2 Program logic

A simplified flowsheet is shown in Figure 5.1. A detailed flowsheet is in Appendix I.

5.1.2.1 Initialisation

The program begins by reading in the control data from a data file and defining the bar co-ordinates. The data file contains the number of the run, the initial particle position and velocity, the particle radius, the coefficient of restitution α, the bar size L_b and thickness Y_T, and the parameters which define the vertical bar spacing Y_s and S_y. Y_s is the vertical distance between two adjacent parallel rows of bars and S_y is the mean

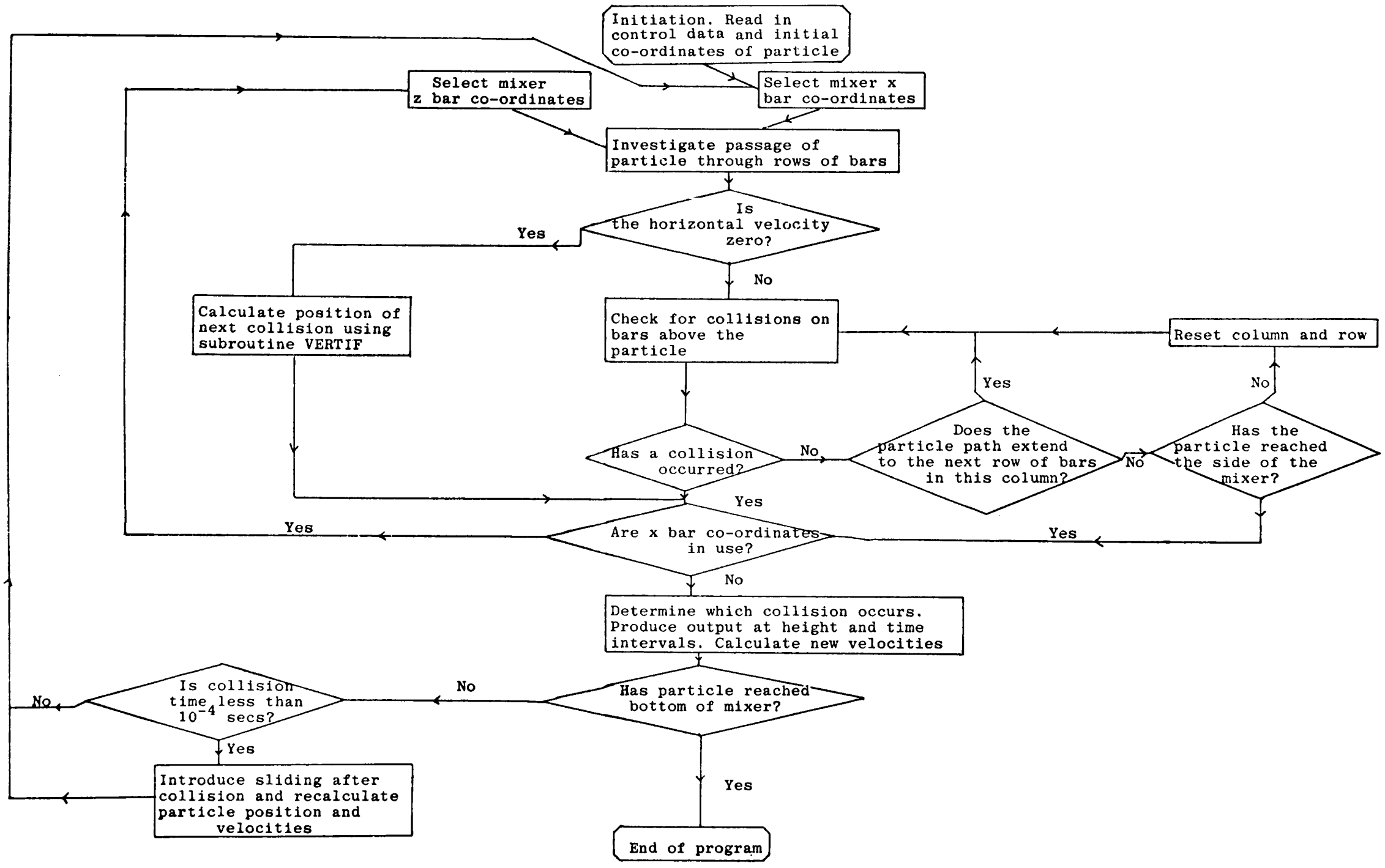


Figure 5.1: Concise program flowsheet

vertical bar spacing in the mixer. Measurements in the program were in dimensional form, though they have been converted into the dimensionless quantities presented here. The co-ordinate system was defined so that y is positive upwards and all values of x and z are positive.

The detailed mixer geometry is controlled by two sub-routines, one for the vertical and another for the horizontal bar spacing. The cross-section of the mixer remained 0.4m square throughout and the horizontal bar spacing was as described in Chapter 4 (see Figures 4.3 and 5.2).

5.1.2.2 Search routine

One way in which this simulation is simpler than that of percolation is that the motion in the x and z directions can be considered independently. A collision between the particle and a bar can be found by two two-dimensional searches, one considering movement in the x-y plane and looking at bars running in the z direction and the other with x and z interchanged. The earliest collision during each of these searches is stored and then the earlier one is recorded. This method can be used because a bar is uniform along its length.

The moving sphere follows a parabolic path such that the co-ordinates of the particle (x,y,z) at time t are defined by the equations:

$$\begin{aligned} x(t) &= V_x t + x_o \\ y(t) &= V_y t - gt^2/2 + y_o \\ z(t) &= V_z t + z_o \end{aligned} \qquad (5.1)$$

where V_x, V_y and V_z are the velocities of the particle after the preceding collision which occurred at the point x_o, y_o, z_o.

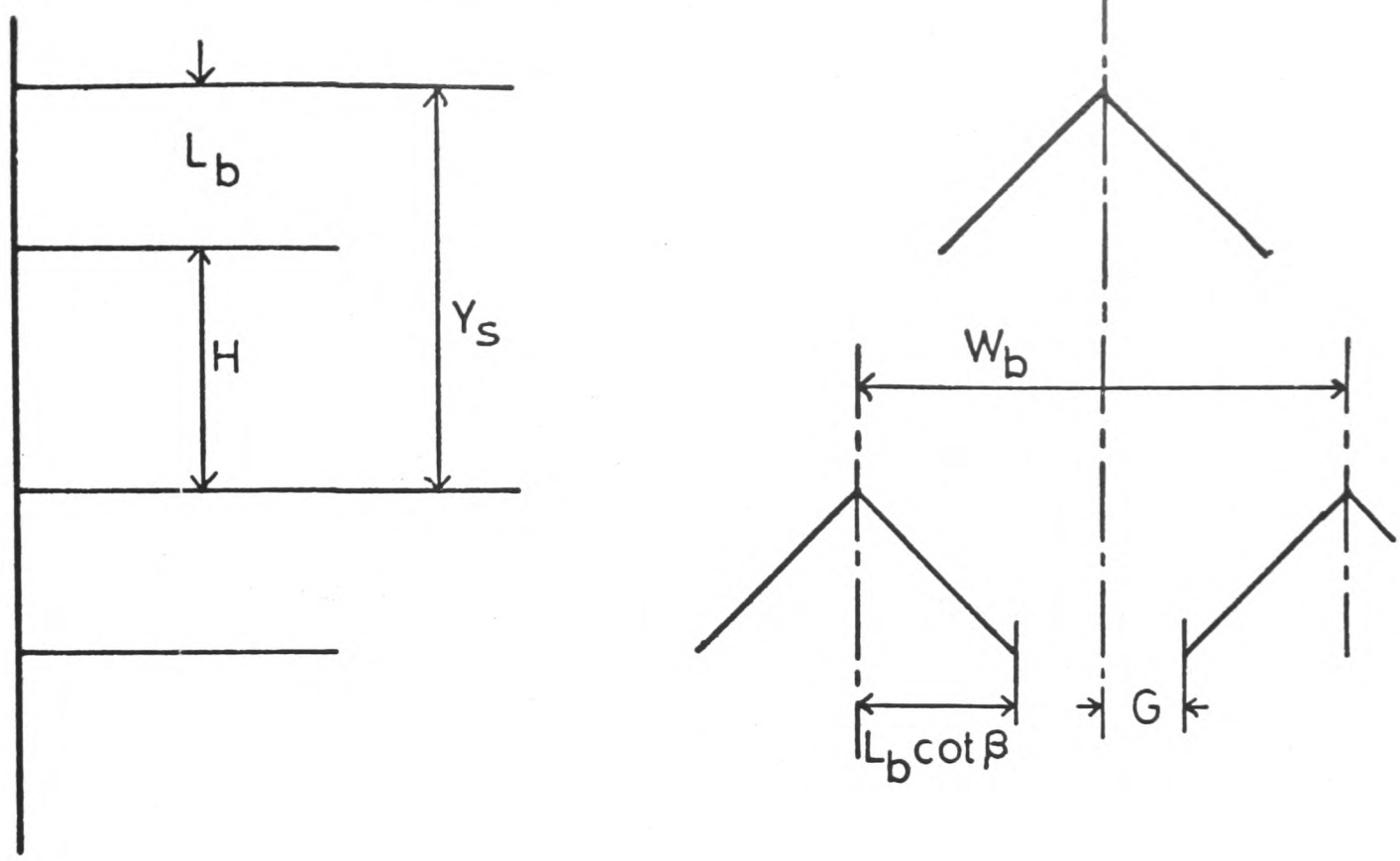


Fig. 5.2 Bar layout in mixer including notation. S_y is the average vertical bar spacing.

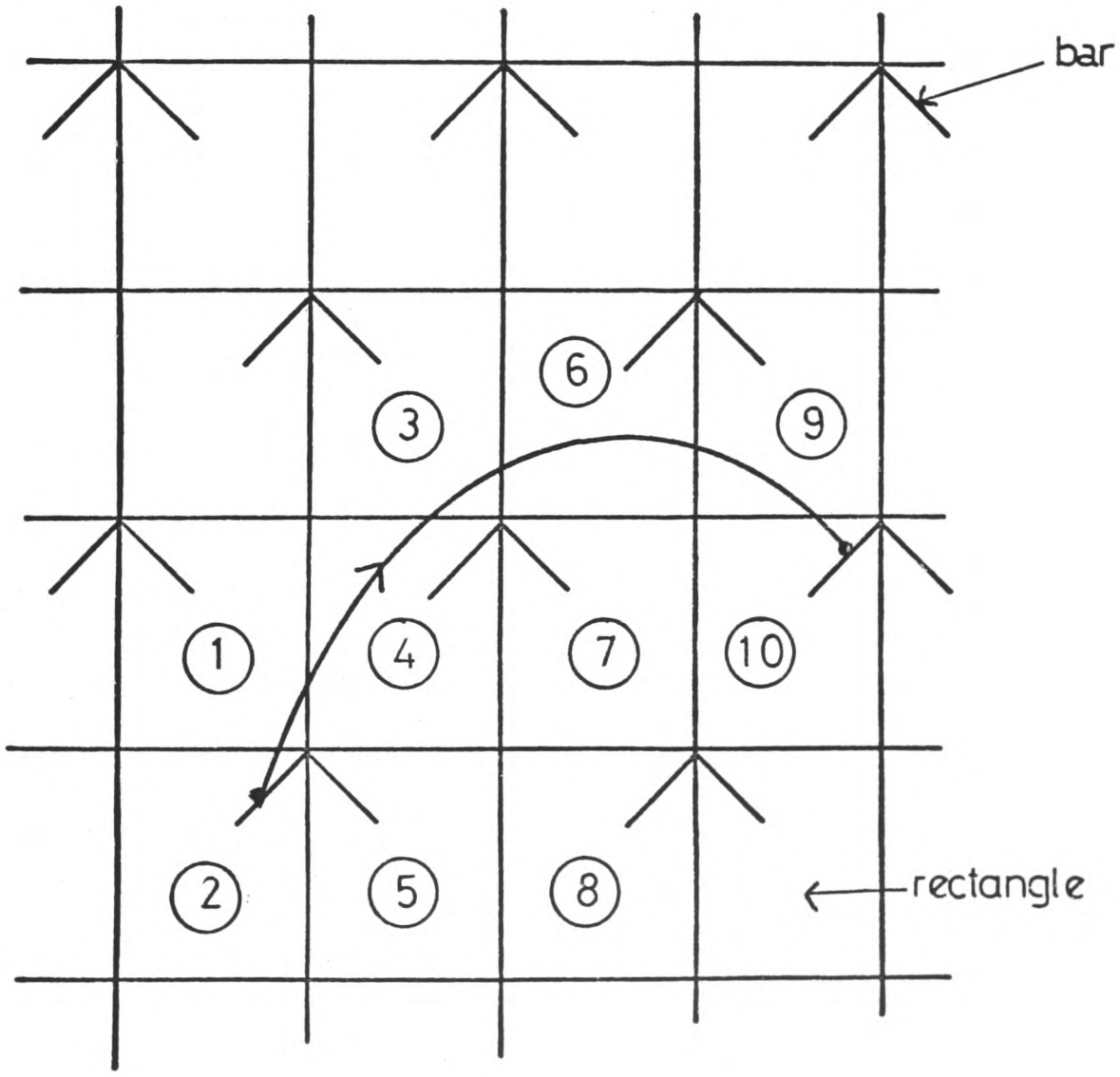


Fig. 5.3 Search routine; division of mixer into rectangles.

Since the lateral velocity remains constant between collisions, it was used as the basis of the search routine. The x-y and z-y planes are divided into rectangles as shown in Figure 5.3 where a possible particle path is shown. The search proceeds by checking whether or not there is a collision between the particle and a bar in one rectangle after another. The first rectangle considered is the highest one through which the particle would pass, if it did not hit a bar first, in the vertical column of rectangles in which the particle had its last collision. Since vertical velocities are never very great, this is never more than a few rectangles above the one in which the last collision occurred (hereafter termed the current rectangle). Each rectangle down to the current one is checked to see whether or not a collision occurs between the particle and the portion of a bar in that rectangle. If a collision occurs, details of it are stored, and the store is updated with details of a new collision if the time at which it occurs is earlier than that of the previously stored collision. If no collision is found then rectangles below the current one are checked if the particle passes through them. Should a collision be found below the current rectangle then further searching is unnecessary as collisions further down the mixer necessarily occur at a later time. It may happen that the particle path leaves the current rectangle through one of its sides in which case this is the only rectangle in the column to be checked for a collision.

If a collision is found in the column in which the current rectangle lies then the search ceases as a collision in another column would occur later. If no collision is found then the search continues in the adjoining column in the direction in which the particle is moving. The same procedure is followed. This

can occur again and again up to the side of the mixer. If no collision is found in a column adjoining a side, the position and time at which the particle hits the side are stored and the search ends. Thus, in summary, whenever a collision is found above the level of the current rectangle the column is checked down to the level at which the previous collision occurred but no further, as collisions elsewhere would necessarily occur later. An example of the order in which rectangles are searched is shown in Figure 5.3.

The foregoing does not apply when the particle is moving with zero lateral velocity. To cope with this case a separate subroutine (called VERTIF) was written. The next collision in this case can be simply determined from the co-ordinates of the last one and the vertical velocity (see section 5.1.2.5).

This search procedure is one of the more efficient ones, though others could have been used. The procedure is carried out for both the x-y and z-y planes and two collisions are stored. The earlier of these is recorded, new velocities are calculated and the search begins again. The run ends when the particle passes through the bottom of a rectangle corresponding to the bottom row of bars in the mixer.

5.1.2.3 Collisions with the bars

It has been noted that the co-ordinates of the intersection of the particle path with a bar surface are given by the roots of a quadratic equation. The problem can be simplified by considering the particle as a point and adding its radius to the bar co-ordinates as shown in Figures 5.4 and 5.5. The surface produced in Figure 5.5 is curved at the corners of the bar so the approximation in Figure 5.4 was used. In practice the result

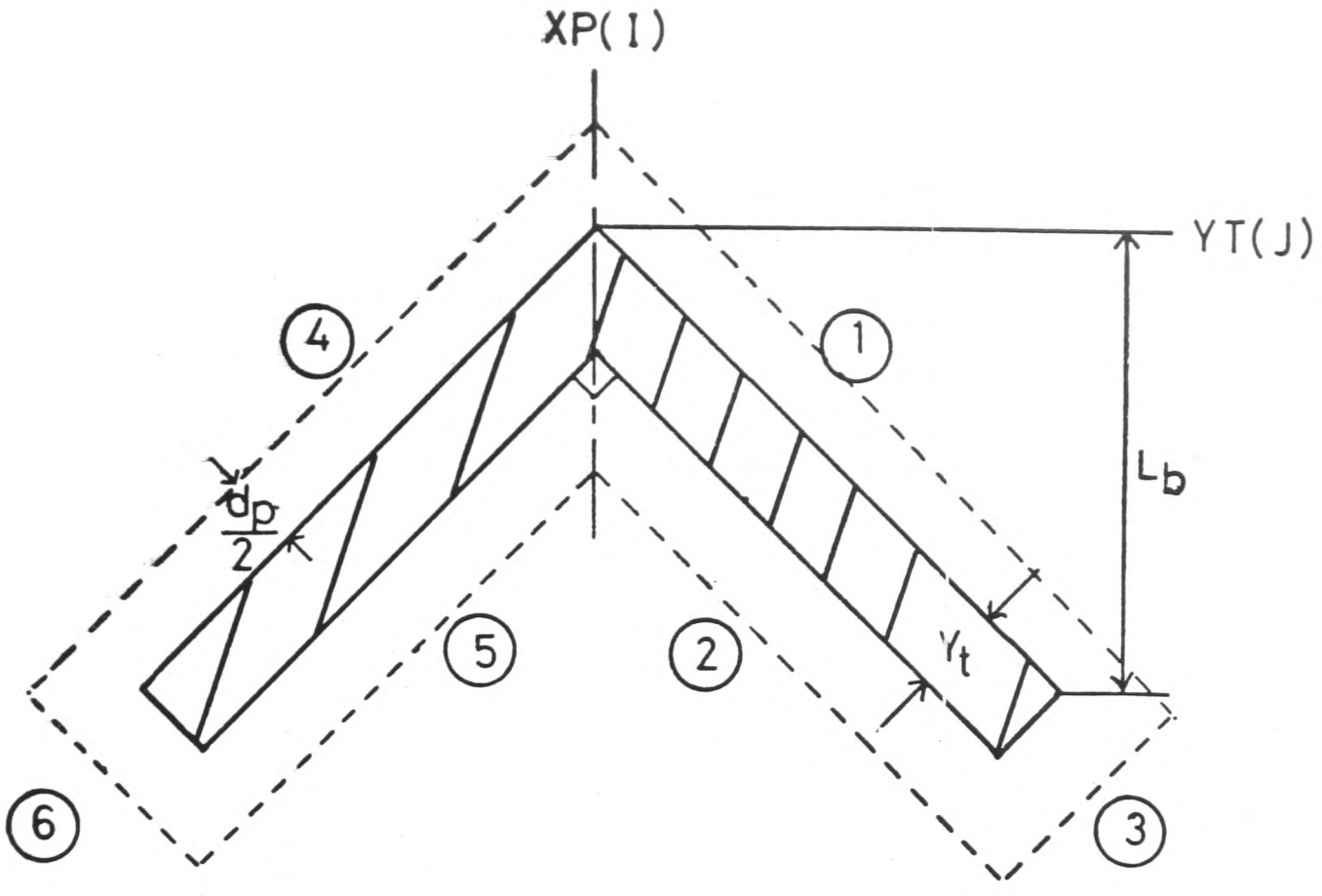


Fig. 5.4 Bar showing approximation to collision surface. Circled figures refer to values of NPLACE, the variable used to describe the type of surface.

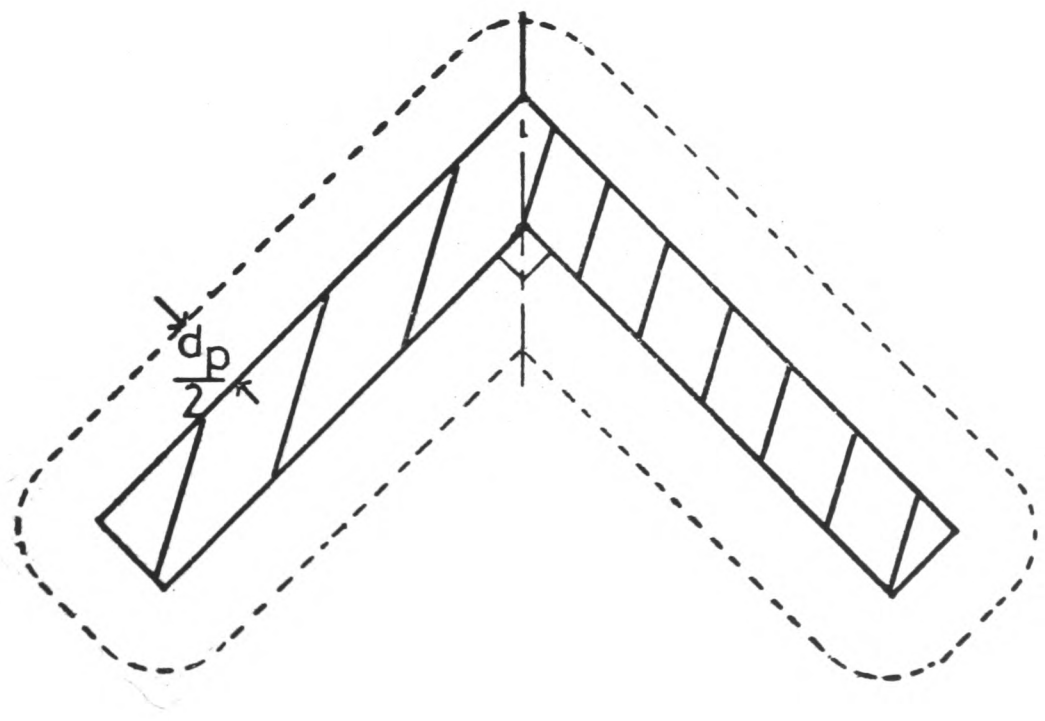


Fig. 5.5 Bar collision surface.

of a collision between a particle and the apex of a bar would depend greatly on secondary effects such as small irregularities at the apex.

Eliminating t between the expressions for x(t) and y(t) in equation 5.1 to obtain the particle path in the x-y plane,

$$y = -g\frac{(x - x_o)^2}{2V_x} + V_y \frac{(x - x_o)}{V_x} + y_o \qquad (5.2)$$

The equations describing the bar surfaces are of the form

$$y = C_1 x + C_2 \qquad (5.3)$$

where $C_1 = \pm 1$ and C_2 is a function of the bar co-ordinates XP(I) and YT(J) (Figure 5.4), L_b and the particle radius. There are six different equations describing the different bar surfaces and these are identified by the value of the variable NPLACE which can take the values 1-8. (7 and 8 refer to collisions with the sides of the mixer). x can be found by eliminating y between equations 5.2 and 5.3. A collision has occurred if the value of x lies between the limits defined by the bar geometry, and if the time at which the collision takes place is positive. The co-ordinates, time and value of NPLACE, are stored if a collision does occur and the search continued.

Special provision was made for a particle which repeatedly collided with the same bar surface at very short intervals. This is discussed in section 5.1.2.7.

5.1.2.4 Collisions with the sides

Whenever the search routine reached a side of the mixer, a collision was recorded and the search stopped. The equations describing the effective side surfaces in the x-y plane are

$$x = d_p/2$$
$$\text{and} \qquad x = L_M - d_p/2 \tag{5.4}$$

where L_M is the length of one side of the mixer. Substitution in equation 5.2 gives y.

5.1.2.5 Collisions with the bars - zero lateral velocity

If V_x or V_z equals zero, a situation occurring at the beginning of each run, then y cannot be calculated from equation 5.2. A separate subroutine was written for this situation. If $V_x = 0$, the next collision occurs at $x = x_o$. The corresponding values of y, t and z can be found from knowledge of whether the particle is above or below the bar in the rectangle in which it lies and its vertical velocity. Details are shown on the flowsheet in Appendix I.

At the time when the routine was written it appeared that it might have been necessary to use the subroutine iteratively when V_x or V_z was small, as the error in calculating the co-ordinates of a collision is greatest in this situation. Thus provision was also made for particles moving vertically upwards though this part of the program was never used.

5.1.2.6 Velocities after collision

The vertical velocity of the particle on impact is $(V_y - gt)$ while the horizontal velocities remain unaltered during flight. New velocities are calculated by resolving the impact velocities into components parallel and normal to the collision surface. Components parallel to the surface remain unchanged while the normal component is reversed in direction and multiplied by the coefficient of restitution α. The velocities are then resolved to give V_x, V_y and V_z.

Constant values of the coefficient of restitution were used, though it would have been simple to make α a function of the impact velocity.

5.1.2.7 Sliding

Occasionally a particle would undergo many collisions on the same bar surface, gradually moving along it as these occurred. This situation usually arose when the vertical and lateral velocities were small and particularly if the coefficient of restitution were low. Rather than record upward of ten or twenty collisions within a very small time interval, the collisions are replaced by assuming that the particle slides down the bar. Only the first collision on the bar is recorded. The procedure involves recalculation of the particle velocity at an apparent starting position for the next collision, i.e. the bottom of the bar. The routine was invoked when the time between collisions was less than 10^{-4}s. With the exception of those runs with $\alpha \leqslant 0.4$, the routine was rarely used and thus it was unlikely to affect the results.

5.1.2.8 Output

Six channels of output are used by the program. These record:

(i) the control data such as the bar size and co-ordinates and the particle properties.

(ii) the co-ordinate and time of each bounce.

(iii) intermediate information such as interstitial velocities.

This file was useful when debugging the program but was not printed unless an error occurred.

(iv) the particle position at preset height intervals (10mm).

(v) the particle position at preset time intervals (0.05s).

(vi) the passage of the particle between bars. The x-y and z-y planes are considered separately and each is divided into twelve columns of rectangles as before. Whenever the particle passes through a row of bars for the first time, its x (or z) co-ordinate at a height YT(I) - L_b is calculated and the column in which this lies recorded. The number of times the particle passes through a row in each column is calculated. There are two types of row in each plane, one with half-bars at each end and one without, and thus four arrays of twelve numbers are produced. If the variance of each of these arrays is compared with the random variance, the probability that the distribution is random can be calculated, which indicates the mixing characteristics for the particle being used.

5.1.3 Program development

The program was built up gradually. The original version incorporated most of the basic ideas though single precision variables were used throughout and the particle was restricted to motion in two dimensions. Bar surfaces were as in Figure 5.5 and the height of the mixer corresponded to the one built. More than thirty runs were done with this program, though none were analysed. A number of problems arose, chief among which were:

(i) Different runs with all the variables the same but different particle starting positions gave widely varying results because of the small quantity of data produced. In the second

version of the program the mixer was therefore made five times as high.

(ii) The solution of the equations of motion to determine the point of the next collision often produced solutions corresponding to the previous collision. This was due to round-off errors in the calculation of the time at which the collision occurred. Thus collisions which happened at times less than 10^{-5}s after the previous one were disregarded in later versions of the program unless they were with the sides of the mixer.

(iii) The program would occasionally miss a collision with a curved surface. The equations describing these surfaces were of the form

$$(x - C_3)^2 + (y - C_4)^2 = d_p^2/4 \qquad (5.5)$$

Elimination of y between equations 5.2 and 5.5 produces a quartic, which in this version of the program was solved to a specified accuracy by a library routine written for the Numerical Algorithms Group (NAG) library. The program then checked whether the roots of the equation lay within the boundary conditions defined by the bar geometry and the radius of the particle. Because of the size of the numbers being manipulated, the accuracy of the solution was often poor and the roots of the equation would not lie on the circle and were occasionally outside the limits defined by the boundary conditions. The check on the limits was made less stringent in later versions but this did not completely solve the problem.

Whilst the changes described above were being incorporated into the second version of the program, an alteration to allow motion in three dimensions was made. This version was only run

a few times; it worked moderately well though the mixer still did not seem large enough. Its height was therefore increased by a further factor of five which brought another problem with it. The program was now too long to run on Oxford University's ICL 1906A computer. The possibility of a transfer to a more powerful computer was considered but a change to the bar surfaces shown in Figure 5.4 was chosen instead. There was now no longer any problem with quartic equations and the program ran in a reasonable time.

A series of programs to analyse the results was written and the runs recorded in Table 5.1 begun. Trouble was experienced with the second run due to the computer not recording a collision correctly because of inadequate precision. Other results showed that a collision at about y = 20m gave a slightly different result from one at about 10m even though the geometry of the collision was exactly the same in each case. These problems were solved by altering most of the important variables to double precision, a change from the use of approximately 11 significant figures to 20. The program was now virtually in its final form and other alterations were trivial.

New subroutines for the solution of polynomial equations later became available. These were also written for the NAG library but used the method of Grant and Hitchins (1971). They were rewritten using double precision and were then incorporated into the program allowing the bar surfaces shown in Figure 5.5 to be used. In this form a successful run of the program took over an hour and runs were done in sections, with the core image stored at the end of each part. Because of this only three runs were attempted with this version of the program, two of which were successful (nos 39 and 44). The other failed approximately half-

Table 5.1 Results of Mixer Simulation

RUN	$\frac{L_b}{S_y}$	$\frac{Y_t}{S_y}$	$\frac{Y_s}{S_y}$	$\frac{d_p}{S_y}$	α	$\frac{u}{\sqrt{gS_y}}$	$\frac{uS_y}{D_y}$	$\frac{\Delta\bar{r}_r}{S_y}$	$\frac{uS_y}{D_r}$
				x 10^{-1}					
1	0.595	0.085	1.333	0.800	0.8	0.359	2.50	1.442	0.270
2	"	"	"	"	0.7	0.505	2.43	1.530	0.275
3	"	"	"	"	0.6	0.622	4.02	1.475	0.395
3D	"	"	"	"	"	0.618	5.33	1.561	0.329
4	"	"	"	"	0.5	0.737	5.46	1.652	0.291
5	"	"	"	"	0.4	0.852	7.41	1.680	0.337
6	"	"	"	"	0.3	1.026	7.95	1.715	0.302
7	"	"	"	"	0.2	1.078	17.65	1.510	0.282
8	"	"	"	"	"	1.068	15.05	1.452	0.377
9	"	"	"	"	0.1	1.049	94.83	1.262	0.256
10	"	"	"	"	0.9	0.229	1.58	1.446	0.154
11	"	"	"	0.267	0.8	0.364	2.27	1.504	0.204
12	"	"	"	1.333	"	0.338	3.30	1.158	0.351
13	"	"	"	1.867	"	0.289	4.48	0.969	0.460
14	"	"	"	$6x10^{-5}$	"	0.381	2.13	1.564	0.230
15	"	"	"	0.800	0.7	0.475	3.97	1.491	0.270
16	"	"	"	"	0.8	0.346	3.55	1.484	0.207
17	"	"	"	"	0.95	0.175	0.98	1.456	0.097
18	"	"	"	2.400	0.8	0.264	5.06	0.940	0.434
19	"	"	"	2.133	"	0.280	5.86	1.031	0.314
20	"	"	"	0.533	"	0.358	3.90	1.589	0.266
21	"	"	"	1.067	"	0.336	2.89	1.390	0.244
22	"	"	"	1.600	"	0.305	5.05	1.172	0.283
24	"	"	1.000	0.800	"	0.330	3.89	1.505	0.206
25	"	"	1.133	"	"	0.336	3.56	1.457	0.254
26	"	$3x10^{-6}$	1.333	"	"	0.322	3.35	1.505	0.291
27	"	0.027	"	"	"	0.348	2.33	1.501	0.272
28	"	0.053	"	"	"	0.345	4.02	1.556	0.244
29	"	0.080	"	"	"	0.354	2.68	1.464	0.321
30	"	0.107	"	"	"	0.361	2.83	1.337	0.266
31	"	0.133	"	"	"	0.374	3.05	1.383	0.269
32	0.333	0.085	"	"	"	0.541	1.24	2.474	0.134
33	0.400	"	"	"	"	0.513	1.79	2.121	0.208
34	0.467	"	"	"	"	0.462	1.34	1.899	0.245
35	0.533	"	"	"	"	0.407	3.05	1.572	0.213
36	0.600	"	"	"	"	0.359	2.29	1.426	0.273
37	0.667	"	"	"	"	0.275	5.63	1.117	0.355
38	0.595	"	"	"	"	0.392	2.60	1.498	0.231
39	"	"	1.067	"	"	0.326	2.65	1.490	0.251
40	"	"	1.200	"	"	"	3.12	1.408	0.254
41	"	"	1.267	"	"	0.338	3.75	1.507	0.169
42	"	"	0.933	"	"	0.328	4.38	1.472	0.201
43	"	"	1.333	"	0.7	0.523	3.50	1.420	0.435
44	"	"	"	"	0.6	0.625	4.58	1.481	0.280
45	"	"	0.867	"	0.8	0.326	4.27	1.508	0.149
46	"	"	0.800	"	"	0.331	4.43	1.539	0.182
47	"	"	0.733	"	"	0.302	5.13	1.375	0.226
48	"	"	0.667	"	"	0.284	5.23	1.360	0.184
49	"	"	1.333	"	"	0.338	3.18	1.449	0.267
50	"	"	"	"	"	0.353	2.29	1.365	0.251
51	"	"	"	"	"	0.343	2.72	1.417	0.287

RUN	$\frac{L_b}{S_y}$	$\frac{Y_t}{S_y}$	$\frac{Y_s}{S_y}$	$\frac{d_p}{S_y}$	α	$\frac{u}{\sqrt{gS_y}}$	$\frac{uS_y}{D_y}$	$\frac{\Delta\bar{r}_r}{S_y}$	$\frac{uS_y}{D_r}$
				x 10^{-1}					
52	"	"	"	"	"	0.335	3.99	1.391	0.277
53	0.892	0.128	1.000	1.200	"	0.311	4.01	1.441	0.179
54	0.446	0.064	1.500	0.600	"	0.320	3.72	1.227	0.336
55	0.357	0.051	1.600	0.480	"	0.321	2.78	1.087	0.363

Height of particle at start of runs, y/S_y = 802

S_y: 37.5mm (1-52); 25.0mm (53); 50.0mm (54); 62.5mm (55).

way through, though sufficient data were obtained for analysis.

All the results were stored on magnetic tape so that they could be reanalysed if necessary.

5.2 Results

5.2.1 Data analysis

The variables that could be altered may be divided into particle properties and mixer dimensions. Of the former, the diameter and coefficient of restitution of the particle were varied over a wide range. The bar size and thickness and the quantities which define the vertical spacing were the dimensions varied. The horizontal bar spacing remained the same as in Figure 4.3. Initial x and z co-ordinates of the particle were chosen using random numbers and initial values of V_x, V_y and V_z were zero.

Results are presented in dimensionless form with S_y chosen as the characteristic length as the height of mixer necessary to give good mixing is important. A characteristic time is then $\sqrt{S_y/g}$. The dependent variables tabulated are the radial and axial Peclet numbers, the dimensionless velocity and the root mean square lateral jump.

5.2.1.1 Falling velocity

Graphs of the change in height of the particle with time were produced by the computer graph plotting system and found to be approximately linear (Figure 5.6). Estimates of the mean downward particle velocity could be obtained from the output at intervals of one bounce, 10mm or 0.05s, though differences between these were typically less than 1 in 10^3. The values of $u/\sqrt{gS_y}$ in Table 5.1 are based on the least squares regression (Appendix

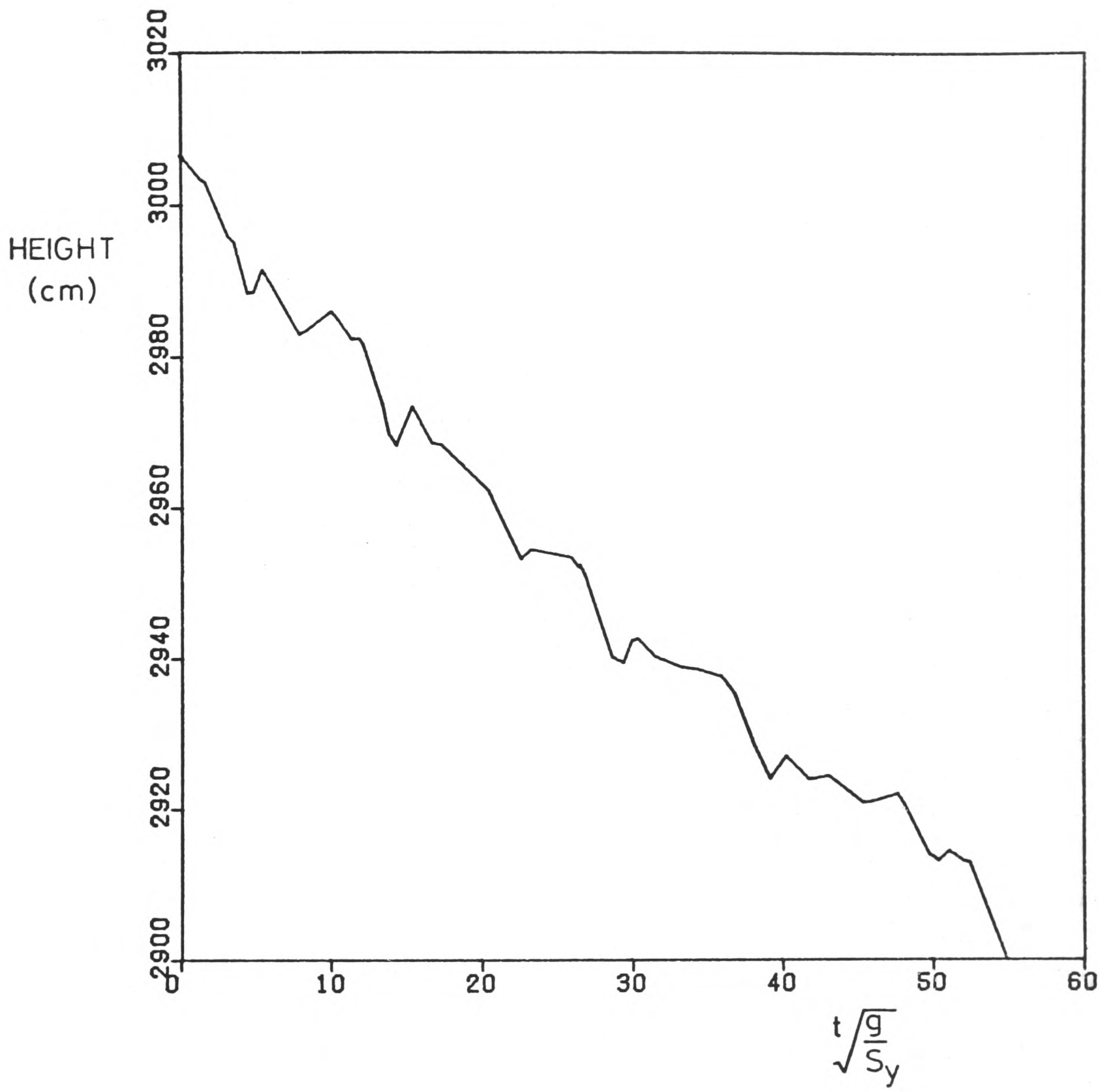


Fig. 5.6 Variation of particle height with time. First 56 bounces only. Run No. 15.

II) to the output at intervals of one bounce. Entry effects were minimised by disregarding the first ten points (Masliyah and Bridgwater, 1974).

5.2.1.2 Diffusion coefficients and Peclet numbers

The determination of diffusion coefficients from numerical data of the type produced by the simulation has been considered by Masliyah and Bridgwater (1974). They show that for a system with short-range order and long-range randomness,

$$|\overline{S_{Jw}}|^2 = J\,|\overline{S_{1w}}|^2 + K_1 \qquad (5.6)$$

where S_{Jw} is the rectilinear jump fluctuation vector in the w direction after J jumps, S_{1w} is the rectilinear jump fluctuation vector in the same direction for one jump and K_1 is a constant. This equation applies for values of J greater than some number which characterises the extent of the short-range order. They then derive the diffusion equation for the system in a manner similar to that used by Einstein (1926) to show that

$$\sigma^2(\Delta w) = 2D_w\tau \qquad (5.7)$$

where $\sigma^2(\Delta w)$ is the variance of displacements in the w direction at time τ and D_w is the diffusion coefficient in that direction. They also show that for τ' greater than some small value,

$$|\overline{S_{Jw}}|^2 = 2D_w\tau' + K_2 \qquad (5.8)$$

where τ' is the mean time for J jumps and K_2 a constant. This is a consequence of the random nature of the system.

The variances of the verticle particle displacements $\sigma^2(\Delta y)$ for various time intervals τ, for a typical run (no. 40), are shown in Figure 5.7. The variance is calculated from the distance between the actual position of the particle after time τ

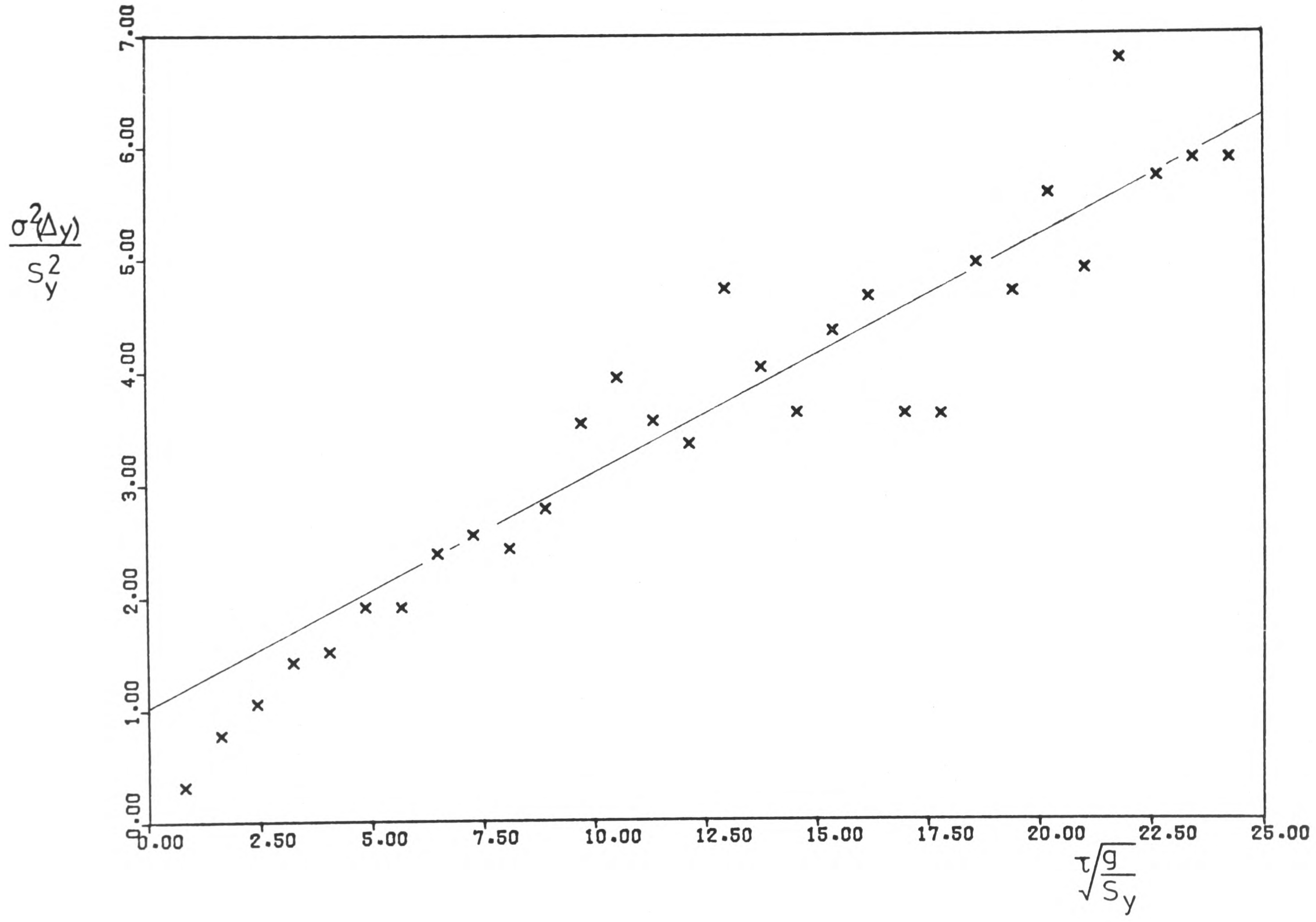


Fig. 5.7 Relationship between $\sigma^2(\Delta y)$ and time interval. Run No. 40.

and the position if the particle had travelled with the mean velocity derived from a least squares fit to the output at constant time intervals. Apart from local order at short time intervals, the points are spread evenly about the regression line, which was fitted to those points with values of τ, $4.8 < \tau\sqrt{g/S_y} < 24.3$. A weighted least squares fit was used (Appendix II) with the weights proportional to the number of values used to calculate the variances. The diffusion coefficient, and hence axial Peclet number uS_y/D_y, can be calculated from the slope of the line using equation 5.7.

The relationship between $|\overline{S_{Jy}}|^2$ and the number of bounces is similar in form (Figure 5.8) and the ratio of the slopes of the regression lines equals $C_s/(g/S_y)^{\frac{1}{2}}$ where C_s is the number of collisions per second.

Figure 5.9 shows the relationship between the variance of particle displacements in the lateral direction $\sigma^2(\Delta r)$ and time interval τ, for run no. 40. The particle is constrained to remain within the confines of the mixer at all times and thus the variance tends to a limit at long time intervals. However the diffusion coefficient can be estimated from the straight portion of the graph.

5.2.1.3 Other variables

Other quantities calculated from the data include the mean collision frequency, the mean, variance and distribution of the times between collisions and the mean bounce length in vertical and lateral directions. The root mean square lateral jump $\Delta\bar{r}_r$, which is tabulated in Table 5.1, is based on those jumps which did not involve a collision with a side wall and therefore refers to an infinitely wide mixer.

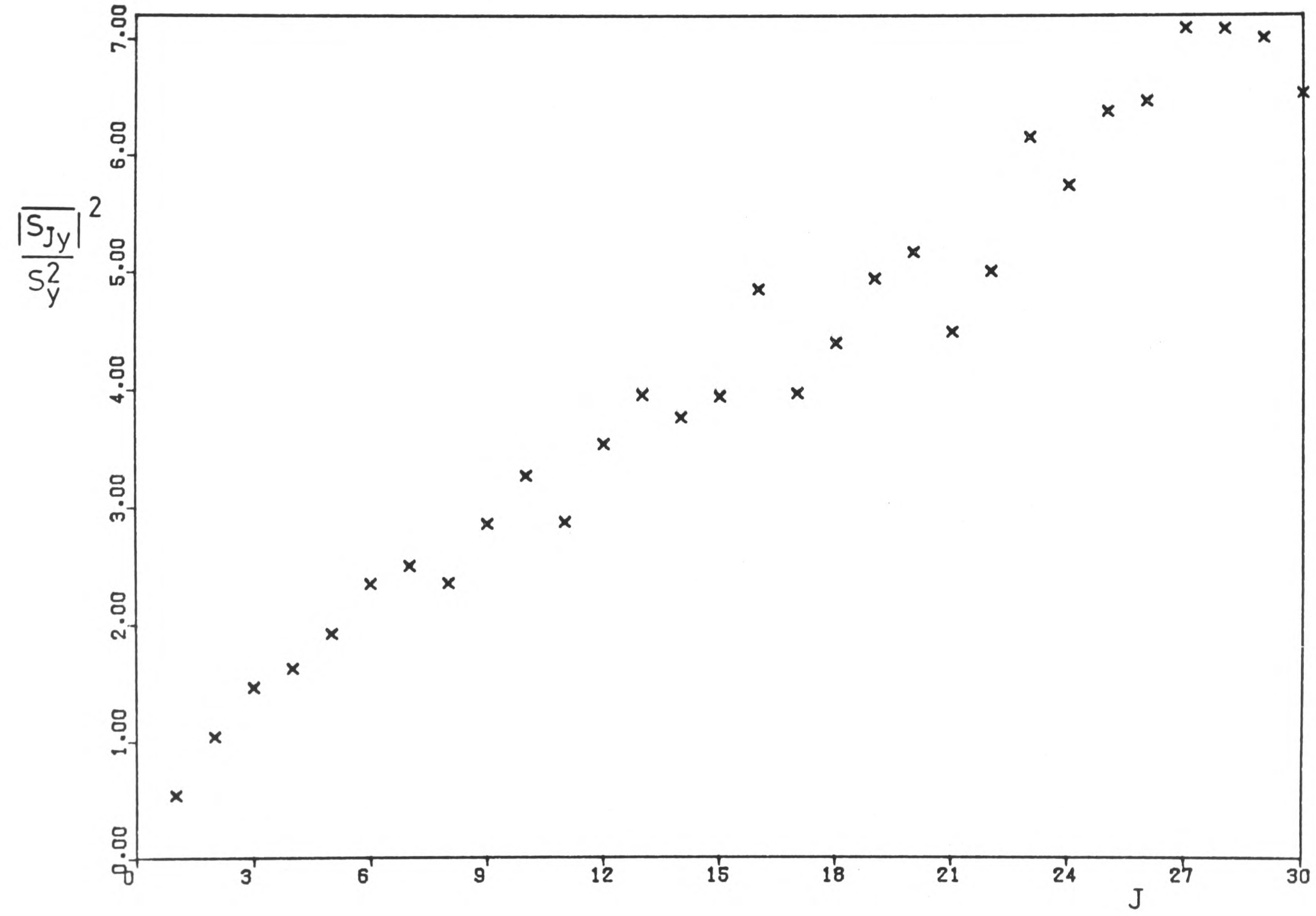


Fig. 5.8 Relationship between $|\overline{S_{Jy}}|^2$ and number of jumps, J. Run No. 40.

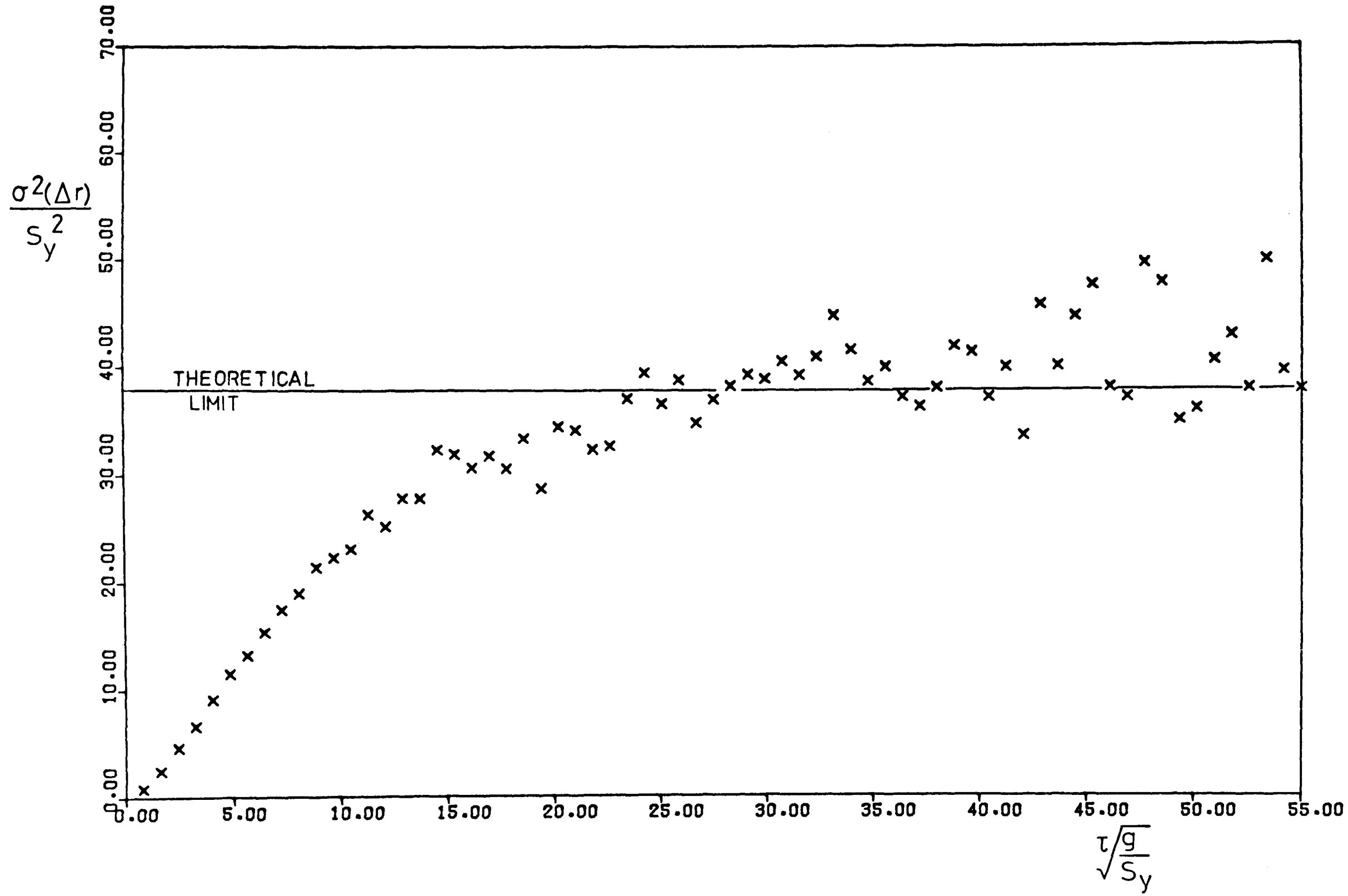


Fig. 5.9 Relationship between $\sigma^2(\Delta r)$ and time interval. Run No. 40.

5.2.2 General considerations

The output from the sixth channel (section 5.1.2.8) was analysed as follows. If the mixer produced a totally random distribution of material then there should be an equal probability of the particle passing through a row of bars in each of the twelve columns. If side effects due to the finite radius of the particle are neglected, and the probabilities are equal to 1/12, then the variance of the number of times the particle passed through rectangles in each column is given by the binomial distribution. For 200 rows of bars this equals 200 x 1/12 x 11/12 = 15.3. F tables can be used to compare the actual variance with this figure and hence determine the probability that the distribution is random. The 95% confidence limits are 0.44 and 1.75 and values of F outside these limits would indicate either ordering of material or inefficient operation. Generally distributions were not statistically different from random with the exception of those runs with low coefficients of restitution.

The number of collisions per second, which is related to the interstitial velocities and the bar spacing, remained approximately constant in the range 16-19 for most experiments. Exceptions were runs in which α was very high (0.95) or very low ($\leq$0.2) and for which $d_p/S_y \geq 0.213$. In all these cases the value was greater but did not exceed 23. If α is high the interstitial velocities will be higher and if d_p is large the distance between collisions is reduced. The high value at low values of α may be due to the ordering of the particle motion as discussed above.

A typical distribution of the times between collisions is shown in Figure 5.10. The mean time between collisions and the mean vertical jump are related; they were considered to be of less importance than the lateral jumps which indicate how well

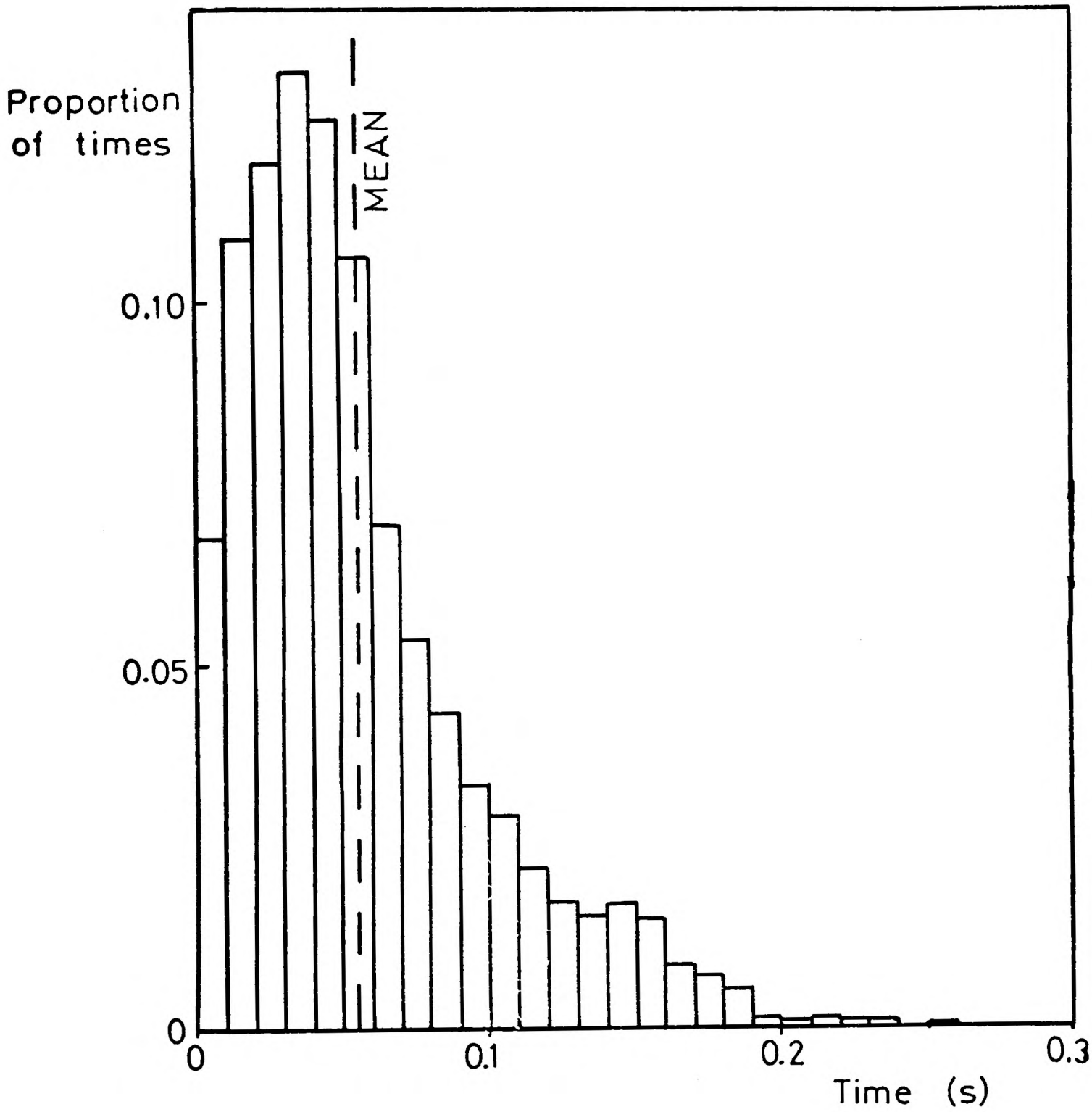


Fig. 5.10 Distribution of times between collisions. Run No. 50.

the equipment is likely to perform as a distributor.

5.2.3 Different programs and reproducibility

Results are reported from three different programs. The first one, used only for runs 1-3, employed single precision arithmetic throughout and used the bar surfaces in Figure 5.4. This was replaced by a double precision version which was used for all other runs except numbers 38, 43 and 44. In these cases the version which employed the bar surfaces shown in Figure 5.5 was used.

The effect of these changes is shown in Figures 5.11-5.14. Figure 5.11 shows the change in the particle velocity. The three values for a coefficient of restitution of 0.6 are almost coincident, though there is more scatter at other values of α. The five points produced by the double precision program with different initial positions for $\alpha = 0.8$ indicates the accuracy of the values. Thus there is apparently no significant difference between the single and double precision programs but the use of curved collision surfaces leads to a slightly higher velocity. This is to be expected as the curved surfaces produce a larger gap between adjacent bars, making it easier for a particle to fall through it. The effect is considered further in section 5.2.6.

Figure 5.12 shows that the use of different programs has no significant effect on the root mean square lateral jump; the magnitude of the possible error in the results is indicated by the values from the double precision program at $\alpha = 0.8$.

The effect on the axial and radial Peclet numbers is shown in Figures 5.13 and 5.14. Again the results at $\alpha = 0.8$ indicate that the differences between the programs are not significant because of the scatter in the values.

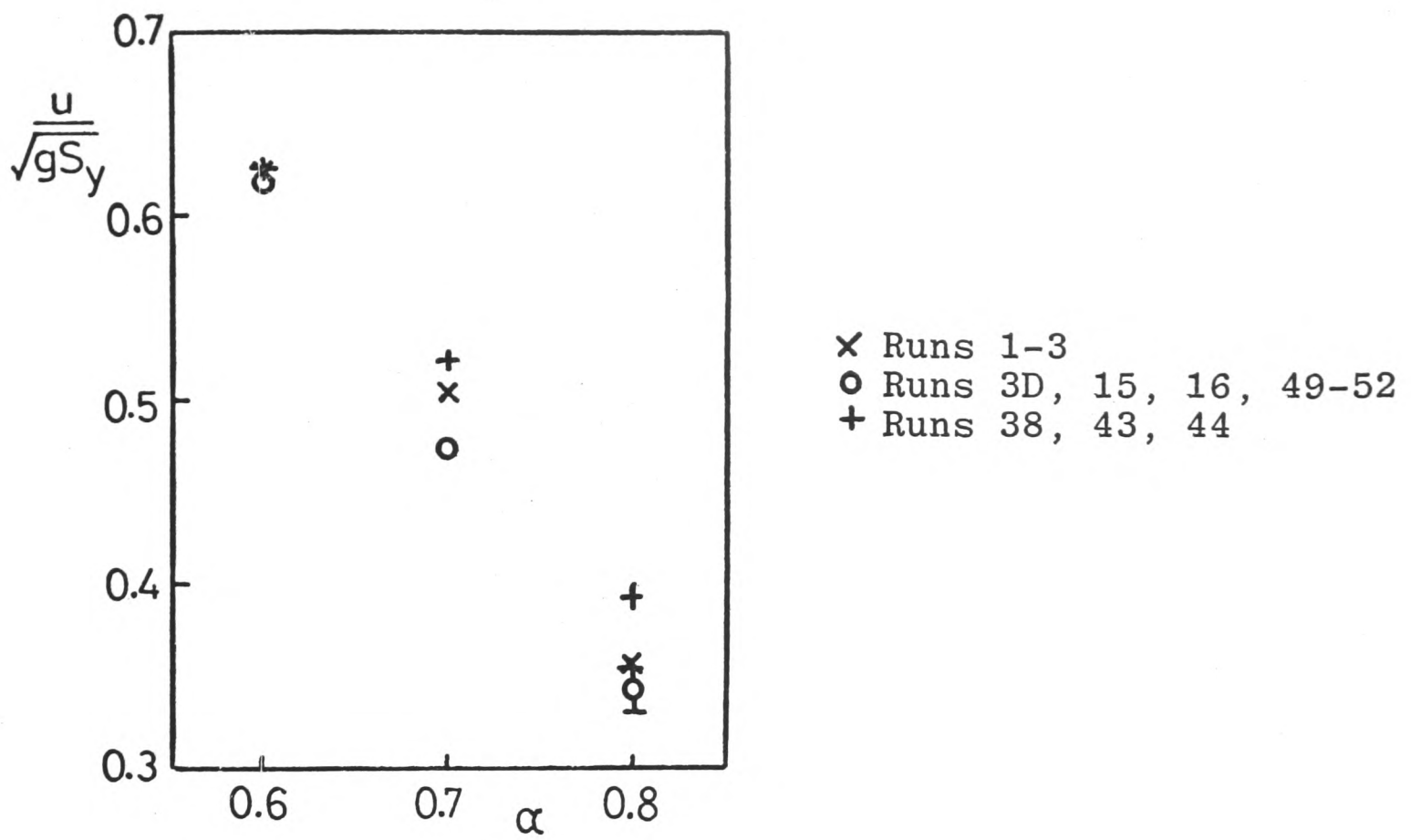


Fig. 5.11 Consistency of results. Effect on particle velocity.

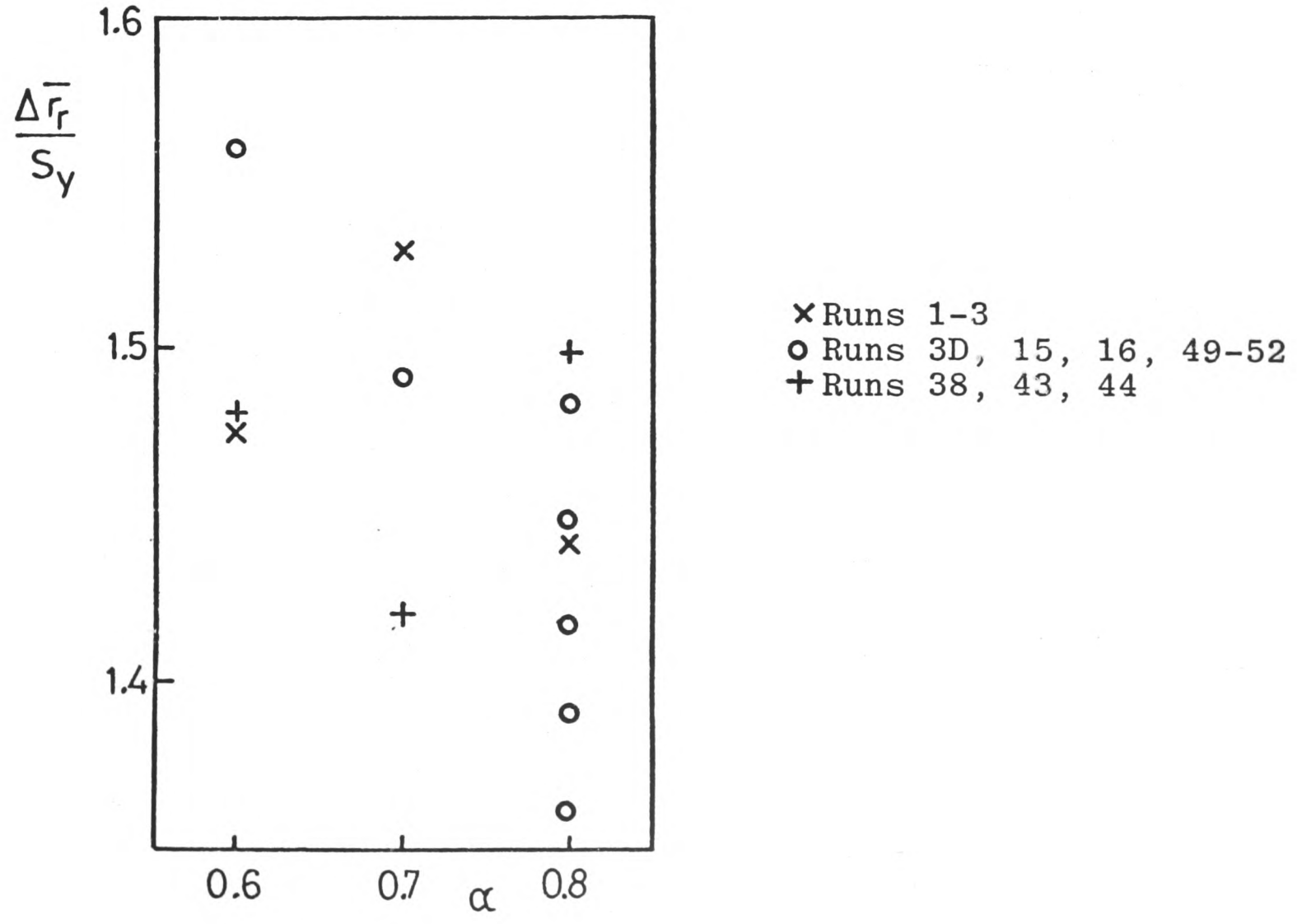


Fig. 5.12 Consistency of results. Effect on root mean square lateral jump.

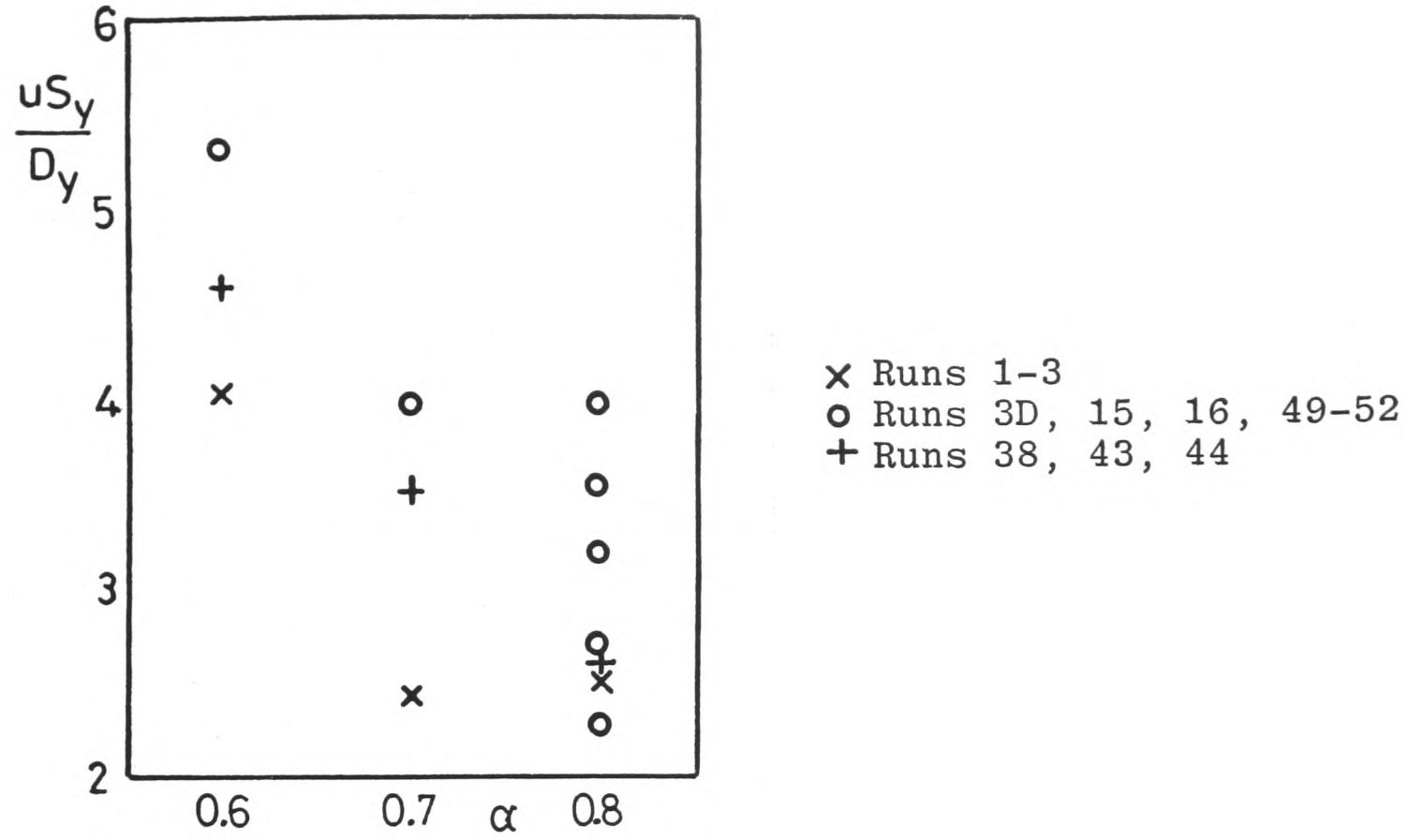


Fig. 5.13 Consistency of results. Effect on axial Peclet number.

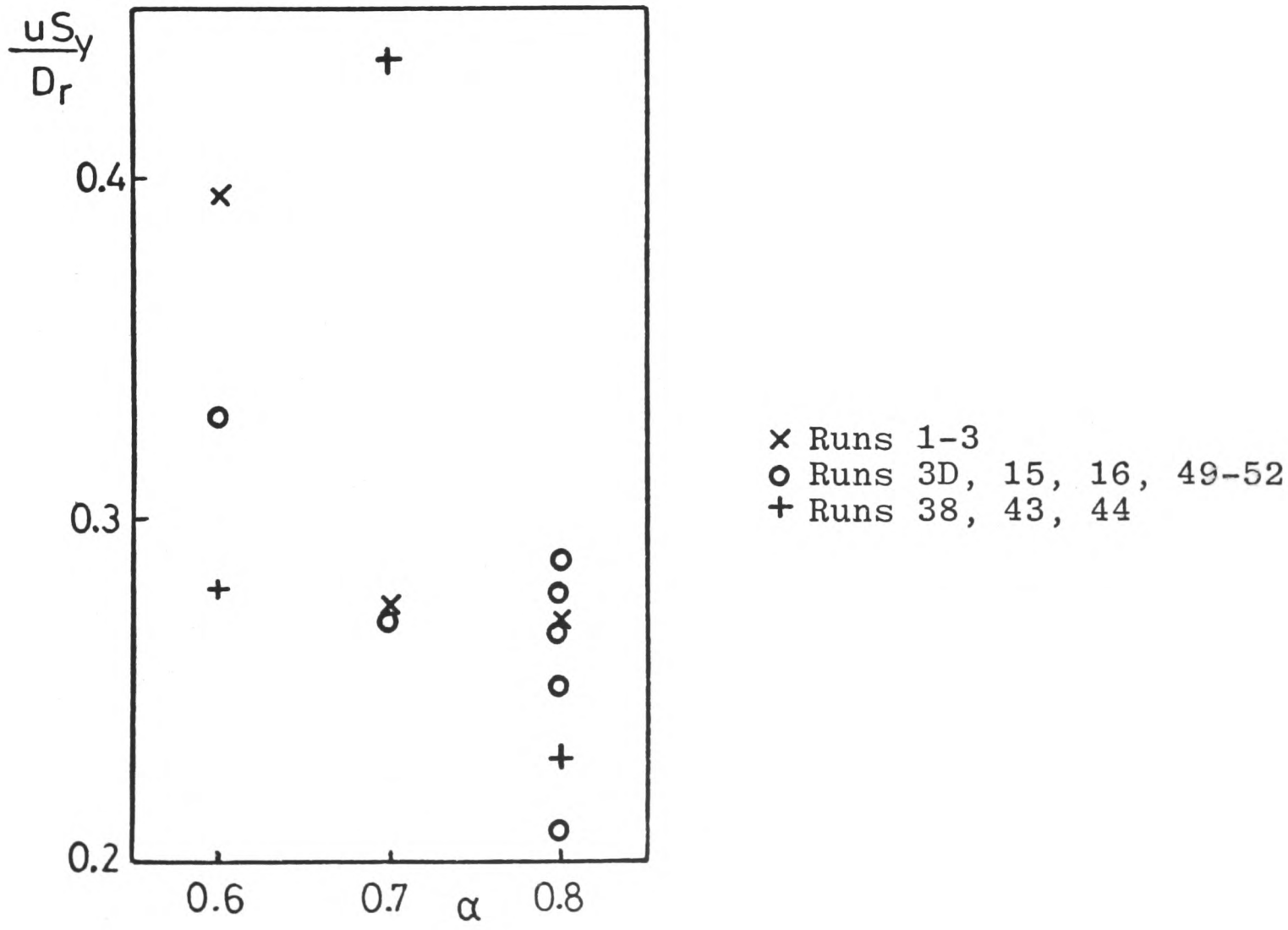


Fig. 5.14 Consistency of results. Effect on radial Peclet number.

Since runs with the version of the program which used curved collision surfaces produced slightly different velocities, they were not considered in the following sections.

5.2.4 Coefficient of restitution

The dimensionless velocities varied by a factor of six between those at very low and those at very high coefficients of restitution. The plot is linear over most of the range (Figure 5.15).though the value for $\alpha = 0.1$ is anomalous. Theoretically the plot should also pass through the point (1.0, 0.0).

Anomalous behaviour for $\alpha \leq 0.2$ is also shown by the root mean square lateral jump (Figure 5.16) and the axial Peclet number (Figure 5.17). The former increases as α decreases from 0.95 to 0.3 but then decreases sharply. The latter shows an approximately linear relationship for $0.3 < \alpha < 0.95$ but increases to about 16 at $\alpha = 0.2$ and 95 at $\alpha = 0.1$. This behaviour at low values of α may be related to the increased use of the sliding routine in the program.

Changes in the radial Peclet number are less dramatic, results varying by a factor of 3 over the range. An impression of the relation between uS_y/D_r and α is shown in Figure 5.18. The former varies little for $\alpha < 0.6$, but then decreases from about 0.35 to 0.1 as α increases to 0.95. This almost exactly corresponds to the change in $u/\sqrt{gS_y}$ for $0.6 \leqslant \alpha \leqslant 0.95$ and thus the diffusion coefficient is approximately constant over this range. The increase in the radial Peclet number at lower values of α may explain the experimental observation that lead shot (which has a low coefficient of restitution) was not dispersed as well as other materials by the three-dimensional mixer. If this is the

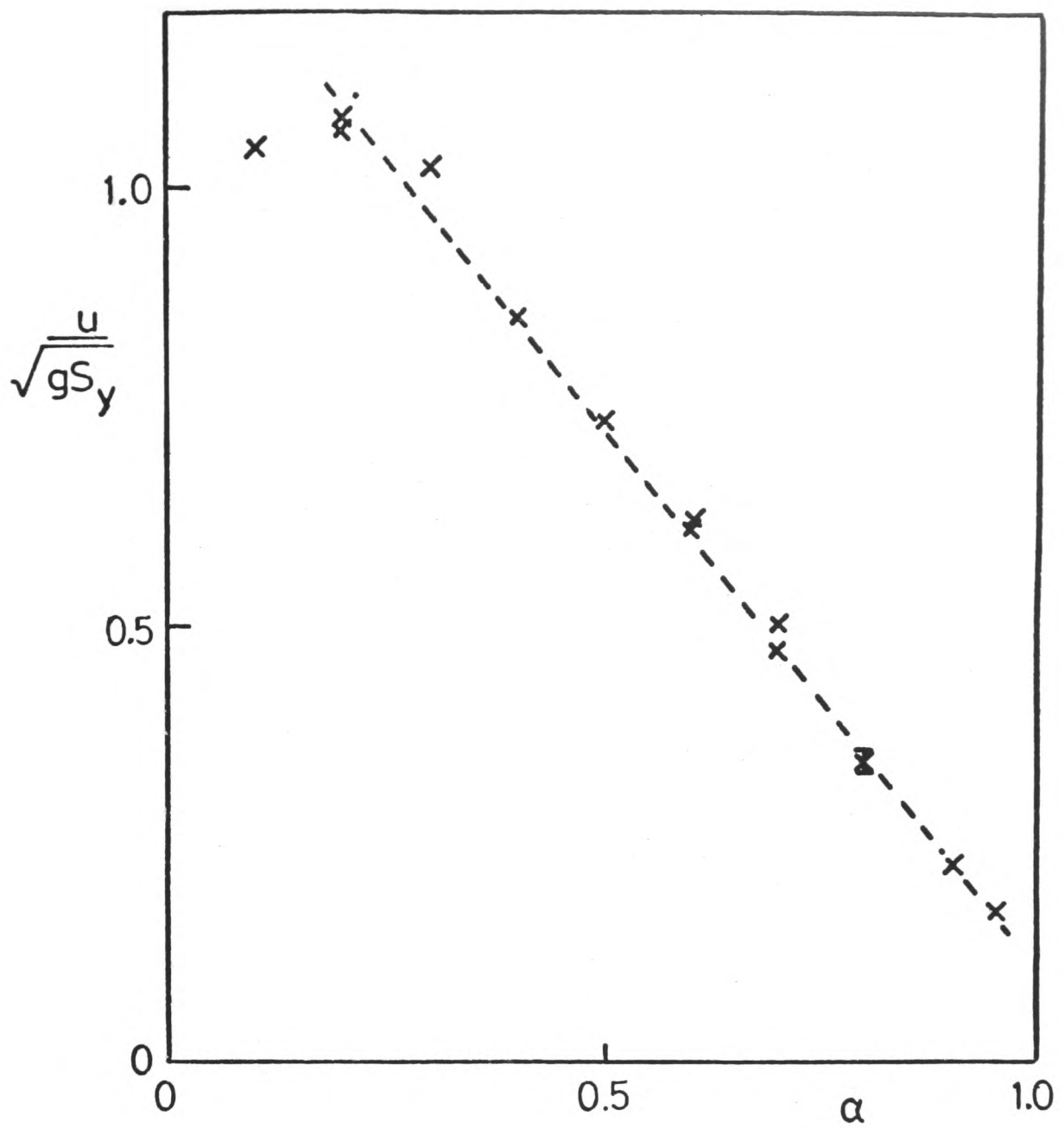


Fig. 5.15 Coefficient of restitution. Effect on particle velocity.

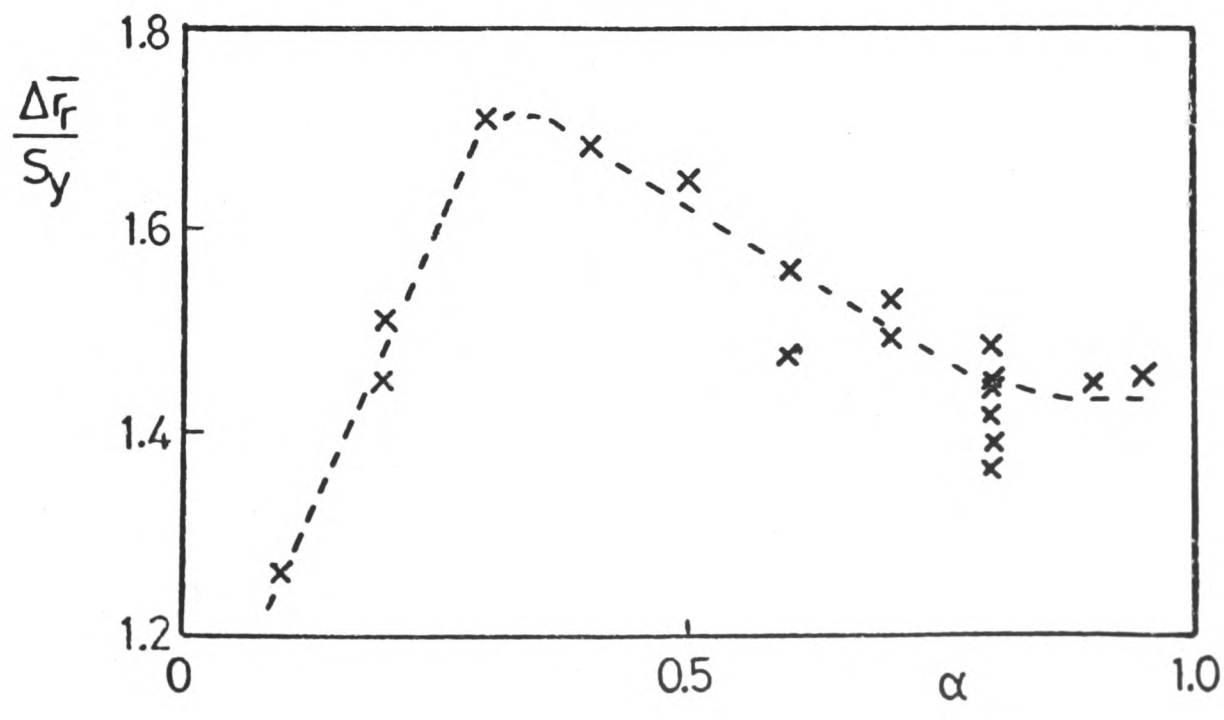


Fig. 5.16 Coefficient of restitution. Effect on root mean square lateral jump.

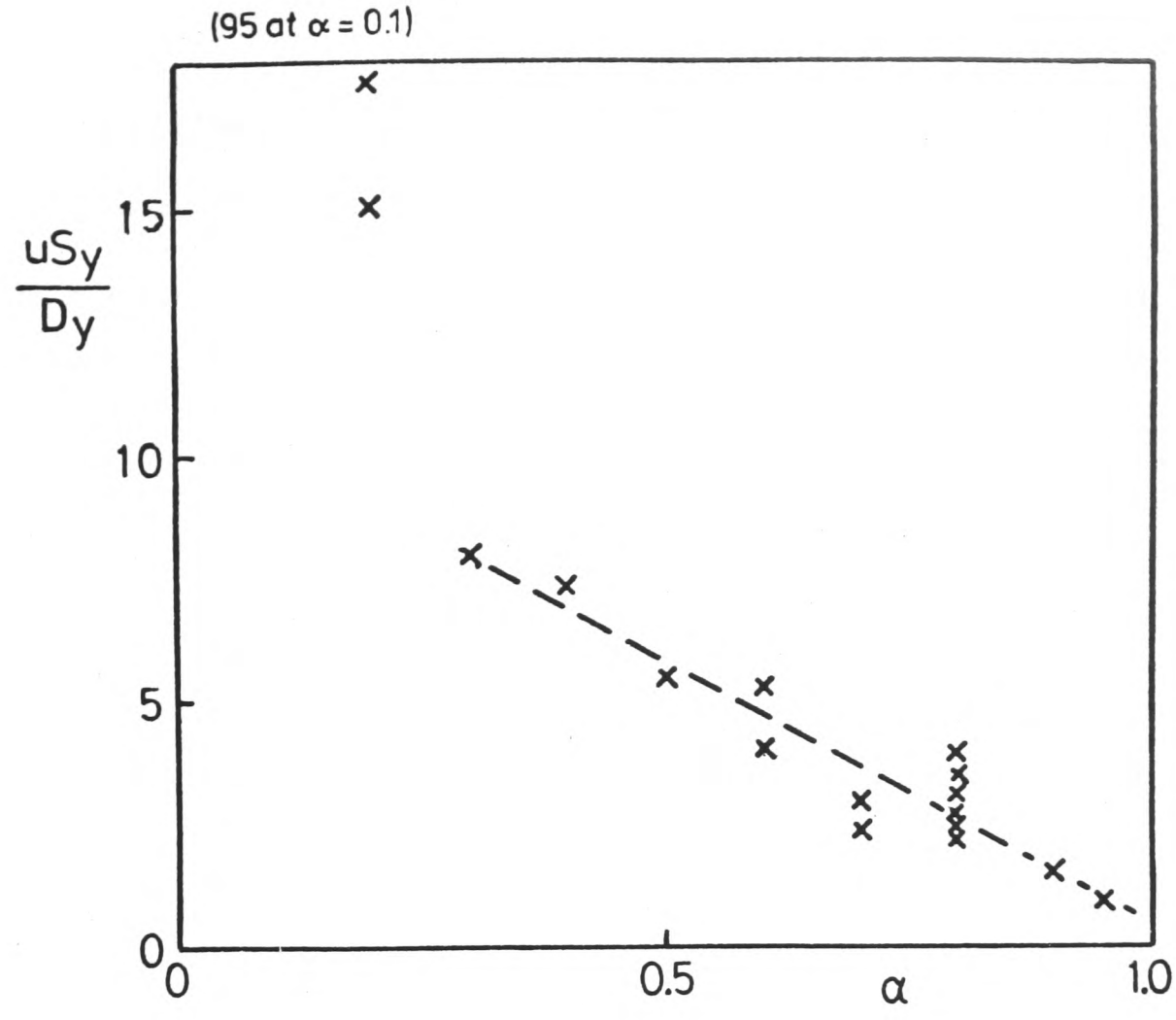


Fig. 5.17 Coefficient of restitution. Effect on axial Peclet number.

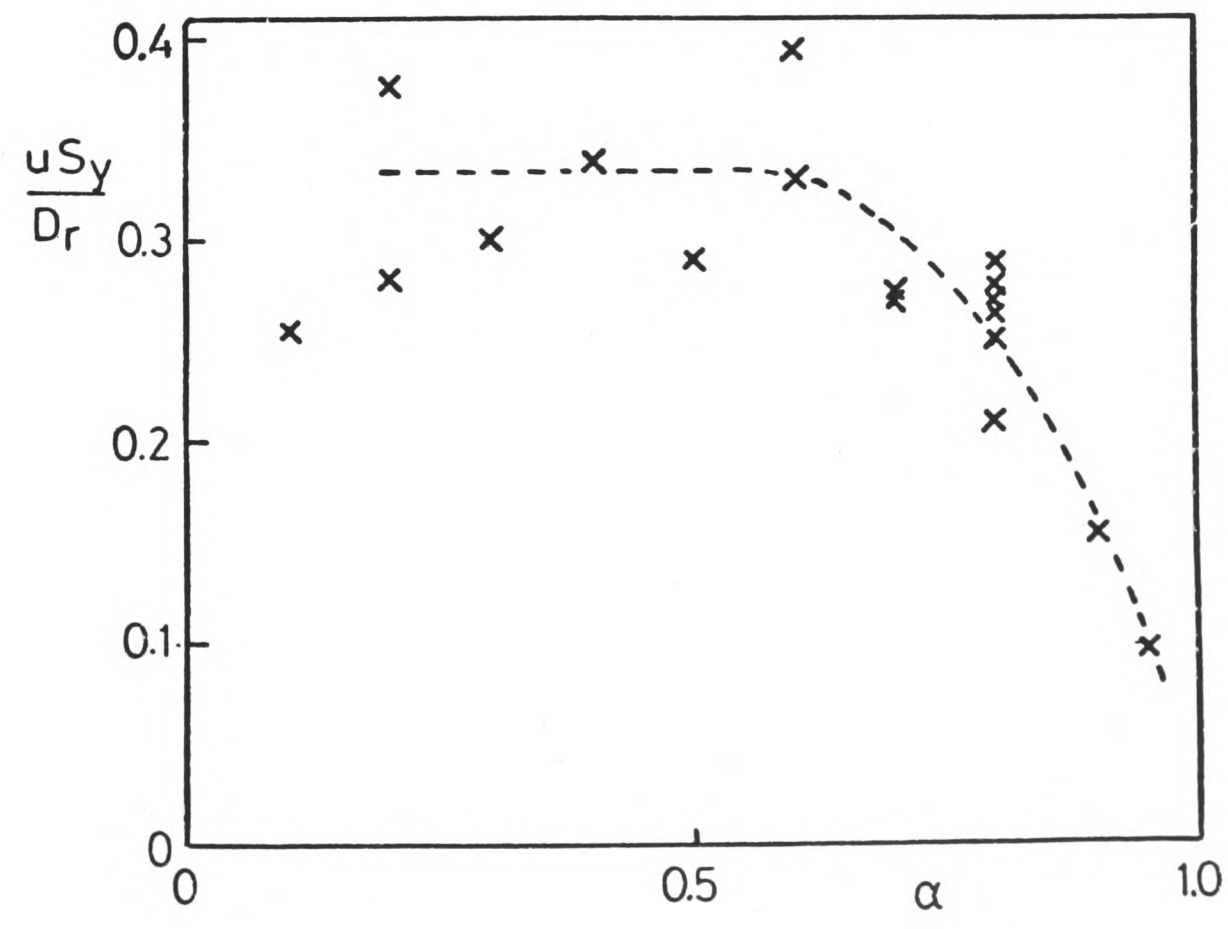


Fig. 5.18 Coefficient of restitution. Effect on radial Peclet number.

case, an increase in the height of the unit would have improved its distribution. The graphs of $\sigma^2(\Delta r)/S_y^2$ against $\Delta y/S_y$ (fig 5.42) confirm this. The limiting value of the former is reached after an interval of about 0.5m for run 16 (Pe_r = 0.207, α = 0.8) and after about 0.7m for run 6 (Pe_r = 0.302, α = 0.3). The effective height of the unit built was 0.6m.

A reduction in the coefficient of restitution would be expected to give a greater downward velocity as the particle would lose more energy per collision. The rate of loss of potential energy by the particle, mgu, is equal to the rate of loss of kinetic energy due to collisions. If V_f is the impact velocity and V_i the rebound velocity, the latter equals C_s. $(m\overline{V_f^2}/2 - m\overline{V_i^2}/2)$, or $m\overline{V_f^2}\bar{C}_s(1-\alpha^2)\overline{\sin^2\theta_f}/2$ applying equation 3.57. Since, from figure 5.15, u is proportional to α, $\overline{V_f^2}$ is proportional to $\alpha/(1-\alpha^2)$ if $\sin^2\theta_f$ is not a function of α. Unfortunately the data to confirm this was not available, though interstitial velocities might be expected to increase with the coefficient of restitution.

5.2.5 Particle diameter

The other particle property that could be altered in the program was the diameter. The maximum value is limited by the size of the gap between bars at the end of a row and the side of the mixer. The program logic would not accept the value zero and so the value $d_p/S_y = 6 \times 10^{-6}$ was used instead.

Figure 5.19 shows that, as would be expected, smaller particles fall through the mixer faster as there is more room for them to pass through rows of bars. The decrease in the root mean square lateral jump for larger particles (Figure 5.20) is due to the centres of such particles not having to travel so far

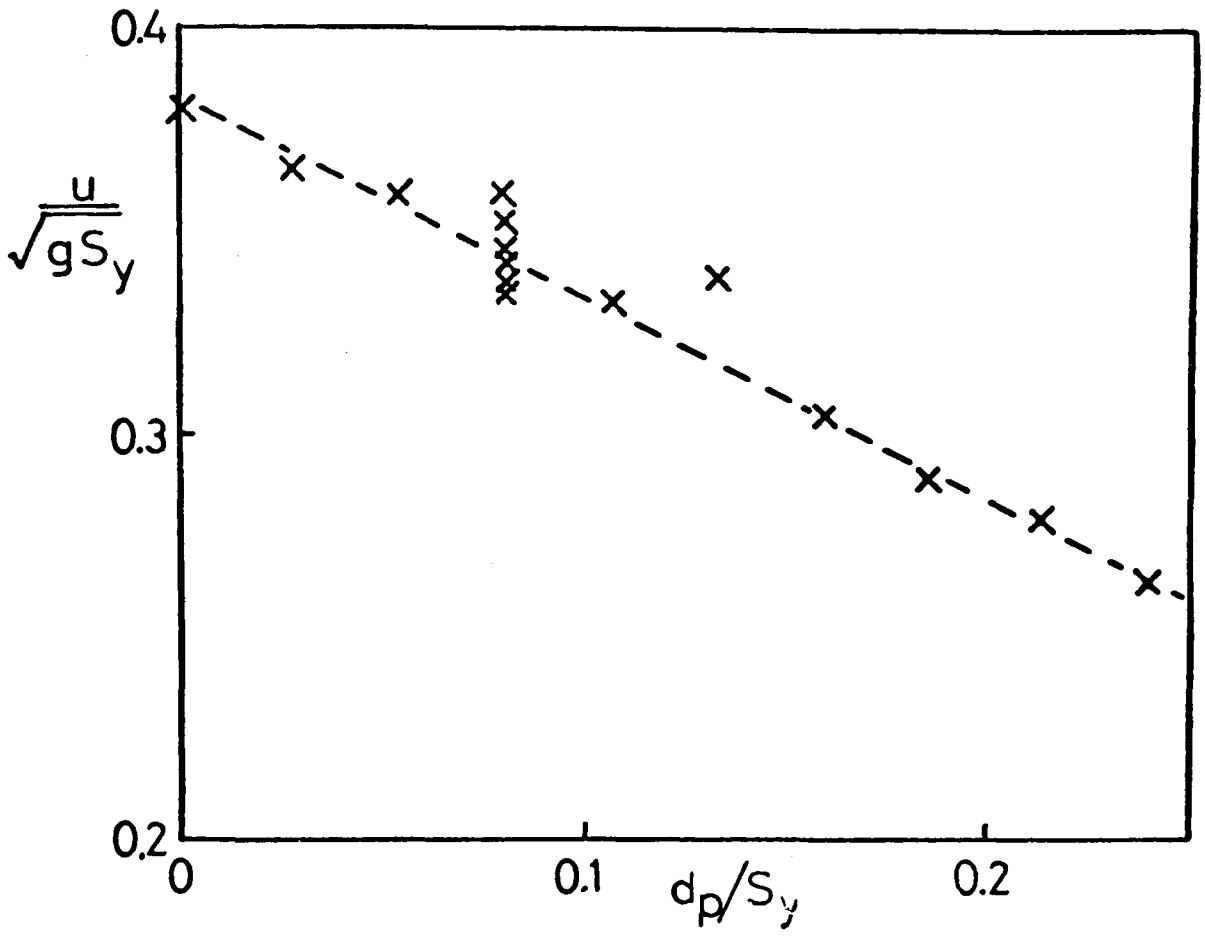


Fig. 5.19 Particle diameter. Effect on velocity.

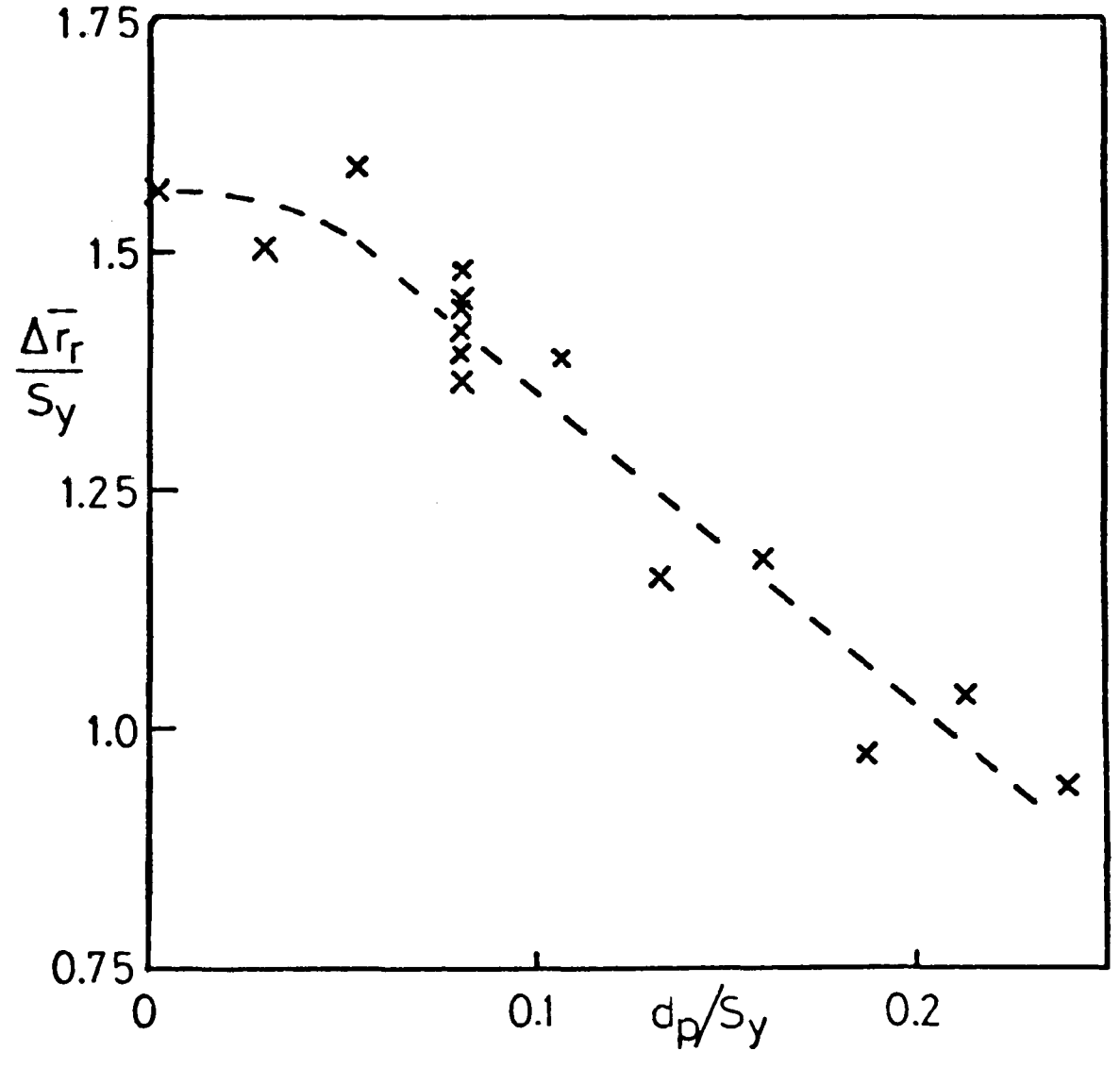


Fig. 5.20 Particle diameter. Effect on root mean square lateral jump.

from one collision to the next and also because, being larger, the particles have a greater chance of colliding with a bar. These effects combine to result in lower axial and radial Peclet numbers for smaller particles (Figures 5.21 and 5.22) which therefore diffuse faster.

In the three-dimensional mixer design, the maximum value of d_p/L_b chosen was approximately 0.1, i.e. $d_p/S_y = 0.06$. Changes in the Peclet numbers are relatively small below this value and thus the marked reduction in the values of D_r and D_y at high values of d_p/S_y is unlikely to have any practical significance.

5.2.6 Bar size

Increasing the bar size decreases both the velocity of the particle and the root mean square lateral jump as shown in Figures 5.23 and 5.24. The effect is similar to that caused by increasing the size of the particle as described in the previous section. However both axial and radial Peclet numbers increase with increasing L_b/S_y (Figures 5.25 and 5.26) and thus more diffusion per unit height of mixer is obtained if smaller bars are used, at least for a 3mm dia. particle with $\alpha = 0.8$. This may be a consequence of the increase in the mean jump length.

If the straight collision surfaces (Figure 5.4) are replaced by curved ones (Figure 5.5), there is an increase in the effective gap between the bars, which for the conditions in runs 38, 43 and 44 is 16%. This is equivalent to a reduction in L_b/S_y from 0.595 to 0.555 if straight surfaces are used, and Figure 5.23 indicates that this would lead to an increase in $u/\sqrt{gS_y}$ to 0.395, which agrees well with the effect in Figure 5.11. Thus the use of straight rather than curved collision

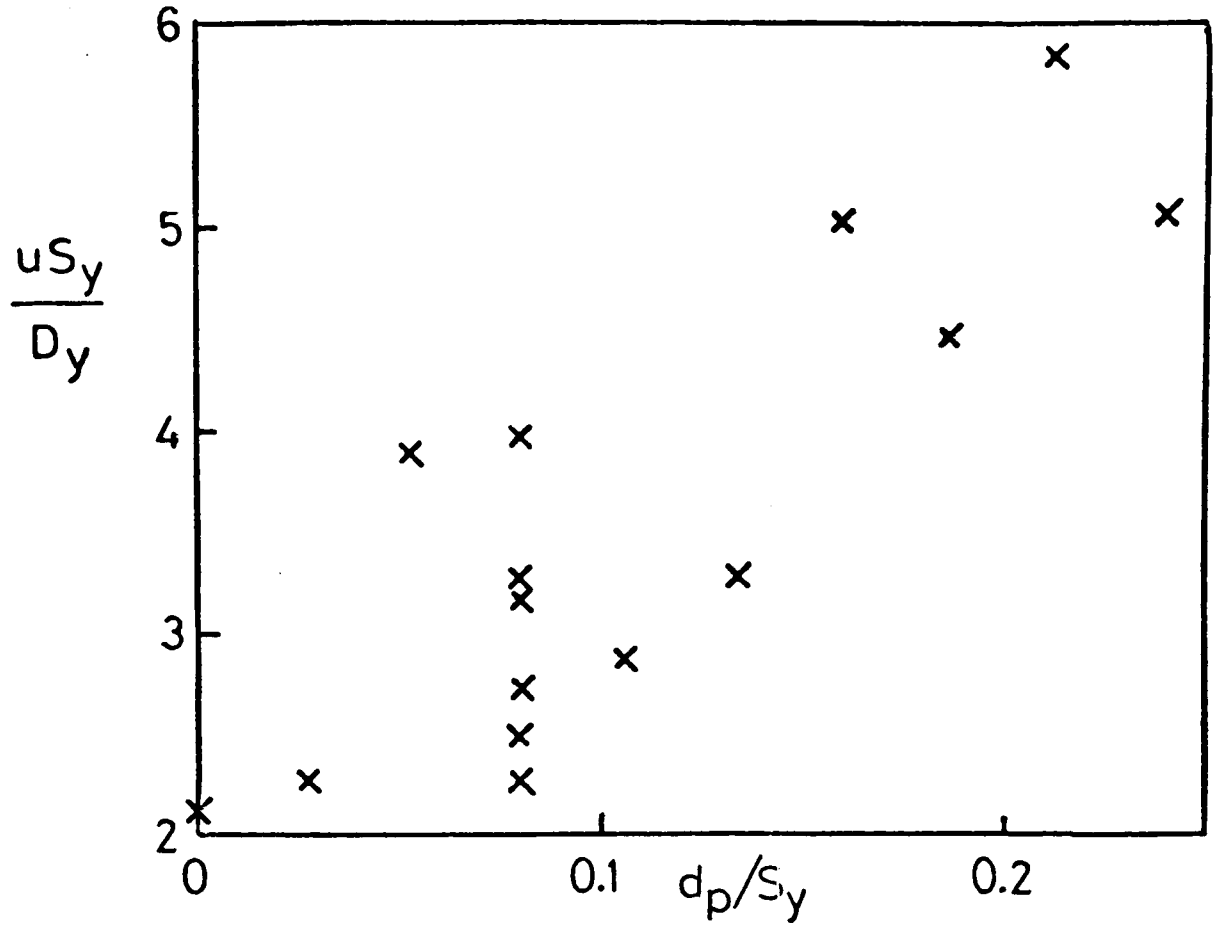


Fig. 5.21 Particle diameter. Effect on axial Peclet number.

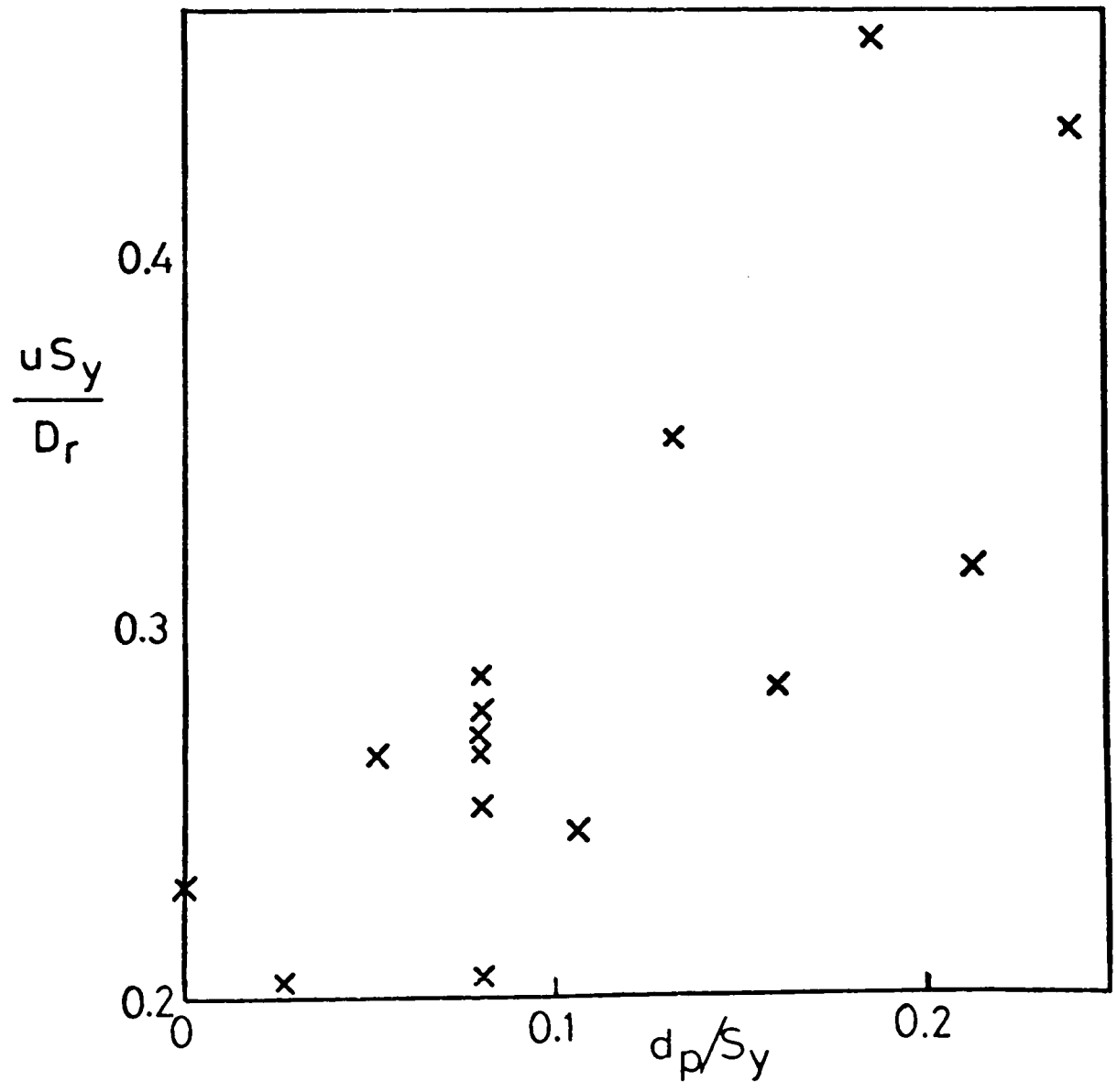


Fig. 5.22 Particle diameter. Effect on radial Peclet number.

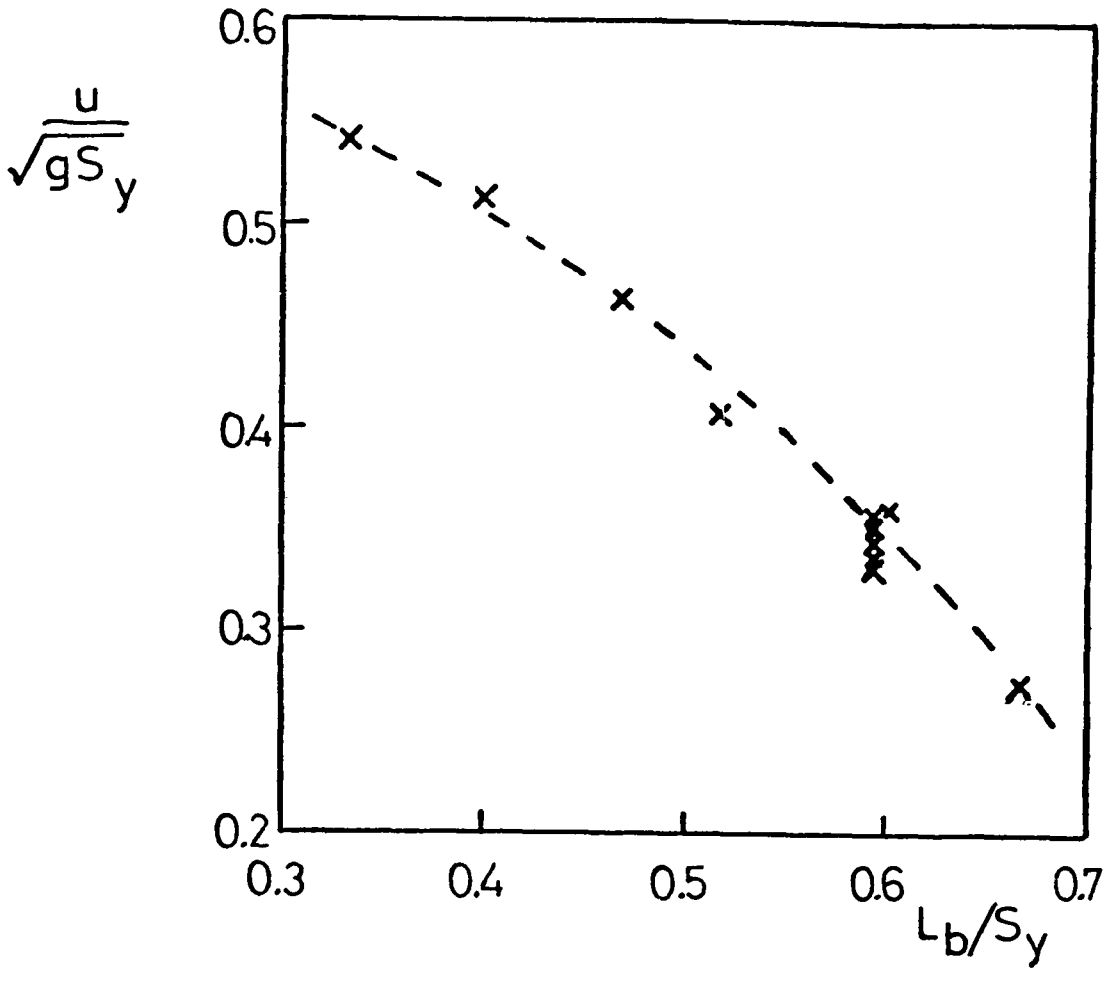


Fig. 5.23 Bar size. Effect on velocity.

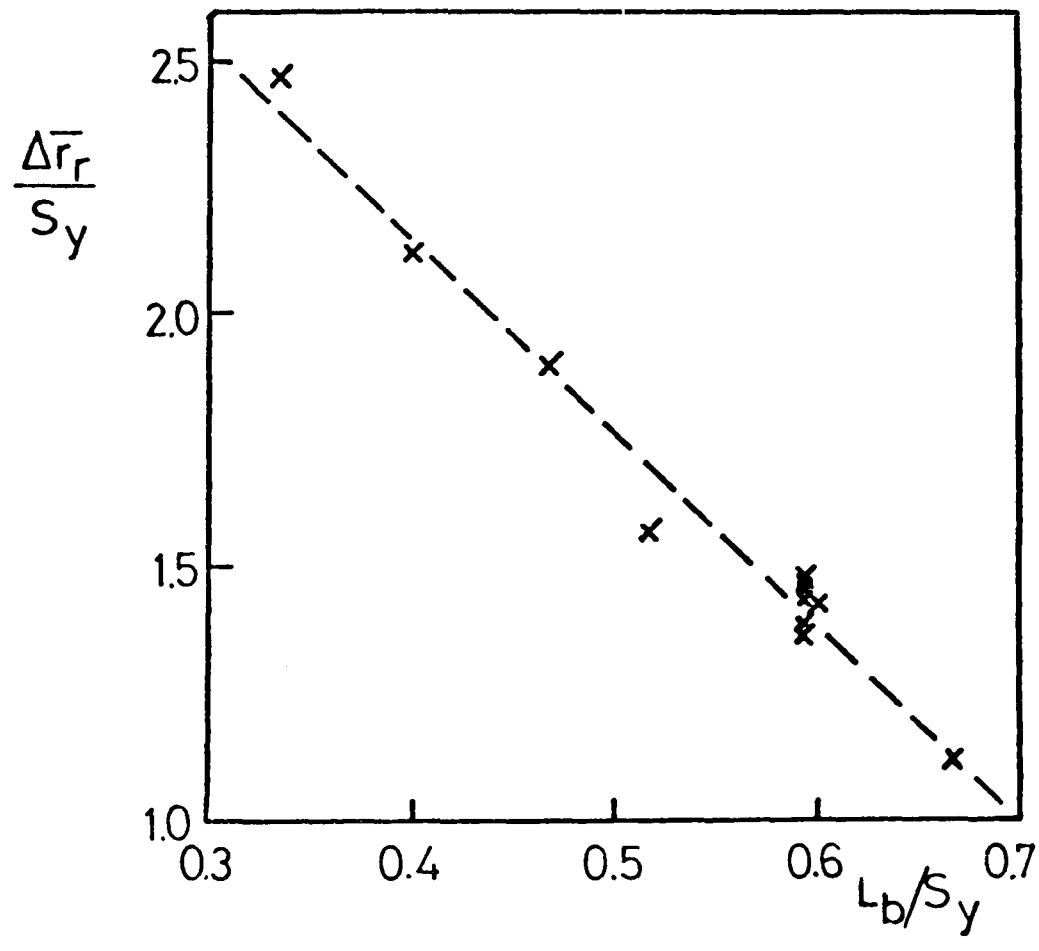


Fig. 5.24 Bar size. Effect on root mean square lateral jump.

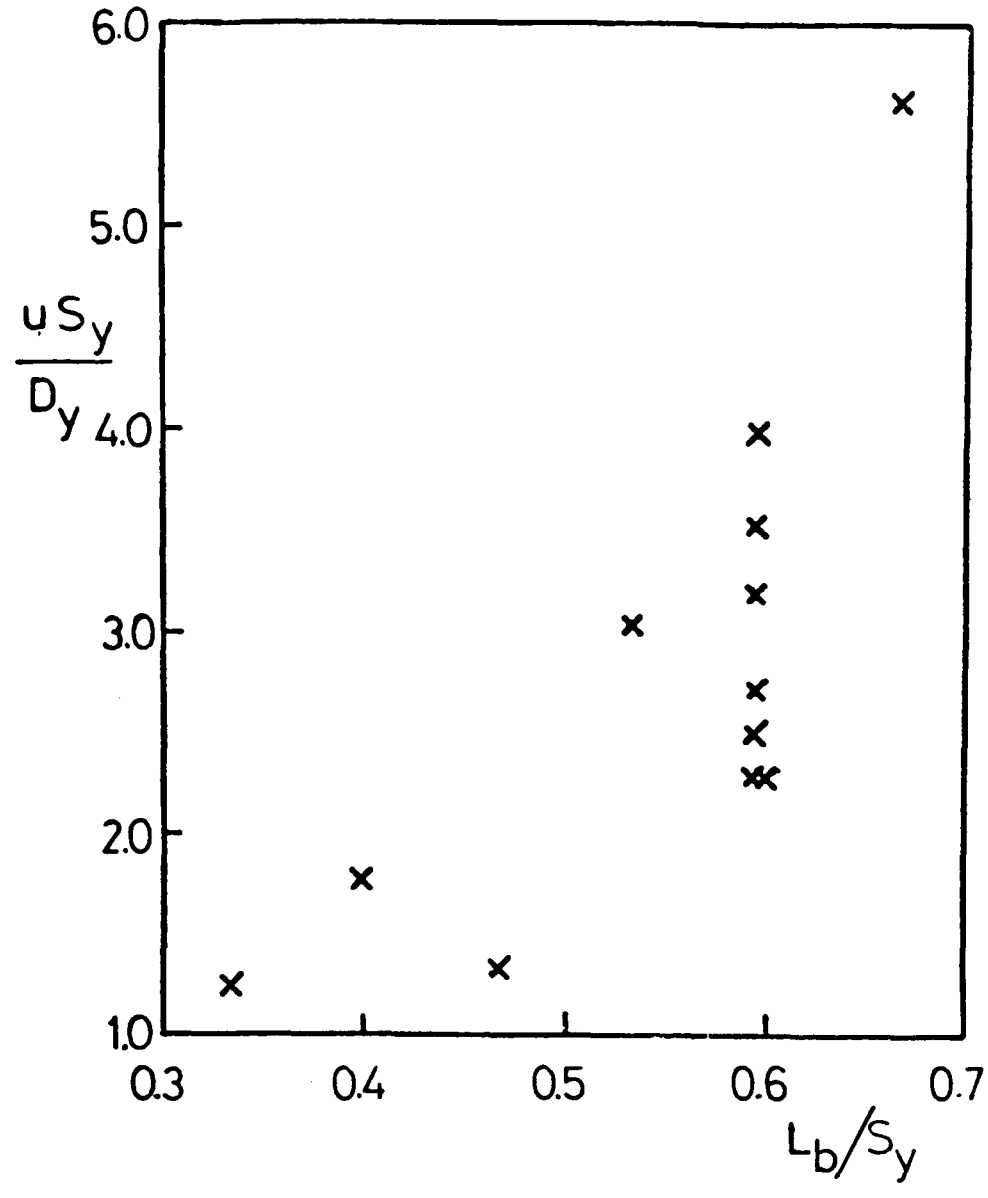


Fig. 5.25 Bar size. Effect on axial Peclet number.

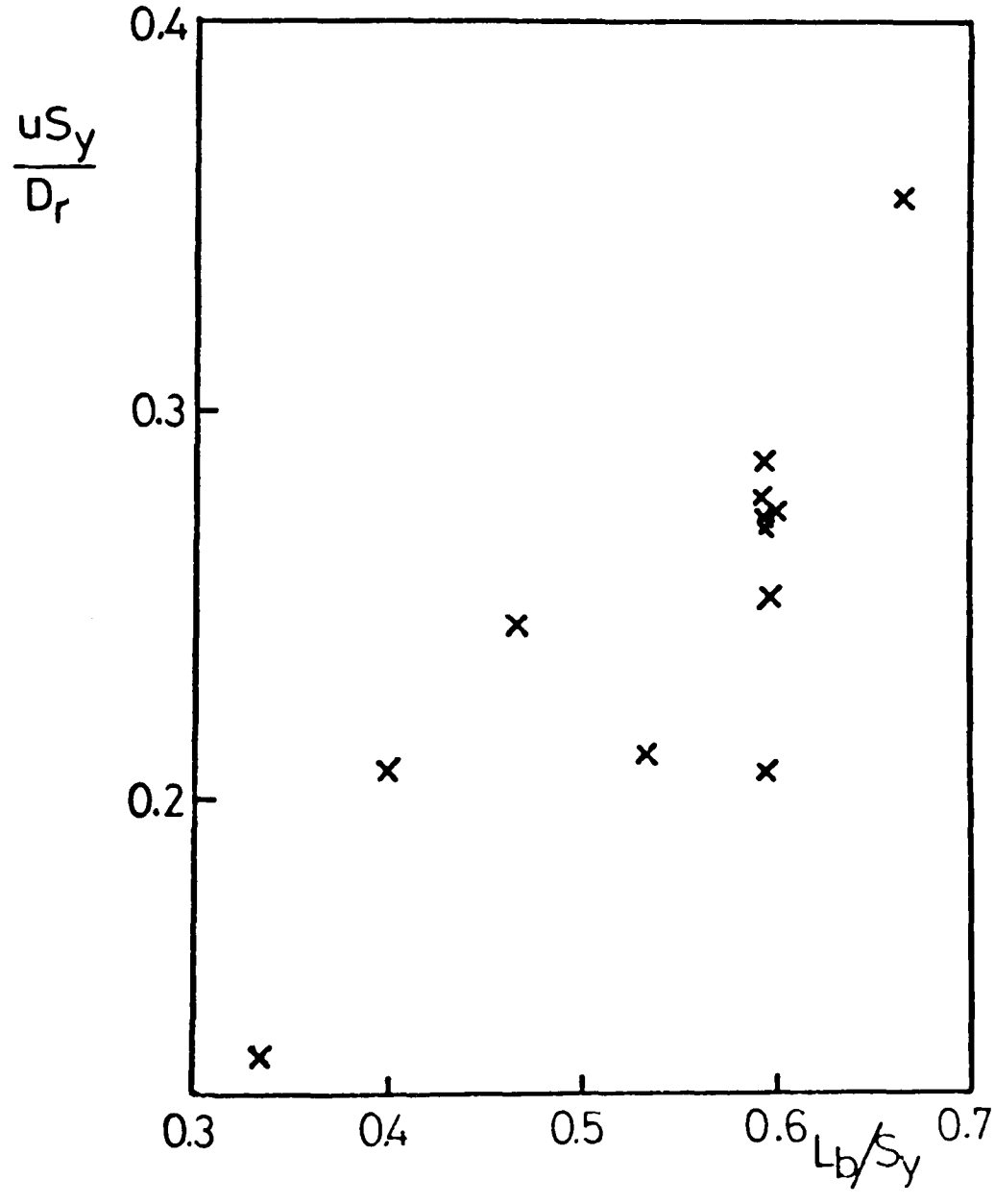


Fig. 5.26 Bar size. Effect on radial Peclet number.

surfaces is reasonable if allowance is made for the change in the effective bar size.

5.2.7 Bar thickness

It was expected that changes in the thickness of a bar would have, at most, a small effect. The slight increase in velocity with Y_t/S_y (Figure 5.27) presumably arises because when the particle is travelling upwards and hits the underside of a bar, it does not have so far to travel. The corresponding slight decrease in $\Delta\bar{r}_r/S_y$ (Figure 5.28) is probably due to the reduction in voidage. Any effect on the Peclet numbers is eclipsed by the scatter in the results (Figures 5.29 and 5.30).

5.2.8 Bar spacing (i)

Two quantities describe the bar spacing. Y_s is the distance between two adjacent parallel rows of bars while S_y is the mean vertical bar spacing. Thus in the unit shown in Figure 4.3 Y_s is 50mm and S_y is 37.5mm.

A slight change in the particle velocity is apparent from Figure 5.31 though changes in the root mean square lateral jump are obscured by scatter (Figure 5.32). The axial Peclet number shows a marked decrease as Y_s/S_y increases (Figure 5.33), whereas the radial Peclet number shows a corresponding slight increase (Figure 5.34). This implies that an improvement in the design of these mixers could be achieved by mounting the pairs of rows of parallel bars closer together, presumably because this increases the probability of a particle collision with a bar. Corroboration is provided by the corresponding reduction in $u/\sqrt{gS_y}$. It was also noticed that in run 48 ($Y_s/S_y = 0.667$) there were approximately 16% more collisions than in those runs with $Y_s/S_y = 1.333$.

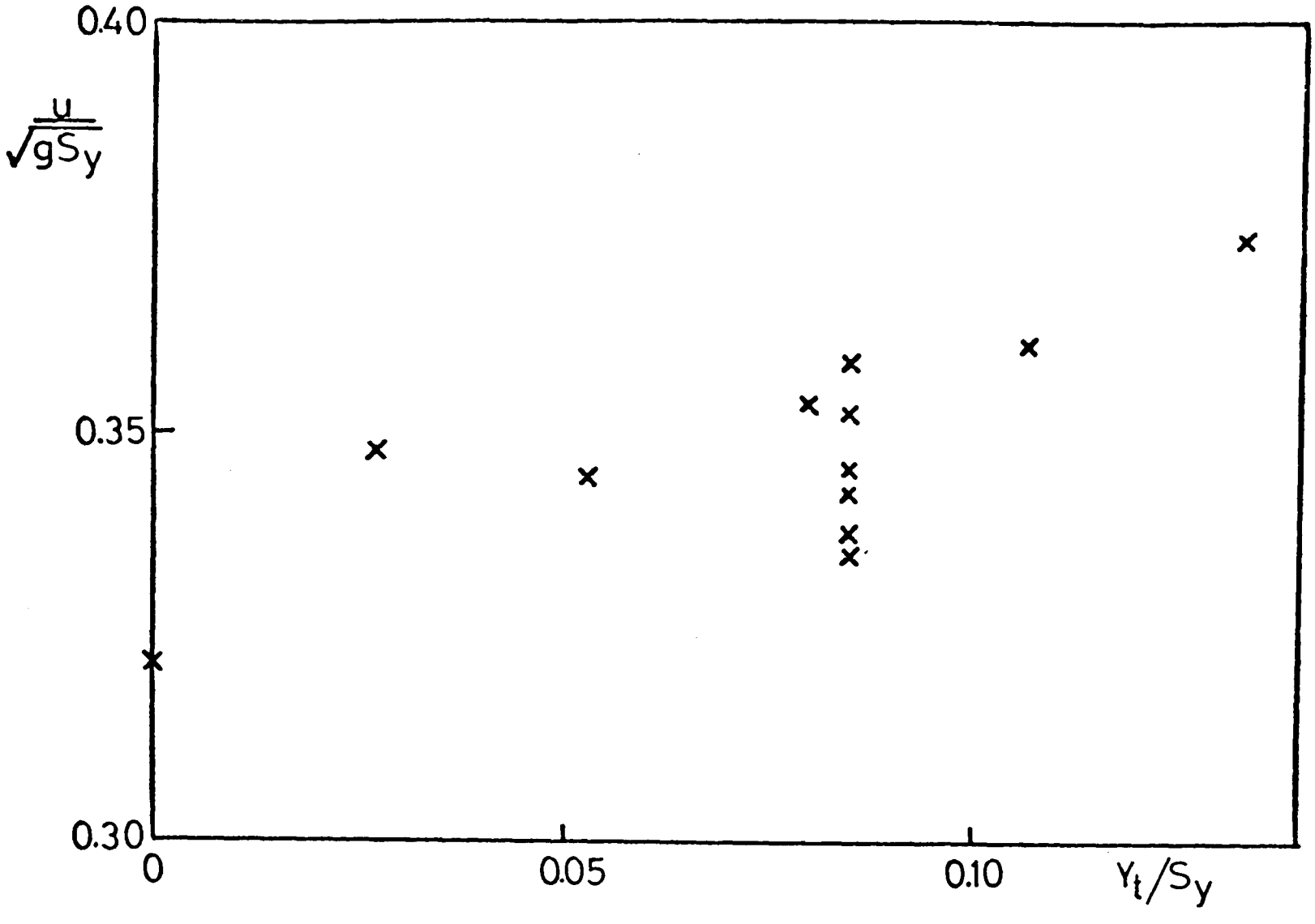


Fig. 5.27 Bar thickness. Effect on velocity.

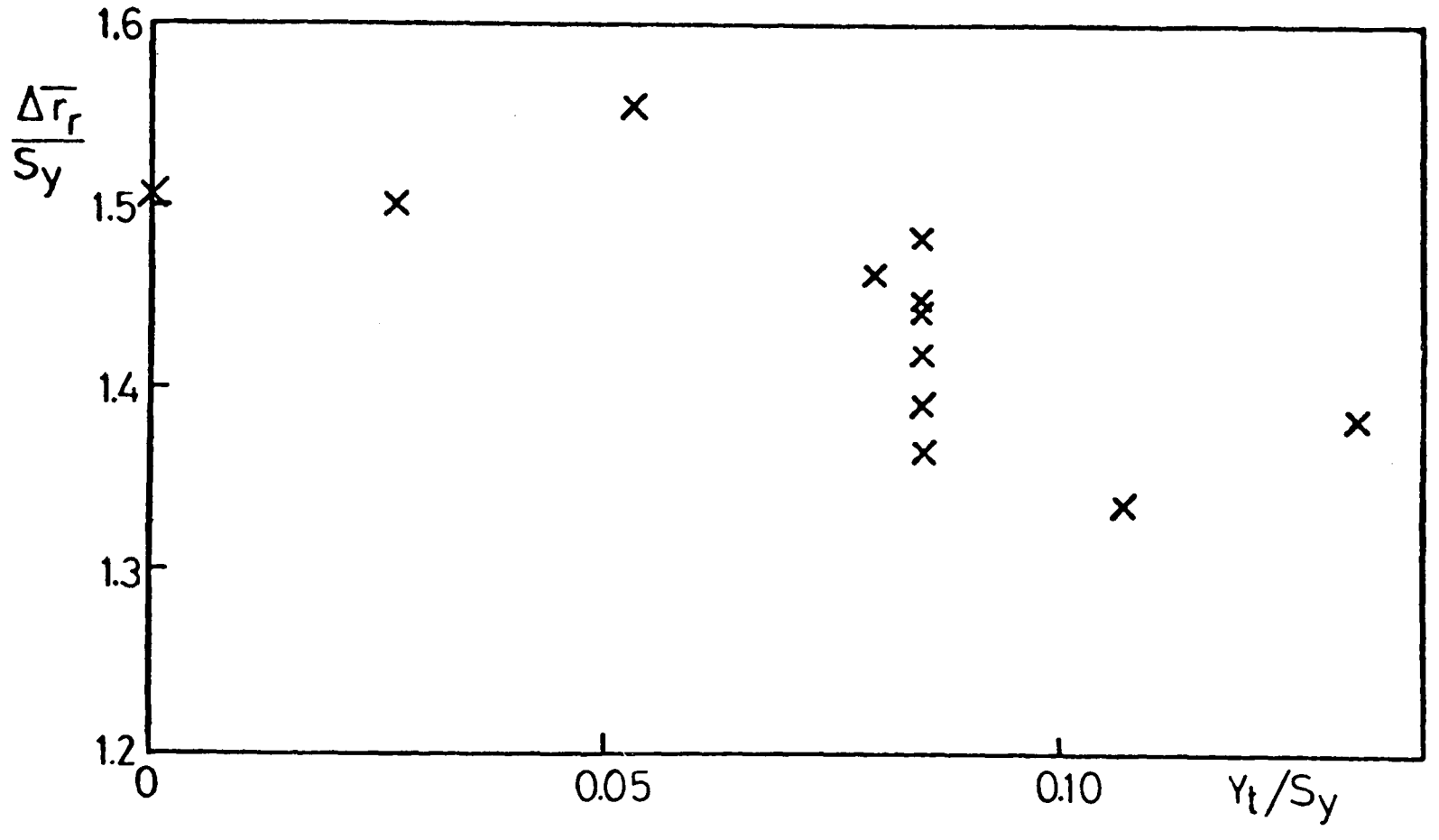


Fig. 5.28 Bar thickness. Effect on root mean square lateral jump.

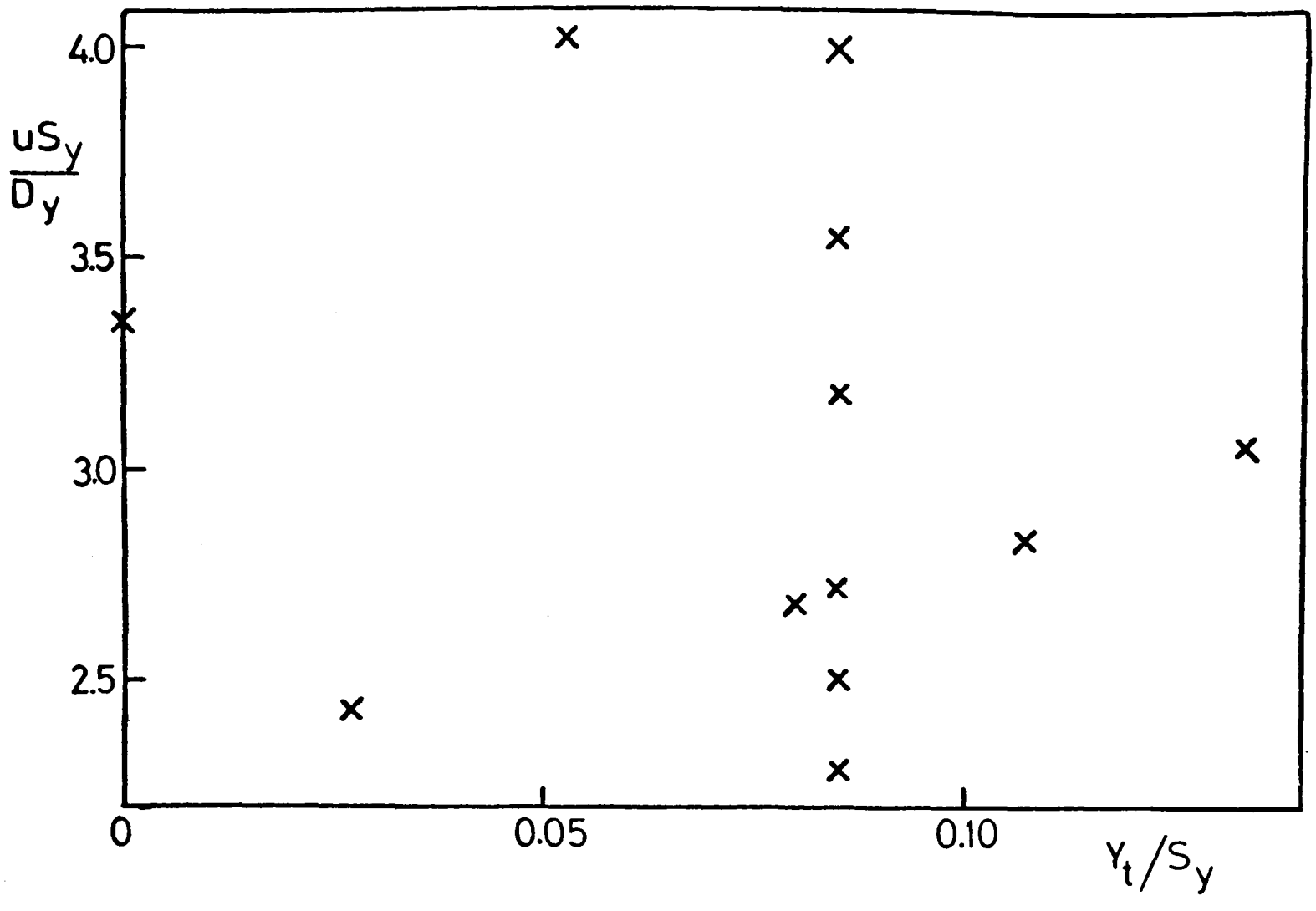


Fig. 5.29 Bar thickness. Effect on axial Peclet number.

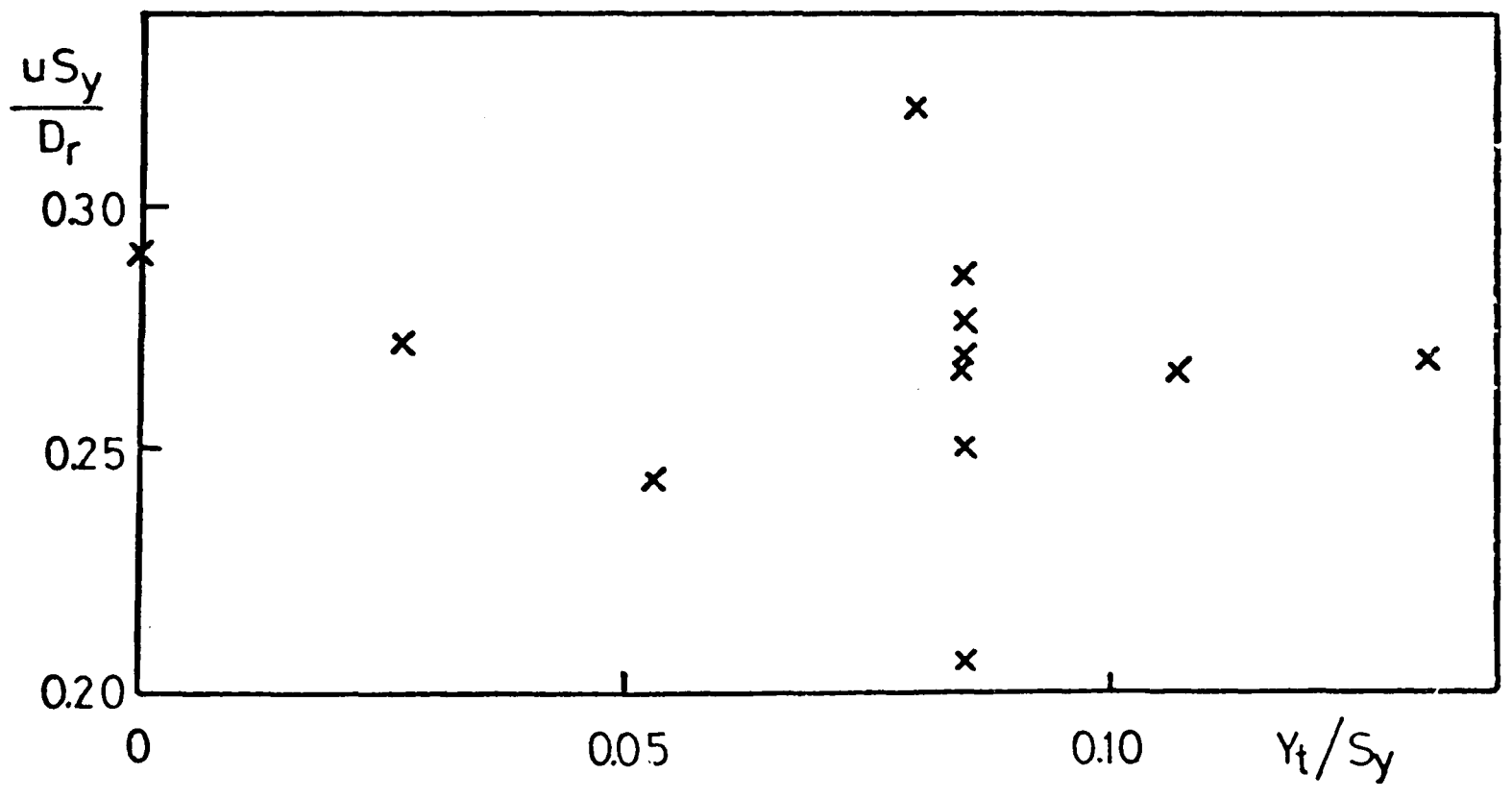


Fig. 5.30 Bar thickness. Effect on radial Peclet number.

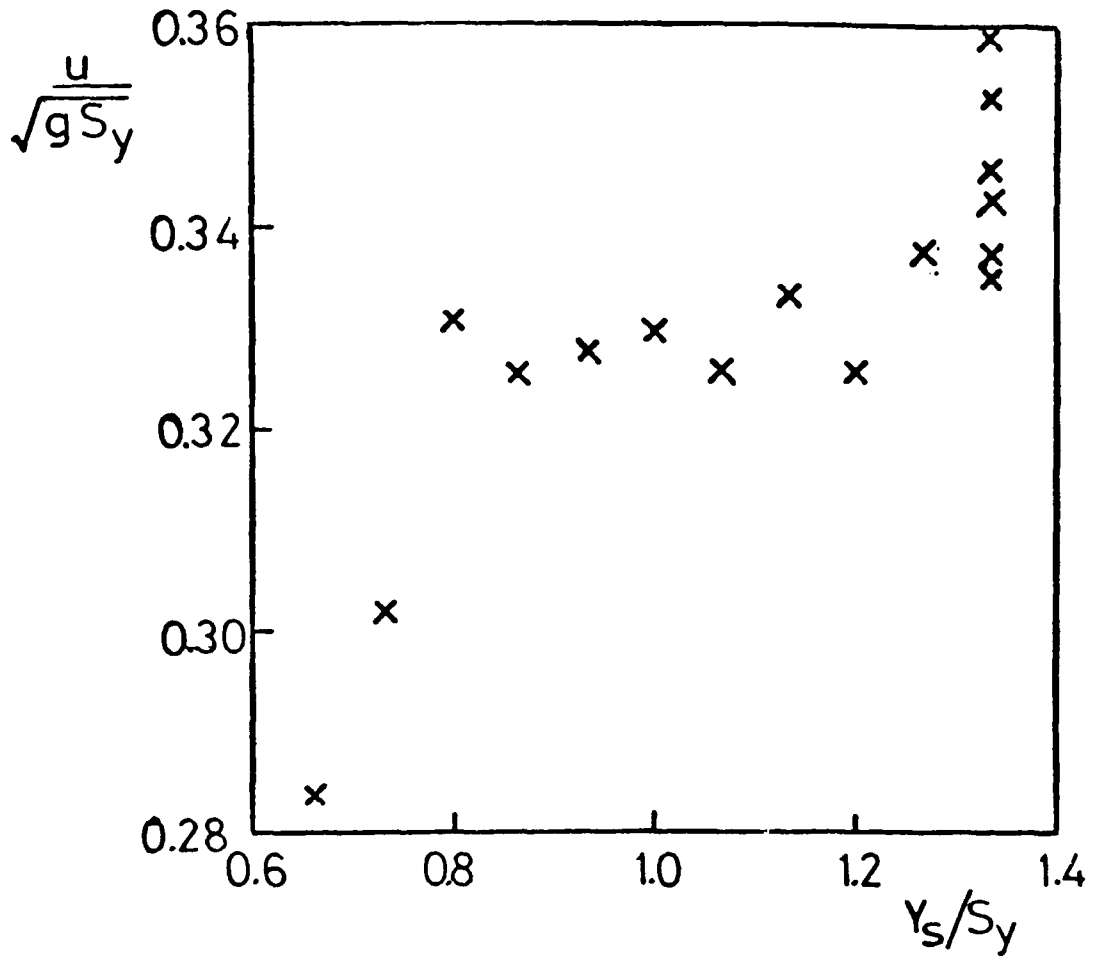


Fig. 5.31 Bar spacing (i). Effect on velocity.

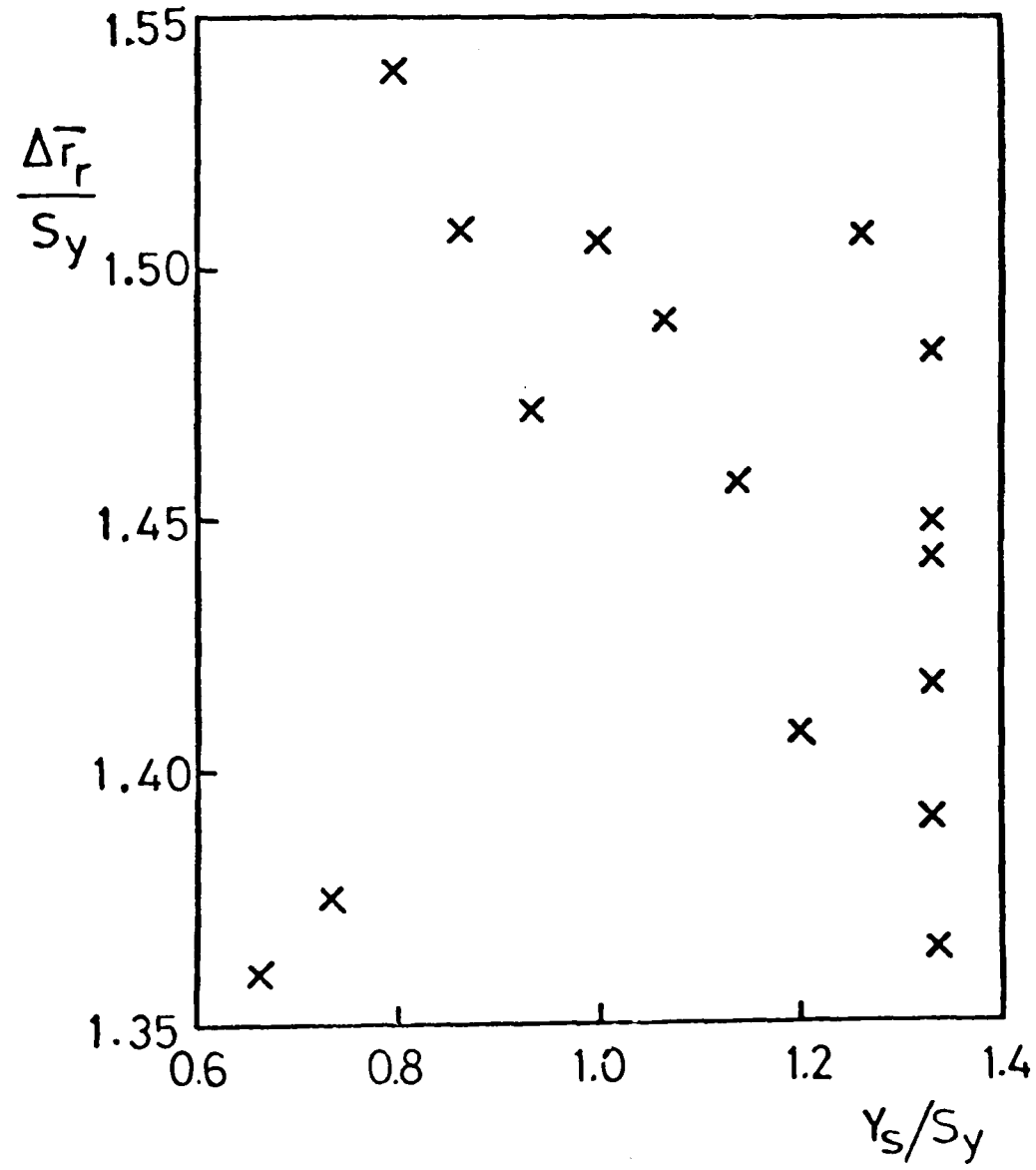


Fig. 5.32 Bar spacing (i). Effect on root mean square lateral jump.

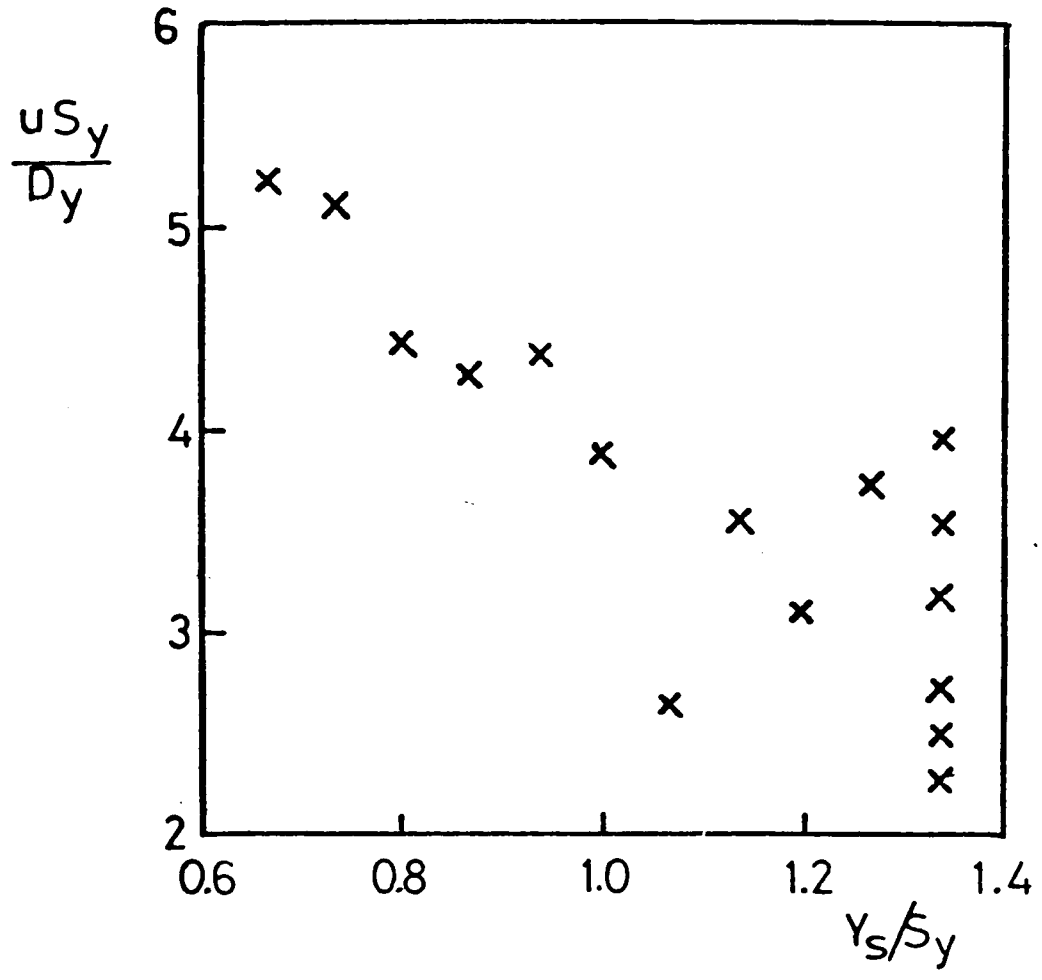


Fig. 5.33 Bar spacing (i). Effect on axial Peclet number.

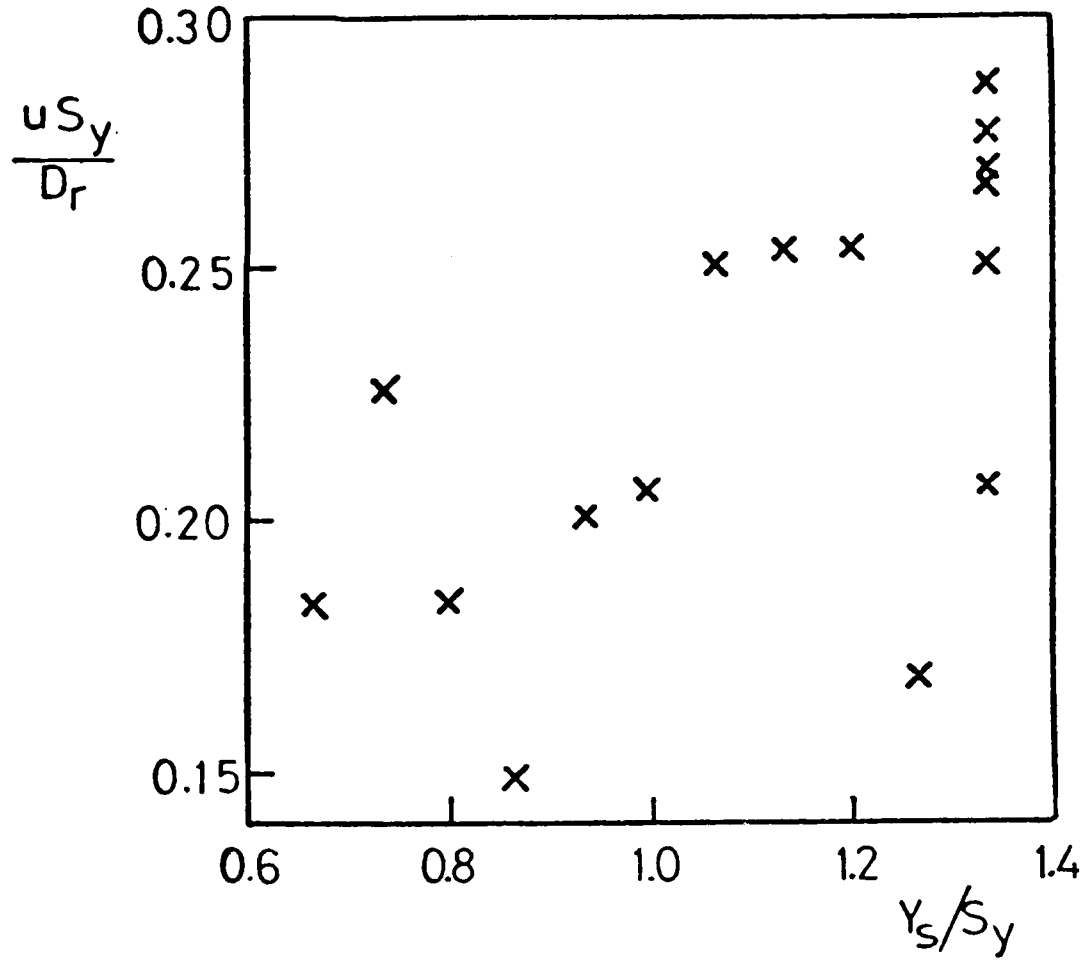


Fig. 5.34 Bar spacing (i). Effect on radial Peclet number.

5.2.9 Bar spacing (ii)

The effect of changes in S_y is important as, if there is only a limited amount of space available for the equipment, it is essential that the consequences of a decrease in the voidage can be accurately assessed. The results are shown in dimensionless form in Figures 5.35-5.38 where W_b is the horizontal bar spacing (Figure 5.2).

The dimensionless velocity is virtually constant over the range of values of S_y used (Figure 5.35). As expected, a reduction in voidage leads to a corresponding increase in the root mean square lateral jump (Figure 5.36). Changes in the axial Peclet number (Figure 5.37) are apparently obscured by scatter in the results and Figure 5.39 presents a clearer picture, whence D_y is proportional to $S_y^{1.9}$. From Figure 5.35, $u \propto \sqrt{S_y}$ which implies that $Pe_a \propto S_y^{-0.4}$. The radial Peclet number increases with S_y/W_b (Figure 5.38). Figure 5.40 indicates that $D_r \propto S_y^{0.8}$ whence $Pe_r \propto S_y^{0.7}$ if $u \propto \sqrt{S_y}$. Thus the diffusion coefficient per unit height of mixer apparently increases slightly as S_y/W_b increases, though the change is small (Figure 5.41).

5.3 Modelling

5.3.1 Limiting displacements

The most important of the dependent variables in this analysis is the radial diffusion coefficient, since this determines the rate at which materials disperse. The graph of $\sigma^2(\Delta r)$ vs τ from which this is calculated reaches a limiting value; at higher values of τ the two positions of the particle are independent. This limit could be predicted as follows.

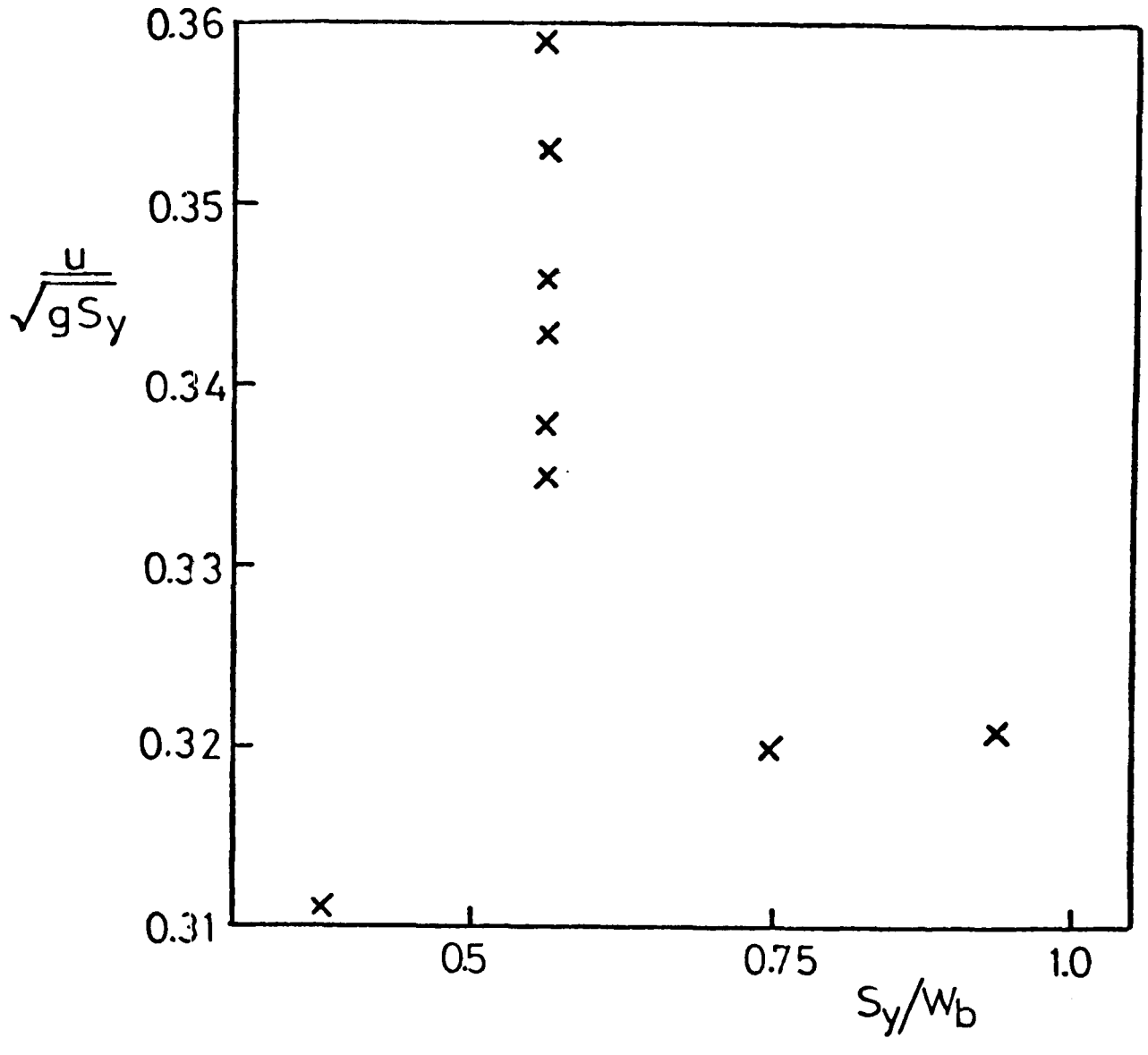


Fig. 5.35 Bar spacing (ii). Effect on velocity.

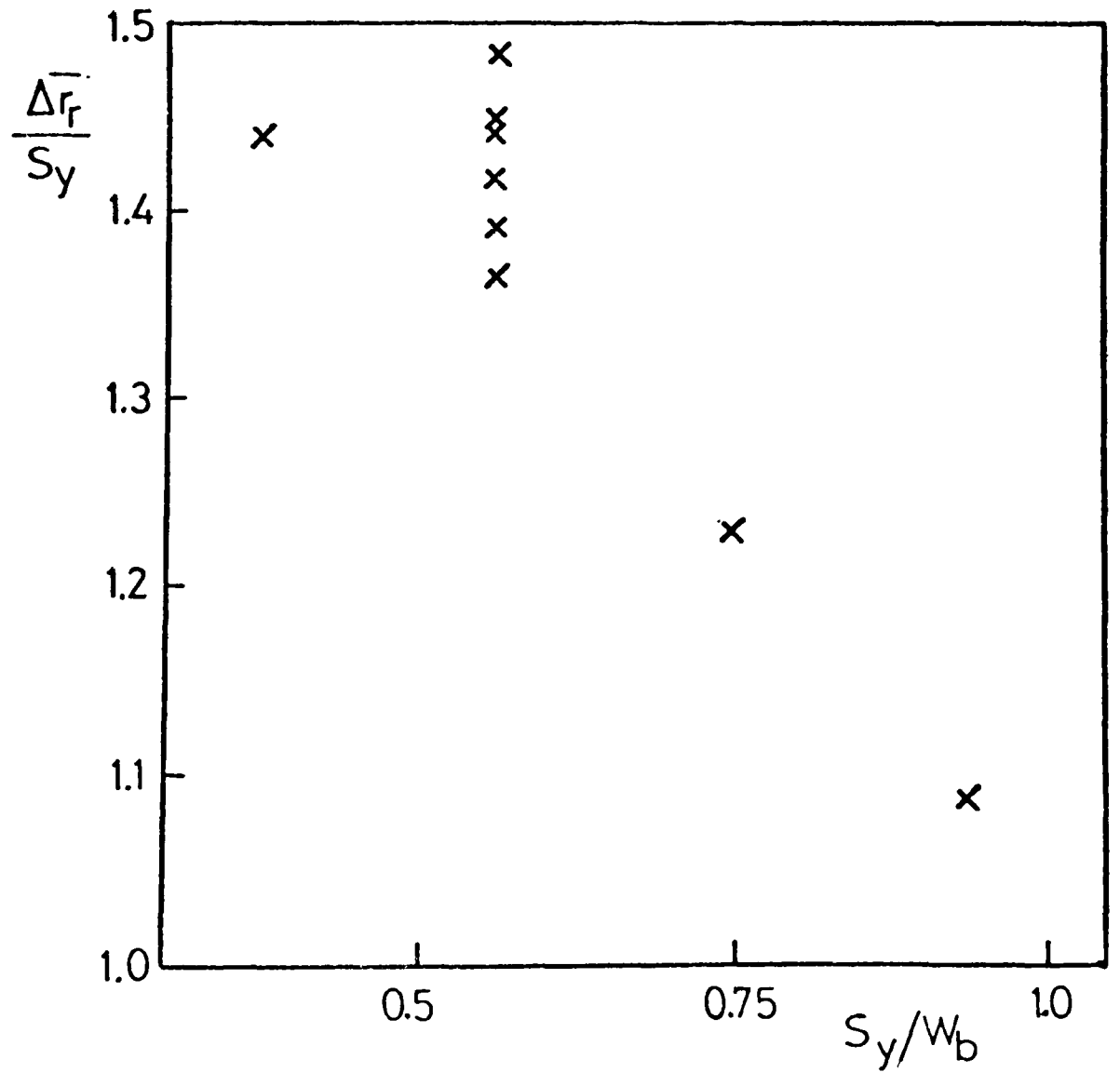


Fig. 5.36 Bar spacing (ii). Effect on root mean square lateral jump.

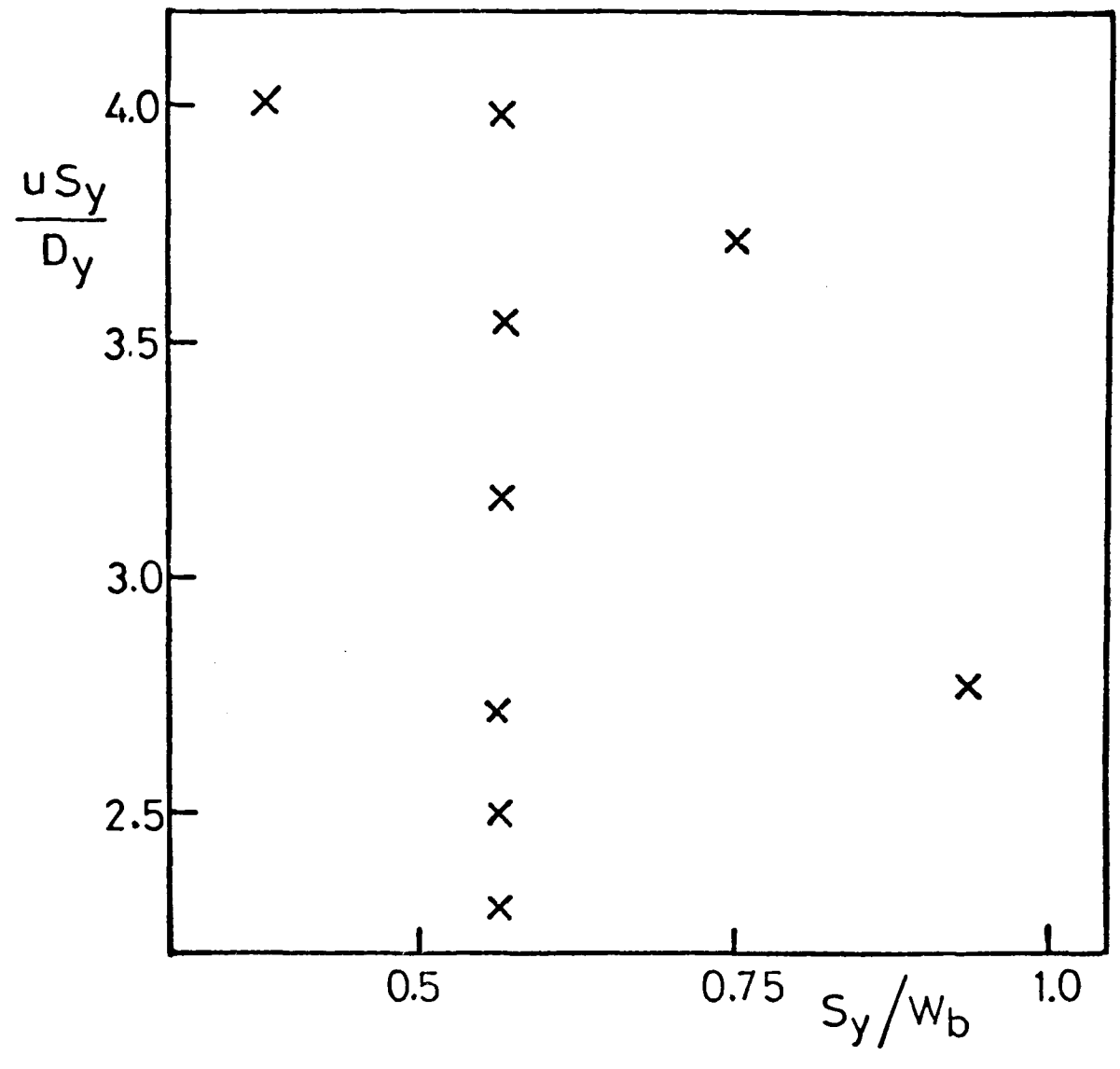


Fig. 5.37 Bar spacing (ii). Effect on axial Peclet number.

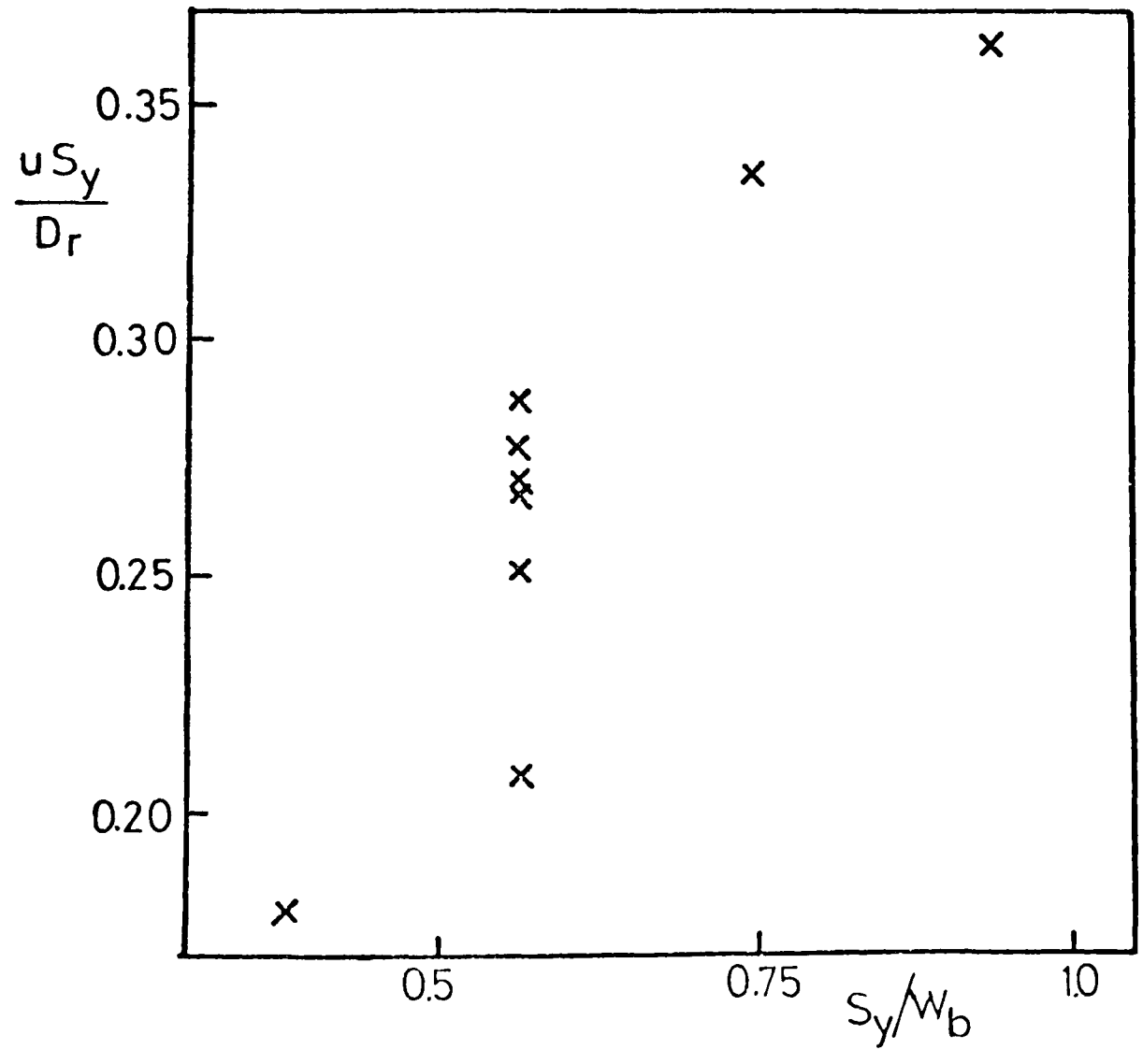


Fig. 5.38 Bar spacing (ii). Effect on radial Peclet number.

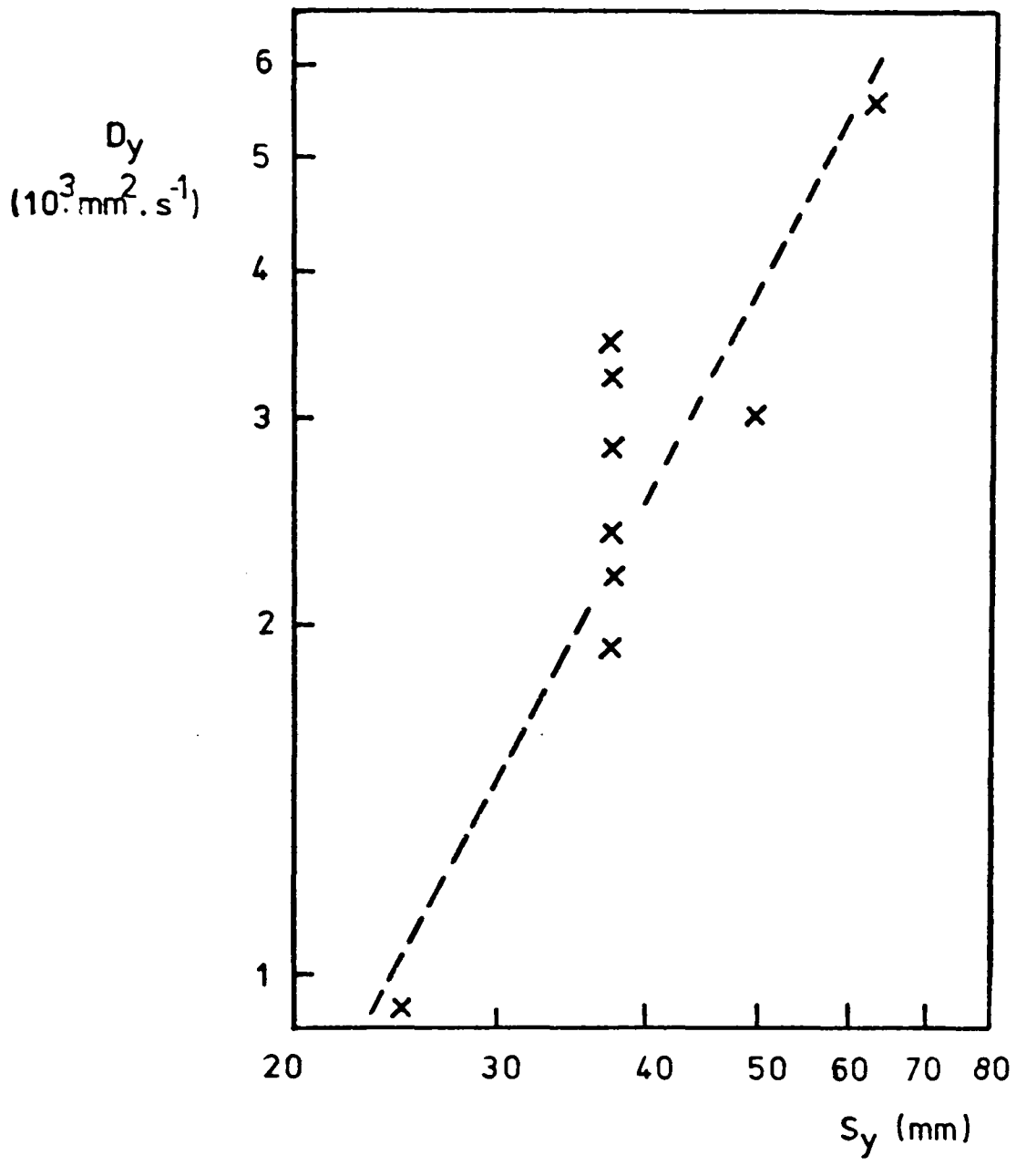


Fig. 5.39 Bar spacing (ii). Effect on axial diffusion coefficient.

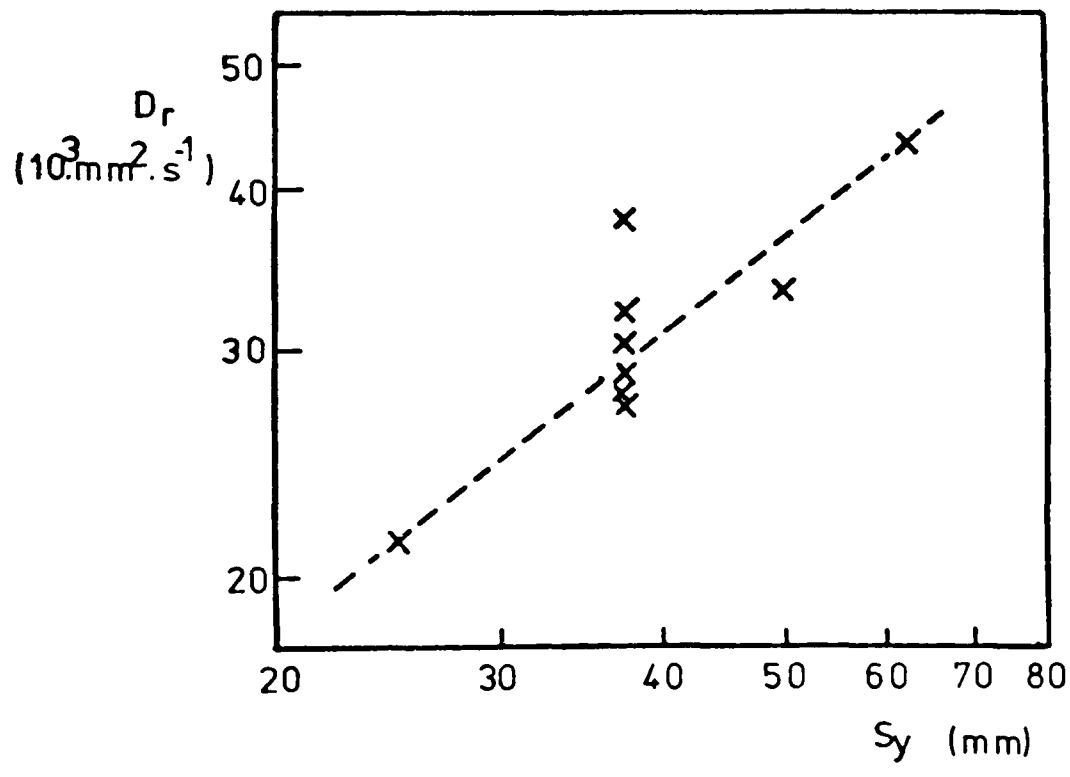


Fig. 5.40 Bar spacing (ii). Effect on radial diffusion coefficient.

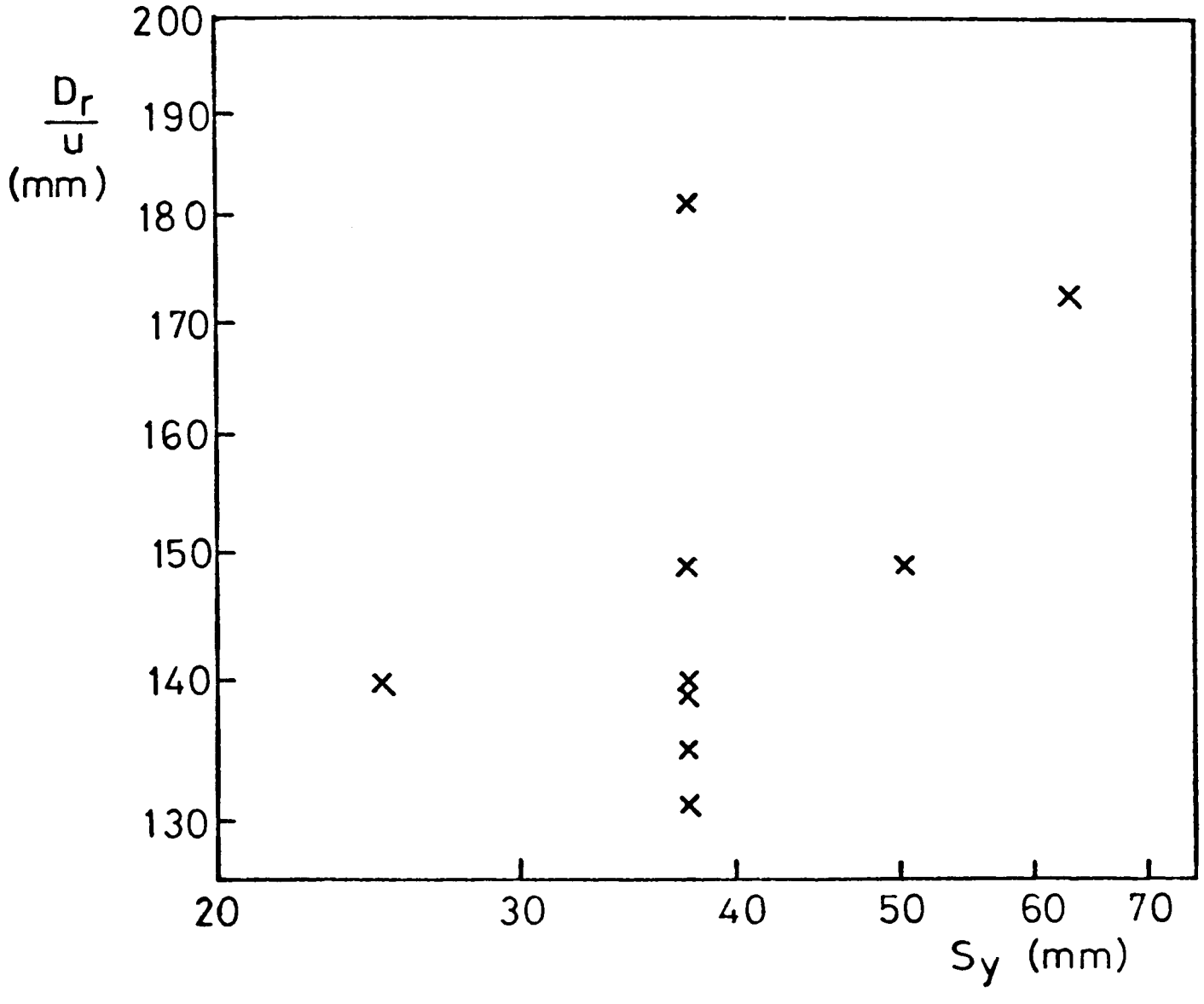


Fig. 5.41 Bar spacing (ii). Effect on D_r/u.

If motion in the x direction is independent from that in the z direction, only one need be considered at a time. When the limiting variance is reached the lateral co-ordinates of the two particle positions are independent of each other. For the output at preset time intervals it is reasonable to assume that there are no constraints on the particle position due to the bar layout and there is a uniform probability that the x co-ordinate of the particle lies between $d_p/2$ and $L_M-d_p/2$. The mean value of x is $L_M/2$ and by definition

$$E(x - L_M/2)^2 = \int_{d_p/2}^{L_M-d_p/2} (x - L_M/2)^2 f_1(x)\ dx \qquad (5.9)$$

where $f_1(x)$, the probability distribution of x, is $1/(L_M-d_p)$. Integrating equation 5.9,

$$E(x - L_M/2)^2 = (L_M - d_p)^2/12 \qquad (5.10)$$

If two random values of x are chosen, x_A and x_B, then

$$E(x_B - x_A)^2 = E(x_A - L_M/2)^2 + E(x_B - L_M/2)^2$$

$$= (L_M - d_p)^2/6 \qquad (5.11)$$

Similarly $E(z_B-z_A)^2 = (L_M-d_p)^2/6$ and if the distributions are independent the variance of the joint distribution is $(L_M-d_p)^2/3$. Disregarding d_p and substituting for L_M, the limiting value of $\sigma^2(\Delta r)/S_y^2$ is 37.9, which agrees quite well with Figure 5.9. The output at present height intervals produces a similar plot (Figure 5.42).

The output at intervals of one bounce leads to a different limit as the probability distribution is no longer approximately uniform. The most important deviation from a random distribution is that due to collisions on the side walls. If it can be assumed that the distribution between the sides is uniform despite

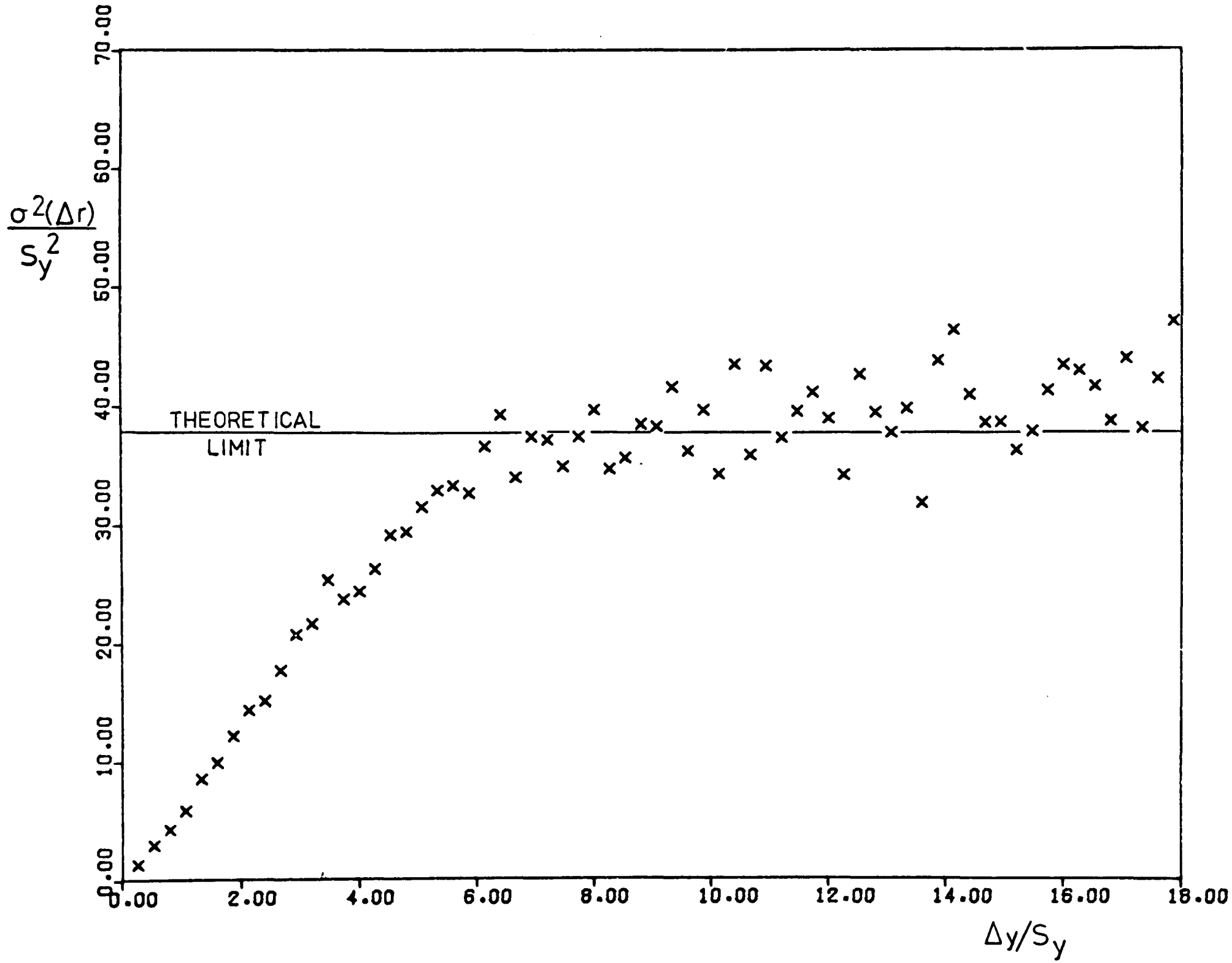


Fig. 5.42 Relationship between $\sigma^2(\Delta r)/S_y^2$ and $\Delta y/S_y$. Run no. 40.

the overlap of bars the limit can be found as follows.

If the probability that a collision taken at random is with the side of the mixer is Y_c, then for $d_p/2<x<L_M-d_p/2$, if $f_2(x)$ is the probability distribution of x,

$$\int_{d_p/2}^{L_M-d_p/2} f_2(x)\,dx = 1 - Y_c$$

whence $f_2(x) = (1-Y_c)/(L_M - d_p)$ for $d_p/2<x<L_M - d_p/2$. As before,

$$E(x - L_M/2)^2 = \int_{d_p/2}^{L_M-d_p/2} (x - L_M/2)^2 f_2(x)\,dx \qquad (5.12)$$

Integrating, allowing for delta functions area $Y_c/2$ at $x = d_p/2$ and $x = L_M - d_p/2$,

$$E(x - L_M/2)^2 = (L_M - d_p)^2 (1 + 2Y_c)/12 \qquad (5.13)$$

and the limit of $\sigma^2(\Delta r)$ as $\tau \to \infty$ is $(L_M - d_p)^2(1 + 2Y_c)/3$.

Y_c was generally around 0.15 though runs 7 and 8 ($\alpha = 0.2$) gave 0.22-0.23 and run 9 ($\alpha = 0.1$) 0.13. A simple model to explain this was derived. Part of the mixer is shown in Figure 5.43. Since $\Delta\bar{r}_r/S_y$ is generally about 1-2 (Table 5.1), a particle colliding with surface A or surface B might be expected to then hit the side wall. If each top surface is hit with equal probability, and collisions with the lower surfaces disregarded, then surfaces similar to A and B will be hit one time in six and the proportion of collisions with the side walls will be 1/7 or 0.14. If this value is used the limit of $\overline{|S_{Jr}|}^2/S_y^2$ is 48.8, in good agreement with Figure 5.44.

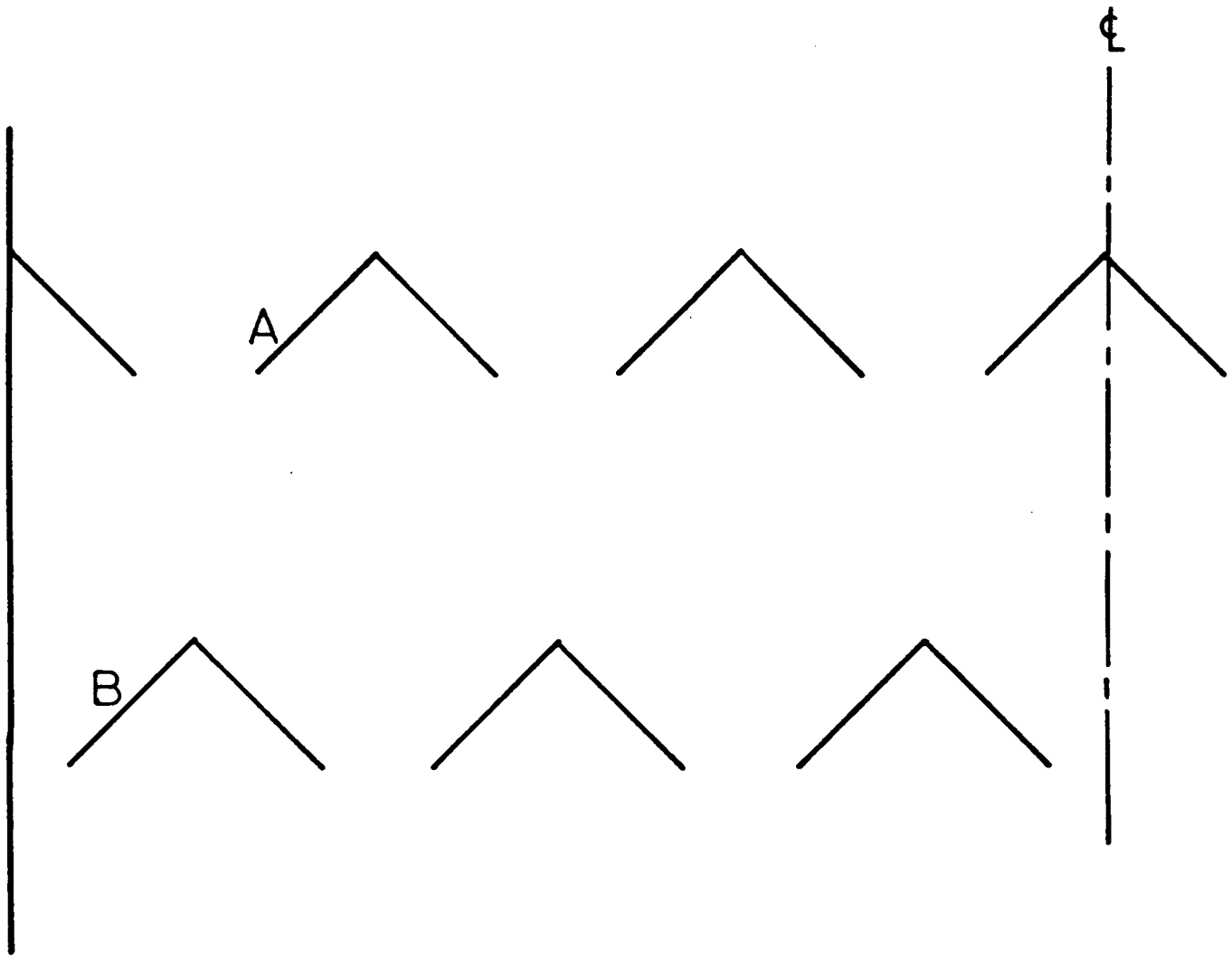


Fig. 5.43 Bounces on the side of the mixer.

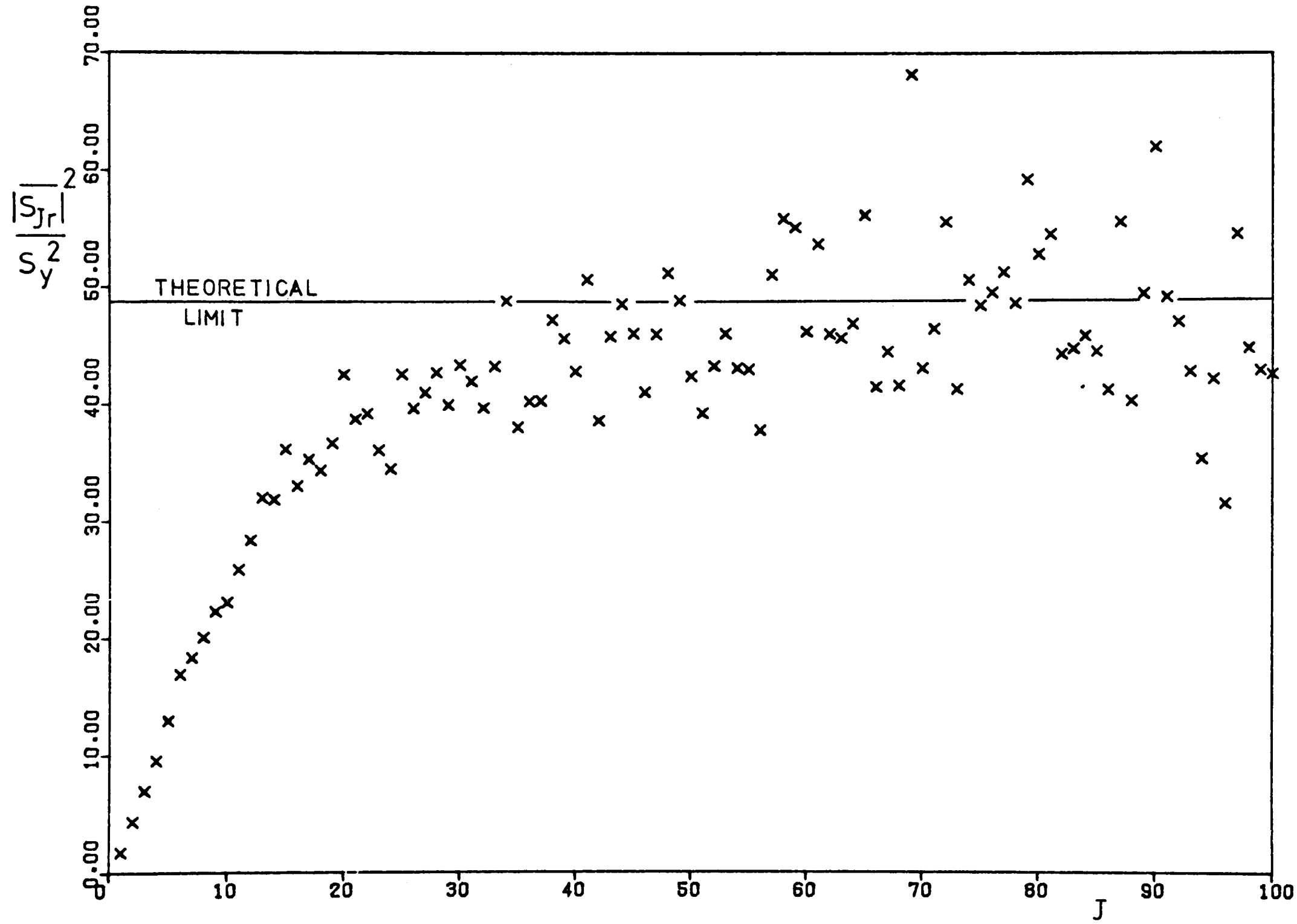


Fig. 5.44 Relationship between $|\overline{S_{Jr}}|^2/S_y^2$ and number of jumps, J. Run No. 40.

5.3.2 Velocity of inelastic particles

Since the mixers are based upon mechanisms which occur during spontaneous percolation, the theories described in Chapter 3 could be used. As before two different models are possible, one to account for the behaviour of an inelastic particle, the other for a partly elastic one. Only outline derivations are presented as the methods are very similar to those described earlier.

Consider an inelastic particle hitting a bar with velocity V_f. The motion of the particle is restricted to two dimensions. Since $\alpha = 0$, the particle is assumed to roll down the bar if it is spherical or slide down if it is not. If the velocity after impact is V_a and the mass of the particle is m, then equations 3.12 and 3.13 may be applied (see Figure 5.45). Thus, as before

$$E_{Li} = \frac{mV_f^2}{4}(1 - \cos 2\theta_f) \qquad (5.14)$$

where E_{Li} is the energy lost on collision and θ_f is the angle between the path of the particle at the instant of collision and the bar. If θ_f is assumed to be uniformly distributed between O and $\pi-2\beta$, the mean value of E_{Li} is

$$E_L = \int_0^{\pi-2\beta} \frac{mV_f^2}{4} \cdot \frac{1-\cos 2\theta_f}{\pi-2\beta} \, d\theta_f$$

which, if V_f is not a function of θ_f, can be integrated to give

$$E_L = \frac{mV_f^2}{2}\left[\frac{1}{2} + \frac{\sin 4\beta}{4(\pi-2\beta)}\right] \qquad (5.15)$$

If the particle then rolls down the plane equation 3.17 applies, whereas if the particles slides with coefficient of friction μ

$$\frac{mV_f^2}{2} + mgl\sin\beta = E_{Li} + \frac{mV^2}{2} + \mu mgl\cos\beta \qquad (5.16)$$

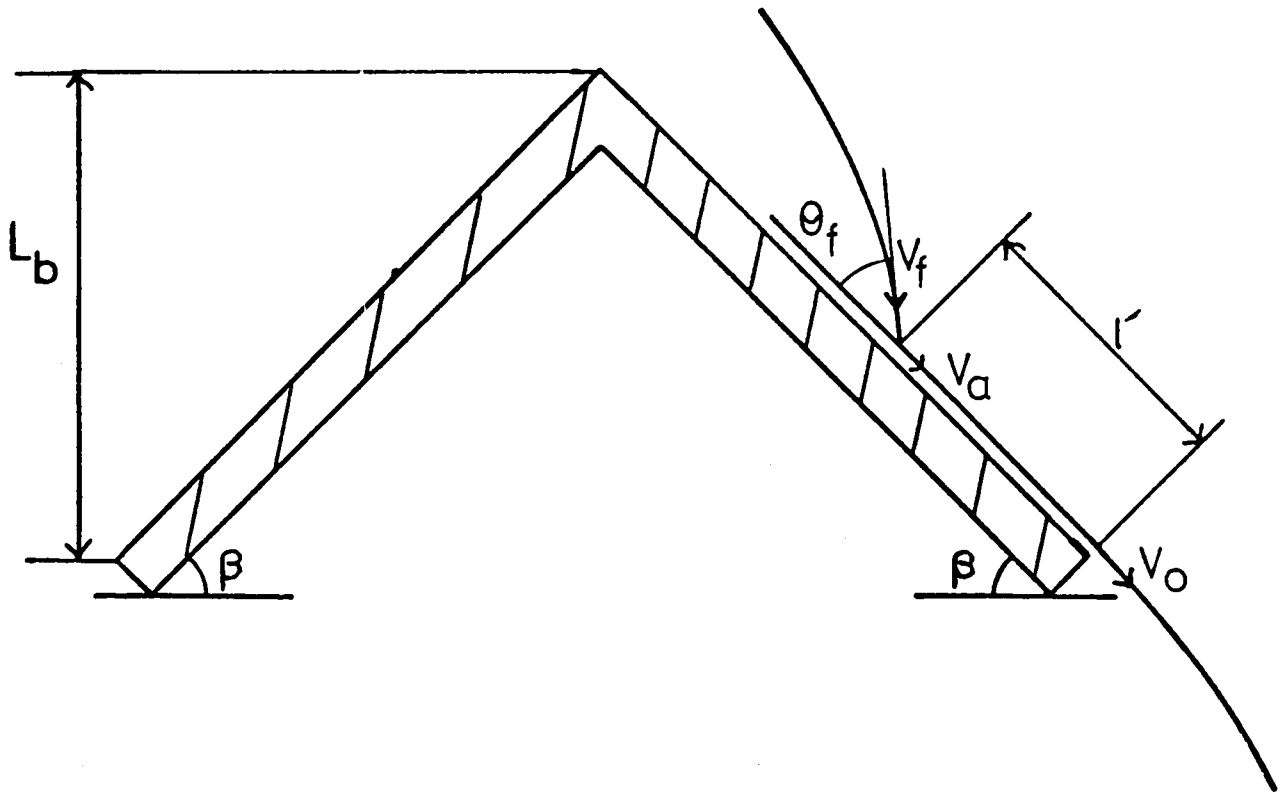


Fig. 5.45 Impact of a particle on a mixer bar.

Averaging and combining equations 3.17, 5.15 and 5.16,

$$\frac{(1 - k_2)\, V_f^{\,2}}{2} + glk_3 = \frac{k_1 V^2}{2} \qquad (5.17)$$

where $k_2 = 0.5 + \sin 4\beta/(4\pi - 8\beta)$, if sliding occurs $k_1 = 1$, $k_3 = \sin\beta - \mu\cos\beta$ and if rolling occurs, $k_1 = 1.4$, $k_3 = \sin\beta$.

The velocity of the particle as it leaves the bar V_o is given by

$$V_o^{\,2} = \frac{1}{k_1}\left[(1-k_2)V_f^{\,2} + 2k_3 g l' \right] \qquad (5.18)$$

where l' is the distance on the plane traversed by the particle. If l' is uniformly distributed between O and $L_b/\sin\beta$ then the average value of $V_o^{\,2}$ is

$$\overline{V_o}^2 = \int_0^{L_b/\sin\beta} \frac{V_o^{\,2}\sin\beta\, dl'}{L_b} =$$

$$\frac{1}{k_1}\left[(1-k_2)V_f^{\,2} + \frac{k_3 g L_b}{\sin\beta} \right] \qquad (5.19)$$

Substituting $V = dl/dt$ in equation 5.17 and integrating

$$t = \sqrt{\frac{k_1}{k_3 g}}\left[\{(1-k_2)V_f^{\,2} + 2k_3 g l'\}^{\frac{1}{2}} - \{(1-k_2)V_f^{\,2}\}^{\frac{1}{2}} \right] \qquad (5.20)$$

The mean time spent by a particle on a plane $\bar{t}$ is given by

$$\bar{t} = \int_0^{L_b/\sin\beta} \frac{t\sin\beta}{L_b}\, dl'$$

$$= \frac{\sqrt{k_1}\sin\beta}{k_3 g l}\left[\frac{1}{3k_3 g}\left(\left[(1-k_2)V_f^{\,2} + \frac{2k_3 g L_b}{\sin\beta}\right]^{\frac{3}{2}} - \left[(1-k_2)V_f^{\,2}\right]^{\frac{3}{2}} \right) - L_b \frac{(V_f^{\,2})^{\frac{1}{2}}(1-k_2)^{\frac{1}{2}}}{\sin\beta} \right] \qquad (5.21)$$

The equations which describe the motion of a particle in

free-flight are similar to those applied in the percolation model though β is a constant in this situation. They are

$$V_1 = V_o \sin\beta \tag{3.21}$$

$$V_H = V_o \cos\beta \tag{3.22}$$

$$\bar{h} = \overline{(V_2^2 - V_1^2)}/2g \tag{3.29}$$

$$\overline{V_2} - \overline{V_1} = g\bar{t}' \tag{3.33}$$

$$V_f^2 = \overline{V_2}^2 + \overline{V_H}'^2 \tag{3.34}$$

where the velocity of a particle leaving a plane is resolved into components V_H in a horizontal direction and V_1 downwards, and V_f is resolved into V_H' horizontally and V_2 downwards. $\bar{t}'$ is the mean time spent by the particle during free flight and $\bar{h}$ is the mean vertical distance travelled by the particle during this time. If, as in the mixer built, $\beta < 45^o$, there is no possibility of a particle rolling up a plane. The mean vertical distance travelled by a particle while on a plane is $L_b/2$ and hence

$$u = \frac{\bar{h} + L_b/2}{\bar{t} + \bar{t}'} \tag{5.22}$$

$\bar{h}$ can be estimated from the bar spacing in the mixer. Assume the probability that a particle passes through a row of bars without a collision p_c is proportional to the size of the gap between the bars and that the probability that a particle hits a bar in a given row is not related to the probability that it will hit a bar in any other row. An estimate of p_c is then $G/(G + L_b\cot\beta)$ where $2G$ is the size of the horizontal gap between bars (Figure 5.2), assuming $d_p << G$ and $d_p << L_b$. The particle has a probability $1-p_c$ of hitting one of the first row of bars, in which case it will have fallen an average vertical distance $H + L_b/2$ where H is the vertical distance separating rows of bars.

The probability that a particle will pass through q-1 rows of bars and hit the qth is $p_c^{q-1}(1-p_c)$ and the mean vertical distance travelled is $qH + (2q-1)L_b/2$. Thus

$$\bar{h} = \sum_{q=1}^{\infty} p_c^{q-1} (1-p_c)\left[qH + (2q-1)L_b/2 \right]$$

$$= \frac{H + L_b}{(1-p_c)} - \frac{L_b}{2}$$

$$= \frac{(G + L_b\cot\beta)(H + L_b)}{L_b\cot\beta} - \frac{L_b}{2} \qquad (5.23)$$

Though derived for a two dimensional mixer, these equations might be expected to apply approximately to a three-dimensional unit. Combining equations 5.19, 5.21, 3.21, 3.22, 3.29, 3.33, 3.34, 5.22 and 5.23 and inserting the dimensions used in the mixer that was built, $\bar{h}/S_y = 1.2$ and $u/\sqrt{gS_y} = 1.6$. This is in reasonable agreement with the limiting value of $u/\sqrt{gS_y}$ of 1.3 predicted from the intercept in Figure 5.15.

5.3.3 Partly elastic particles

Equations 3.54-3.61 can be applied directly in this case, the only difference being that θ_i and θ_f are the angles between the particle path and the plane, and not the tangent to a sphere. If the mean lateral movement in each direction is $L_b + 2G$, i.e. a bounce from the middle of the side of one bar to the middle of the adjacent side of the next bar, and $\bar{h}$ can be calculated as in section 5.3.2 then the mean free path is

$$\lambda = \sqrt{\bar{h}^2 + 2(L_b + G)^2} \qquad (5.24)$$

If λ is not a function of α and as before, $\overline{\sin^2\theta_f} = 0.5$, then

$$u = 0.5 \left[\frac{2g\ \lambda\sqrt{(1-\alpha^2)/2}}{1+\sqrt{(1+\alpha^2)/2}} \right]^{\frac{1}{2}} \qquad (5.25)$$

Combining equations 5.24 and 5.25 it is found that $u/\sqrt{gS_y}$ varies from 0.63 at $\alpha = 0.3$ to 0.48 at $\alpha = 0.8$ for the three-dimensional mixer. Though the direction of the change is correct this does not agree with Figure 5.15, probably because of the dependence of V_f^2 on α described in Section 5.2.4.

5.4 Summary

The purpose of the work described in this chapter has been to derive data which will be of assistance in the design of the mixers or distributors described in Chapter 4. The computer programs described enabled the effects of changes in mixer dimensions and particle properties to be simulated. Differences between the programs used have been shown to have only a small effect on the results. The most important conclusions may be summarised thus:

(i) The particle velocity varies over quite a wide range as the coefficient of restitution changes. The values of the radial diffusion coefficient indicate that the mixer built may not have been high enough to cope adequately with particles with a low coefficient of restitution such as lead shot.

(ii) Changes in the particle diameter over the range for which the equipment was designed have only a small effect.

(iii) Smaller bars, within the limits used, lead to higher radial diffusion coefficients. On physical grounds it would be expected that indefinitely shortening the bar length would eventually lead to a reduction in diffusion. For practical use the bars have to be large enough to prevent particles passing straight through the mixer and hence simulation of bars smaller than $L_b/S_y = 0.333$ was not attempted.

(iv) Mounting the parallel rows of bars closer together without changing the average vertical spacing (i.e. decreasing H while keeping S_y constant (Figure 5.2)), increases the number of collisions per unit height and hence improves the dispersion.

(v) Increasing the overall height of the mixer while keeping the number of bars constant has only a small effect on the performance; slightly better results are achieved if higher values of S_y are employed.

(vi) Limiting values of the variance of the displacements of the particle can be accurately predicted. Application of the models used to describe percolation leads to results which are not so accurate though the errors generally do not exceed 50%.

In summary, those changes which increase the amount of free space in the equipment, i.e. smaller bars, smaller particles and larger vertical bar spacing, improve the performance of the mixer.

CHAPTER 6

STATISTICS OF SAMPLES

6.1 Introduction

Methods of analysing mixtures using correlation coefficients have recently been investigated by a number of workers. It was thought that such an approach would be necessary to generalise results from the mixers described in Chapter 4 and this provided the motivation for the work reported in this chapter. A particular feature of the three-dimensional mixer is that a particle passing through it is subjected to forces in two orthogonal directions and the equations derived here allow for this.

Correlation coefficients have been used in response to the inadequacy of the variance of sample* compositions as a mixing index. For example, when comparing mixtures the size and number of samples taken in each case are usually different and the values of the variance are not directly comparable. Information about the positions of samples is usually discarded when the variance is calculated, and it is generally not possible to predict the variance of other sizes of sample. Considerations of this sort are important in fields other than the mixing of powders.

Many mixers smooth out long-range variations in composition by their convective action, and thus many poor mixtures consist of 'clumps' of material in which the fraction of one of the components is greater than it is in the mixture as a whole. When such a situation occurs, the non-randomness found on sampling is

---

* In this work the term sample refers to a single assessment of the composition of the mixture from which it was withdrawn.

due to short-range correlation between neighbouring samples and may be characterised by a correlation coefficient.

A mixture may therefore pass through the following stages:

(i) Initially the components are totally segregated. The variance of such a mixture is p(1-p) for a two component mixture, where p is the proportion of one of the components. At this stage the variance is independent of the size of samples chosen.

(ii) An intermediate stage between randomness and total segregation in which the variance is a complicated function of the sample size.

(iii) The random state where the probability of finding an element of one material in any place is the same throughout the mixture. The variance is then inversely proportional to the size of the samples.

The random state is the best that can be achieved; production of an ordered mixture is impossible with the mixers currently available. In some mixing systems the random state is not achieved in practice. This occurs in the mixing of segregating powders, and can even happen when cohesive powders which do not segregate are being mixed (Orr and Shotton, 1973). Many mixtures investigated are therefore in state (ii).

The first application of the correlation coefficient to the study of mixtures of solids was by Landry (1944) who discussed the sampling of coal in order to analyse its ash content. Emery (1951) was also interested in this problem and derived variance - sample size relationships for linear samples using three different forms of the correlation coefficient. It was later concluded in a survey by Bertholf (1955) that his analysis was not applicable to coal sampling, since variations

in ash content arise from long-range, not short-range, segregation.

Attempts to use correlation theory in the sampling of solids mixtures have recently been surveyed by Kristensen (1976). An early contribution was the work of Danckwerts (1953) who suggested the use of the 'scale' and 'intensity' of segregation, quantities based on the correlation coefficient and variance respectively, as means of characterising mixtures. Subsequently workers assumed expressions for the correlation coefficient and derived variance-sample size relationships based on these. However, many of these studies are restricted to long thin samples. Means of applying the approach to two-dimensional samples have been suggested by Bourne (1968) and Kristensen (1973b), but little progress was made.

6.2 Formulation

6.2.1 Correlation coefficients

The efficiency of different grids for sampling materials has been considered by Dalenius et al. (1961) who found that there is no unique optimum sampling pattern. Bourne (1967) suggested that a mixture could be considered as a three-dimensional array of cubic units, which he termed "unit samples". This approach is particularly advantageous since chemical analysis usually requires finite samples and if a mixture is to be completely analysed, cubic samples provide the simplest means of covering all space. These unit samples, which might be the smallest samples which can conveniently be taken, represent the smallest scale of scrutiny that is of concern.

The variance of the compositions of the unit samples, σ_o^2, can be related to the variance of N of them taken together, σ_N^2.

The lack of randomness at the scale of the unit samples may be characterised by the correlation coefficient between their compositions.

If x_i and x_j represent the compositions of any pair of unit samples a distance r apart, the correlation coefficient can be defined thus:

$$\rho(r) = \frac{E(x_i-\bar{x}_i)(x_j-\bar{x}_j)}{\sqrt{E(x_i-\bar{x}_i)^2 E(x_j-\bar{x}_j)^2}} \qquad (6.1)$$

In the absence of long-range correlation, the means of different groups of samples are the same, i.e. $\bar{x}_i = \bar{x}_j = \bar{x}$. Hence

$$\rho(r) = \frac{E(x_i-\bar{x})(x_j-\bar{x})}{E(x_i-\bar{x})^2} = \frac{C(x_i,x_j)}{V(x_i)} \qquad (6.2)$$

where $C(x_i, x_j)$ represents the covariance of x_i and x_j and $V(x_i)$ represents the variance of x_i. Both x_i and x_j are drawn from the series $x_1, x_2 \ldots x_N$. The mean of the series $\bar{x}$ is given by

$$\bar{x} = \frac{1}{N} \sum_{i=1}^{N} x_i$$

Then

$$V(\bar{x}) = V\left(\frac{1}{N}\sum_{i=1}^{N} x_i\right) = \frac{1}{N^2} V\left(\sum_{i=1}^{N} x_i\right) \qquad (6.3)$$

$$= \frac{1}{N^2}\left[\sum_{i=1}^{N} V(x_i) + 2 \sum_{i=1}^{N}\sum_{\substack{j=1 \\ i\neq j}}^{N} C(x_i,x_j)\right]$$

But the variance of the unit samples $V(x_i)$ equals σ_o^2. Substituting equation 6.2 in 6.3,

$$V(\bar{x}) = \frac{1}{N^2}\left(N\sigma_o^2 + 2\sigma_o^2 \sum_{r=1}^{r_m} n_r \rho(r)\right)$$

$$\sigma_N^2 = \frac{\sigma_o^2}{N}\left(1 + \frac{2}{N}\sum_{r=1}^{r_m} n_r \rho(r)\right) \qquad (6.4)$$

where n_r is the density function of samples a distance r apart and r_m is the maximum distance over which correlation occurs. In the absence of any correlation $\rho(r) = 0$ for all r and σ_N^2 is inversely proportional to N.

Equation 6.4 was derived by Madow and Madow (1944) and applies to exhaustive sampling of a mixture. They and Cochran (1946) compare systematic and random sampling procedures. Their approach was generalised to two-dimensional samples by Quenouille (1949) who also considered the efficiency of using different sampling techniques in different directions. These workers expressed their results in a similar form to equation 6.4, i.e. in equations relating the variance with the sample size using a correlation coefficient.

6.2.2 Definition of distance between samples

It is convenient to measure distances in terms of the dimension of the unit samples. Thus the distance between two samples is equal to the distance between their mid-points divided by the length of one side of a unit sample. In a one-dimensional situation this leads to unambiguous results, but in two and three-dimensional mixtures there are at least two ways of defining the distance between samples. These different conventions have been considered by Bourne (1968).

Method 1: The distance is equal to one plus the number of unit samples separating the pair being considered, passing from one unit sample to another only by routes orthogonal to the sides of the unit samples. A direct route must be used.

Method 2: The distance is equal to the length of the vector joining the centres of the pair of unit samples being considered divided by the length of one side of a unit sample. Bourne (1968)

then rounded this to the nearest integer, but this is not essential.

The correct method in a given situation depends on the process which created the mixture. Method 1 implies a non-isotropic process and is of particular use when two independent orthogonal processes are in operation, as occurs with the three-dimensional mixer. Method 2 implies an isotropic process and should be used when no directional operations are involved.

A 2 x 3 mixture is shown in Figure 6.1 as an example, with the distances between the pairs of samples tabulated according to the two different methods. In this simple case,

$$\frac{\sigma_6^2}{\sigma_o^2} = \frac{1}{6}\left[\ 1 + \frac{1}{3}\left(7\rho(1) + 6\rho(2) + 2\rho(3)\right)\right] \text{ using method 1}$$

or

$$\frac{\sigma_6^2}{\sigma_o^2} = \frac{1}{6}\left[\ 1 + \frac{1}{3}\left(11\rho(1) + 4\rho(2)\right)\ \right]$$

using method 2, with the distances rounded off to the nearest integer.

If method 1 is used, it will be shown that a general expression for such formulae can be derived and often summed analytically, whereas if the second method is used, numerical summation is necessary.

6.2.3 Models for the correlation coefficient

The relationship between $\rho(r)$ and r depends on the unit sample size and on the mixture, although $-1 \leq \rho(r) \leq +1$, $\rho(o) = 1$ and $\rho(\infty) = 0$ for the case of short-range correlation. Positive values of $\rho(r)$ indicate positive correlation, the normal type encountered in powder mixtures, though negative correlation is possible. Scott (1974) considers that, generally, for powder mixtures, a three parameter model for $\rho(r)$ is necessary but that

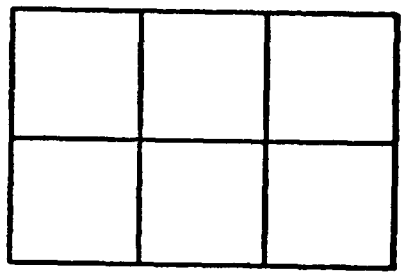


Fig. 6.1 The number of pairs of unit samples in a 2 x 3 array,

Distance	Number of pairs of unit samples	
	Method 1	Method 2
1	7	11
2	6	4
3	2	0

if the size of the unit samples is such that they contain more than a few particles, and if $\rho(r)$ monotonically decreases, a single parameter model will suffice. A plot of the relationship between $\rho(r)$ and r is termed a correlogram. Various workers have suggested the use of different correlograms; linear and exponential ones have been suggested as models for populations occurring in practice (Cochran, 1946) and there is some experimental evidence for their existence (Zweig, 1956; Hall and Godfrey, 1965). These forms, equations 6.5 and 6.6, will therefore be used.

(i) Linear $\rho(r) = 1 - er \quad r \leq {}^{1}/_{e}$

$\rho(r) = 0 \quad r > {}^{1}/_{e}$ (6.5)

(ii) Exponential $\rho(r) = a^{r} \quad 0<a<1$ (6.6)

where a and e are constants. The use of a particular form in a given situation can only be justified by the presence of experimental data.

There have not been many experimental determinations of $\rho(r)$ for real mixtures. One of the most extensive investigations was by Hall and Godfrey (1965) who produced a series of binary mixtures of a non-Newtonian material by an extrusion technique, using a coloured tracer to distinguish between the constituents. Enlarged photographs of each mixture were divided into 3600 samples by superposition of a square grid and each sample was analysed visually. The correlation coefficient was calculated for each mixture. The results obtained suggest that the exponential formulation $\rho(r) = a^{r}$ is adequate for their mixtures. Figure 6.2 shows a correlogram as given by Hall and Godfrey for their mixture B5 with the distances calculated using method 2. Their original data has been re-analysed to give a correlogram with the distances calculated using method 1. A least squares

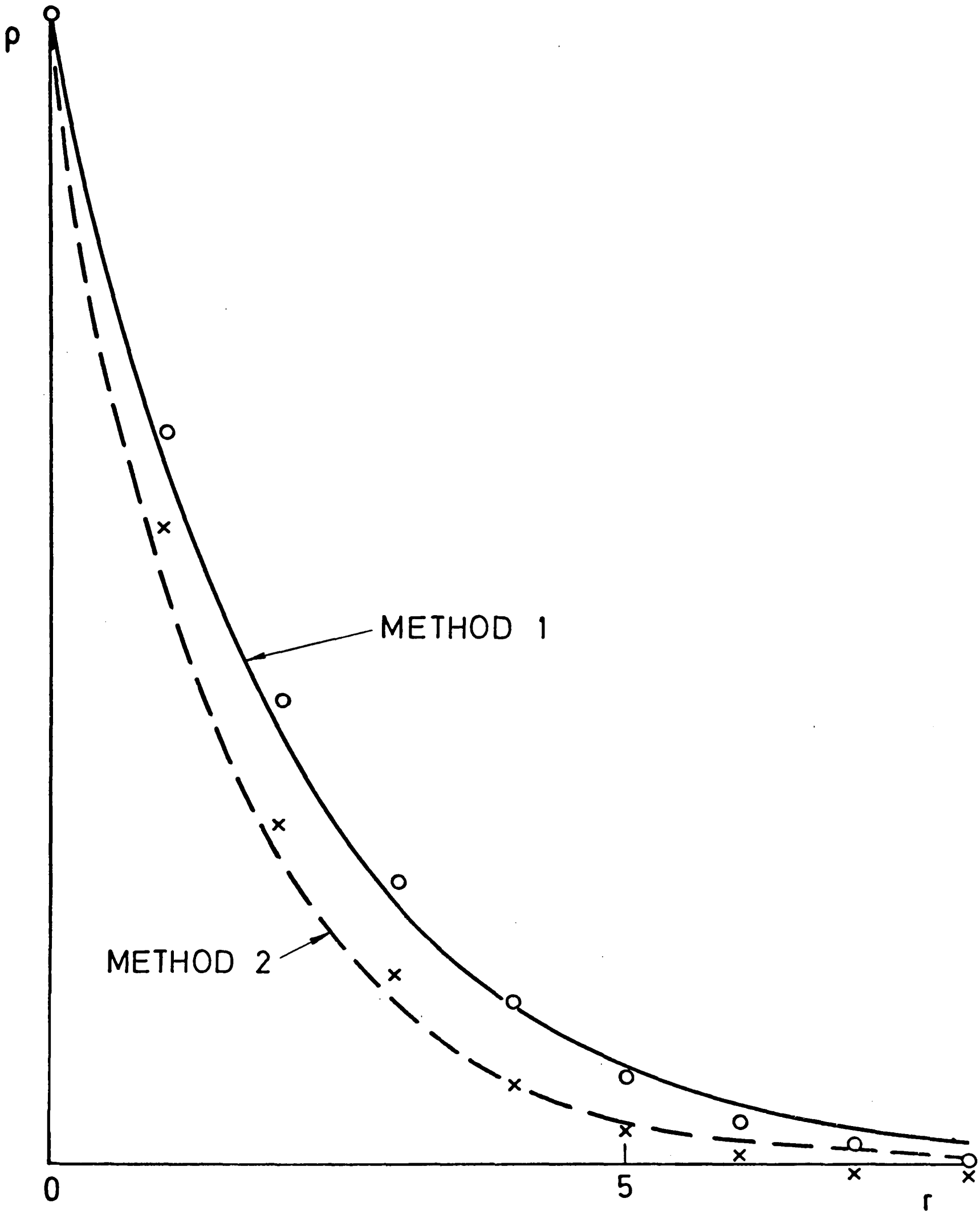


Fig. 6.2 Correlogram for expt. B5 by Hall and Godfrey (1965). Distances by methods 1 and 2.

fit to the first nine points of each plot yielded $\rho(r) = 0.521^r$ and $\rho(r) = 0.613^r$ respectively and these curves are also included on Figure 6.2. These relationships will be used later for illustrative purposes.

Zweig (1956) investigated the optical density of uniformly exposed photographic emulsions. The density of small samples was found to be correlated and different films produced linear and exponential correlograms. With the exception of Lacey and Mirza (1976a, 1976b), who studied long-range segregation, workers in the field of powder mixing have based their results on considerably fewer examples. Kristensen (1973b, 1973d) and Schofield (1970) are among those who present correlograms of powder mixtures.

6.3 Variance - sample size relationships

Mixtures may be evaluated in a number of ways. They may be analysed along a row, over a plane, or over a block.

(i) Linear samples

The density function, n_r, for linear samples may be derived as follows. Figure 6.3 shows a linear sample with 8 unit samples; it can be seen that there are 7 pairs of units next to each other, 6 pairs distance two units apart and so on. Thus, in general, there are (n - k) unit samples which are distance k apart where n is the number of unit samples in the sample.

From equation 6.4, the expression for the variance of a linear sample is:

$$\frac{\sigma_N^2}{\sigma_o^2} = \frac{1}{n}\left[1 + \frac{2}{n} \sum_{k=1}^{n-1} (n-k)\rho(k) \right] \qquad (6.7)$$

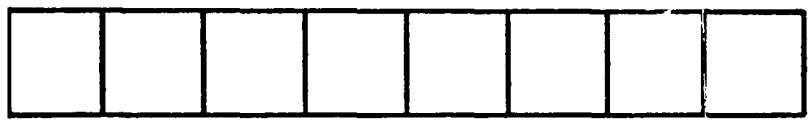


Fig. 6.3 Linear sample containing 8 unit samples.

(ii) Rectangular samples

Consider a pair of unit samples chosen from an (m x n) array and let them be distance k apart in the n direction and distance j apart in the m direction. If the first method of measuring distances is used they are (j + k) apart, whereas if the second method is used they are $\sqrt{j^2 + k^2}$ apart. If the n direction is taken alone, it can be seen that there are (n-k) pairs of unit samples distance k apart in this direction in each of the m lines of unit samples. Now introduce the criterion that the pairs of unit samples must also be a distance j apart in the positive m direction, If the distance k is proscribed there are two pairs of samples the required distance apart, AB and A'B' (Figure 6.4). There are (m - j) positions for this arrangement and therefore n_r is 2(m - j)(n - k). This method excludes double counting of unit sample pairs. This formula applies only to samples in different rows. In calculating the variance-sample size relationship for a rectangular sample, pairs of unit samples that lie in the same row must be considered as well. From equation 6.4, the expression for the variance of a rectangular sample is therefore:

$$\frac{\sigma_N^2}{\sigma_o^2} = \frac{1}{mn}\left[1 + \frac{2}{mn}\left\{m\sum_{k=1}^{n-1}(n-k)\rho(k) + n\sum_{j=1}^{m-1}(m-j)\rho(j) + 2\sum_{j=1}^{m-1}\sum_{k=1}^{n-1}(m-j)(n-k)\rho(j,k)\right]\right. \qquad (6.8)$$

the first two summations coming from pairs of unit samples in the same rows, the third from pairs in different rows. $\rho(j,k)$ is the correlation coefficient between two samples which are j apart in the m direction and k apart in the n direction.

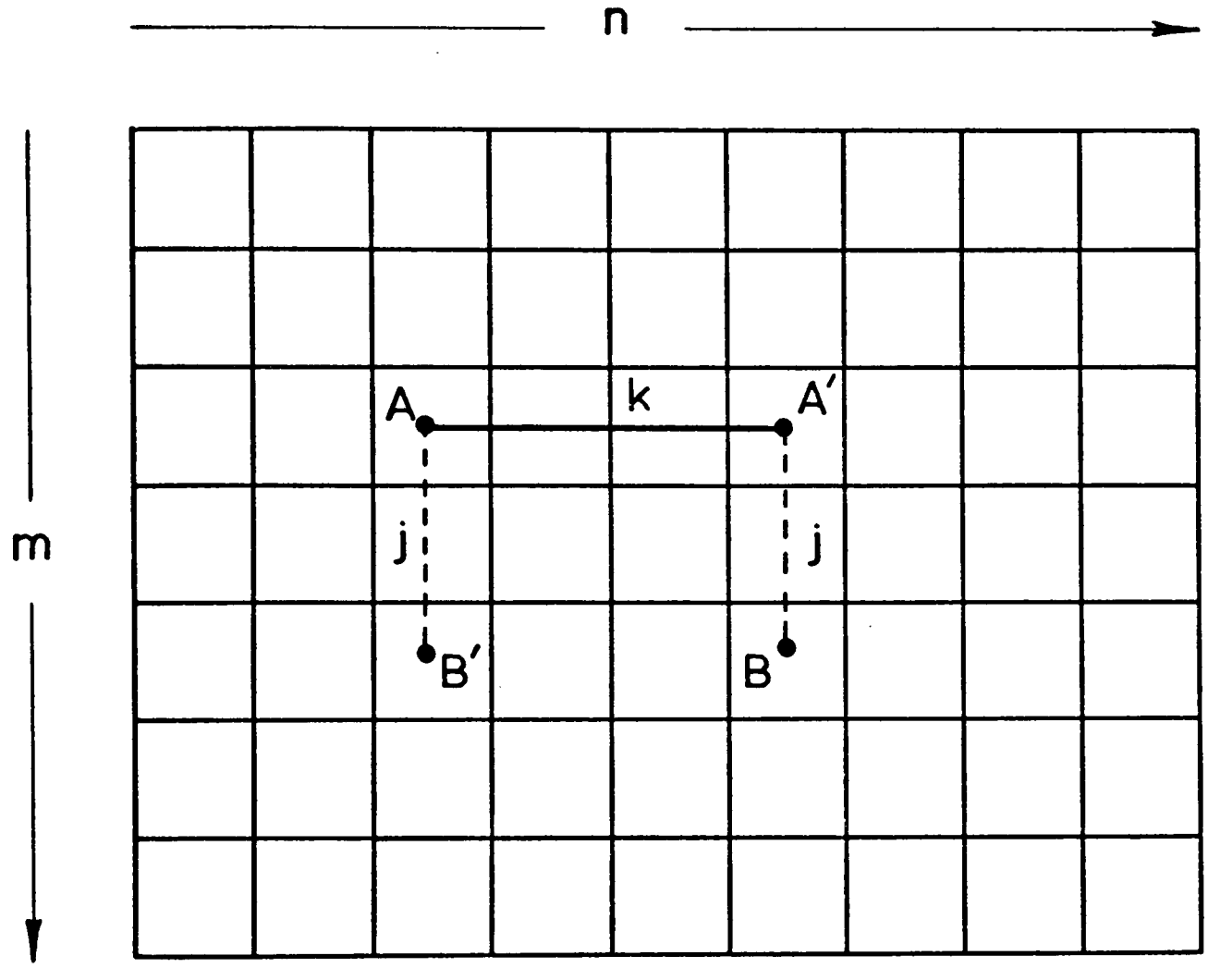


Fig. 6.4 Rectangular sample, dimension 9 x 7 unit samples. k = 3, j = 2. n_r = 2 x (9-3) x (7-2) = 60.

(iii) Three-dimensional samples

A similar approach can be applied to three-dimensional samples. There are $2(m - j)(n - k)$ positions for a pair of unit samples, D, D' in any m, n plane. Two possible positions E, E' for a third unit sample a distance i apart in the positive ℓ direction are shown in Figure 6.5. There are therefore two pairs of unit samples DE and D'E'. $(\ell - i)$ arrangements like this exist and thus there are $4(\ell - i)(m - j)(n - k)$ pairs of unit samples distance $(i + j + k)$ apart using method 1 or $\sqrt{i^2 + j^2 + k^2}$ apart using method 2. In calculating the variance-sample size relationship for a three dimensional block, pairs of unit samples in the same plane and pairs of unit samples in the same row must be considered as well. Hence from equation 6.4 for an $(\ell \times m \times n)$ sample:

$$\frac{\sigma_N^2}{\sigma_o^2} = \frac{1}{\ell mn}\left[1 + \frac{2}{\ell mn}\left[mn \sum_{i=1}^{\ell-1}(\ell-i)\rho(i) + \ell n \sum_{j=1}^{m-1}(m-j)\rho(j) + \right.\right.$$

$$\ell m \sum_{k=1}^{n-1}(n-k)\rho(k) + 2\ell \sum_{j=1}^{m-1}\sum_{k=1}^{n-1}(m-j)(n-k)\rho(j,k) + 2m \sum_{i=1}^{\ell-1}\sum_{k=1}^{n-1}$$

$$(\ell-i)(n-k)\rho(i,k)$$

$$+2n \sum_{i=1}^{\ell-1}\sum_{j=1}^{m-1}(\ell-i)(m-k)\rho(i,j) + 4 \sum_{i=1}^{\ell-1}\sum_{j=1}^{m-1}\sum_{k=1}^{m-1}(\ell-i)(m-j)(n-k)$$

$$\left.\left.\rho(i,j,k)\right]\right] \qquad (6.9)$$

where $\rho(i,j,k)$ is the correlation between samples which are i apart in the ℓ direction, j apart in the m direction and k apart in the n direction.

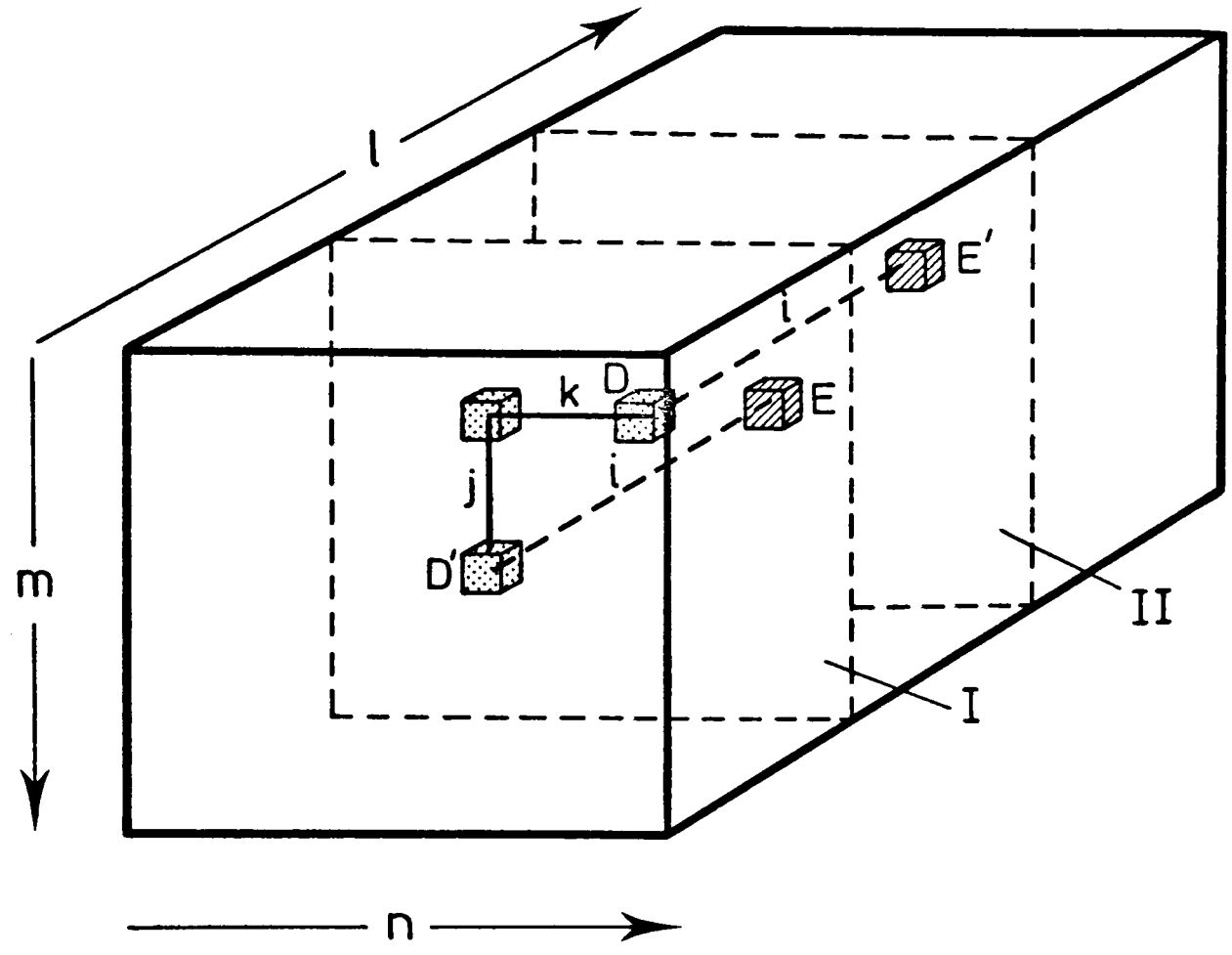


Fig. 6.5 Three-dimensional sample. D, D^1 lie in plane I. E, E^1 lie in plane II.

6.4 Application to particular cases

6.4.1 Method 1

If the distance between unit samples is measured orthogonally, then an exact analytical expression for σ_N^2/σ_o^2 can be developed if a simple expression for $\rho(r)$ is assumed. If $\rho(r) = a^r$, the double and triple summations in equation 6.9 can be split up and summed. For example,

$$\sum_{j=1}^{m-1}\sum_{k=1}^{n-1}(m-j)(n-k)a^{j+k} = \left[\sum_{j=1}^{m-1}(m-j)a^j\right]\left[\sum_{k=1}^{n-1}(n-k)a^k\right]$$

The general term in these summations may be found. If $G' = n-k$, then

$$\sum_{k=1}^{n-1}(n-k)a^k = a^n\sum_{G'=1}^{n-1}G'a^{-G'}$$

$$\text{Now let } R = \sum_{G'=1}^{n-1}a^{-G'} = \frac{a^{-(n-1)}-1}{1-a}$$

Then

$$-a\frac{dR}{da} = \sum_{G'=1}^{n-1}G'a^{-G'} = \frac{(n-1)a^{-(n-1)}-na^{-(n-2)}+a}{(1-a)^2}$$

Thus

$$\sum_{k=1}^{n-1}(n-k)a^k = \frac{1}{(1-a)^2}\left[(n-1)a-na^2+a^{n+1}\right] \qquad (6.10)$$

Substitution of such results in equations 6.6-6.9 leads to general expressions for σ_N^2/σ_o^2. Results for some commonly occurring special cases are given below.

(i) Cubic sample

If the sample is cubic, $\ell = m = n$. If $\rho(r) = a^r$, the three summations for pairs of unit samples in the same row are equal to

$$\frac{3n^2}{(1-a)^2}\left[(n-1)a-na^2+a^{n+1}\right]$$

The three summations for pairs of unit samples in the same plane are equal to

$$\frac{6n}{(1-a)^4}\left[(n-1)a-na^2+a^{n+1}\right]^2$$

The summation for pairs of unit samples not in the same plane is

$$\frac{4}{(1-a)^6}\left[(n-1)a-na^2+a^{n+1}\right]^3$$

Adding these together and substituting in equation 6.9 gives

$$\frac{\sigma_N^2}{\sigma_o^2}=\frac{1}{n^3}\left[1+\frac{2}{n^3(1-a)^6}\left[(3n^3-3n^2)a-(9n^3-6n)a^2+\right.\right.$$

$$(10n^3+6n^2-4)a^3-(6n^3+6n)a^4+(3n^3-3n^2)a^5-n^3a^6+$$

$$3n^2a^{n+1}-12na^{n+2}+(12-6n^2)a^{n+3}+12na^{n+4}+3n^2a^{n+5}+$$

$$\left.\left.6na^{2n+2}-12a^{2n+3}-6na^{2n+4}+4a^{3n+3}\right]\right] \qquad (6.11)$$

For large n, ignoring terms in $\frac{1}{n}$ of order greater than 3,

$$\frac{\sigma_N^2}{\sigma_o^2}=\frac{1}{n^3}\left[1+\frac{2a(a^2+3)}{(1-a)^3}\right]=\frac{1}{n^3}\left[\frac{1+a}{1-a}\right]^3 \qquad (6.12)$$

(ii) Square sample

Putting m = n in equation 6.8, substituting for the summations, and collecting terms,

$$\frac{\sigma_N^2}{\sigma_o^2}=\frac{1}{n^2}\left[1+\frac{2}{n^2(1-a)^4}\left[2an(n-1)+2a^2(1-2n^2)+2a^3n(n+1)\right.\right.$$

$$\left.\left.+2na^{n+1}-4a^{n+2}-2na^{n+3}+2a^{2n+2}\right]\right] \qquad (6.13)$$

For large n, ignoring terms in $\frac{1}{n}$ of order greater than 2,

$$\frac{\sigma_N^2}{\sigma_o^2}=\frac{1}{n^2}\left[1+\frac{4a}{(1-a)^2}\right]=\frac{1}{n^2}\left[\frac{1+a}{1-a}\right]^2 \qquad (6.14)$$

(iii) Linear sample

Equation 6.7 leads to

$$\frac{\sigma_N^2}{\sigma_o^2} = \frac{n(1-a^2)-2a(1-a^n)}{n^2(1-a)^2} \qquad (6.15)$$

For large n, ignoring terms in $\frac{1}{n^2}$,

$$\frac{\sigma_N^2}{\sigma_o^2} = \frac{1}{n}\left[1 + \frac{2a}{1-a}\right] = \frac{1}{n}\left[\frac{1+a}{1-a}\right] \qquad (6.16)$$

Equation 6.15 has previously been derived by Bourne (1967). The result for a linear sample is analogous to that for a series of samples taken at different times from a continuous blender and thus this equation is consistent with the limiting case considered by Goldsmith (1966) in his study of semi-continuous blending.

If a correlation coefficient of the form (1-er) is used, where e<1, then a different approach to the summation is required. This is illustrated by the following example.

Consider an m x n sample in which 1/e, the maximum distance over which correlation extends, is less than the length of one side of the sample. If r<m and r<n, the number of pairs of unit samples a distance r apart, where r = i+j, is given by

$$n_r = n(m-r)+m(n-r) + 2\sum_{s_r=1}^{r-1}(n-s_r)(m-[r-s_r])$$

Pairs of unit samples where r>m or r>n are not considered and hence

$$n_r = 2mnr - (n+m)r^2 + \frac{r}{3}(r^2-1)$$

But

$$\frac{\sigma_N^2}{\sigma_o^2} = \frac{1}{nm}\left[1+\frac{2}{nm}\sum_{r=1}^{1/e} n_r(1-er)\right]$$

and hence

$$\frac{\sigma_N^2}{\sigma_o^2} = \frac{1}{nm}\left[1 + \frac{2}{nm}\left(\frac{1}{60e^4} - \frac{n+m}{12e^3} + \frac{4nm-1}{12e^2} + \frac{n+m}{12e} - \frac{5nm-1}{15}\right)\right]$$

(6.17)

provided 1/e is an integer. If that is not the case, an exact analytical result is still possible if the upper limit of the summation is changed to the integer below 1/e. For large n and m, ignoring higher order terms,

$$\frac{\sigma_N^2}{\sigma_o^2} = \frac{1}{nm}\left[1 + \frac{2}{3}\left(\frac{1}{e^2} - 1\right)\right] = \frac{1}{3nm}\left[1 + \frac{2}{e^2}\right] \qquad (6.18)$$

The corresponding result for the three-dimensional case is:

$$\frac{\sigma_N^2}{\sigma_o^2} = \frac{1}{\ell mn}\left[1 + \frac{2}{\ell mn}\left(-\frac{1}{1260e^6} + \frac{\ell+m+n}{180e^5} - \frac{3\{\ell m+\ell n+mn\}-1}{90e^4}\right.\right.$$

$$+ \frac{6\ell mn-\{\ell+m+n\}}{36e^3} - \frac{7}{180e^2} + \frac{15\ell mn+\{\ell+m+n\}}{45e}$$

$$\left.\left. - \frac{105\ell mn-7\{\ell m+\ell n+mn\}-6}{210}\right)\right] \qquad (6.19)$$

For large 1, m and n, ignoring higher order terms,

$$\frac{\sigma_N^2}{\sigma_o^2} = \frac{1}{\ell mn}\left[1 + 2\left(\frac{1}{6e^3} + \frac{1}{3e} - \frac{1}{2}\right)\right] = \frac{1}{3\ell mne}\left[2 + \frac{1}{e^2}\right] \qquad (6.20)$$

6.4.2 Method 2

If distances between pairs of samples are measured vectorially, then a numerical solution is necessary. Substitution of $\rho(r) = a^r$ or $(1-er)$ in equation 6.9 where $r = \sqrt{i^2 + j^2 + k^2}$ leaves the equation in a form which can be summed numerically.

6.5 Discussion

Bourne (1967, 1968) and Scott and Bridgwater (1974) have found it convenient to use a correlation coefficient equal to a^r using a = 0.5 when comparing results, and the same function has been used here. Figure 6.6 shows how the variance-sample size relationship is affected by the type of sampling method employed.

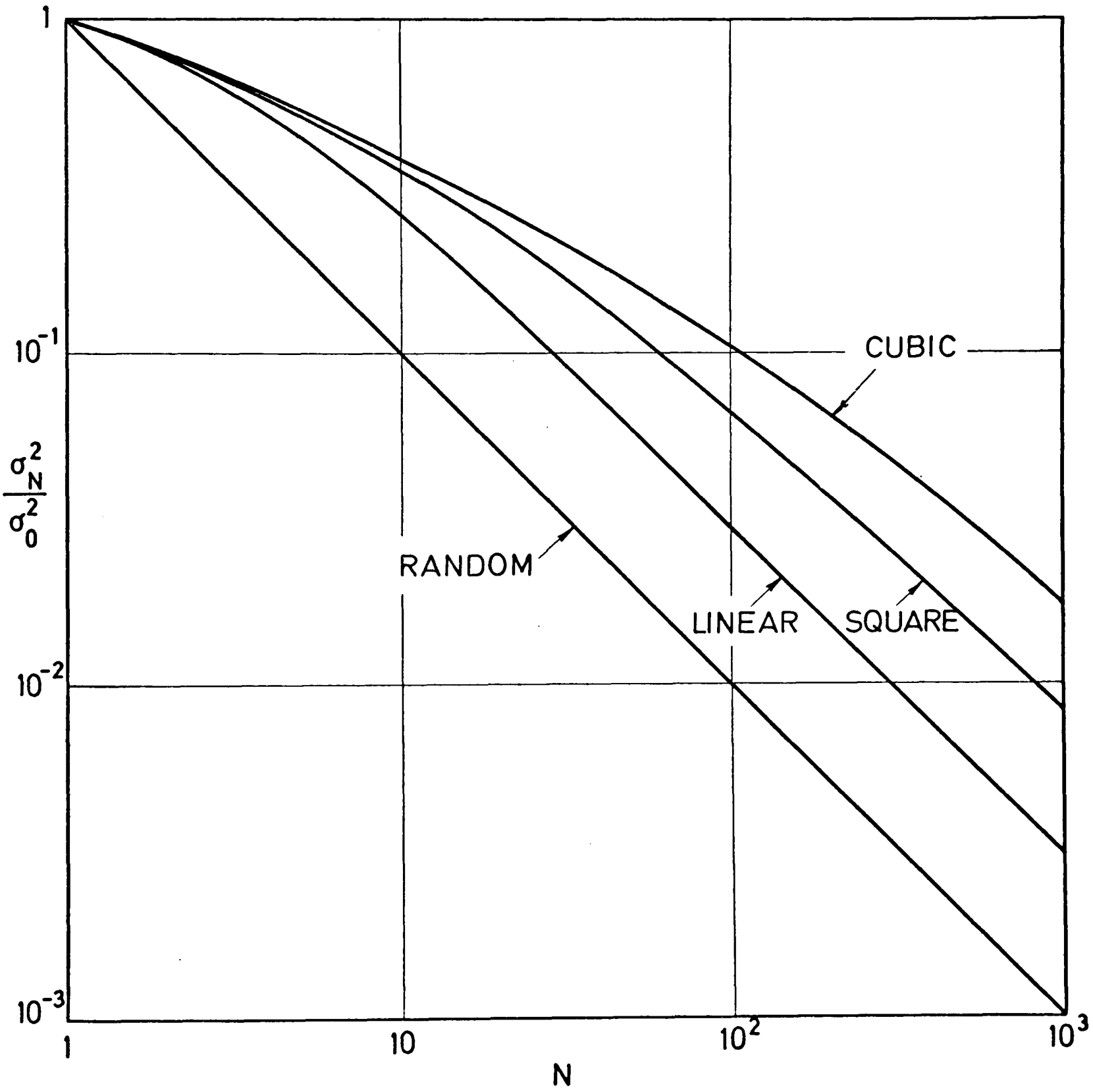


Fig. 6.6 Variance-sample size relationships for different shape samples. $\rho(r) = 0.5^r$. Method 1.

At a sufficiently large sample size, all the curves reach a limiting gradient of -1. The systematic increase in variance with the increasing dimensionality of the sample for a specified number of unit samples N is caused by the necessarily greater compactness of samples of higher dimensionality.

At large sample sizes, all curves become parallel to the random line and the relationship between variance and sample size is given by equations 6.12, 6.14, 6.16, 6.18 and 6.20. This is illustrated in Figure 6.7, which shows the effect of altering the value of 'a' for square samples. If experimental data yield a straight line offset from the random line at a sufficiently large sample size, then the value of 'a' may be deduced from the distance between the two lines, provided that $\rho(r) = a^r$ is an acceptable form of the correlation coefficient. Even if the form of the correlation coefficient is unknown, the value of the offset provides a simple means of assessing the amount of correlation present in the mixture. The offsets in Figure 6.7 are consistent with equation 6.14. Similar considerations apply to other formulations of the correlation coefficient. In general, from equations 6.12, 6.14, and 6.16 if Y_I is the intercept of the extrapolated straight line portion on the y - axis of a plot such as Figure 6.7,

$$a = \frac{(Y_I^{1/d} - 1)}{(Y_I^{1/d} + 1)} \qquad (6.21)$$

where d denotes the dimensionality of the sample, equalling one for a linear sample, two for a square sample and three for a cubic sample.

Figure 6.8 shows the effect of changing the shape of samples for samples that are 5 and 10 unit samples wide, the other dimen-

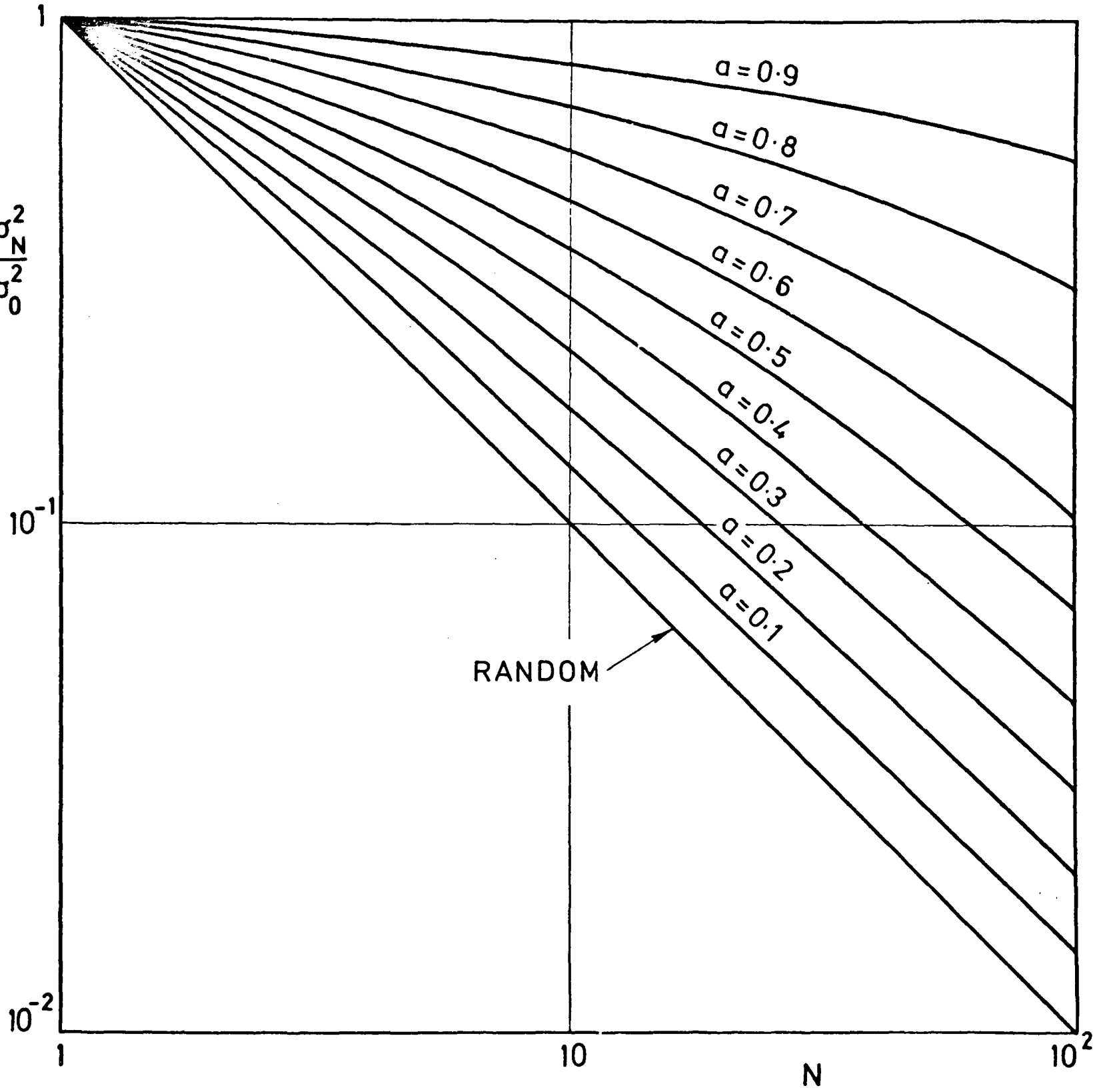


Fig. 6.7 Variance-sample size relationships for square samples. $\rho(r) = a^r$. Method 1.

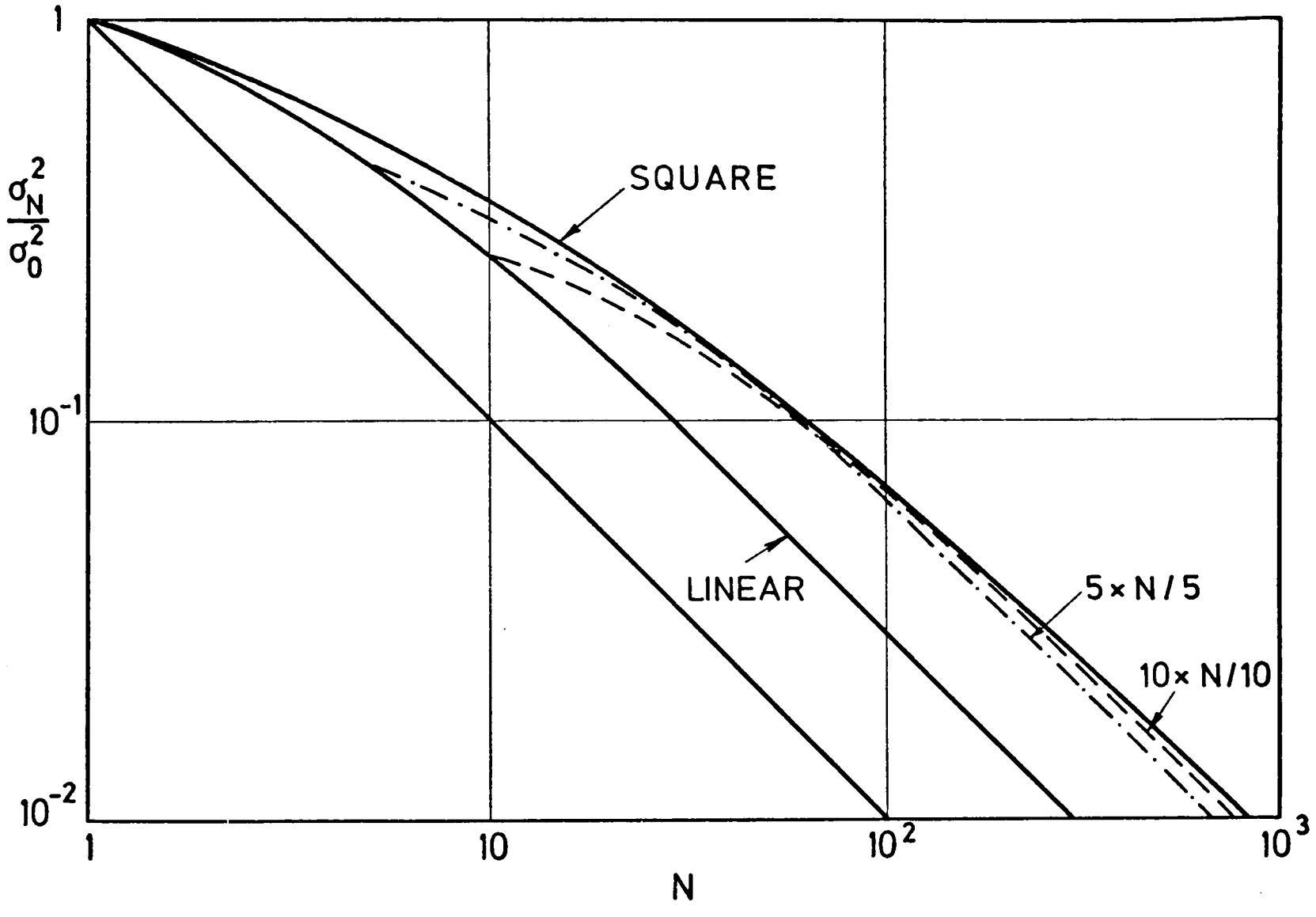


Fig. 6.8 Variance-sample size relationships for rectangular samples, $\rho(r) = 0.5^r$. Method 1.

sion being N/5 and N/10 respectively. Consider the 5 x N/5 curve. It must necessarily start on the linear curve at N = 5, pass through the curve for squares at N = 25 and then fall below the curve for squares owing to the loss of compactness at large sample sizes.

Vector formulations (method 2) are compared with the orthogonal formulation (method 1) for square samples using $\rho(r) = 0.5^r$ in Figure 6.9. As expected, rounding off increases the variance. Also shown is the result employing a linear correlogram $\rho(r) = 1-er$, choosing the value of e so as to give correlograms of equal area, i.e. equal linear scales of segregation given by $\int_0^\infty \rho(r)\, dr$ (Danckwerts, 1953).

Hence $$\frac{1}{2e} = \int_0^\infty a^x dx = -\frac{1}{\ln a}$$

and $$e = -\frac{1}{2} \ln \frac{1}{2}$$

The experimental variance-sample size relationships obtained from the data of Hall and Godfrey can be checked against the values predicted from the experimentally determined correlation coefficient and equation 6.13. Agreement between the two is good as shown by Figure 6.10. The vector formulation (i.e. employing the vector form for $\rho(r)$ and the vector measurement of distances) gives a virtually identical curve.

Correlograms were calculated for all the three-dimensional mixer experiments and three of them are shown in Figure 6.11 as examples. In only a few cases was there much correlation between samples; experiment 5 showed most due to a pronounced pattern in the results and a least squares fit to this correlogram gave $\rho(r) = 0.639^r$, also shown in Figure 6.11. The correlograms from experiments 11 and 15 could not be satisfactorily represented by a smooth curve of this form nor by a straight line. These were

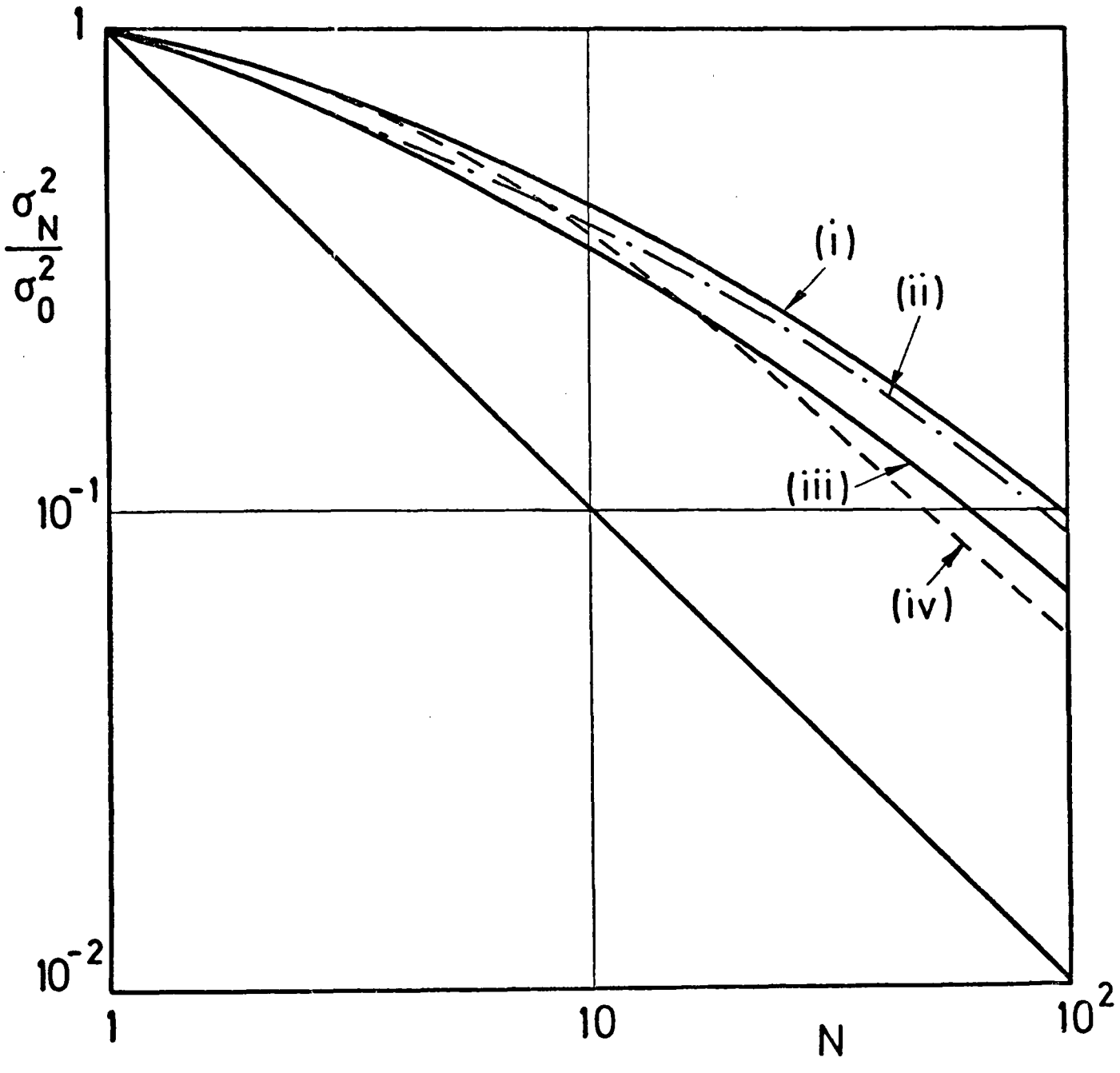


Fig. 6.9 Variance-sample size relationships.

i. Vector measurement. Method 2 $\rho(r) = 0.5^r$, with rounding off.

ii. Vector measurement. Method 2 $\rho(r) = 0.5^r$, without rounding off.

iii. Orthogonal measurement. Method 1. $\rho(r) = 0.5^r$.

iv. Orthogonal measurement. Method 1. $\rho(r) = 1+\frac{r}{2}\ \ell n\frac{1}{2}$

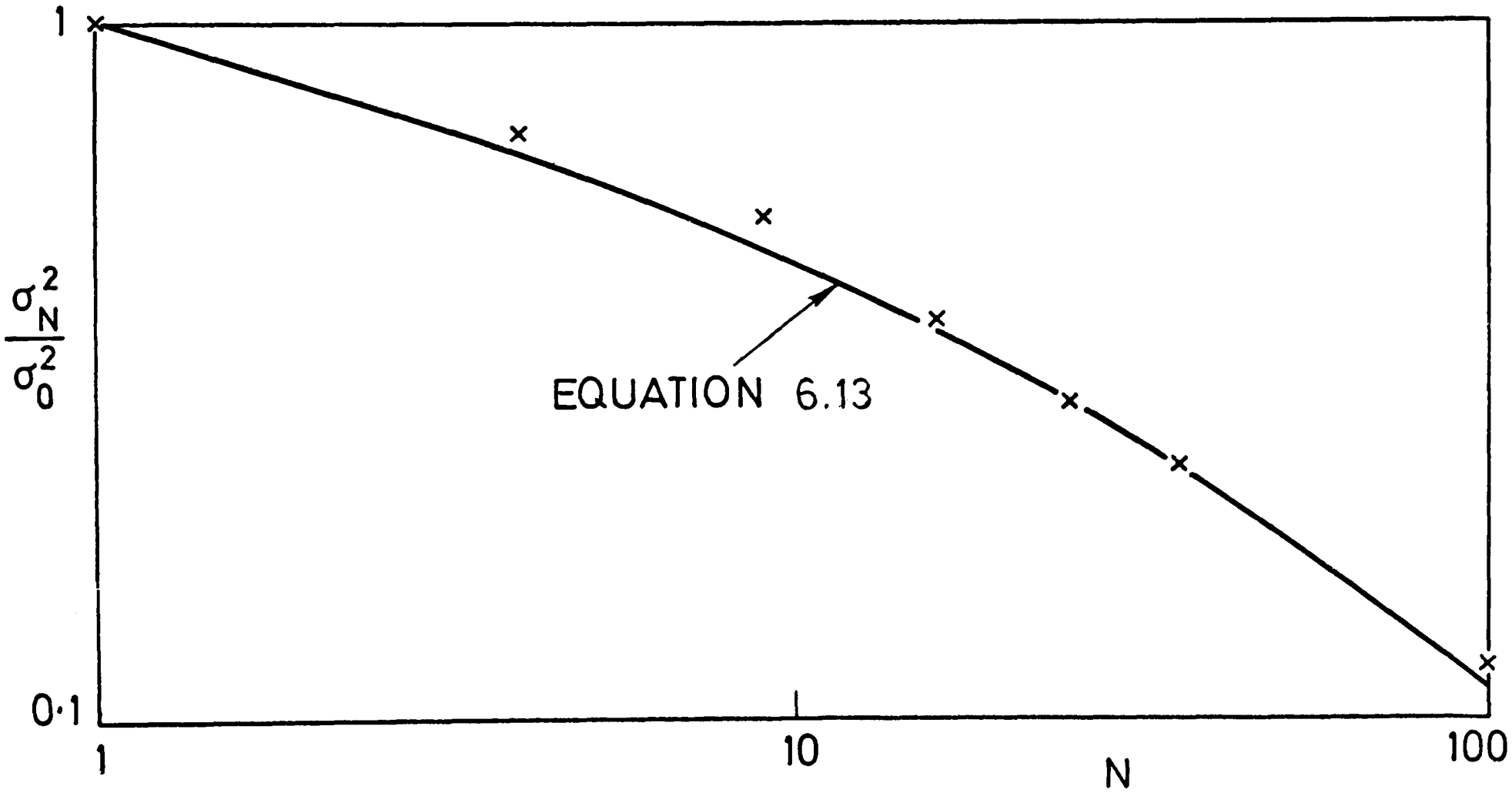


Fig. 6.10 Variance-sample size relationship for Hall and Godfrey's experiment B5 compared with that predicted by equation 6.13. x = experimental results.

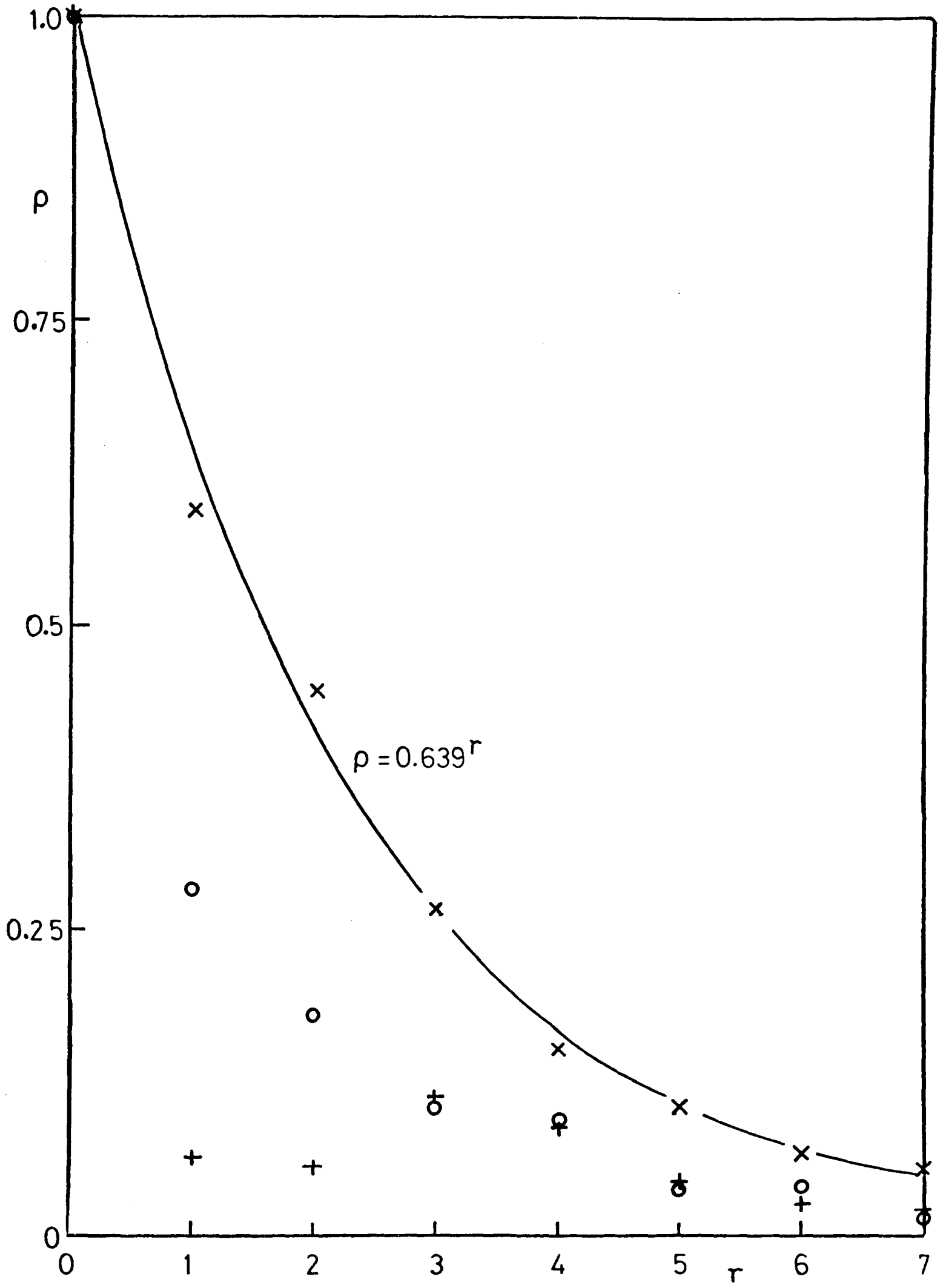


Fig. 6.11 Correlograms derived from three-dimensional mixer experiments, Table 4.1. × expt. 5, lead shot; + expt. 11, ballotini; o expt. 15, lead shot.

typical of most of the results; values of ρ were generally small and positive for r<10 but the correlograms could not be described by simple equations. This approach to these results was not pursued further.

Other workers have produced related studies. Landry (1944) presented an analysis of what he called a "partly segregated" coal, defined as one in which there are islands of segregation, or non-randomness, in a background of randomness. He showed that the variance of the ash content in samples containing n_1 equal-sized pieces of coal, σ_n^2, was given by

$$\frac{\sigma_n^2}{\sigma_o^2} = \frac{1}{n_1}\left[\, 1 + (n_1-1)\bar{\rho}_n \,\right] \qquad (6.22)$$

where $\bar{\rho}_n$ was a mean correlation coefficient, the average over all possible pairs of samples. He went on to derive the expression

$$\frac{\sigma_n^2}{\sigma_o^2} = N^{B_n-1} \qquad (6.23)$$

for a "compact" sample made up of N unit samples, where B_n = log (1+a)/log 2 and $\rho(r) = a^r$. This leads to a straight line relationship between σ_n^2 and N on a log-log plot, as opposed to those developed here. Since work by Scott and Bridgwater (1974) on point samples gives graphs of the same form as those here, it seems likely that Landry has incorrectly evaluated n_r, possibly due to the arbitrariness of the form of sample that he chose. Kristensen (1976) has recently confirmed this point.

Bourne (1967, 1968) discussed Landry's work and also considered correlation in linear samples using the approach developed here. He was unable to deduce values of n_r for two- or three-dimensional samples but derived numerically some results for square samples containing up to 49 unit samples using method

1. Kristensen (1973a-e) extended the work on linear samples using a similar method, to include cases where the correlation coefficient is of the form (1-er). He has also considered the effect of analytical errors on the evaluation of correlation coefficients. He has looked at two-dimensional samples but did not make any generalisations. Stange (1967) also considered correlation in linear samples and derived results similar to those obtained by Bourne and Kristensen.

Scott and Bridgwater (1974) derived expressions for the variance of linear, circular and spherical samples in terms of the correlation coefficient between infinitely small elements. This approach has the advantage that no decision has to be made as to the size of the unit sample to be employed (though in practical situations this will often be predetermined), but the disadvantage that determination of the correlogram for powder mixtures is relatively difficult. They obtained an expression for the variance

$$\sigma^2 = \frac{p(1-p)}{S_a^2} \int_{S_a} N(r)\rho(r)dr \qquad (6.24)$$

where p was the proportion of one of the components by volume, S_a the size of the sample, and N(r) the density function for element pairs of lag r when both elements come from the same sample. The present work leads to estimates of the variance at a particular sample size which are lower than those obtained by Scott and Bridgwater. This is because in their approach the correlation coefficient is evaluated between elements whereas here it is evaluated between unit samples and correlation within unit samples is not included.

6.6 Conclusions

It has been shown that, in general, the statistical properties of a mixture sampled at a certain level of scrutiny can be represented in terms of a variance of and correlation coefficient between unit samples. This conclusion applies strictly to true binary mixtures. However, multicomponent mixtures could be treated by considering them as pseudo-binary mixtures in which the second component is composed of all the species except the first. Correlograms for each different component can be derived in turn and thus it is possible to have a mixture for which it may be said that some components are well-mixed and others are not.

By means of the derivation of the density function between pairs of samples, n_r, it has been shown that the variance of any regular sample may be related to its size and the correlation coefficient. General expressions for one, two and three dimensions have been found which include the special cases looked at by earlier workers. Both exponential and linear correlation coefficients have been used, as have different methods of measuring distance.

The value of the offset Y_I between the straight line portion of the log σ_N^2/σ_o^2 vs. log sample size curve and the random mixture curve has been noted as a means of assessing the amount of correlation present in a mixture. If a mixture shows correlation of the form $\rho(r) = a^r$, it is found that for linear, square and cubic samples

$$a = \frac{Y_I^{1/d} - 1}{Y_I^{1/d} + 1}$$

where d denotes the dimensionality of the sample.

Because this analysis was designed to cope with the results of the mixer experiments, macroscopic samples have been considered. Though a consideration of correlation between point samples gives more information about the detailed structure of a mixture, information about unit samples is easier to obtain and thus these results are more useful.

CHAPTER 7

STRAIN-INDUCED PERCOLATION. EQUIPMENT

7.1 Introduction

7.1.1 Previous work

It has long been known that dilation accompanies substantial shearing of a granular material (Reynolds, 1885). Failure of such a material is localised and concentrated in narrow planes called slip planes or failure zones, the formation of which has been described by Roscoe (1967). When a granular material is strained, the ratio of shear stress to normal stress rises until failure occurs. The shear stress then decreases to a value at which unlimited strain can take place. The particular region that fails depends on local irregularities in the packing and on the stress distribution. Thus failure zones are found between blocks of material in which only elastic deformation occurs.

Roscoe (1970) has reviewed the use of the simple shear apparatus to study failure zones in soils. Measurements using X-ray and γ-ray photography indicated that they were generally about ten particle diameters thick. Other evidence for their existence has been summarised by Scott (1974). It is in such zones that strain-induced percolation occurs.

Some early experiments on strain-induced percolation were performed by Willemse (1961). He used a vertical cylinder, 44mm in diameter, fitted with a shaft rotating at 30 r.p.m., from which pins extended to the walls. The materials used were nylon and polypropylene spheres; the latter were smaller though exact sizes are not recorded. Willemse reported that for widely

divergent particle properties, demixing was complete after approximately sixty revolutions, though for less dissimilar particles an equilibrium concentration distribution was set up where the rate of fall due to percolation equalled the rate of rise due to diffusion. Unfortunately the experimental procedure and results are poorly reported and some of the quantities are not well-defined, thus limiting the usefulness of the study.

Campbell and Bridgwater (1973) studied percolation in a vertical failure zone adjacent to a roughened wall in a thin rectangular hopper. The behaviour of tracer particles in this zone was recorded by a cine camera moving down with the bulk of the material, which was supported by a piston. The rough edge wall was 120 grit sandpaper and experiments were performed with spherical glass and tungsten carbide particles. Percolation was observed for $d_p/d_b<0.5$ when all particles had the same density and persisted up to seven bulk particle diameters from the wall. With soda glass particles the failure zone appeared to increase from five particle diameters at a piston speed of 4mm s^{-1} to about fifteen particle diameters at 33m s^{-1}. A detailed analysis of the results has not been presented (Campbell, 1975). It is possible that the motion observed in these experiments may be characteristic of a hopper corner, rather than a side.

Sugimoto and Yamomoto (1973) also studied percolation in a two-dimensional hopper. An empirical expression relating the relative movement between different spherical particles was found, based on the density and diameter ratios between the particles. Only a limited range of ratios were used, 0.7 to 2.0 for ρ_p/ρ_b and 0.7 to 1.3 for d_p/d_b.

The only extensive study of strain-induced percolation has

been by Scott (1974). He showed that the phenomenon could be studied in a reciprocating shear cell and developed apparatus that could be used to produce large amounts of data relatively quickly. In a long series of experiments he investigated the effects of bed and particle properties on percolation velocities, which he found were a sensitive function of the diameter ratio between percolating and bulk particles, though the effect of the density ratio remained uncertain. Among the other quantities investigated was self-diffusion of the bulk particles for which an X-ray technique was used (Scott and Bridgwater, 1976).

More recent work includes that of Tranter (1976), who has shown that percolation rates are reduced by the presence of interstitial fluid and West (1976), who investigated strain-induced percolation in a two-dimensional shear cell. Stephens (1976) has measured percolation rates in an annular cell.

Since the work reported here is an extension of Scott's, his methods and equipment will be described in detail later.

7.1.2 Variables affecting percolation

A simple physical picture of strain-induced percolation has been described by Scott and will be summarised here. If an observer in an idealized horizontal failure zone (figure 7.1) were travelling with the average local velocity of the bulk material, then bulk particles with a different y co-ordinate to the observer would have a systematic velocity relative to him, while particles at the same y co-ordinate would not. There would also be a random fluctuating velocity component superimposed on the systematic motion. A smaller particle, if it were too large for spontaneous percolation, would be held by contact with at least one bulk particle below it. Eventually the random motion of the bulk particles would leave a gap through which the smaller

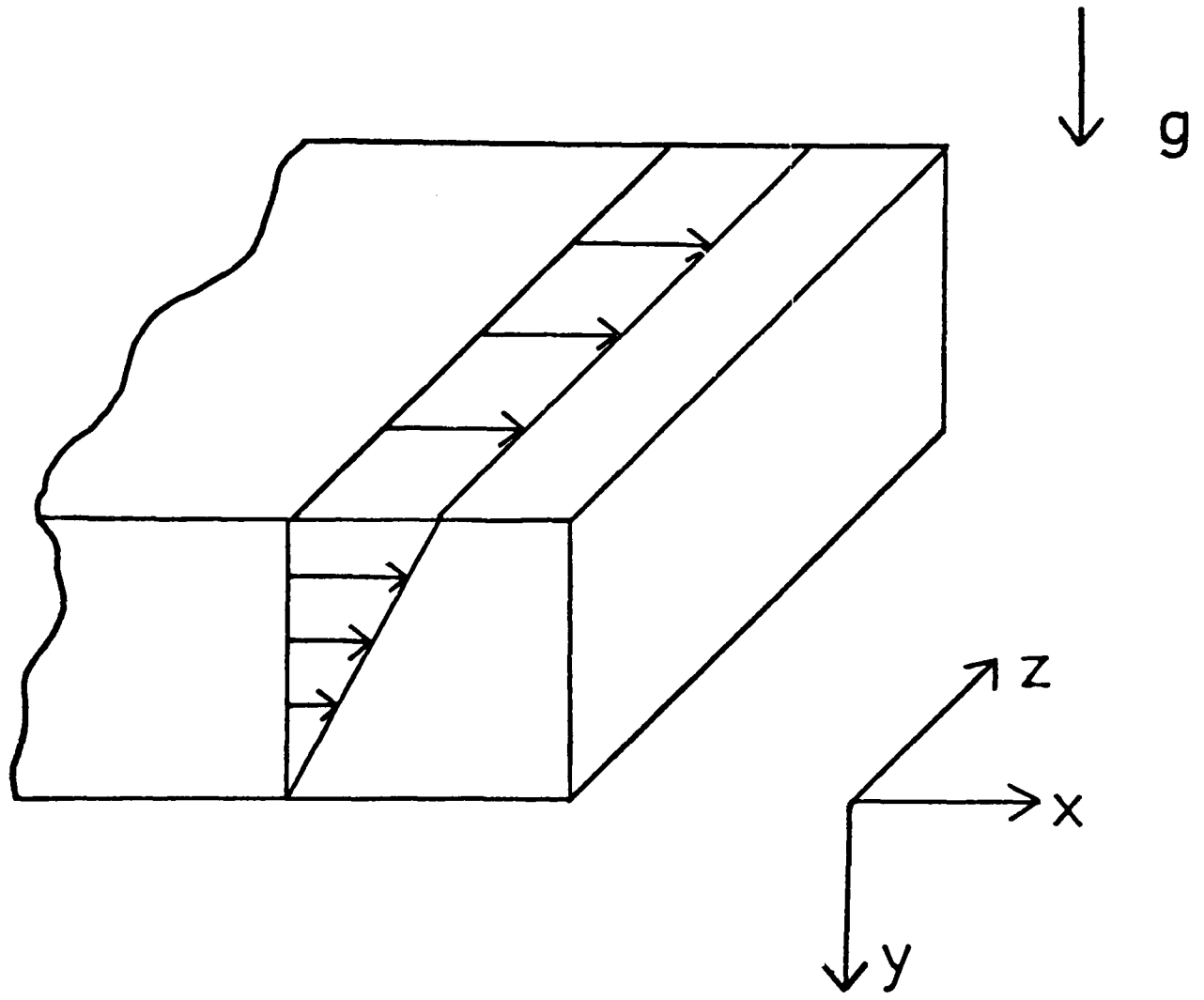


Figure 7.1: Idealized horizontal failure zone. The velocity profile in the failure zone, arbitrarily taken as linear, is also shown.

particle could fall and it would then be restrained by another layer of bulk particles. Percolation was thus represented as a release-capture process rather than steady downwards motion. Recently West (1976) has confirmed that this mechanism holds for percolation in two-dimensions. However this is not likely to be so if the percolating particle is only slightly smaller than the bulk particles as such a particle may also be expected to experience random upward motion in the same manner as the larger ones.

A consequence of this mechanism is that the relative sizes and shapes of percolating and bulk particles will be the major controlling factors, while relative densities will be less important. If the bulk material is not mono-sized, its size distribution and degree of segregation will also be of importance. Of the other material properties, elastic moduli may have the most effect on percolation rates, if the normal stress is sufficient to cause significant deformation of the particles. A high normal stress will also lead to compaction of the bed and consequently the production of smaller gaps for percolating particles. It may also reduce percolation rates by preventing the release of particles. The other variable which might be expected to have a significant effect on percolation is the rate of shear strain. Deformation of an element of material under shear is characterised by the angle through which the sides of the element are rotated. Relative horizontal distances traversed by bulk particles are proportional to the tangent of this angle and thus the rate of strain is proportional to the rate of change of the tangent of the angle. The void fraction of the bulk material in the cell has been shown by Scott to vary only slightly and he assumed that the material in the cell was in its

critical state (Roscoe et al., 1958), an assumption which will be discussed in Chapter 8. Those variables which may be important in strain-induced percolation are listed in Table 7.1.

Three dependent variables can be used to characterise the motion of the percolating particle.

(i) The average vertical distance through which a percolating particle falls per unit of shear strain. If the strain rate in a failure zone is $\dot{\gamma}$ and the average vertical velocity is u, the mean distance dropped per unit of strain is $u/\dot{\gamma}$. Now $u/\dot{\gamma}$ equals $\bar{y}/\gamma$, where $\bar{y}$ is the average vertical distance dropped by a percolating particle in a strain γ, thus replacing the unit of time by that of strain.

(ii) The distribution of vertical velocities about the mean. In a shear cell this is represented by the distribution of residence strains.

(iii) The random fluctuating velocity components orthogonal to the percolation direction.

Both (ii) and (iii) may be described by diffusion coefficients.

Scott used dimensional analysis to divide dependent and independent variables into groups. Those groups of interest in this work are:

(i) Dimensionless percolation velocity, $u/\dot{\gamma}d_b$

(ii) Dimensionless diffusion coefficients, $D/\dot{\gamma}d_b^2$, ud_b/D

(iii) Particle diameter ratio, d_p/d_b

(iv) Particle density ratio, ρ_p/ρ_b

(v) Dimensionless measure of strain rate, $d_b\dot{\gamma}^2/g$

(vi) Dimensionless normal stress, σ_y/E_b

(vii) Elastic modulus ratio, E_p/E_b

Table 7.1: Variables affecting percolation

Quantity	Symbol	Dimensions
Bulk particle size represented by a statistical diameter	d_b	L
Bulk particle shape		-
Percolating particle size represented by a statistical diameter	d_p	L
Percolating particle shape		-
Bulk particle density	ρ_b	ML^{-3}
Percolating particle density	ρ_p	ML^{-3}
Dynamic coefficient of friction between bulk particles	μ_b	-
Dynamic coefficient of friction between bulk and percolating particles	μ_p	-
Static coefficient of friction between bulk and percolating particles	μ_s	-
Elastic modulus of bulk particles	E_b	$ML^{-1}T^{-2}$
Elastic modulus of percolating particles	E_p	$ML^{-1}T^{-2}$
Coefficient of restitution between bulk and percolating particles	α	-
Normal stress on material	σ_y	$ML^{-1}T^{-2}$
Rate of shear strain of material	$\dot{\gamma}$	T^{-1}
Acceleration due to gravity	g	LT^{-2}
Void fraction of the bulk material	ε	-
Humidity		-

As a change of material affects various different properties, effects due to this are hard to classify under one heading.

7.2 Scott's equipment

The equipment used by Scott in his experiments was a simple shear apparatus (SSA), developed from those used for testing soils.

The first version of the SSA consisted of a perspex cell which was sheared by pushing backwards and forwards by hand. The first motor-driven version, the Mk. IIA, is shown in figures 7.2 and 7.3. Essentially the cell (figure 7.2) consists of a box, the cross-section of which can be changed from a rectangle to a parallelogram. Two opposite sides, A, are hinged at the bottom, the other two sides, B, are fixed and the top, C, is free to float on top of the bulk material. The base plate of the Mk. IIA was made by sticking 1½" dia. hemispheres on a metal plate and drilling holes between them through which a percolating particle could fall. The base plate is moved backwards and forwards and the material is subjected to shear strain. A percolating particle is detected as it is fed to the top of the cell and again as it falls out the bottom.

Difficulties with the base plate of the Mk. IIA led to its replacement by the Mk. IIB and finally by the Mk. III. This version, which differed from the Mk. II only in the cell design, could produce repeatable results, though the data was subject to random scatter and Scott had to repeat some of his experiments. However, by the end of his work, the apparatus could be run reasonably reliably, though the mechanism used to feed a percolating particle into the cell was still subject to frequent failure. Difficulties were also experienced with the electronic detection

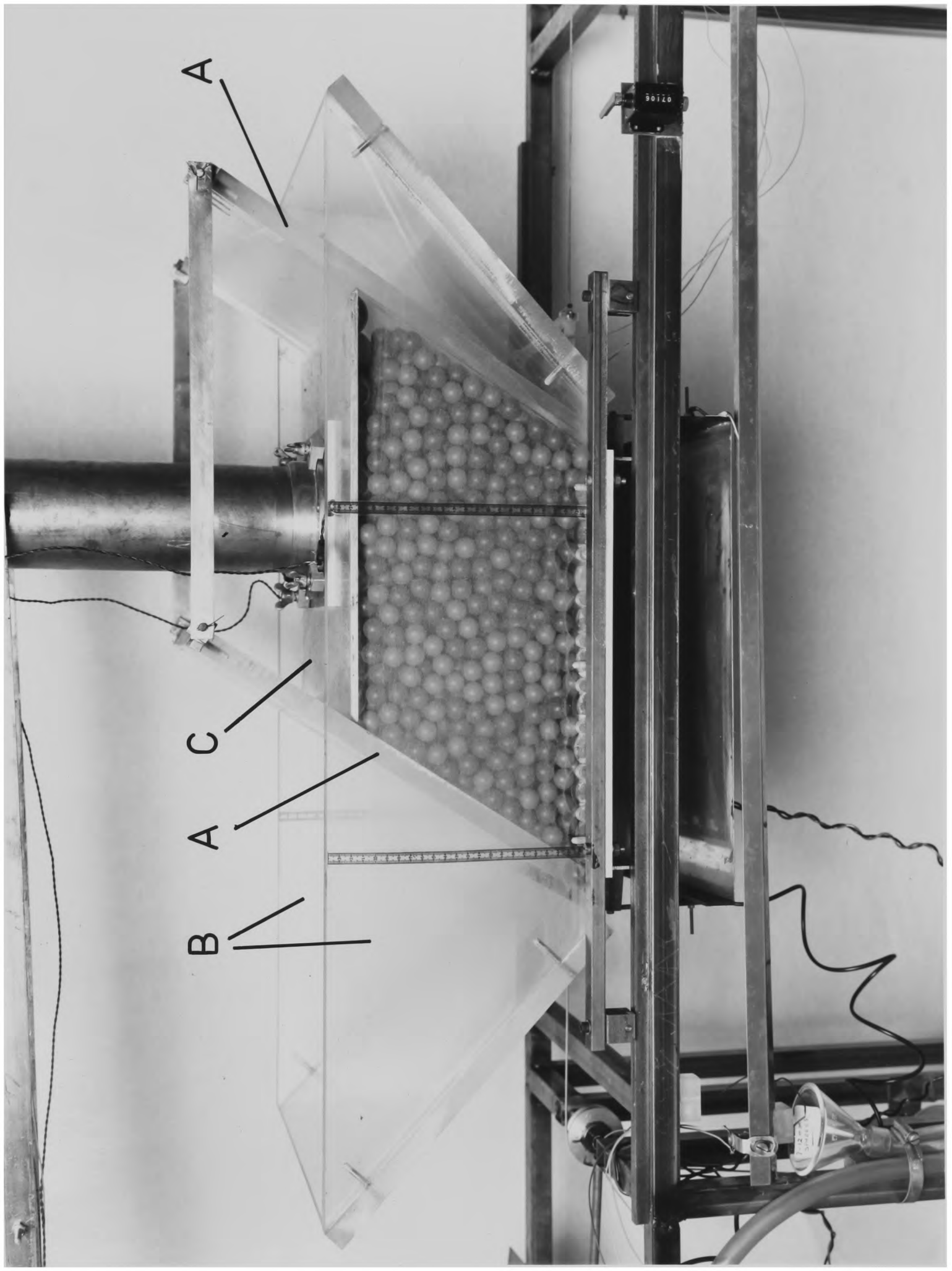


Figure 7.2: Close-up of the cell of the SSA Mk. IIA.

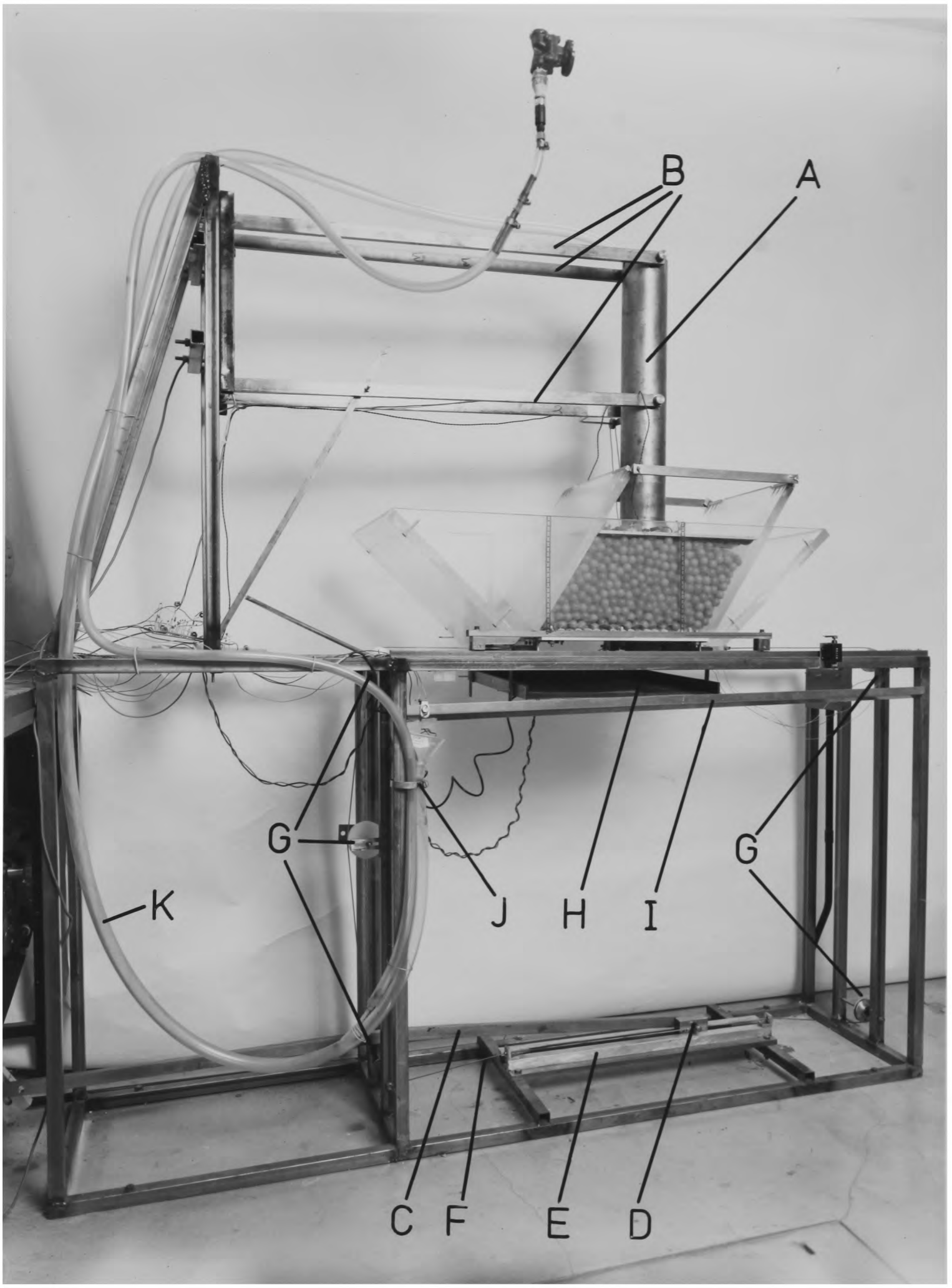


Figure 7.3: The SSA Mk. IIA.

equipment used to record the residence time of a particle in the cell. The apparatus inherited from Scott was modified for use in this study and will therefore be described in some detail.

7.2.1 The cell

The base plate of the SSA Mk. III was designed to prevent jamming of particles in the corners and to pass larger particles than the Mk. II. It consisted of 1½" phenolic resin spheres fixed onto nine ½" diameter steel rods, held in ball races mounted in an undercarriage (figure 7.4). Gear wheels were located on the ends of the rods and as the base moved, the gears ran along a fixed rack (figure 7.5). The spheres were forced to rotate in a direction such that bulk balls tended to be pulled out of a corner which was closing up. The ratio between the rate of rotation of the spheres and that of the end walls was about 2.5 to 1. The end walls, A (figure 7.4), were made from 3/8" thick aluminium alloy and were bolted to ½" steel rods, B, also running in ball races but mounted 5mm above the other bars. Metal pieces, C, which fitted in with the end row of spheres, were attached to the end walls to prevent jamming of the bulk balls. The arrangement of the base plate spheres, D, was chosen so that 18.6mm dia. bulk balls would not fall out even if considerable flexing of the steel rods occurred, though spheres up to 15mm dia. would fall out spontaneously.

The side walls of the cell, E, were fixed to the undercarriage and made from ¾" thick perspex sheet. The underside of the lid had 1½" dia. hemispheres stuck onto it. The lid was not fixed to the cell but was held in place by a 4" diameter vertical steel tube, A (figure 7.3), which was attached to the rest of the frame by four parallel rods, B, fitted with bearings at each end.

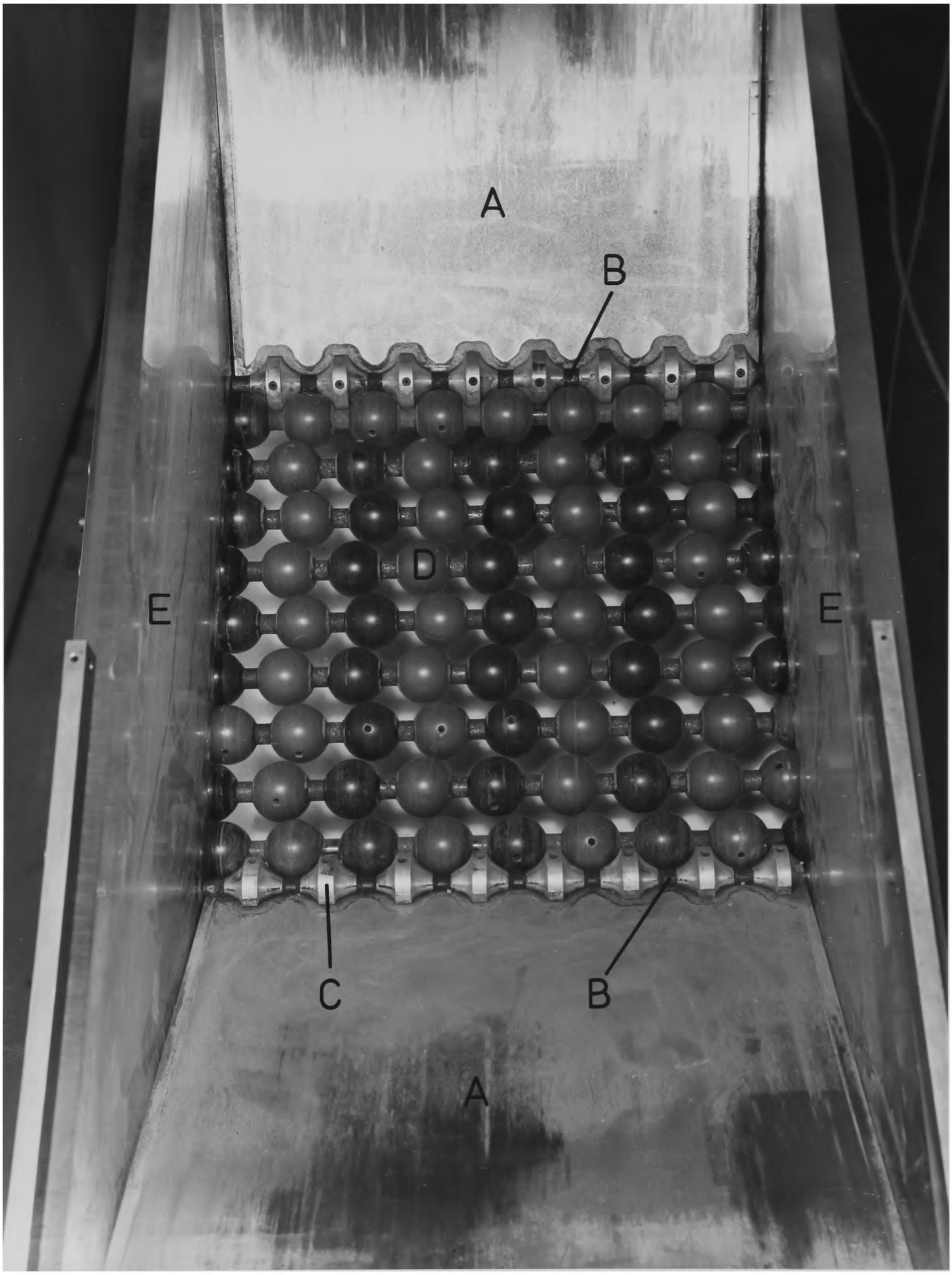


Figure 7.4: Base of the SSA Mk. III.

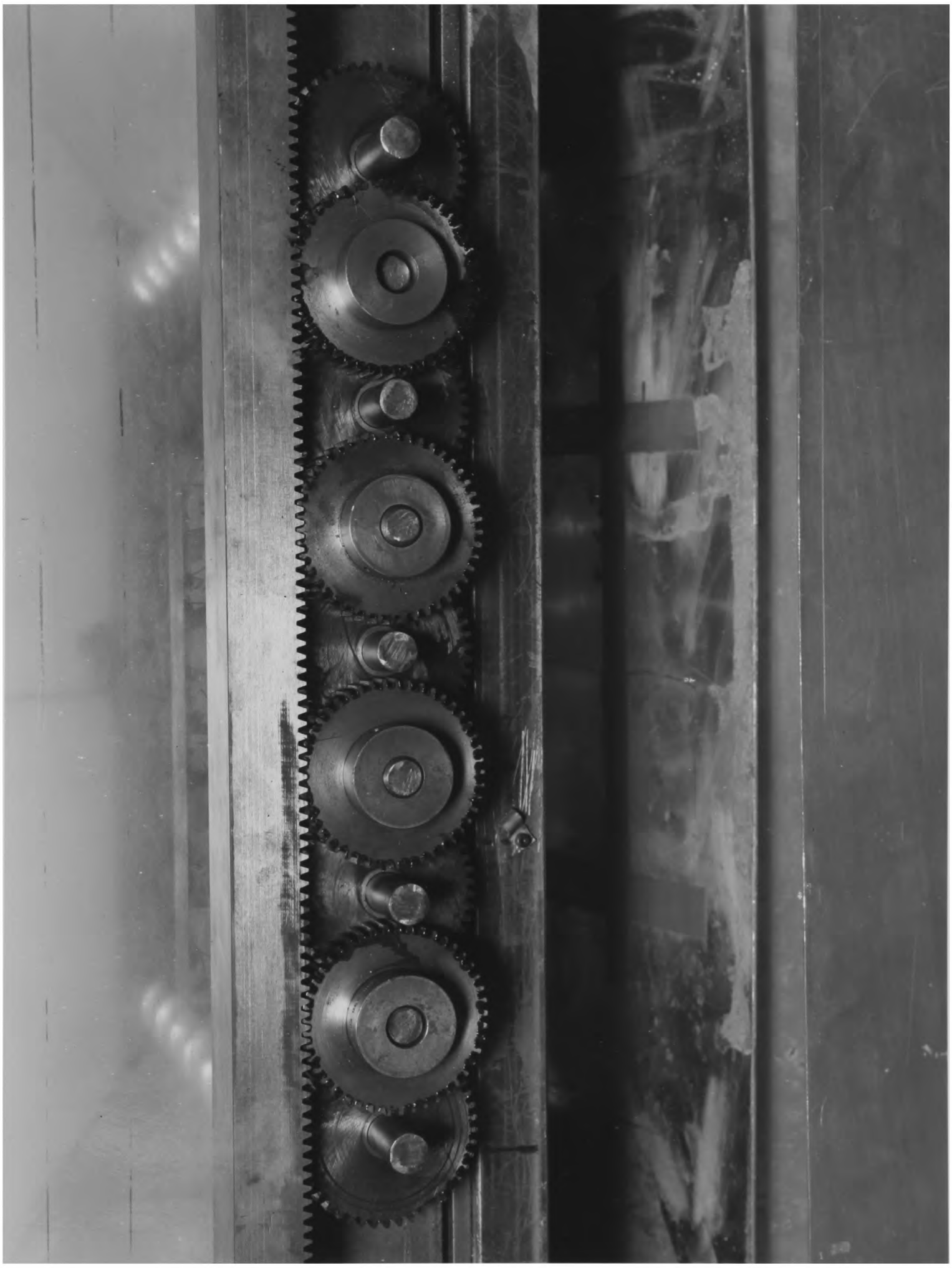


Figure 7.5: The SSA Mk. III showing rack and gear wheels.

The dimensions of the cell were 354mm long by 355mm wide by 246mm high. This wall height and all bed height measurements were taken from the centre-line between the base bars. The cell ran on four ball races which fitted into a grooved track, mounted on the welded square steel framework.

7.2.2 The driving system

A 0.5 h.p. electric motor was used to drive a variable throw crank through a 'Kopp' variable speed drive. The throw, and hence the stroke length of the cell, could be altered by turning a screw thread on the crank. This carried a stub axle about which a connecting rod, C (figure 7.3), turned. The other end of the connecting rod was attached to a slider, D, which ran in a horizontal track, E, bolted to the frame near floor level. 1/16" stainless steel cable, F, was attached to the slider and to both ends of the base plate via pulleys, G. Thus the base plate was pulled first one way and then the other as the slider moved backwards and forwards and the strain rate varied with simple harmonic motion over a stroke. Two strokes formed a cycle, the term applied to the movement of the cell occurring during one revolution of the crank.

7.2.3 The particle feeding and detection system

The system detected a single percolating particle as it entered and left the bed. It was then conveyed to the top of the cell again while the apparatus ran continuously.

The percolating particle entered the bed via a tube inserted in the lid with a trapdoor in it. This mechanism was operated by a cam on the undercarriage of the cell, which moved a lever that was attached to the trap door by string. As the particle fell into the bed it cut a light beam falling on a photocell and

thus started a timer. A microphone insert (Eagle M.C.45), fixed to the bottom of a steel tray, H (figure 7.3), under the cell, produced a pulse which was used to stop the timer when a particle hit the tray. The elapsed time displayed on the timer was fed in BCD format through a KDP punch interface to an Addo type 7 tape punch where it was recorded on 1" paper tape.

The steel tray was mounted at an angle to the horizontal so that the particle would roll into a sloping channel, I, and then operate another photocell, J, the pulse this time being used to reset the timer. The particle was then returned to the top of the cell by pneumatically conveying it in a 28mm dia. pipe, K.

At the end of an experiment the paper tape was removed and analysed on the Oxford University ICL 1906A computer.

7.2.4 Prevention of electrostatic charging

After prolonged running of the cell, the balls in the bed became electrostatically charged and small percolating particles acquired a coating of dust. Though it was shown that this did not affect percolation velocities, it tended to retard rolling on the tray and in the channel and was prevented by passing humidified air through the bed. Air from the main was passed at 3 m^3h^{-1} through a water height of 120mm in a bubble column. The water was heated to 23^{o}C, the temperature being controlled by a thermostat. The air was then fed via a water trap to four points on the lid of the apparatus, A in the photograph of the SSA Mk. V, figure 7.6.

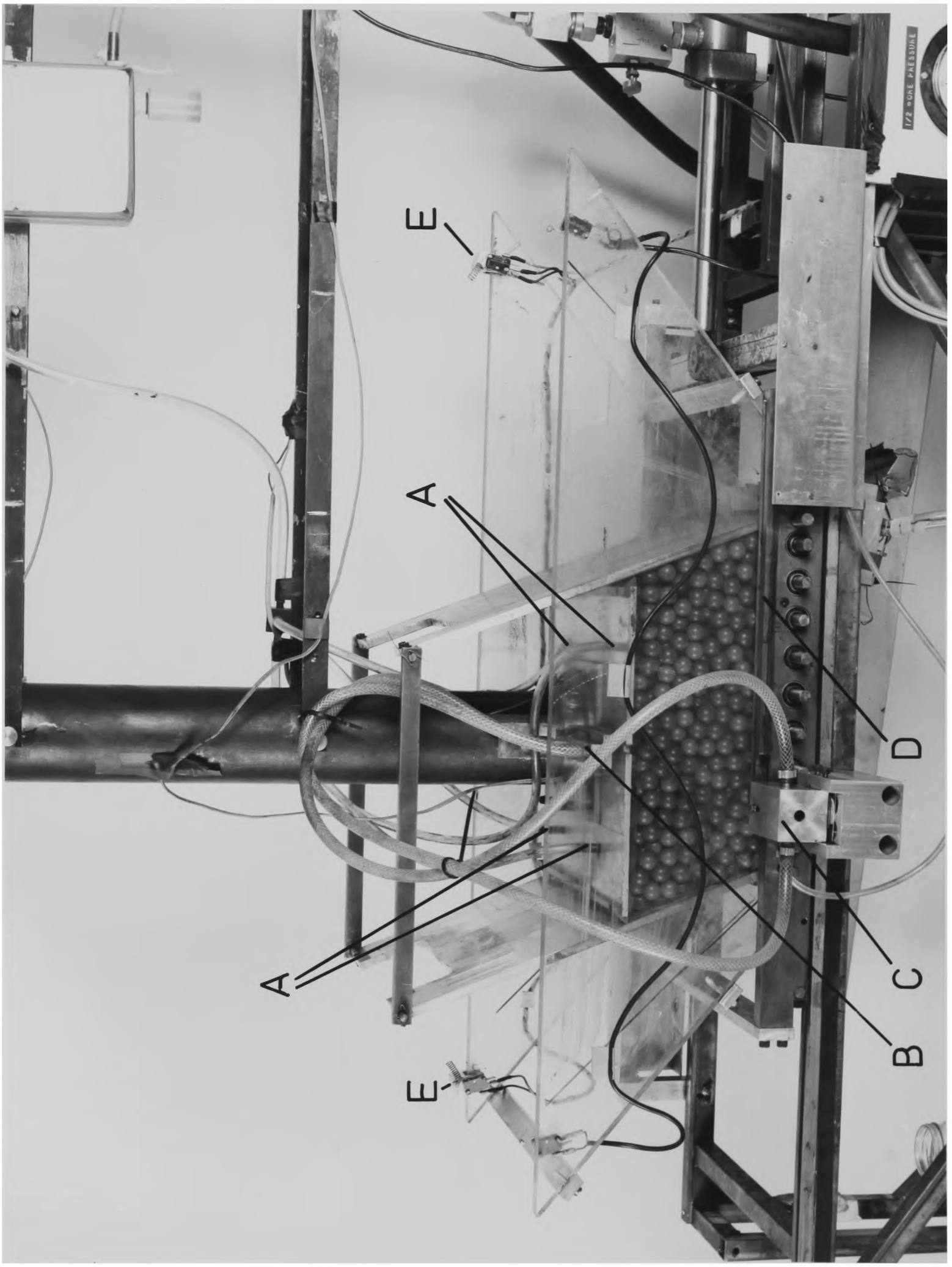


Figure 7.6: Close-up of the cell of the SSA Mk.V.

7.3 Versions of the SSA used in this study

7.3.1 The SSA Mk. IIIA

Two changes to the Mk. III were made in order to study the lateral movement of percolating particles in a failure zone and the new version was then known as the Mk. IIIA. These involved the installation of an improved particle feeding mechanism and construction of a new collection tray to be fixed below the cell.

The existing particle feeder was inadequate as it frequently failed to operate correctly. The best method of operating the trapdoor which allowed the particle to drop into the cell appeared to be the use of compressed air to move a piston and a double-acting air operated piston was designed and installed, B, (figure 7.6). Air flows were regulated by a valve, C, which was operated by a stepped piece of brass, D, screwed onto the cell undercarriage and adjustable so as to allow operation of the particle feeder at any point in the cycle. A new feeder was constructed at the same time, this version admitting only one particle to the cell each cycle, irrespective of the number of particles in the feedpipe.

For these experiments it was not possible to devise a simple method of returning the percolating particle to the top of the cell, whilst recording its exit position. A collection tray (figure 7.7), containing 64 45mm square compartments, was constructed from aluminium alloy. Its base was covered with foam rubber to reduce the likelihood of a particle bouncing from one division to another. The tray was fixed underneath the cell so that each compartment was directly below a different gap between the base plate spheres. This method prevented the simultaneous determination of residence times but these had already been found by Scott (1974).

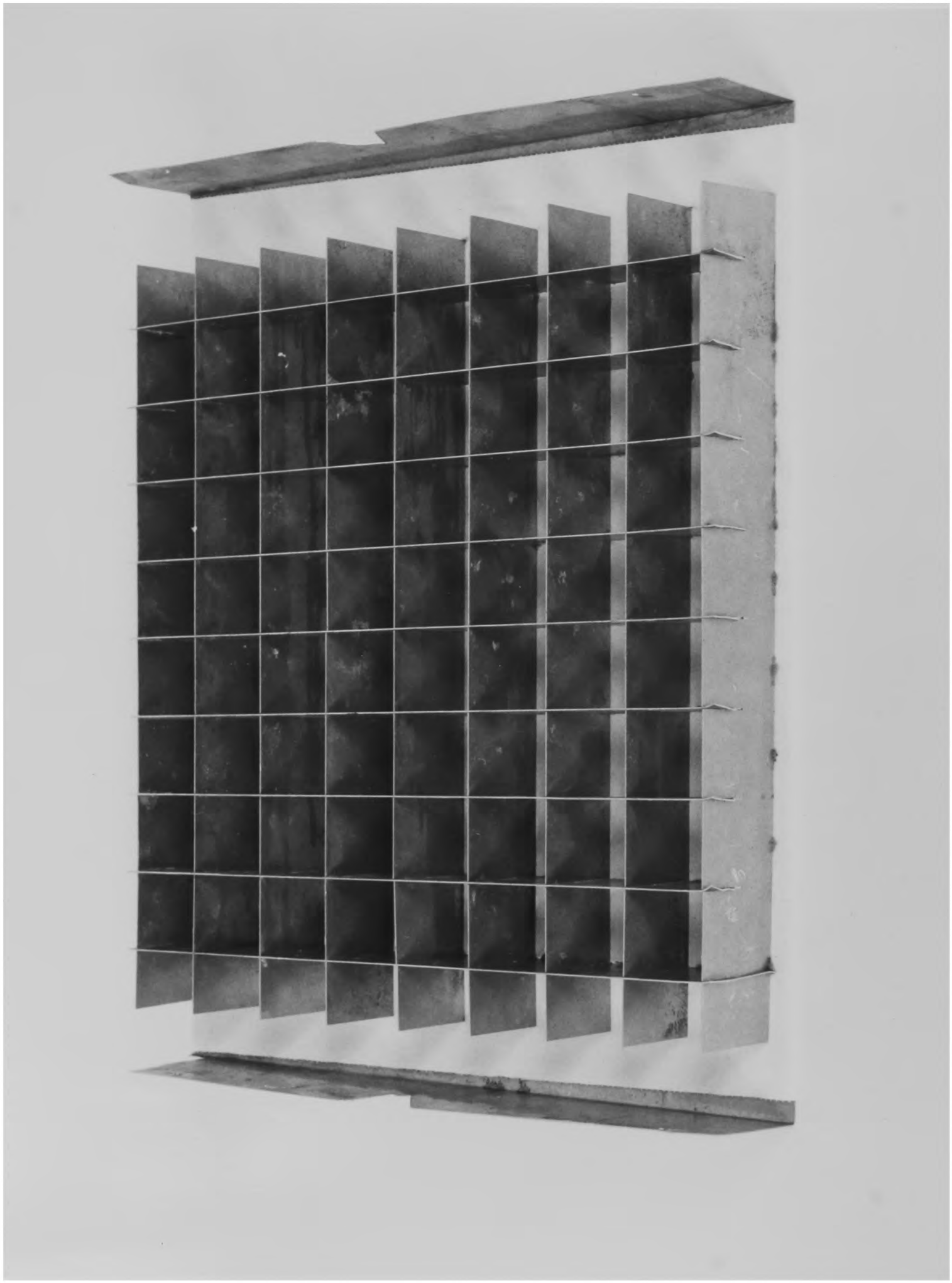


Figure 7.7: Collection tray of the SSA Mk. IIIA.

Experiments were performed by loading the tube above the feeder with particles and admitting one to the cell each cycle. A possible defect in this method was that as the feeder operated once each cycle, there could be a number of percolating particles in the cell at the same time, especially if relatively large particles were in use.

7.3.2 The SSA Mk. V

7.3.2.1 The driving system

Conversion of the SSA Mk. III so that the cell could be strained at a constant rate was considered desirable so that the effect of changes in the rate of strain could be properly understood. This involved the installation of a hydraulically operated drive mechanism and the new version of the SSA was known as the Mk. V.

Methods of achieving constant velocity reciprocating motion include the use of double-acting cylinders and rotary actuators. The latter are advantageous when only a small space is available, but as this was not an important criterion, a double-acting cylinder was chosen. In such a cylinder the cross-sectional area of the cylinder rod is exactly half the full bore area. The hydraulic circuit is designed so that the annulus side is constantly connected to the pump and movement of the piston produced by connecting the full bore either to the tank or to the pump. The ram is then driven with equal force in each direction.

The cylinder chosen was a Keelavite 3544, A (figure 7.8), with a bore area of 1.767 in^2 and a piston rod, B, 26" long. With this unit it was hoped that strain rates of the order of 4 s^{-1} could be obtained.

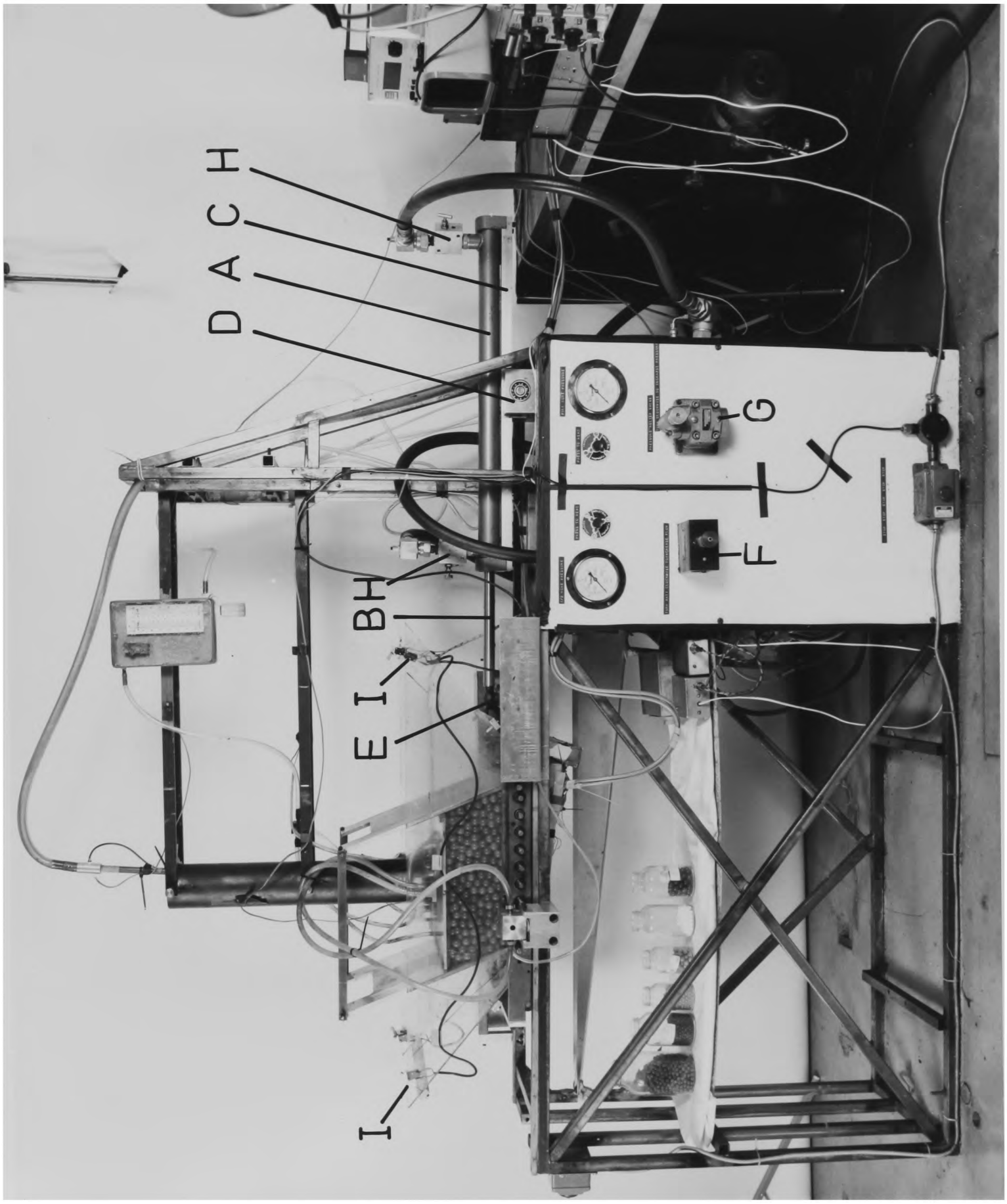


Figure 7.8: The SSA Mk.V.

The cylinder mounting is visible in figure 7.8. Since a piston should not be subjected to side forces, the cylinder was left free to rotate by bolting it onto a plate, C, pivoted at its centre thus permitting motion in a vertical plane. The whole assembly was also free to swivel in a horizontal plane about a bearing in the bottom of the support, D. The piston was connected to the cell via a universal coupling, E.

The hydraulic circuit used to drive the piston is shown in figure 7.9. Oil from the tank is pumped through two filters, one in the tank and the other in the line, at a pressure controlled by the relief bypass valve. A micrometer type valve controls the flowrate and hence determines the speed of the piston. Combined flow restrictors and non-return valves are mounted at each end of the cylinder to ensure that the pressure in the system is sufficient to operate the electro-hydraulic servo-valve which controls the direction of movement of the piston. The second relief valve is used to depressurise the system and so stop the piston without changing the flow settings or switching the pump off. The oil returns to the tank via a water-cooled single pass shell and tube heat exchanger.

Operation is as follows. When the piston is moving into the cylinder, the flow is into the annulus and the full bore side is connected via the servo-valve to the tank. Microswitches, E (figure 7.6) fixed to the side walls of the cell operate this valve so that the flow direction changes when the end walls reach a certain angle. As the operation of the valve was not sufficiently rapid to prevent the end walls damaging the switches, springs were fitted to them. When the switch is triggered, the servo-valve is operated via a relay and the flow direction changes. Both the annulus and the pump are connected to the full

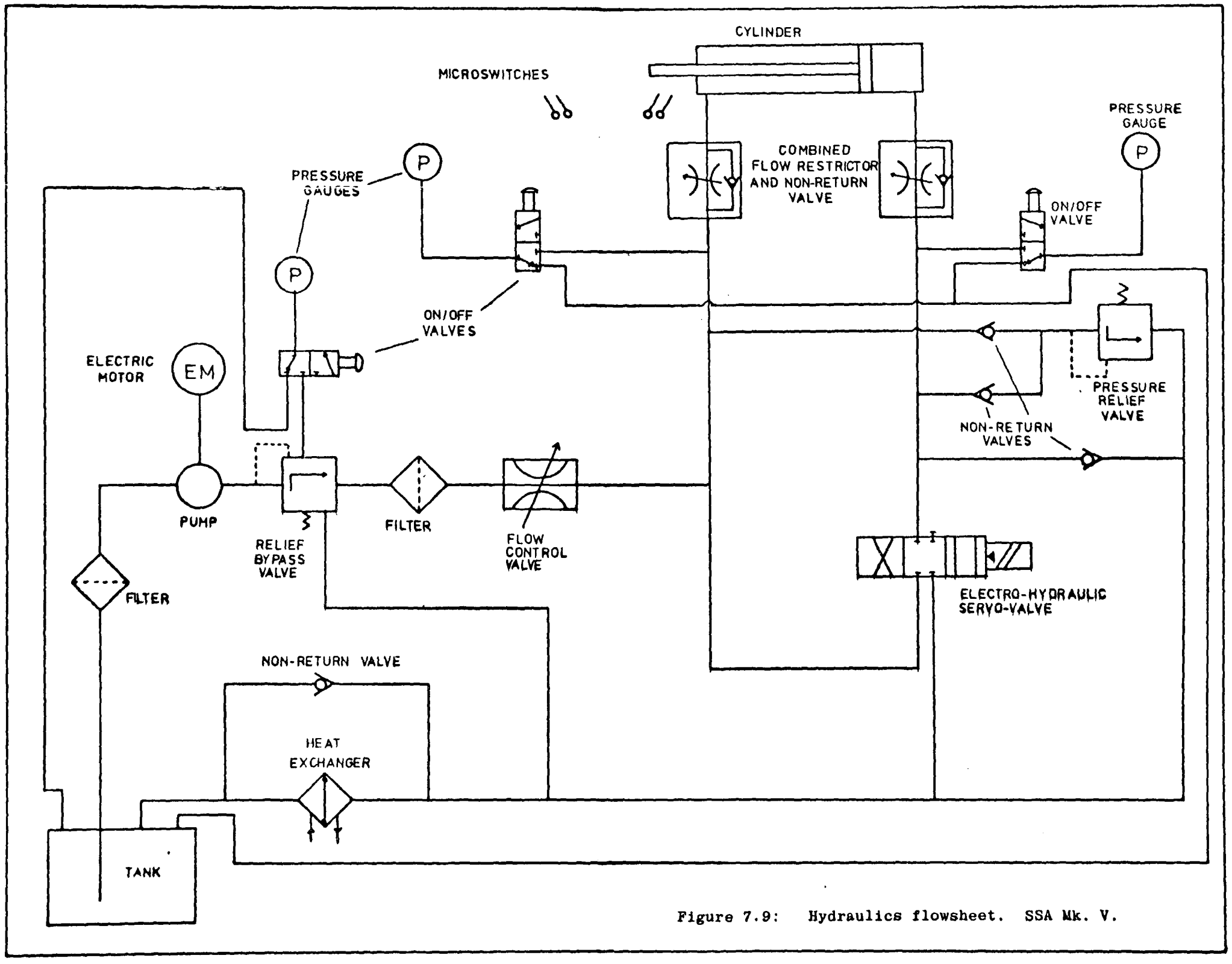


Figure 7.9: Hydraulics flowsheet. SSA Mk. V.

bore side of the piston and there is no flow into the tank. The piston moves out of the cylinder as the full bore area is greater than that of the annulus. Initially an accumulator was installed between the servo-valve and the heat exchanger in an attempt to even out the return flow, but the pressure in the circuit was insufficient for it to be of any use.

Installation of the equipment produced few problems. The power pack, comprising the tank, first filter, pump, 25 h.p. motor, relief bypass valve, on/off valve and pressure gauge were situated, with the heat exchanger, in a basement below the rest of the equipment to reduce noise. Most of the connections were made with ¾" or 1" i.d. high pressure hose, though a few were made with steel pipe. The flow controller, F (figure 7.8), relief valve, G, pressure gauges and their associated on/off valves were mounted on a control board, while the servo-valve was fixed directly on to the back of the relief valve. The combined flow restrictors and non-return valves, H, were mounted on each end of the cylinder.

The microswitches were also connected to a cathode-ray tube which was used to ensure that the cell moved at the same speed in each direction. Impulses from the switches were visible on the screen and the flow restrictors adjusted so that the distances between two pairs of successive impulses were the same.

7.3.2.2 Safety precautions

Because of possible danger from the rapidly moving cell, stop buttons were installed in easily accessible places. One was mounted on the end of the framework, A (figure 7.10), another on the bottom of the control board (figure 7.8) and a third in the basement with the power pack. The reset and start switches were mounted with an isolator, well away from the

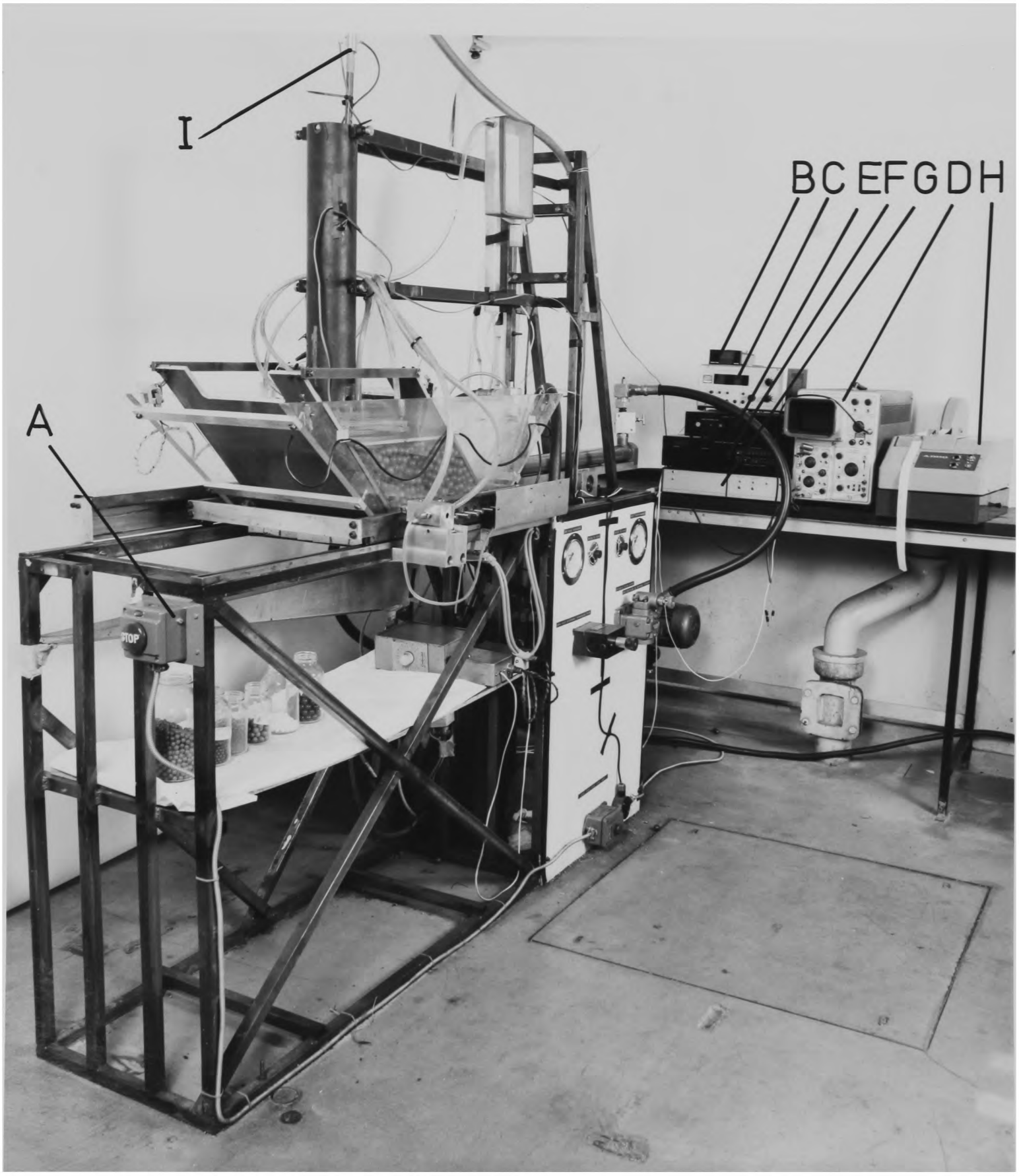


Figure 7.10: The SSA Mk.V and electronic equipment.

equipment. Overrun safety switches, I (figure 7.8), were fixed to the cell walls about half an inch past the microswitches and these also turned the pump off.

A level control was installed in the oil tank and this switched the pump off if the oil level fell below a certain height. The control was never triggered due to a leak, though it occasionally went off during start-up when the oil was cold.

The temperature in the tank was measured by a thermocouple connected to a digital thermometer, B (figure 7.10). Though the heat exchanger was connected directly to the main water storage tank, there was always a danger of fouling. On the one occasion when this occurred, the temperature rose by about 20^{o}C and the heat exchanger was taken apart and cleaned. The normal oil running temperature was 50-55^{o}C.

7.3.2.3 Particle detection

The particle detection system was changed at the same time as the drive, so that lateral diffusion could be investigated simultaneously with the measurement of percolation velocities. The feeder used with the Mk. IIIA was fitted with a phototransistor and light source, originally a small bulb. The lifetime of bulbs proved short and they were replaced by a fibre optic system. A quartz-halogen bulb was mounted in a housing on the cell lid and incoherent Fibrox light guides used to beam the light on to the phototransistor. When a particle fell into the cell, the light beam was broken and a pulse transmitted to the timer, C (figure 7.10). This pulse was also transmitted to the second beam on the cathode-ray tube, D, enabling the feed to be accurately positioned in the centre of a stroke.

A new collection tray (figure 7.11) was constructed from dural and hung beneath the cell. Particles fell from the cell



Figure 7.11: Collection tray of the SSA Mk.V.

into one of eight channels, separated from each other by foam rubber. An Eagle microphone insert, type M.C.25, was affixed to the bottom of each channel and these were connected to a signal conditioning unit, E, which could be adjusted to allow for the different size particles. The system control unit (SCU), F, displayed the number of the channel into which the particle had fallen, channels being numbered sequentially from 1 to 8. The pulse from the microphone also stopped the timer and the elapsed time was also displayed on the SCU. The channel number and time were then read by the punch interface, G, and recorded on paper tape by the punch, H.

The particle then rolled into a collection channel and was returned pneumatically to the top of the cell. Another phototransistor, I, was mounted about a metre above the feeder and the pulse from this was used to reset the system. Thus if for some reason a particle failed to activate a microphone, the timer was reset to zero before the particle entered the cell again. No measurements of the efficiency of the collection tray were made, though observations indicated that only rarely would a particle fail to operate the system. The start and reset pulses worked perfectly though the light guides had to be cleaned regularly to prevent the build-up of dust.

If the sensitivity of the signal conditioning unit were set too high the SCU would occasionally display channel zero due to activation of two microphones by a single particle. However if the sensitivity were too low, more particles would be missed and thus there was an optimum setting of the sensitivity for each particle. Initially there were problems due to activation of the equipment by both electrical and mechanical noise. The use of phototransistors rather than photodiodes was probably helpful here as the

associated circuitry is not so sensitive. However incorrect readings were not eliminated completely and the results were checked for obviously wrong values which were edited out. Few were found and it is thought that the remaining errors in the data are insignificant.

7.3.2.4 The cell and framework

Before experiments were begun with the Mk. V, the cell was overhauled and PTFE washers were fitted to the ends of the base plate rods between the end balls and the side walls. New wheels, diameter $1\,^{5}/_{16}$", were fitted to the cell undercarriage and new track was installed. The undercarriage was strengthened so that it would not distort under the large forces applied when the cell changed direction. The framework was also strengthened considerably by welding on more square tube.

CHAPTER 8

STRAIN-INDUCED PERCOLATION. RESULTS AND DISCUSSION

8.1 Introduction

The purpose of this study was to continue and extend Scott's work. Those of his results taken as proved were:

(i) Percolation velocities measured in different versions of the SSA are not significantly different and hence it was deduced that these were true velocities.

(ii) By performing experiments in a smaller version of the SSA (the Mk. IV) using 6mm dia. bulk material, Scott showed that the dimensionless percolation velocity is independent of the size of the bulk particles.

(iii) Changes in the position of the particle feeder on the lid do not affect the percolation velocity.

(iv) Feeding the percolating particle to the cell at the beginning, middle or end of a stroke does not affect the percolation velocity.

(v) The relationship between the mean residence strain of a percolating particle and the bed height is linear.

Since Scott had performed only a few outline experiments on lateral dispersion using X-rays, this was investigated in the Mk. IIIA first.

8.2 Experiments with the SSA Mk. IIIA

8.2.1 Interpretation of results

If the displacements of a percolating particle are controlled by a random walk mechanism, their distribution is

determined by the diffusion equation. If movement in the x direction (figure 7.1) is not coupled to that in any other orthogonal direction, then each can be considered independently. For a one dimensional system a diffusion law applies thus

$$\frac{\delta c}{\delta t} = D_x \frac{\delta^2 c}{\delta_x^2} \qquad (8.1)$$

where c(x,t) is the probability of finding a particle at position x at time t and D_x is the diffusion coefficient. If all the particles are injected into an infinite system at t = 0, x = 0, the solution is (Crank, 1956)

$$c = \frac{1}{2\sqrt{D_x \pi t}} \exp\left(-\frac{x^2}{4D_x t} \right) \qquad (8.2)$$

The probability of finding a particle between x_1 and x_2 at time t_x is therefore

$$p(x_1<x<x_2) = \int_{x_1}^{x_2} \frac{1}{2\sqrt{D_x \pi t_x}} \exp\left(\frac{-x^2}{4D_x t_x} \right) dx \qquad (8.3)$$

or for the particular case when t_x equals t_m, the mean residence time,

$$p(x_1<x<x_2) = \int_{x_1}^{x_2} \frac{1}{2\sqrt{D_x \pi t_m}} \exp\left(-\frac{x^2}{4D_x t_m} \right) dx \qquad (8.4)$$

This is thus only an approximation when applied to strain-induced percolation in a cell due to axial dispersion; an accurate solution could have been obtained by solving the equation for diffusion in three orthogonal directions coupled with convection in one but experimental accuracy did not warrant it. Application of equation 8.4 to lateral distributions of percolating particles leads to estimates of Dt_m.

Scott had calculated percolation velocities by performing experiments at different bed heights and determining the

regression line between the mean residence strain $\bar{\gamma}$ and the measured bed height h. The latter was obtained by subtracting the distance between the top of the side wall and the lid, measured with calipers, from the height of the side walls less the thickness of the cell lid. Similar procedures were used here; four different bed heights were used and Dt_m plotted against h. The slope of the regression line, determined by a least squares fit (Appendix II), is D/u and, as u is known, D can be calculated.

A complete list of the experiments is in Appendix III.1 and details of the materials used are in Table 8.1. The results of each experiment consisted of an array of 64 numbers. The simplest method of analysing the data was to assume that diffusion in each of the lateral directions is independent and to create two 8 x 1 arrays, one for diffusion in the direction of strain and the other orthogonal to it; an example is shown in figure 8.1. The divisions were numbered 1-8 in the increasing x and z directions. If the 8 x 1 distributions are approximately normal, then the assumption that diffusion in one direction is independent of that in other orthogonal directions is reasonable and equation 8.4 can be used to calculate Dt_m if the number of particles that return to the bulk after reaching the sides of the cell is negligible.

For diffusion in the z direction, the centre of the distributions lies between the 4th and 5th divisions. In order to check that this analysis applied, two estimates of Dt_m were calculated for the first series of experiments, one derived from the proportion of material in divisions 4 and 5 and the second from that in divisions 3-6. The results are shown in figure 8.2. Estimates at different bed heights are approximately equal and one estimate is not consistently larger than the other. The

Table 8.1: Materials used in the experiments in the SSA Mk IIIA

Species	Material	Nominal Diameter	Mean diameter (mm)	Number measured	Density ($kgm^{-3}.10^3$)	Elastic modulus $kNmm^{-2}$
A	Phenolic resin	¾"	18.60	40	1.31	2.8
B	"	1½"	37.20	1	1.31	2.8
C	Acrylic resin	½"	12.44	50	1.19	2.8
D	"	3/8"	9.31	25	1.19	2.8
E	"	7/16"	11.00	25	1.19	2.8
F	"	9/16"	14.09	25	1.19	2.8
G	Glass		11.62	25	2.52	56
H	Acrylic resin	5/16"	7.92	25	1.19	2.8

0	2	0	5	4	1	0	0	12
0	0	4	10	8	2	0	0	24
0	1	16	29	29	9	3	0	87
0	1	7	23	34	12	2	0	79
0	3	5	23	30	11	1	0	73
0	0	4	20	18	6	0	0	48
0	0	3	4	5	1	1	0	14
0	0	1	1	5	2	1	0	10
0	7	40	115	133	44	8	0	347

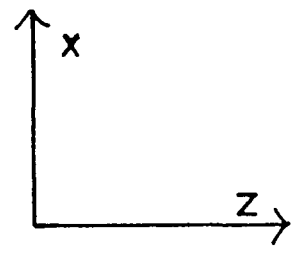


Figure 8.1 Experiment D33, Species E, Table 8.1; 11mm dia. acrylic resin.

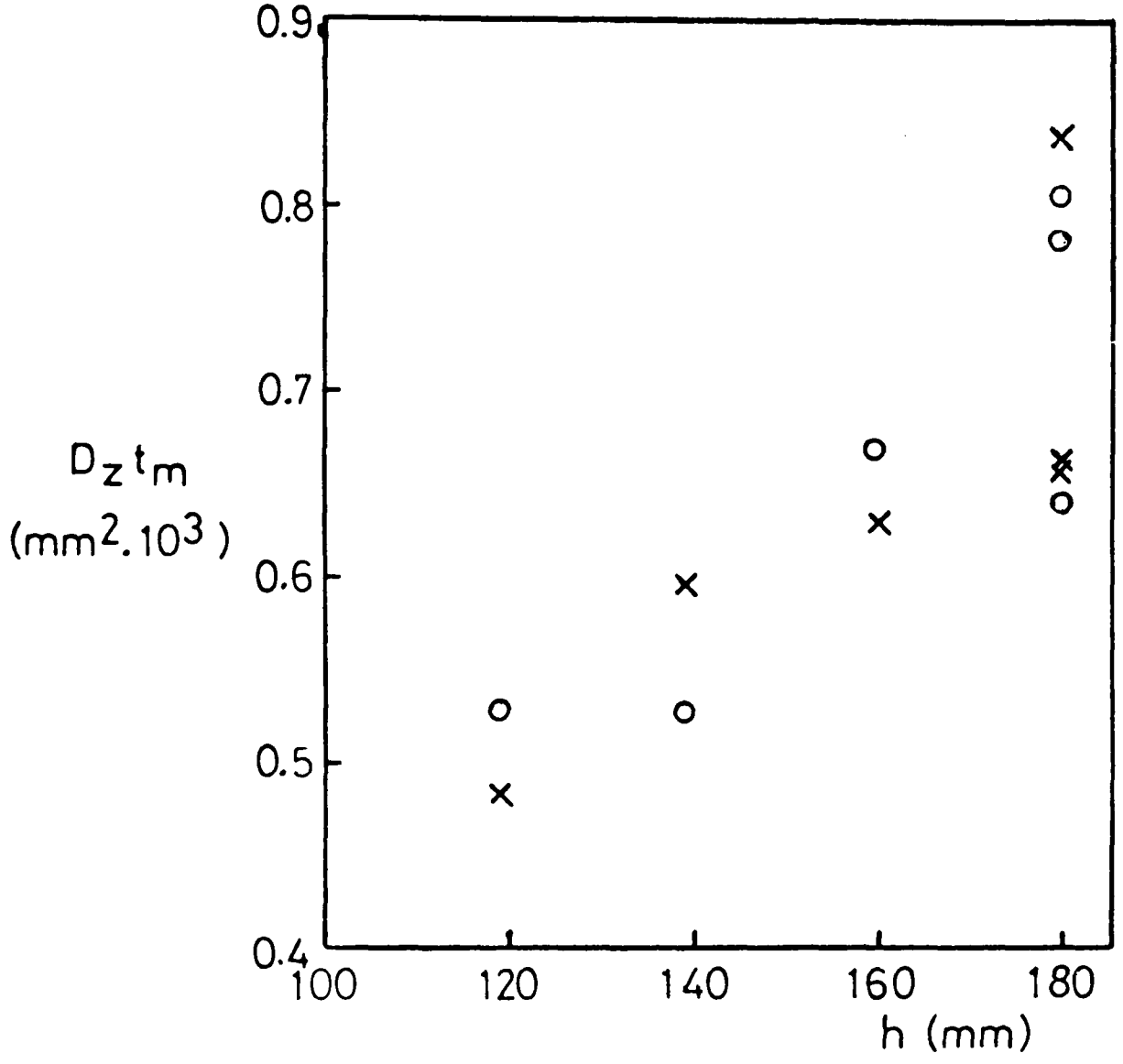


Figure 8.2: Estimates of $D_z t_m$ at different bed heights. Species D.
× Divisions 4-5
o Divisions 3-6
Experiments D5, 7, 8, 10, 12, 14.

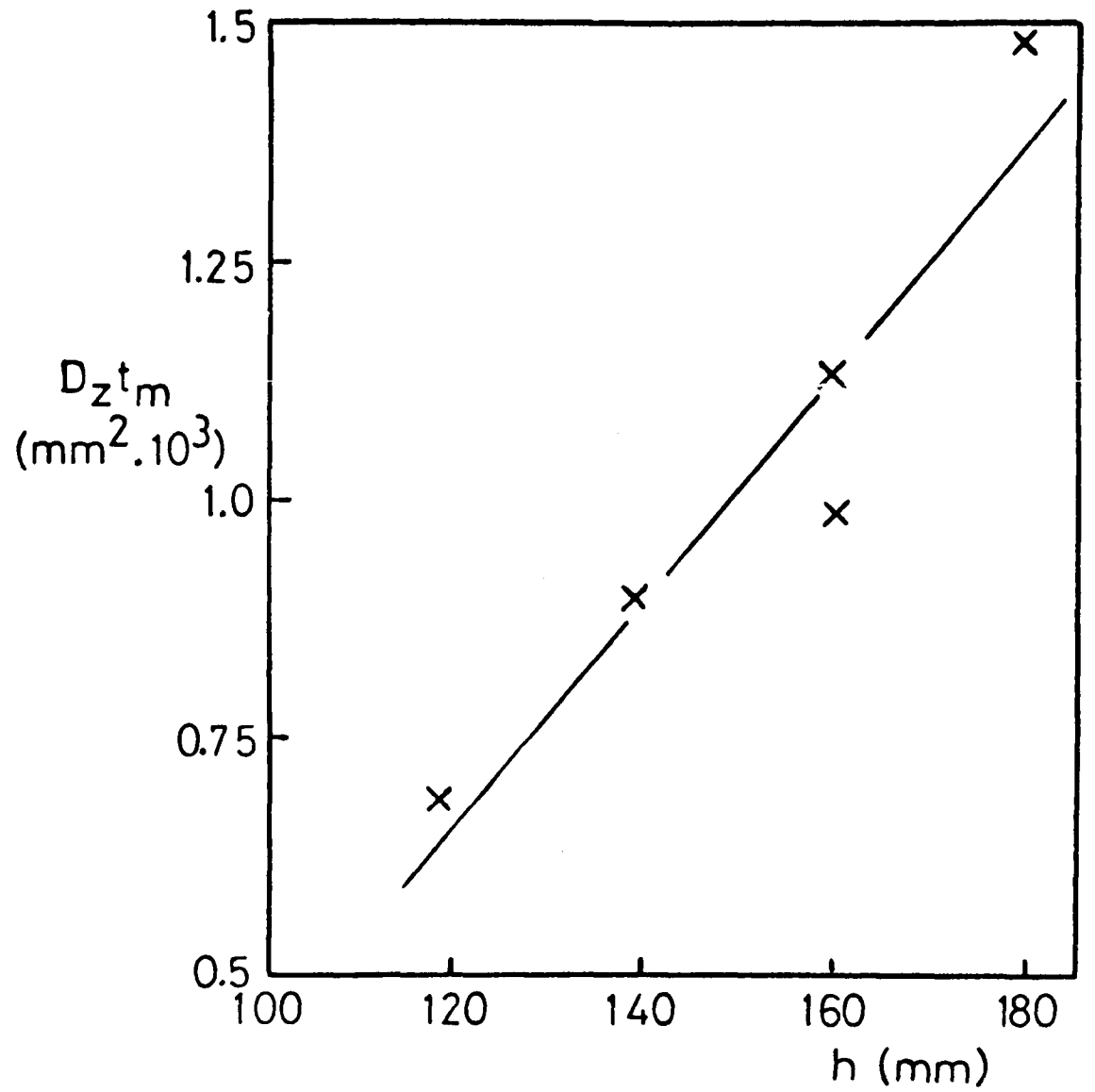


Figure 8.3: Estimates of $D_z t_m$ at different bed heights. Species E. Experiments D9, 11, 13, 15, 39.

figure also demonstrates that the regression between the estimates of $D_z t_m$ and bed height is linear. In the calculation of diffusion coefficients, $D_z t_m$ was derived from divisions 4 and 5 as this was the most accurate value. Incorporation of other values would have required derivation of a weighted mean with the weights based on the sensitivity of the normal distribution at the relevant points. The experimental data were not sufficiently accurate to justify such a step. Another typical graph of $D_z t_m$ vs. h is shown in figure 8.3.

Analysis of particle motion in the direction of strain is more difficult. The mechanism is not purely diffusive but includes reciprocating convective action and the centres of the distributions produced do not lie in the middle of the collection tray (e.g. figure 8.1). To characterize the results numerically, diffusion coefficients were calculated by varying one of the limits in equation 8.4 and leaving the other fixed at the experimental mean position. In all cases, values of Dt_m were found by solving the equation iteratively using a computer. Scott has suggested that percolating particles that reach the walls do not return to the bulk and thus this approach does not have to consider reflections from the walls. The average of the seven possible estimates was used throughout; they did not appear to be ordered in any manner. Figures 8.4 and 8.5 show the actual and mean values plotted against bed height for species E, Table 8.1.

Distributions were tested for normality by calculating their variance from the value of Dt_m, generating the amounts of material in each division from the normal distribution corresponding to this variance and comparing this with the experimental data. The χ^2-test was used to gauge the fits which were generally good enough to justify the use of a diffusion coefficient.

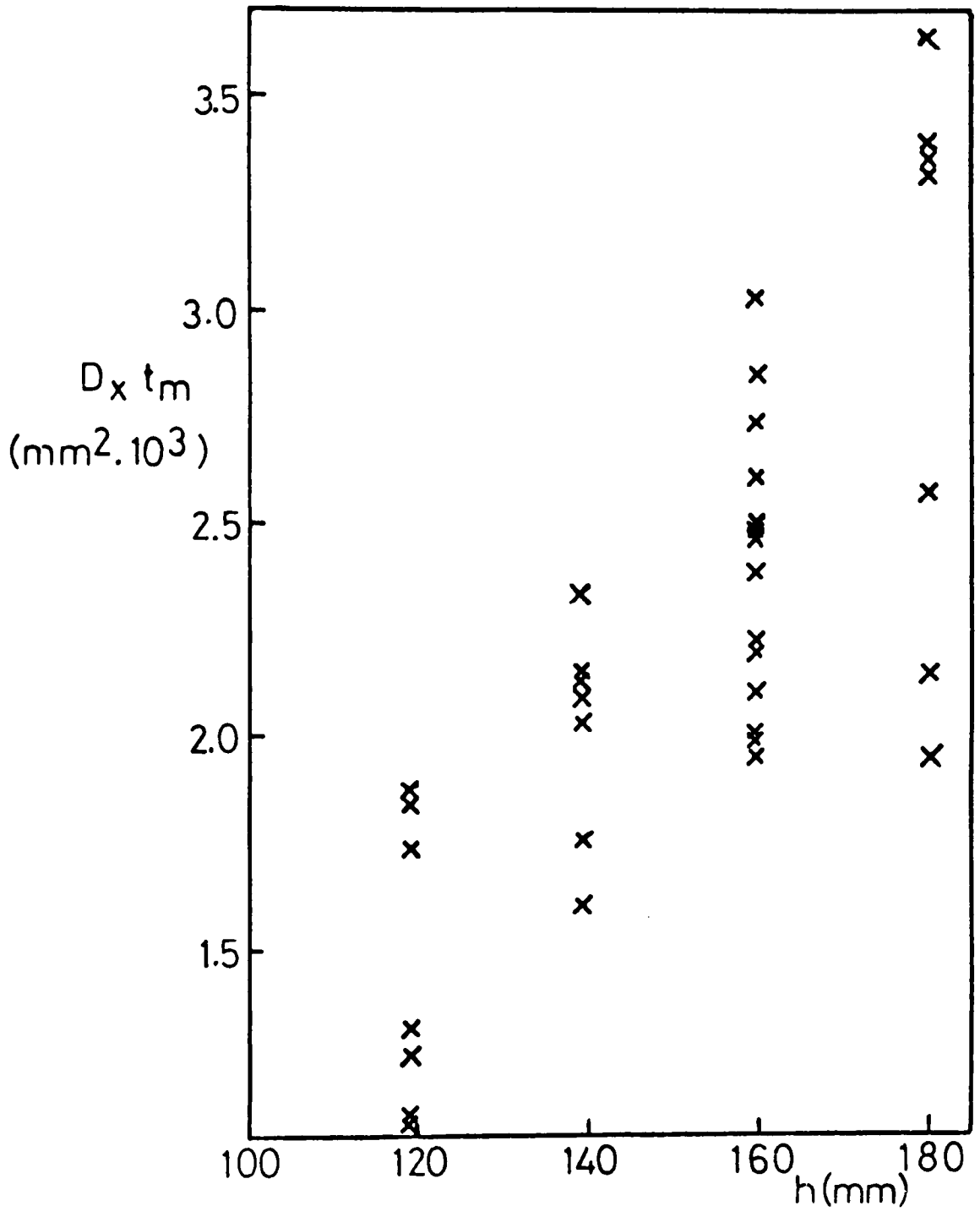


Figure 8.4: Estimates of $D_x t_m$ at different bed heights; individual values. Species E. Experiments D9, 11, 13, 15, 39.

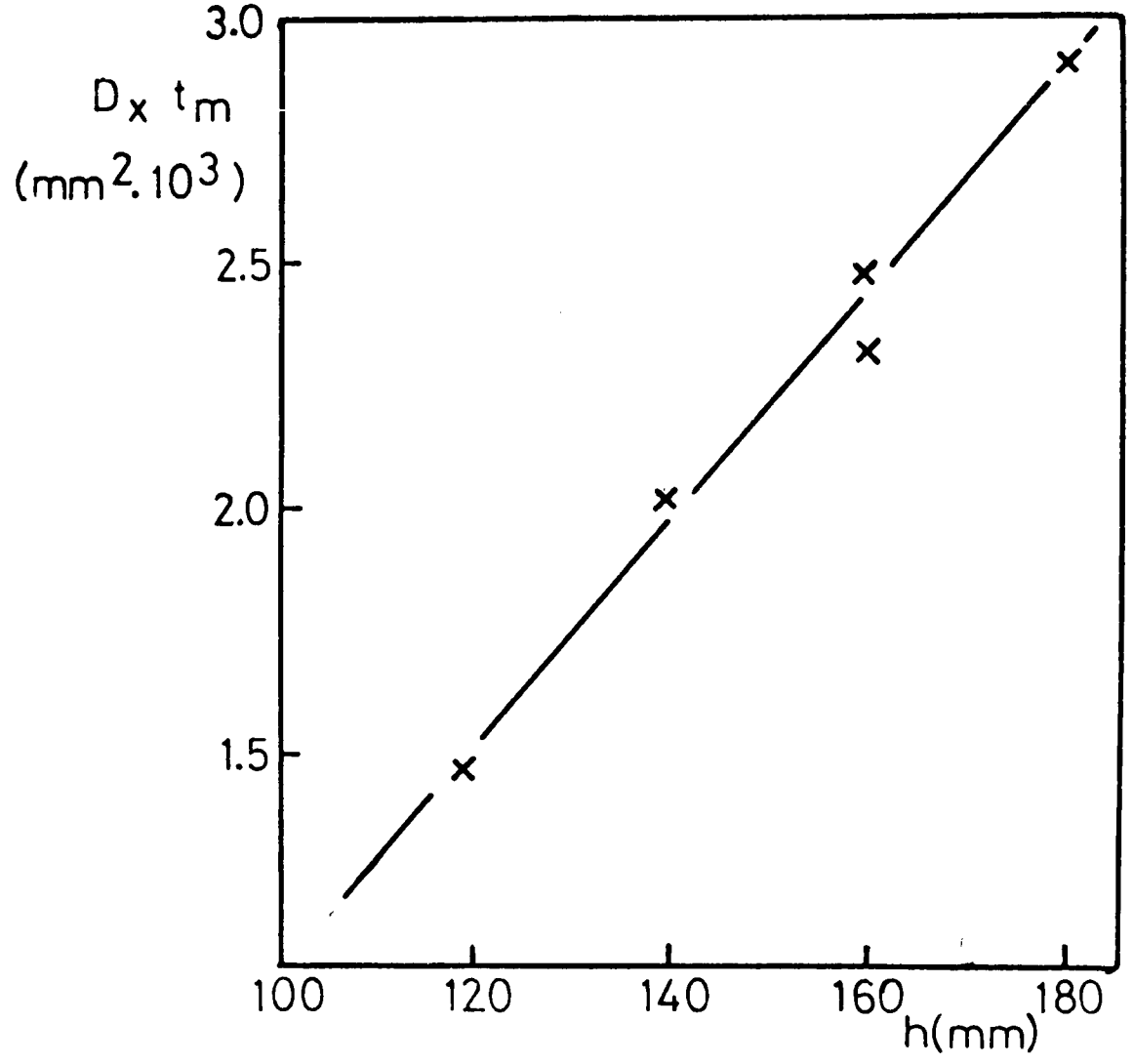


Figure 8.5: Estimates of $D_x t_m$ at different bed heights; mean values. Species E. Experiments D9, 11, 13, 15, 39.

8.2.2 Experimental procedure

Some preliminary experiments (D1-D7) were performed with 9.31 and 12.44mm dia. particles to check that the equipment worked satisfactorily and that reasonable distributions of material were produced. The feeder tube held about 100 particles and was refilled a few times during each experiment. Generally about 350 particles were used except for Species F, Table 8.1, of which only about 90 were available and here the mean of two experiments was employed. Experiments were performed to measure the effects of particle diameter ratio, strain rate and normal stress. The latter was varied by placing weights on the cross-bars which held the 4" diameter cylinder (B, figure 7.3).

The strain per stroke remained constant at 2.0 throughout the experimental programmes with both the SSA Mk. IIIA and Mk. V.

8.2.3 Results and discussion

Five series of experiments were carried out with particles of different sizes, species D, E, F, G and H, Table 8.1. Values of D/u were calculated and estimates of u taken from Scott's work. Results were expressed in dimensionless form as $D/\bar{\dot{\gamma}}d_b^2$ in Tables 8.2 and 8.3. Standard errors in $D/\bar{\dot{\gamma}}d_b^2$ due to scatter about the regression lines varied between 10 and 50% for D_z and 10 and 25% for D_x. The probable errors in u were up to 15%. The results show that changes in $D_z/\bar{\dot{\gamma}}d_b^2$ with particle size ratio are small, there being no significant differences between any of the values. The large differences in distributions are due to the different percolation velocities, i.e. the amount of dispersion depends on the length of time spent by the particle in the cell. Results for glass particles, species G, were comparable with those for acrylic resin particles, species D, E, F and H.

Table 8.2: Experiments to measure lateral diffusion coefficients for different size particles. (i) $D_z/\bar{\dot{\gamma}}d_b^2$

Species	d_p/d_b	$\bar{\dot{\gamma}}_1$ (s^{-1})	σ_{y-2} (kNm^{-2})	D_z/u (mm)	$u/\bar{\dot{\gamma}}d_b$ (from Scott, 1974)	$D_z/\bar{\dot{\gamma}}d_b^2$
D	0.502	0.215	1.36	5.0	0.52	0.14
E	0.593	"	"	12.1	0.20	0.13
F	0.759	"	"	27.0	0.09	0.13
G	0.626	"	"	12.2	0.22	0.15
H	0.427	"	"	2.1	0.92	0.10

Table 8.3: Experiments to measure lateral diffusion coefficients for different size particles. (ii) $D_x\bar{\dot{\gamma}}d_b^2$

Species	d_p/d_b	$\bar{\dot{\gamma}}$ (s^{-1})	σ_y (kNm^{-2})	D_x/u (mm)	$u/\bar{\dot{\gamma}}d_b$ (from Scott, 1974)	$D_x/\bar{\dot{\gamma}}d_b^2$
D	0.502	0.215	1.36	11	0.52	0.32
E	0.593	"	"	23	0.20	0.24
F	0.759	"	"	204	0.09	0.99
G	0.626	"	"	24	0.22	0.23
H	0.427	"	"	6	0.92	0.29

With the exception of species F, values of $D_x/\bar{\dot{\gamma}}d_b^2$ were also comparable. The higher value in this case may be because a large proportion of the percolating particles reached the sides during the experiment.

The results obtained here are higher than those of Scott who tracked percolating particles directly using X-rays. For $d_p/d_b = 0.51$ he found values of $D_x/\bar{\dot{\gamma}}d_b^2$ equal to 0.10 and 0.18 at different bed heights. He also calculated some dimensionless self-diffusion coefficients by a photographic technique and these were 0.06 in the z direction and 0.1 in the x direction.

If the presence of more than one percolating particle in the system at a time affects the percolation velocity, it will presumably reduce percolation rates. Then, if the diffusion coefficient depends mainly on the time spent in the cell, values from these experiments would be expected to be greater than those recorded for single particles.

The effect of increasing the normal load while maintaining a constant fill of material in the cell is shown in figures 8.6 and 8.7. No clear trend is shown by these results because of the experimental scatter. Scott showed that an increase in normal load led to a decrease in percolation velocity and this might have been expected to result in an increase in the diffusion coefficients. Figure 8.8 shows that changes in the strain rate do not significantly affect $D_z t_m$. This is also unexpected as Scott showed that increasing the strain rate caused a significant decrease in percolation velocities. However figure 8.9 shows that $D_x t_m$ rises with increasing strain rate though experimental scatter precludes determination of an exact relationship between the two.

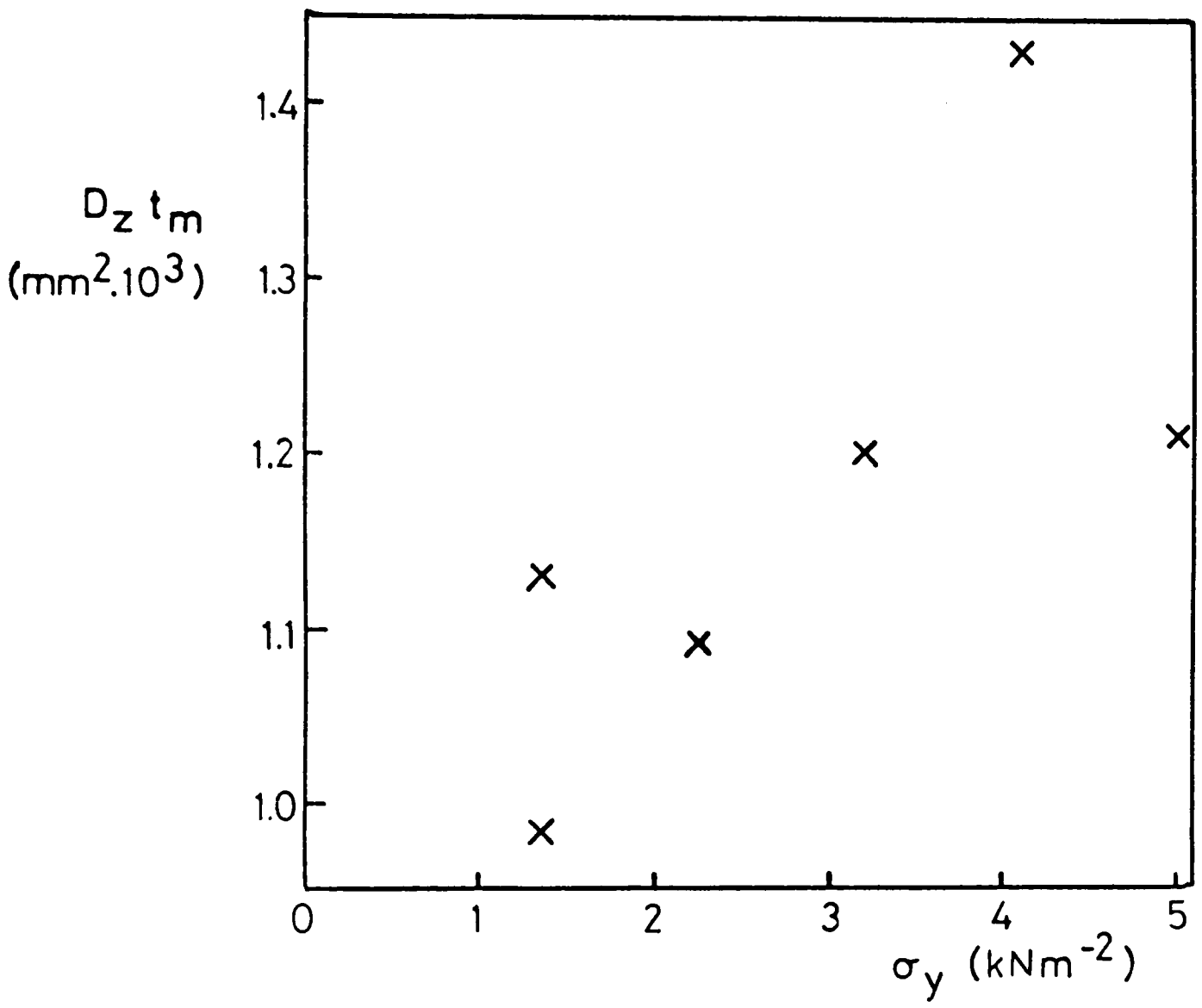


Figure 8.6: Estimates of $D_z t_m$ at different normal loads. Species E. $d_p/d_b = 0.593$, $\bar{\dot{\gamma}} = 0.215\ s^{-1}$.

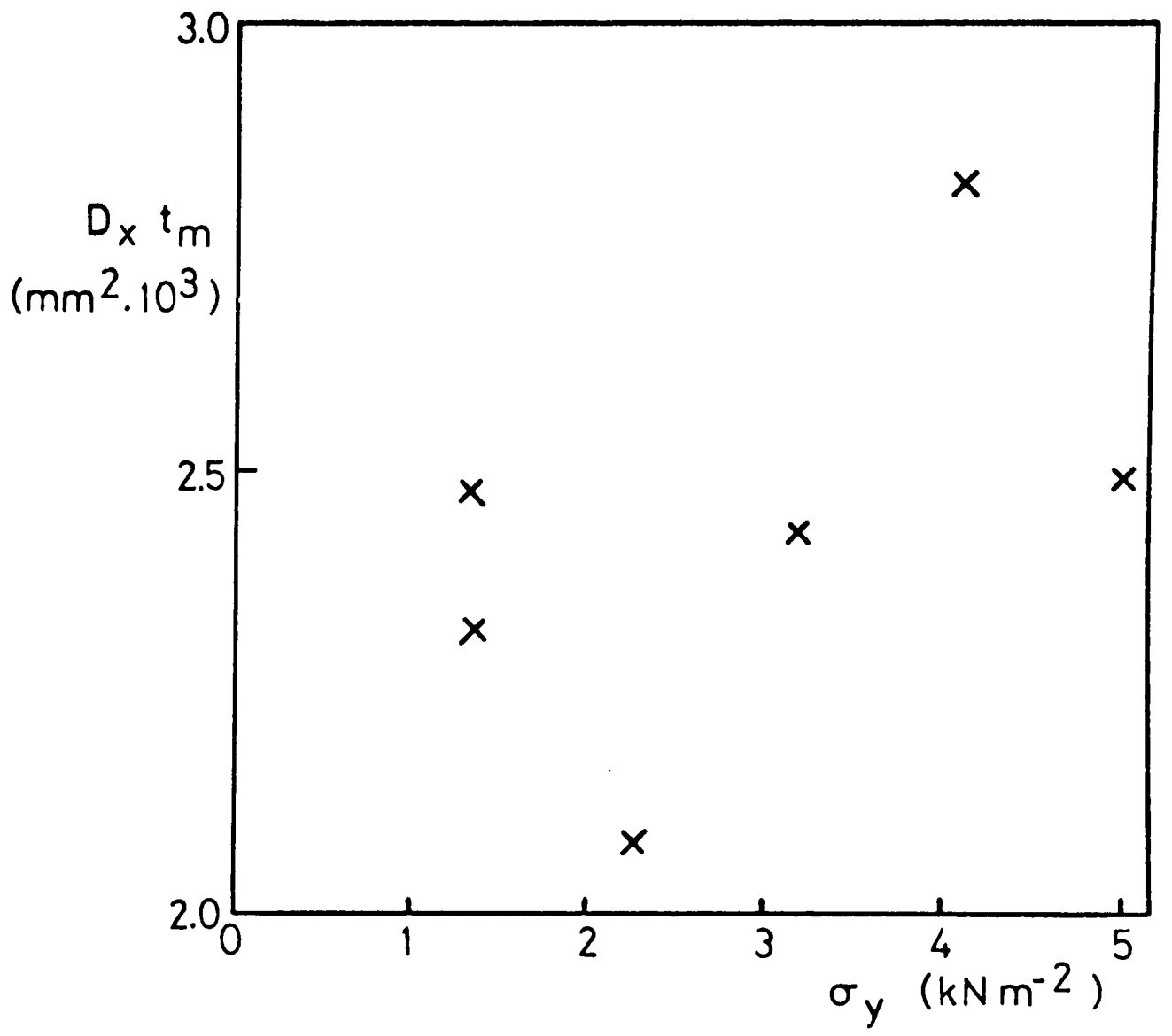


Figure 8.7: Estimates of $D_x t_m$ at different normal loads. Species E. $d_p/d_b = 0.593$, $\bar{\dot{\gamma}} = 0.215\ s^{-1}$.

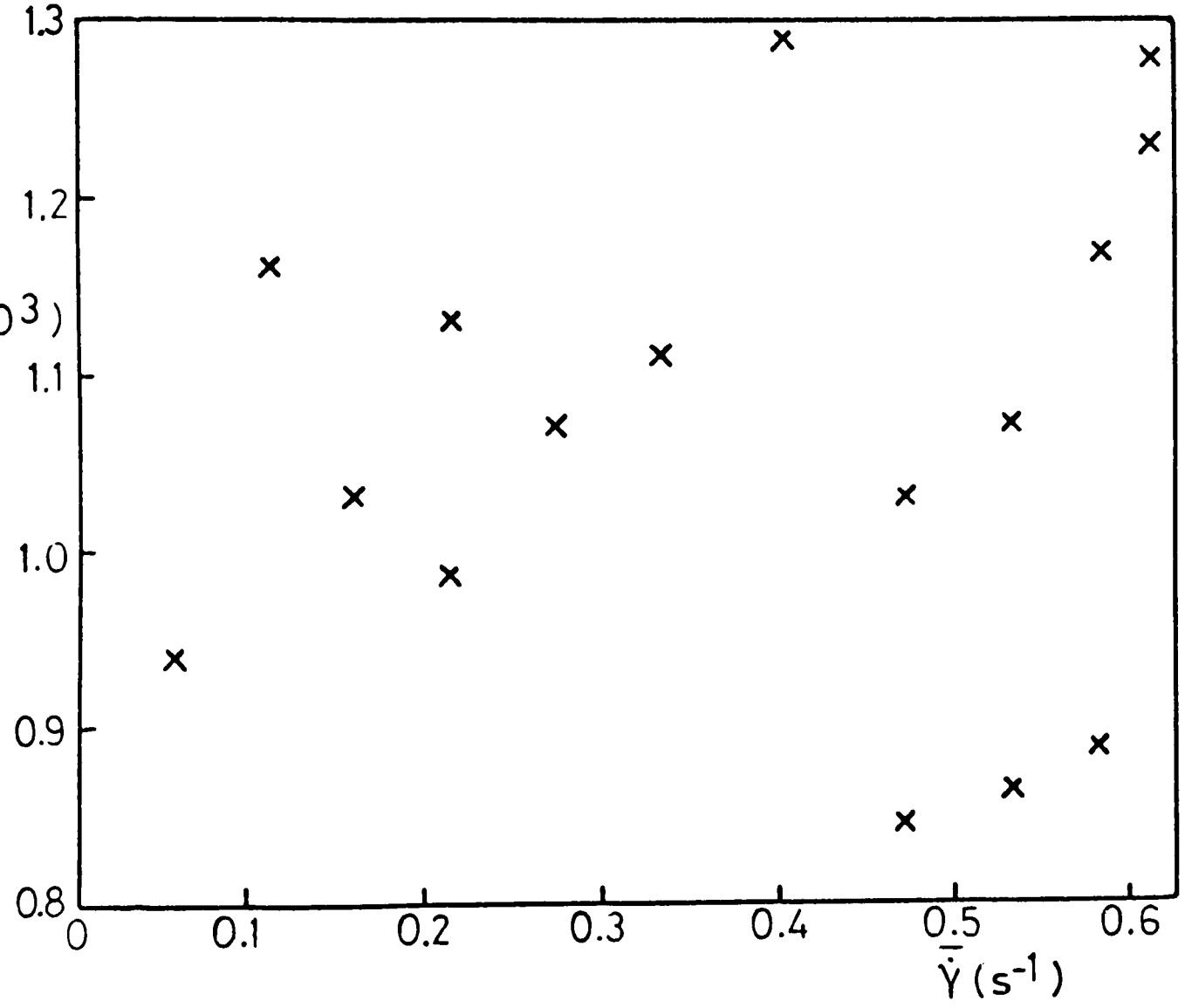


Figure 8.8: Estimates of $D_z t_m$ at different strain rates. Species E. d_p/d_b = 0.593, σ_y = 1.36 kNm^{-2}.

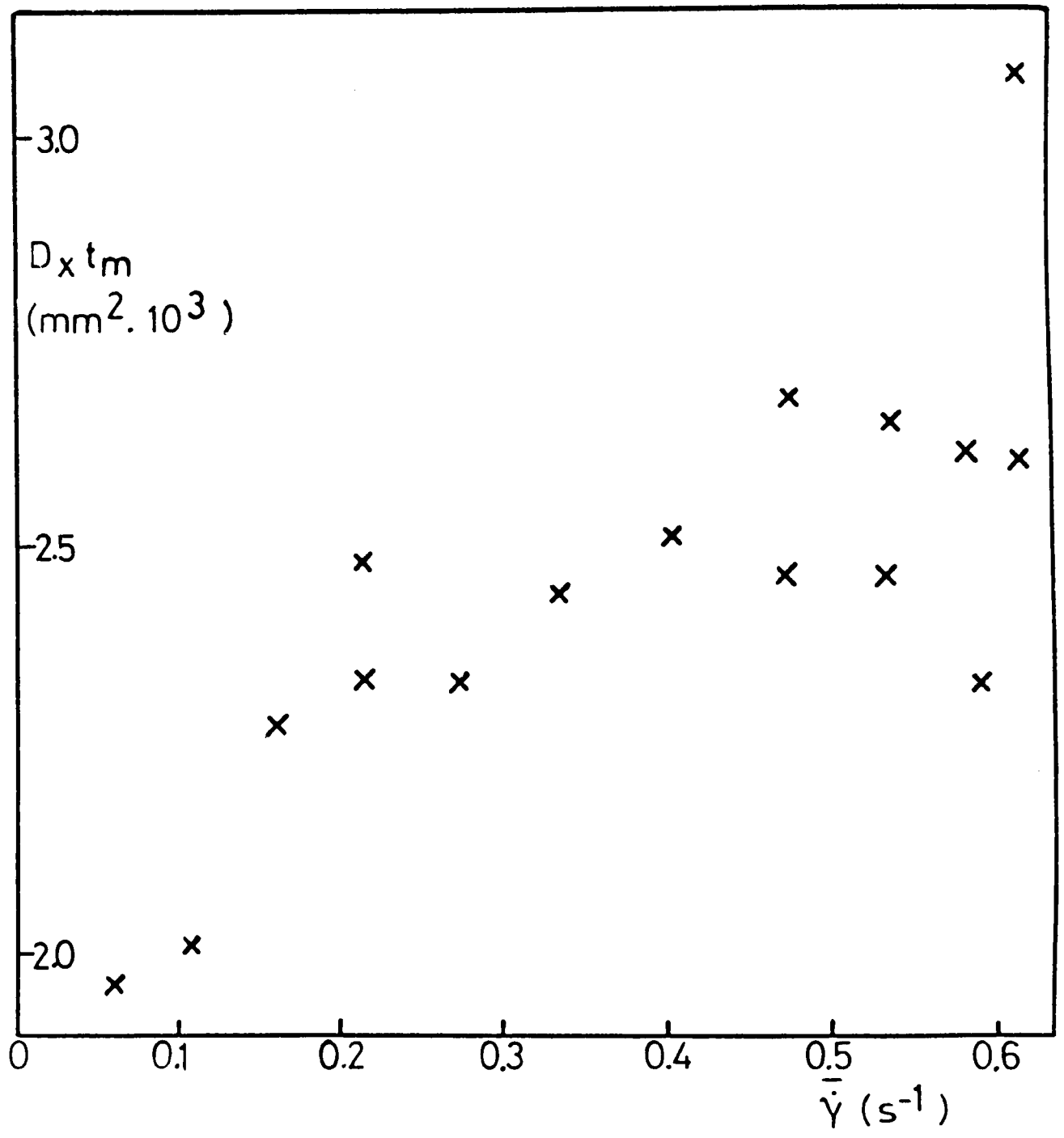


Figure 8.9: Estimates of $D_x t_m$ at different strain rates. Species E. d_p/d_b = 0.593, σ_y = 1.36 kN m^{-2}

8.3 Experiments with the SSA Mk. V

8.3.1 Interpretation of results

A list of the experiments performed is in Appendix III.2 and the materials used are tabulated in Table 8.4. These experiments produced lists of residence times and associated channel numbers. Axial velocities were calculated from a least squares regression (Appendix II) between the mean residence strains and bed heights, generally over a range of heights between 115 and 200mm. The lower limit arose as the side walls hit the central cylinder at lower heights. Scott had suggested that the regression was not linear above 200mm though the cell could cope with values up to about 250mm. The slope of the regression is $u/\dot{\gamma}$ and the results were converted to dimensionless form by dividing by the diameter of a bulk particle. A typical regression is shown in figure 8.10. The intercept of the regression on the bed height axis h_c was positive. The results are tabulated in Table 8.5 together with standard errors calculated from the scatter of the points about the regression lines.

Lateral diffusion coefficients were calculated as described in section 8.2.1 and expressed in terms of the quantity $D_z/\dot{\gamma}d_b^2$. A typical plot is shown in figure 8.11. Intercepts on the bed height axis were widely scattered; no trend was discernible and not all the values were positive.

Axial diffusion coefficients (i.e. those in the y direction) were calculated from the dimensionless variance of the distribution of residence strains, using the axially dispersed plug flow model. From equation 3.10,

$$\frac{\sigma_t^2}{t_m^2} = \frac{\mathrm{var}(\gamma)}{\bar{\gamma}^2} = 2\left[\frac{d_b}{HPe_y}\right]^2 \left[\frac{HPe_y}{d_b} - 1 + \exp\left(\frac{-HPe_y}{d_b}\right)\right] \qquad (8.5)$$

Table 8.4: Materials used in the experiments in the SSA Mk.V

Species	Material	Mean Diameter (mm)	Density ($kgm^{-3}.10^{3}$)	Elastic Modulus ($kNmm^{-2}$)
A	Phenolic resin	18.60	1.31	2.8
B	"	37.20	1.31	2.8
I	Acrylic resin	10.94	1.19	2.8
J	"	6.92	1.19	2.8
K	"	9.48	1.19	2.8
L	"	8.02	1.19	2.8
M	"	10.99	1.19	2.8
N	"	12.51	1.19	2.8
P	"	5.99	1.19	2.8
Q	Aluminium	9.52	7.55	70
R	"	9.52	0.74	70
S	Acrylic resin	5.00	1.19	2.8
T	Steel	7.94	7.77	210
U	Vulkollan	6.35	1.23	0.1
V	Steel	6.35	7.77	210
W	Teflon	9.52	2.13	0.3
X	Glass	9.50	2.52	56
Y	Steel	3.18	7.77	210
Z	"	2.38	7.77	210

Table 8.5: SSA results, Mk.V. $\sigma_y = 1.4\ kNm^{-2}$

Percolating Particle	$\frac{d_p}{d_b}$	$\frac{\rho_p}{\rho_b}$	$\dot{\gamma}$ (s^{-1})	$\frac{u}{\dot{\gamma}d_b}$	s.e$\left(\frac{u}{\dot{\gamma}d_b}\right)$	h_c (mm)	s.e.(mm)(h_c)	$\frac{D_z}{\dot{\gamma}d_b^2}$	s.e$\left(\frac{D_z}{\dot{\gamma}d_b^2}\right)$	Pe_y
J	0.372	0.91	0.400	0.88	0.07	43	9	0.085	0.024	2.5
K	0.510	0.91	0.400	0.26	0.01	62	6	0.038	0.009	3.2
L	0.431	0.91	0.400	0.53	0.02	51	5	0.080	0.010	3.2
M	0.591	0.91	0.400	0.17	0.01	60	7	0.048	0.005	2.4
N	0.673	0.91	0.400	0.090	0.005	79	6	0.029	0.010	2.4
P	0.322	0.91	0.400	1.33	0.04	37	4	0.088	0.016	1.9
J	0.372	0.91	1.000	0.84	0.04	22	7	0.070	0.014	2.9
J	0.372	0.91	0.167	1.17	0.03	30	4	0.094	0.021	1.9
Q	0.512	5.76	0.400	0.42	0.03	45	7	0.067	0.010	3.1
R	0.512	0.56	0.400	0.34	0.02	49	6	0.071	0.009	3.1
J	0.372	0.91	0.667	0.84	0.05	25	9	0.070	0.015	2.2
S	0.269	0.91	0.400	2.24	0.12	23	7	0.088	0.022	1.4
T	0.427	5.93	0.400	0.74	0.02	46	3	0.088	0.012	2.9
U	0.341	0.94	0.400	1.40	0.04	31	4	0.095	0.029	1.9
W	0.512	1.63	0.400	0.36	0.03	38	11	0.054	0.011	2.6
X	0.511	1.92	0.400	0.35	0.03	46	10	0.068	0.025	2.7
Y	0.171	5.93	0.400	7.9	0.8	20	14	0.97	0.12	1.5
Z	0.128	5.93	0.400	9.3	1.0	33	14	1.4	0.9	2.9

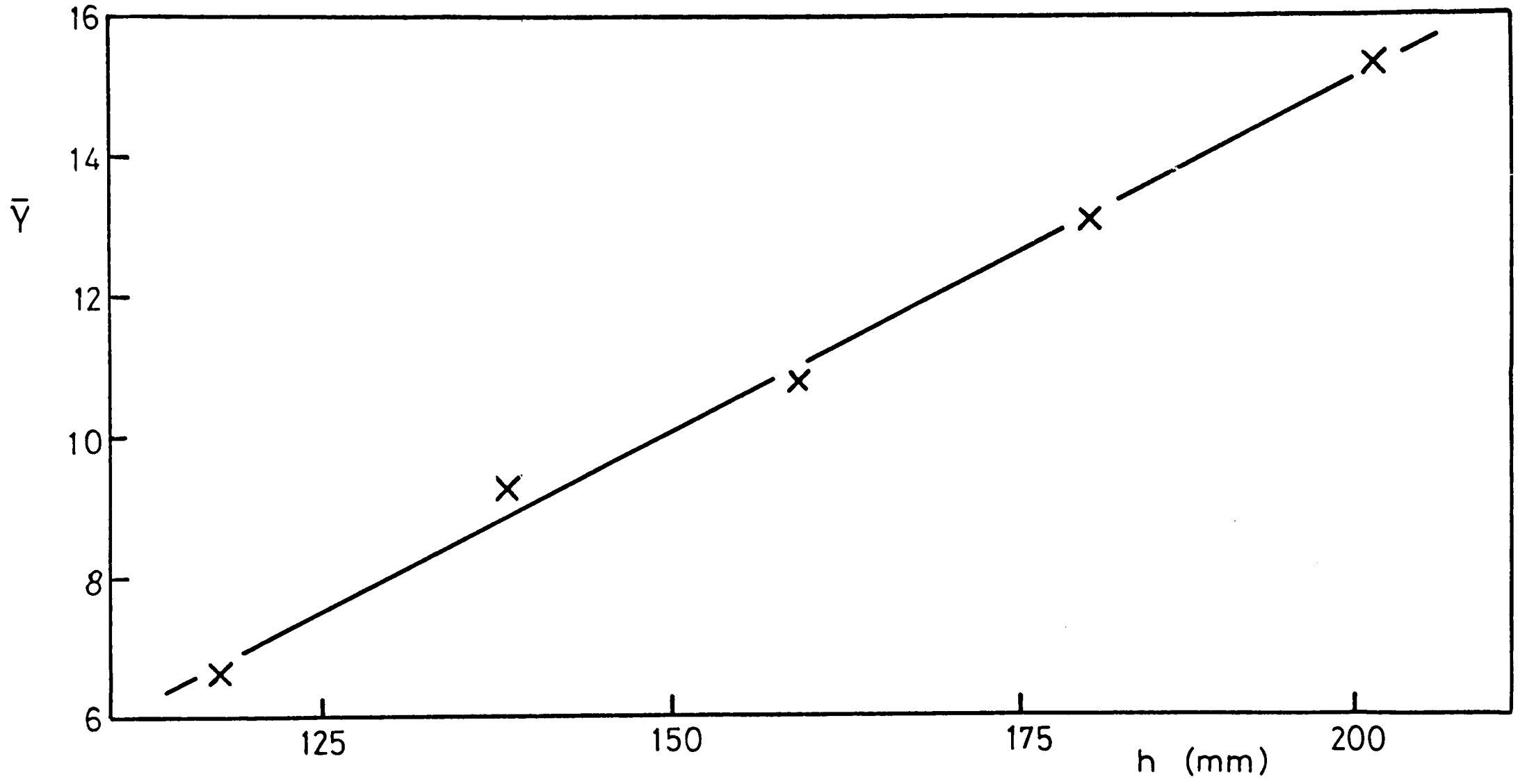


Figure 8.10: Regression between mean residence strain and bed height. Species L, $d_p/d_b = 0.431$, $\sigma_y = 1.40\ kNm^{-2}$, $\dot{\gamma} = 0.4\ s^{-1}$. Experiments 14-17, 23.

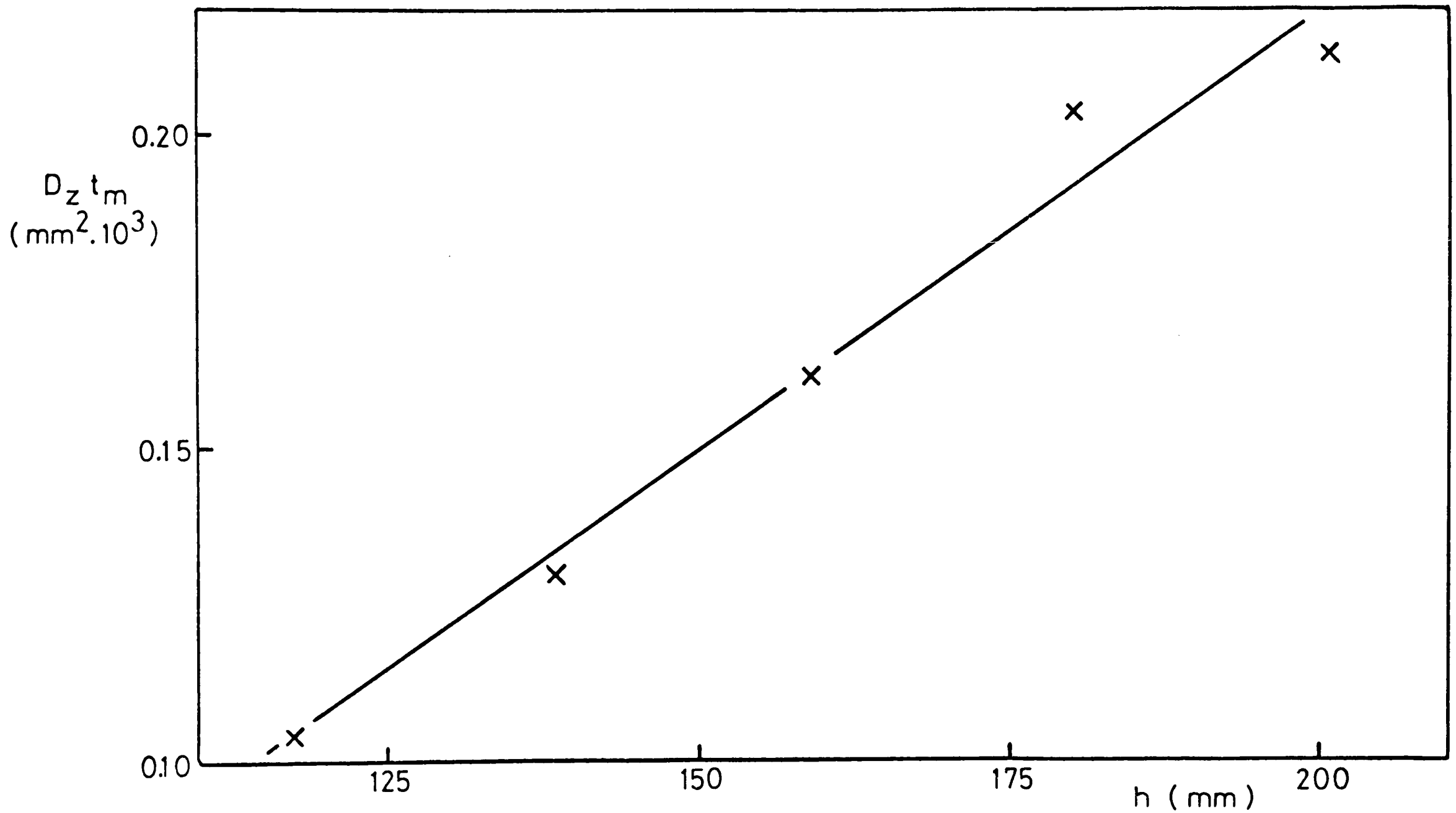


Figure 8.11: Regression between $D_z t_m$ and bed height. Species L, d_p/d_b = 0.431, σ_y = 1.40 kNm^{-2}, $\dot{\gamma}$ = 0.4 s^{-1}. Experiments 14-17, 23.

where H is the height of packing in which diffusion occurs. If $H = h-h_c$ where h is the measured bed height, then

$$\left(\frac{HPe_y}{d_b}\right) = (h-h_c) \cdot \frac{Pe_y}{d_b} \qquad (8.6)$$

HPe_y/d_b was calculated from equation 8.5 for each experiment. From equation 8.6, the regression between this and h has slope Pe_y/d_b and intercepts the h axis at $h = h_c$. Thus Pe_y/d_b was determined by a constrained least squares fit (Appendix II) estimating h_c from the regression between mean residence strain and bed height (e.g. figure 8.12).

Another frequently used method when studying residence times is to model a process as a number of equal-sized ideal stirred tanks in series. This was applied to strain-induced percolation by Scott; the general description may be found in Levenspiel and Bischoff (1963). An ideal stirred tank is a vessel in which the probability of material leaving is independent of the time it has already spent in the vessel. For a pulse input to a system containing J_t tanks of equal volume in series, the output from the J_t th. is given by (Levenspiel and Bischoff, 1963)

$$c = \frac{J_t}{(J_t-1)!}\left(\frac{\gamma}{\bar{\gamma}}\right)^{J_t-1} \exp\left(-\frac{J_t\gamma}{\bar{\gamma}}\right) \qquad (8.7)$$

while the variance of $\gamma/\bar{\gamma}$ is $1/J_t$. Such a model may be applied by equating the number of stirred tanks to the reciprocal of the variance of the dimensionless residence time distribution.

Both axially dispersed plug flow and stirred tank models could be employed. Theoretical distributions predicted by each were compared with the observed distribution using a χ^2-test, dividing dimensionless residence strains into groups 0.1 wide.

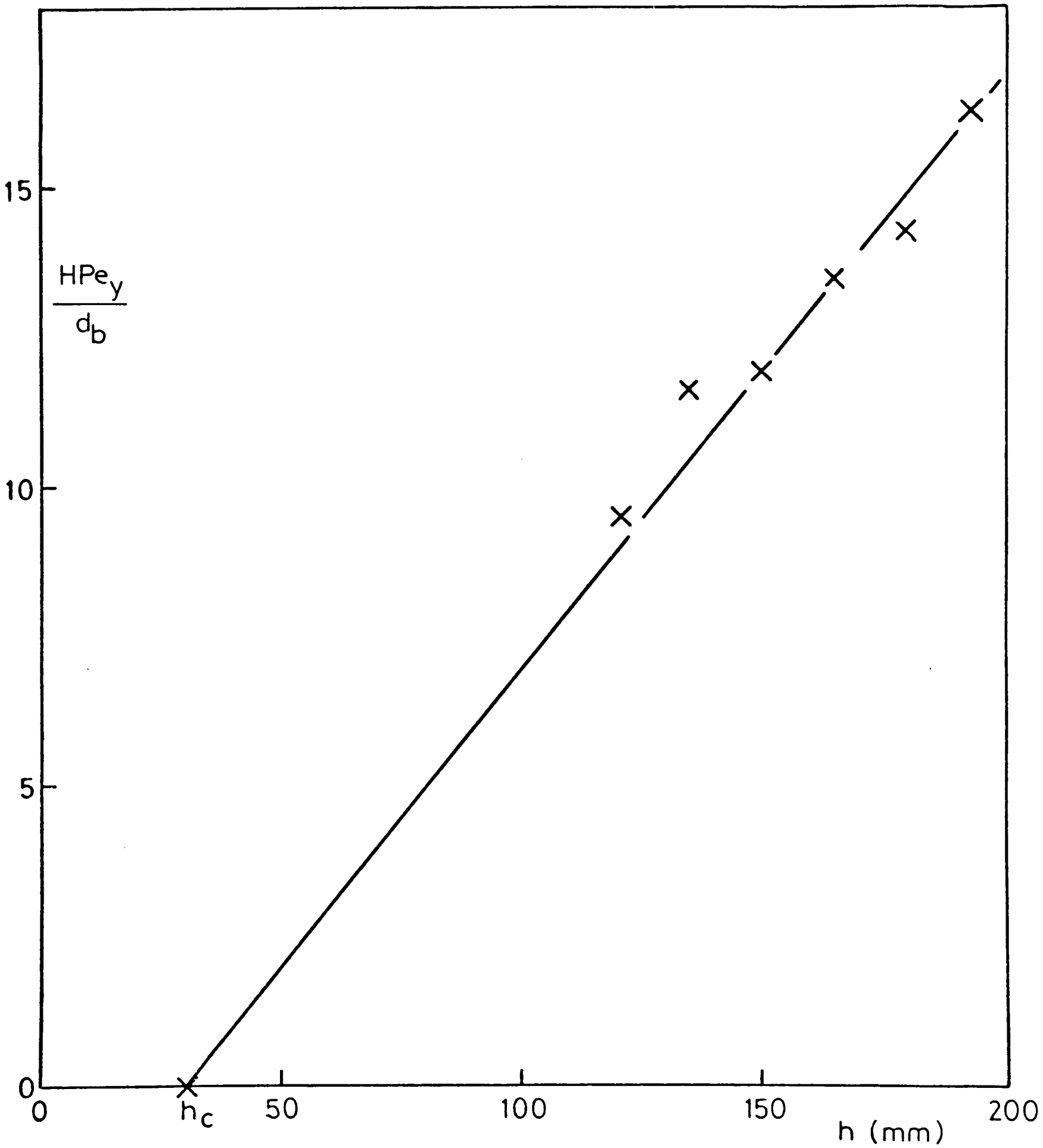


Figure 8.12: Regression between HPe_y/d_b and bed height. Species J, $d_p/d_b = 0.372$, $\sigma_y = 1.40\ kNm^{-2}$, $\dot{\gamma} = 0.167s^{-1}$. Experiments 60, 62, 64, 66, 68,70.

The fit between the experimental and theoretical results varied from one experiment to another, though it was generally better for long mean residence strains. This is probably due to variations in the state of the bulk material, and hence in the number of balls leaving the cell, during a stroke. Thus species N, Table 8.4, $d_p/d_b = 0.673$ was used to compare models. All seven experiments with this material could be described adequately by the axially dispersed plug flow model, all fits being good at the 10% level. In only one case did the stirred tanks model provide a better fit and in two instances the fit was not good at the 1% level. From this it was deduced that the axially dispersed plug flow model was valid and the stirred tanks model was not used further.

A further phenomenon investigated in all experiments was whether mean residence times of those particles which fell into the inner channels were significantly different from those which fell into other channels. The results from the Mk. IIIA indicated that the longer a particle spent in the cell, the greater should be its chance of leaving the system away from the centre.

Mean residence times for individual channels cannot be satisfactorily tested for differences by a t-test as the underlying distributions are known to be skew and so the Mann-Whitney 'U' test was employed. The times on both channels are ranked in order. A value 1 is given to the lowest of the $t_1 + t_2$ times, value 2 to the next lowest and so on, where t_1 and t_2 are the number of readings on each of the channels. Then U is defined (Mann and Whitney, 1947) as

$$U = t_1 t_2 + \frac{t_1(t_1 + 1)}{2} - R_1 \qquad (8.8)$$

or equivalently $U = t_1 t_2 + \frac{t_2(t_2 + 1)}{2} - R_2$

where R_1, R_2 are the sums of the ranks assigned to the t_1, t_2 readings. It can be shown that as t_1 and t_2 increase in size, the sampling distribution of U rapidly approaches the normal distribution with mean $t_1t_2/2$ and variance $t_1t_2(t_1 + t_2 + 1)/12$. Thus the probability that the times on different channels are the same may be determined from the normal distribution.

Application of the test to the residence times grouped in pairs of channels, (4 and 5, 3 and 6, etc.) indicated that in some instances the residence times on the outer channels were significantly greater than those on the inner ones, as expected. This was the case for the experiments with species N, $d_p/d_b = 0.673$ table 8.4, where, in six out of seven cases, the differences were significant at the 5% level. This may be contrasted with the experiments with species L, $d_p/d_b = 0.431$, where in two cases the mean times for channels 4 and 5 were greater than those for 3 and 6, in another two instances differences between the two were not significant and in only one case was the difference significant at the 5% level. The reason for this is not clear though it may also be due to variations in the number of particles leaving the cell during different parts of the cycle.

8.3.2 Experimental procedure

One preliminary experiment (No. 1) checked the operation of the equipment and the computer program used to analyse results. After this the equipment was run for approximately 8 hours each day for about a month. When the reliability of the system had been proved, it was run overnight, a 120 hour week then being normal.

The variables considered were particle size ratios, density ratios, material properties, strain rates, normal stresses and high bed heights.

8.3.3 Effect of particle properties

8.3.3.1 Particle diameter ratio

Dimensionless percolation rates $u/\dot{\gamma}d_b$ are plotted against d_p/d_b in figure 8.13 for $d_p/d_b>0.2$, $\dot{\gamma} = 0.4\ s^{-1}$. They vary by a factor of 25 between 0.090 at $d_p/d_b = 0.673$ and 2.24 at $d_p/d_b = 0.269$. The shape of the graph is as found by Scott though his percolation rates were greater, probably because his experiments were carried out at $0.215\ s^{-1}$ and because the motion of the cell was different. The results are discussed further in section 8.4.

Experiments with smaller particles, species Y and Z, Table 8.4 were also performed. Species Z is small enough to percolate spontaneously whereas species Y is 10% larger than the critical diameter ratio, 0.155. For comparison with spontaneously percolating systems, percolation rates are best expressed in terms of $u/\sqrt{gd_b}$, viz. 0.14 for species Y and 0.16 for species Z. Coefficients of restitution were found by dropping particles onto a horizontal smooth surface made from phenolic resin and measuring the height of rebound. For a height of fall of 0.9m, the coefficients of restitution for both Y and Z were 0.86. These results can be compared with those for spontaneously percolating systems determined by Bridgwater and Ingram (1971). For $\alpha = 0.92$, $d_p/d_b = 0.136$, they found that for a steel percolating particle and glass bulk spheres, $u/\sqrt{gd_b} = 0.22$, 38% more than the value 0.16 ± 0.02 reported here for $\alpha = 0.86$, $d_p/d_b = 0.128$. This is probably because the percolating particle may be trapped by the bulk particles in a moving bed.

The use of small particles led to problems with the sensitivity of the microphones on the collection tray, which had to be increased. This resulted in a greater proportion of incorrect

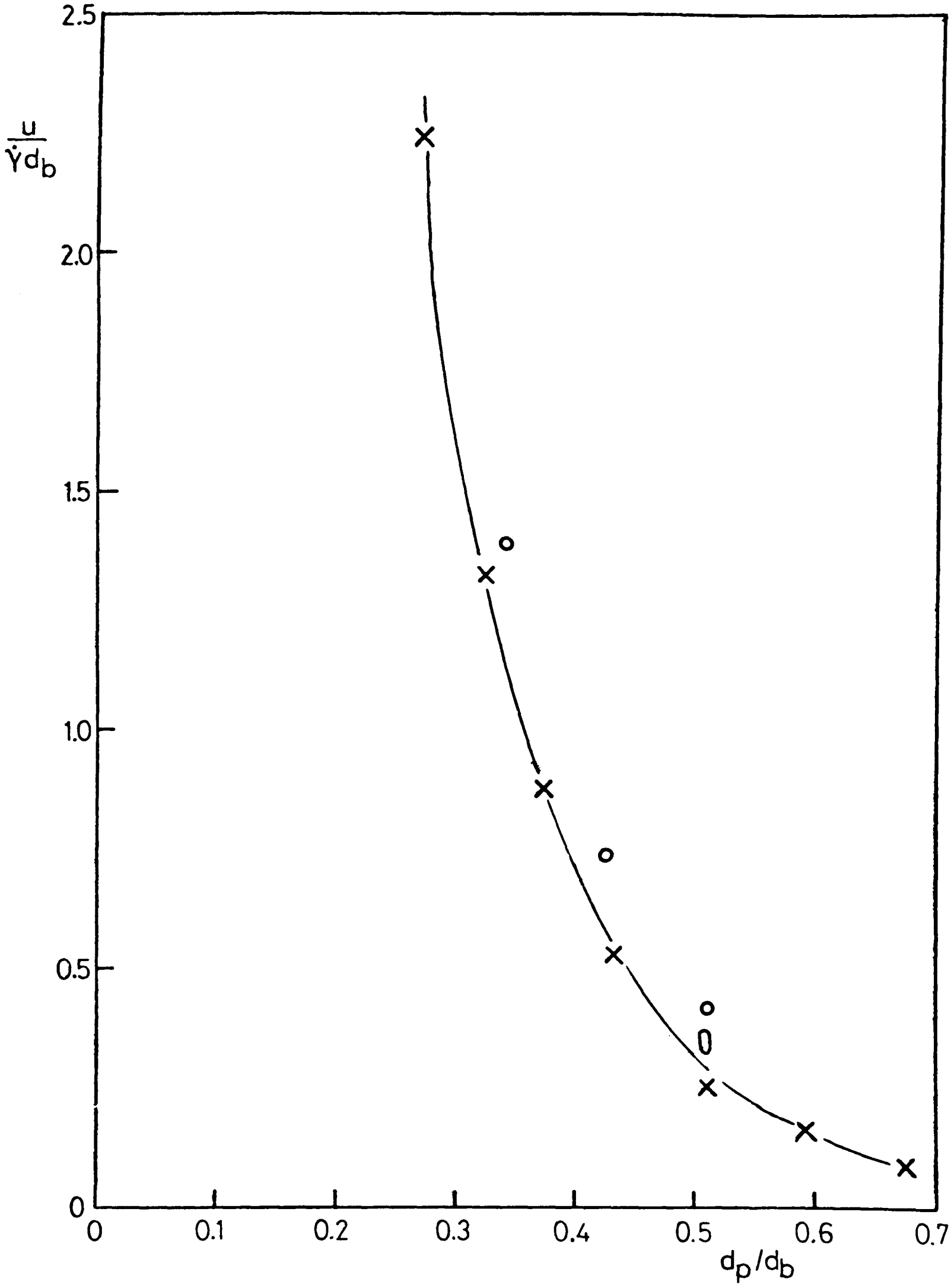


Figure 8.13: Dependence of percolation velocity on particle diameter ratio for $d_p/d_b > 0.2$. $\sigma_y = 1.40\ kNm^{-2}$, $\dot{\gamma} = 0.4\ s^{-1}$.

× Acrylic resin, species J,K,L,M,N,P,S.

o Other materials, species Q,R,T,U,W,X.

readings being recorded and though noticeably wrong values were edited out, it seems possible that the proportion of errors remaining was greater than that in the other experiments. However the regression between the mean residence strains and the bed height remained linear and h_c was reasonable, so it is unlikely that the errors are large.

Generally, errors due to scatter about the regression lines were in the range 5-10%, and hence were greater than those in other quantities. Errors in the bed height, which could be measured to 0.1mm, were negligible; standard errors in the mean residence strain varied but were typically 1-2%. A 0.01mm error in measuring the diameter of a small particle leads to a 1% error in residence strains (Scott, 1974) and hence this is also small.

Scott was unable to correlate the intercept of the regression on the bed height axis with bed or particle properties, but it is now apparent that there is a dependence on particle diameter (figure 8.14). Changes in the intercepts are about five times those in the percolating particle diameters and are presumably due to entry and exit effects as the particle falls into and leaves the cell.

In contrast to the results from the SSA Mk. IIIA, the lateral diffusion coefficient $D_z/\dot{\gamma}d_b^2$ shows a pronounced dependence on d_p/d_b (figure 8.15). It decreases from about 0.09 to 0.03 over the range of d_p/d_b 0.673 to 0.269. This is probably because a larger particle requires access to a larger hole before lateral movement can occur and thus the rate of dispersion of large particles per unit of strain is less. These results are generally lower than those recorded in Table 8.2, possibly because the presence of more than one percolating

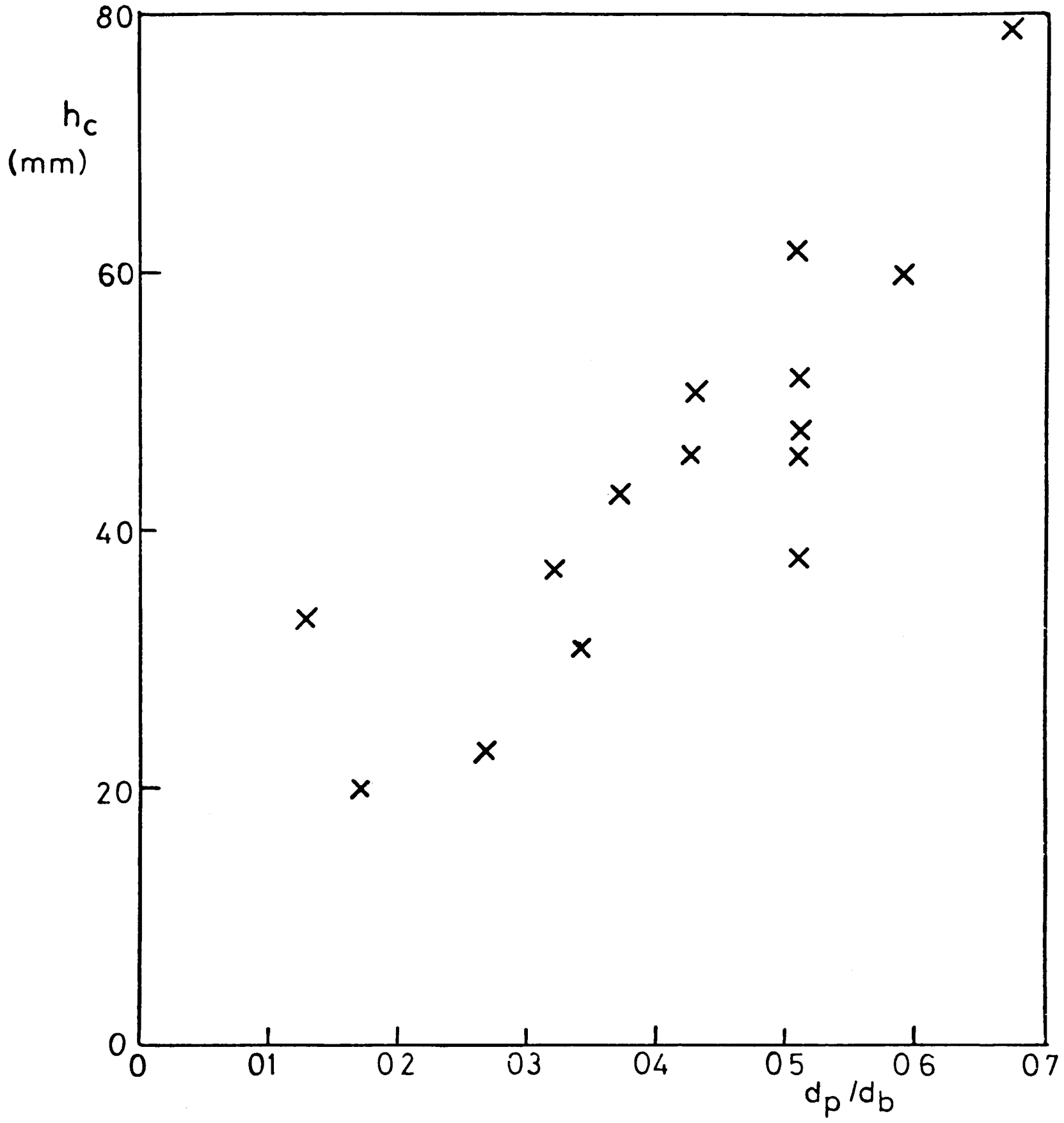


Figure 8.14: Effect of particle diameter ratio on intercept in regression between mean residence strain and bed height, σ_y = 1.40 kNm^{-2}, $\dot{\gamma}$ = 0.4 s^{-1}.

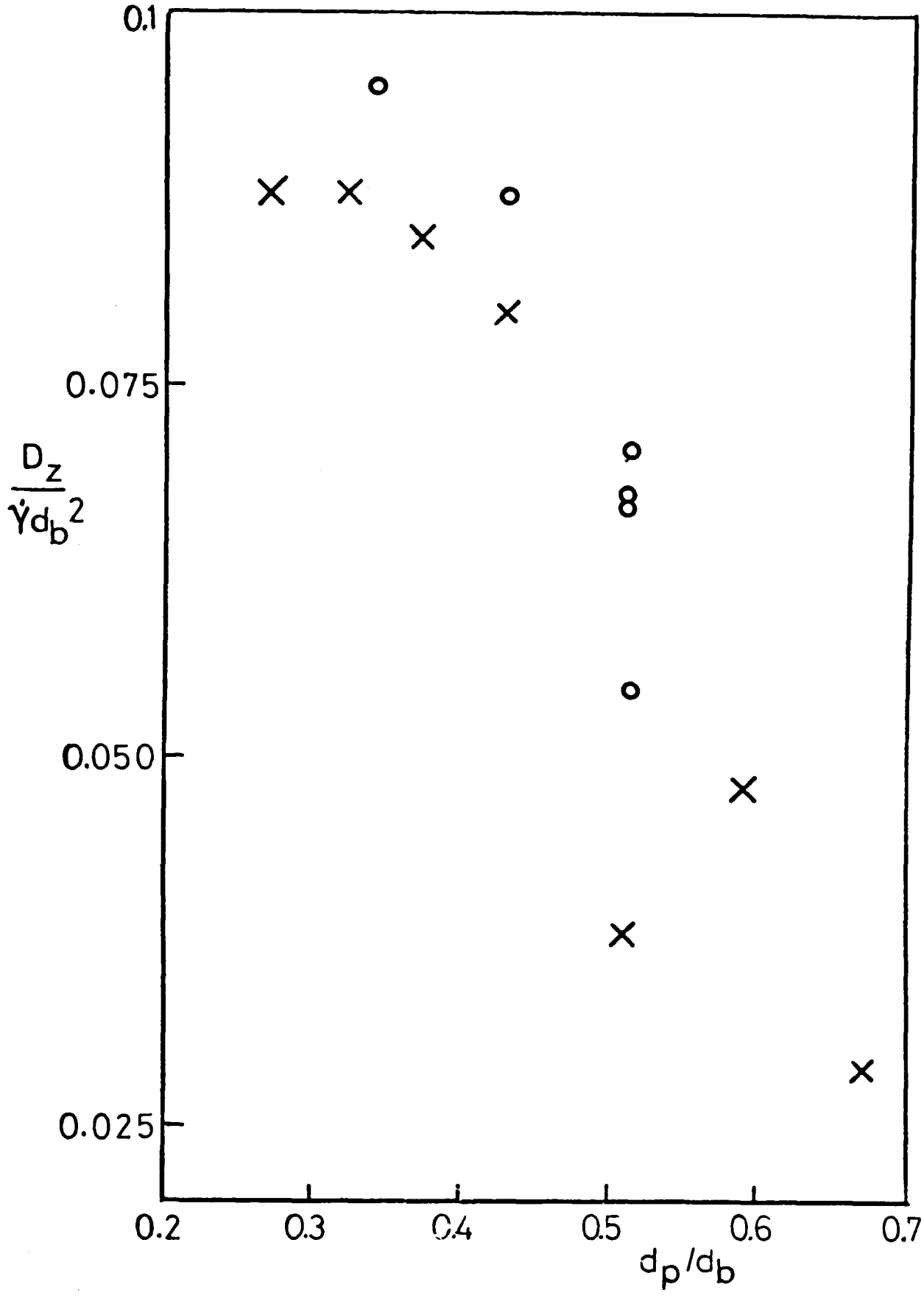


Figure 8.15: Dependence of dimensionless diffusion coefficient on particle diameter ratio for $d_p/d_b > 0.2$, σ_y = 1.40 kNm^{-2}, $\dot{\gamma}$ = 0.4 s^{-1}. × Acrylic resin
o Other materials.

particle in the cell at a time reduces the percolation velocity and hence appears to increase the diffusion coefficient. However the different strain rates and the different motion of the cell may have a larger effect.

The lateral diffusion coefficients of species Y and Z are considerably larger, and correspond to values of Pe_z equal to 8 and 7 respectively. These agree very well with the data for spontaneous percolation; values in the range 6-9 were reported by Bridgwater et al. (1969a) for $0.6<\alpha<1.0$.

Figure 8.16 shows the dependence of the axial Peclet number on particle diameter ratio. With the exception of species Z (spontaneous), there is apparently a slight increase in Peclet number with particle diameter. Thus larger particles undergo slightly less axial diffusion per unit of bed height, probably for the same reasons as their axial diffusion coefficients are lower. Scott's determinations of axial Peclet numbers were 1.7 ± 0.3 at $d_p/d_b = 0.425$ and 8 ± 5 at $d_p/d_b = 0.51$, values of the same order of magnitude as those presented here.

The axial Peclet number for species Z, 2.9, is less than half that for the experiment by Bridgwater and Ingram (1971) described earlier ($d_p/d_b = 0.128$, $\alpha = 0.92$, $Pe_y = 6.3$). This is probably also due to the moving bed effect.

8.3.3.2 Particle density ratio

One series of experiments was done with a hollow aluminium sphere, species R, and another with a similar sphere filled with 'Serebend', a high density alloy with a melting point about $40^{o}C$, species Q. The alloy was injected into the ball in the molten state with a syringe. This gave an increase in the apparent density of the ball from 0.74×10^{3} kg m^{-3} to

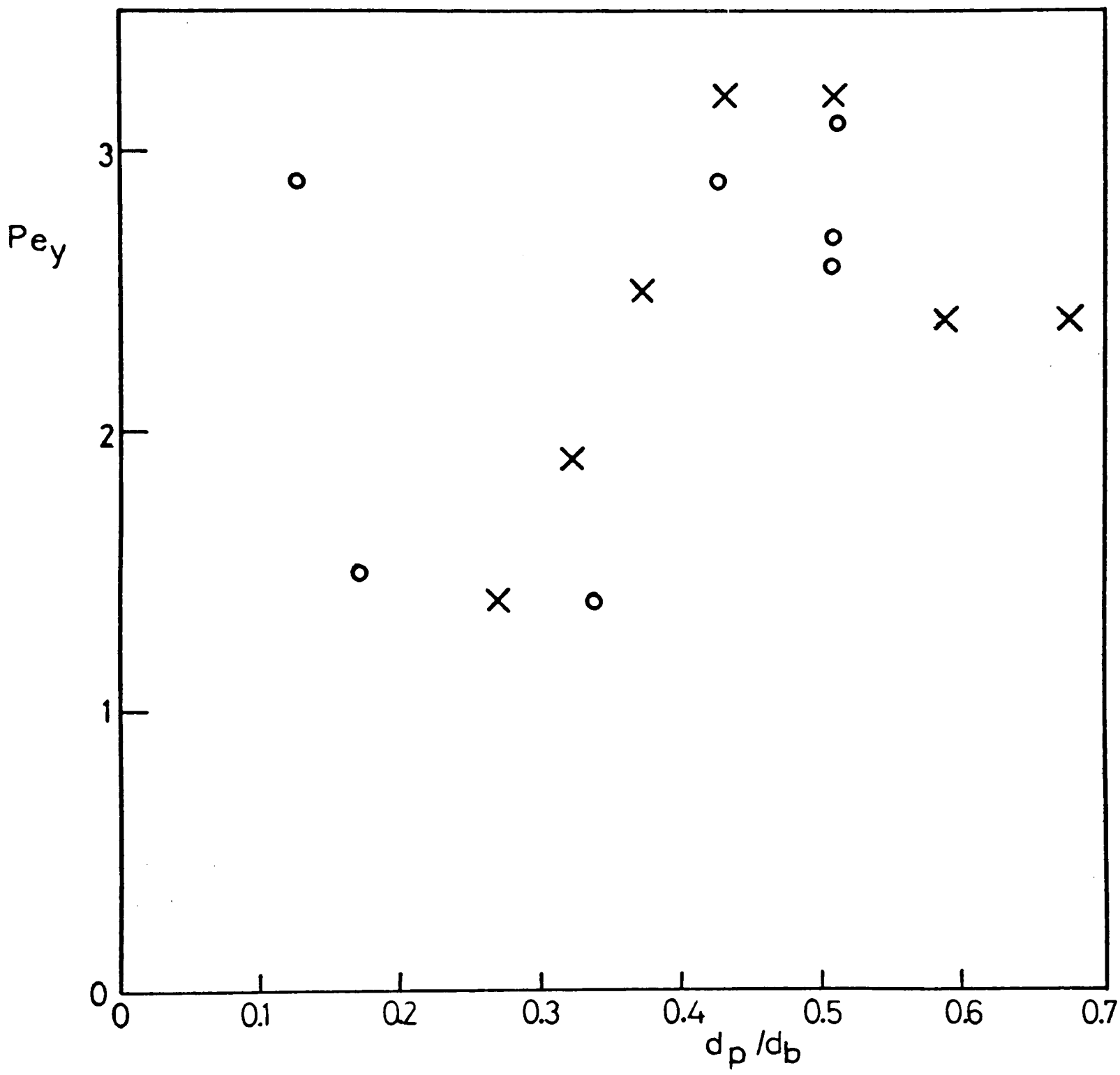


Figure 8.16: Dependence of axial Peclet number on particle diameter ratio. σ_y = 1.40 kNm^{-2}, $\dot{\gamma}$ = 0.4 s^{-1}.
× Acrylic resin
o Other materials.

7.55×10^3 kg m^{-3} whilst the surface properties remained unchanged. Dimensionless percolation rates were 0.42 ± 0.03 at ρ_p/ρ_b = 5.76 and 0.34 ± 0.02 at ρ_p/ρ_b = 0.56, i.e. increasing the density of the ball led to an increase in $u/\dot{\gamma}d_b$. The slopes of the regression lines on which these values were based (figure 8.17) were tested with a t-test (see Appendix II) and a value of t = 2.79 based on 17 degrees of freedom was obtained. The value observed with 5% probability is 2.11 and hence it was concluded that the percolation rates were different, possibly because the greater weight of the heavier ball enables it to force its way into more gaps. This is in contrast to Scott, who was unable to show that there were significant differences as the scatter in his results was too great. Values of h_c for the two series of experiments were not significantly different.

The effect of the density ratio on the diffusion coefficients is small and differences are not significant. Values of $D_z/\dot{\gamma}d_b^2$ = 0.067 ± 0.010 at ρ_p/ρ_b = 5.76 and 0.071 ± 0.009 at ρ_p/ρ_b = 0.56 were recorded and axial Peclet numbers were 3.1 in both sets of experiments. This provides further evidence that diffusion is primarily controlled by the relative particle sizes.

8.3.3.3 Material properties

A range of percolating particles of different materials was tested in the shear cell, but few significant differences were found. Figure 8.13 shows that vulkollan, steel and teflon particles percolate faster than acrylic resin. For steel this is due to its greater density; for teflon and vulkollan it may be related to their elastic moduli which are very low. These are soft materials which are deformed slightly by the normal stress and may be squeezed through slightly smaller

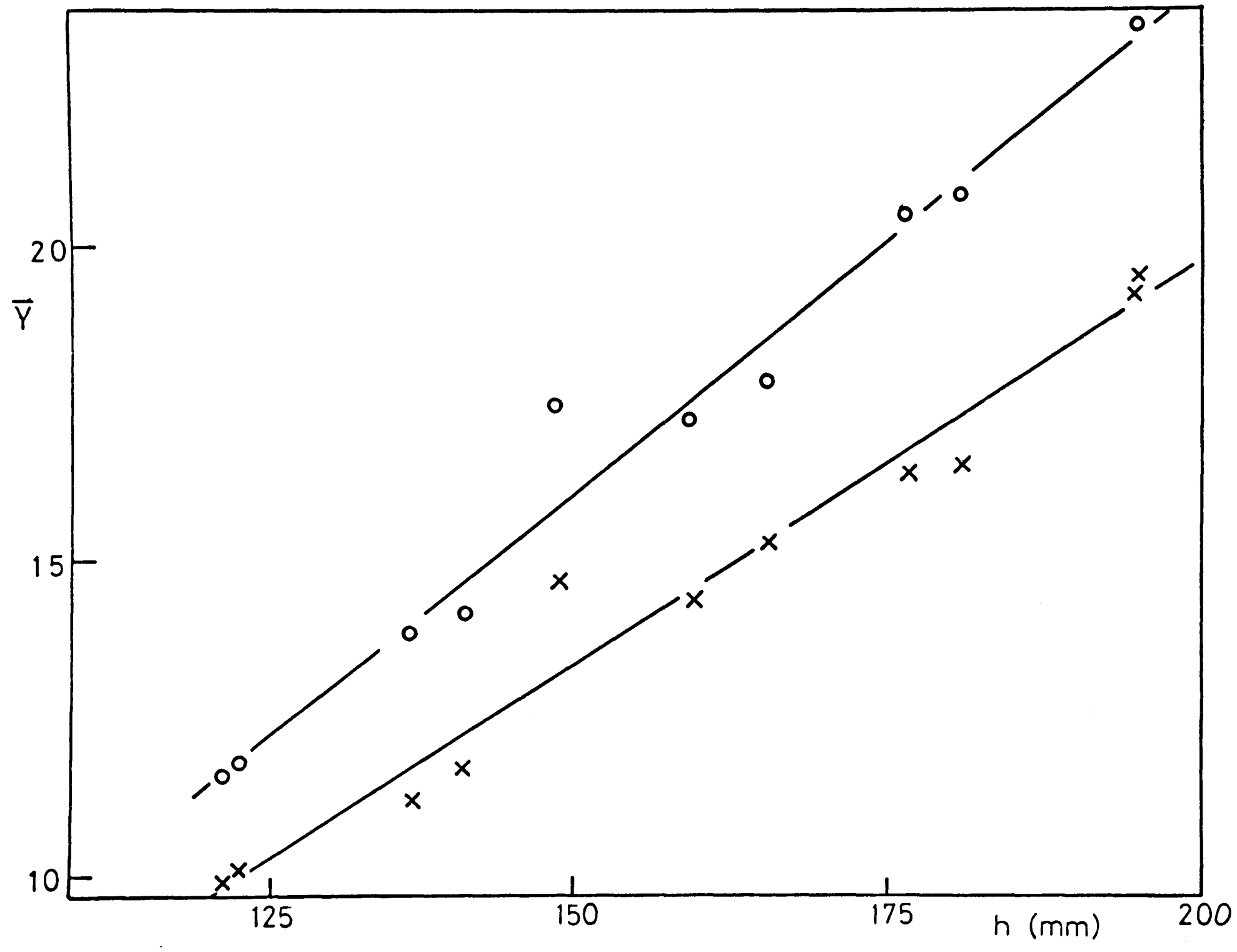


Figure 8.17: Relationship between mean residence strain and bed height. $d_p/d_b = 0.512$, $\sigma_y = 1.40\ kNm^{-2}$, $\dot{\gamma} = 0.4\ s^{-1}$. x Species Q, $\rho_p/\rho_b = 5.76$
o Species R, $\rho_p/\rho_b = 0.56$

gaps. The low friction between the teflon and phenolic resin particles may also be partly responsible.

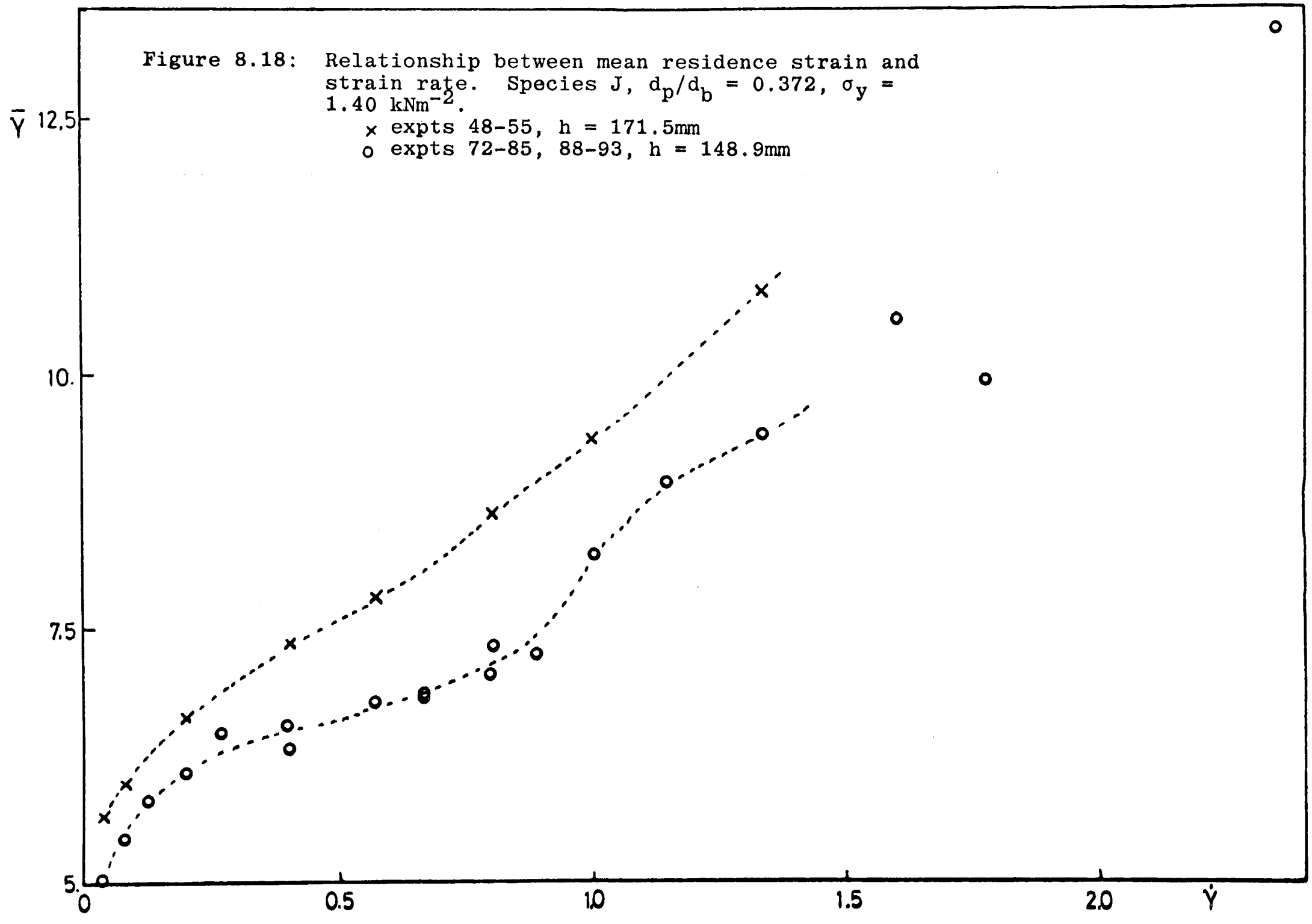
Differences in diffusion coefficients were not significant.

8.3.4 Effect of bed variables

8.3.4.1 Rate of strain

Scott found an approximately linear relationship between mean residence strain and mean rate of strain for a constant fill of the cell. His experiments were checked in the Mk. V to see whether the use of a constant strain rate over a cycle made a difference. The first series, experiments 48-55, figure 8.18, produced an approximately linear relationship with possible slight oscillations about the line. One of Scott's experiments exhibited similar oscillations and a second more extensive series, experiments 72-85, 88-93, was carried out at a lower bed height (figure 8.18). These results showed even greater deviations from linearity. A different approach was then tried; percolation rates were measured at four different strain rates over a range of bed heights. The results were: 1.17 ± 0.03 at $\dot{\gamma} = 0.167\ s^{-1}$, 0.88 ± 0.07 at $\dot{\gamma} = 0.400\ s^{-1}$, 0.84 ± 0.05 at $\dot{\gamma} = 0.667\ s^{-1}$ and 0.84 ± 0.04 at $\dot{\gamma} = 1.000\ s^{-1}$. Thus there is no significant difference for $0.4\ s^{-1} \leqslant \dot{\gamma} \leqslant 1.0\ s^{-1}$ but the percolation rate is significantly faster for $\dot{\gamma} = 0.167\ s^{-1}$. This unexpected finding is compatible with the earlier experiments, as, from figure 8.18, the difference in mean residence strains for $\dot{\gamma} \geqslant 0.4\ s^{-1}$ for the two series of experiments is approximately constant, whereas below this value the differences are appreciably smaller. A consequence is that h_c should decrease with increasing strain rate for $0.4\ s^{-1} \leqslant \dot{\gamma} \leqslant 1.0\ s^{-1}$ and this is found to be so (Table 8.5).

Figure 8.18: Relationship between mean residence strain and strain rate. Species J, d_p/d_b = 0.372, σ_y = 1.40 kNm^{-2}.
× expts 48-55, h = 171.5mm
o expts 72-85, 88-93, h = 148.9mm



From the supposedly linear relationship between mean residence strain and mean rate of strain, Scott had deduced that the relationship between $\bar{\gamma}$ measured at a constant strain rate and $\dot{\gamma}$ would be the same as that between $\bar{\gamma}$ measured at a variable strain rate and $\bar{\dot{\gamma}}$, and hence that $u/\dot{\gamma}d_b$ was proportional to $1/\dot{\gamma}$. His mistake was to assume that h_c was not a function of strain rate and this procedure has now been shown to be unsound.

The oscillations in figure 8.18 may be due to changes in the state of the material in the bed over a cycle. Scott had investigated the variation of the bed height during a cycle using a dial gauge. He was unable to continuously record the bed height but was able to show that the maximum bed height was reached at the end of a stroke and that this was followed by a rapid fall. Further investigations were carried out with the SSA Mk. V using a displacement transducer coupled to a U-V oscillograph so that a continuous record could be obtained. Some typical traces are shown in figure 8.19. They confirm that there is a sharp fall in height as the direction of the cell changes, followed by a rapid climb to an approximately constant bed height. There is then another increase towards the end of a stroke followed by a sharp drop on reversal and the cycle begins again.

These variations can be explained as follows. During the rapid increase in voidage near the beginning of a stroke, the material is dilating prior to achieving the critical state. The second increase is due to the development of free space underneath the lid adjacent to the leading end wall. Such spaces could be observed visually. The drop in height on reversing the direction of strain was also observed by Wroth (1958) during an investigation of 1mm steel balls in an SSA.

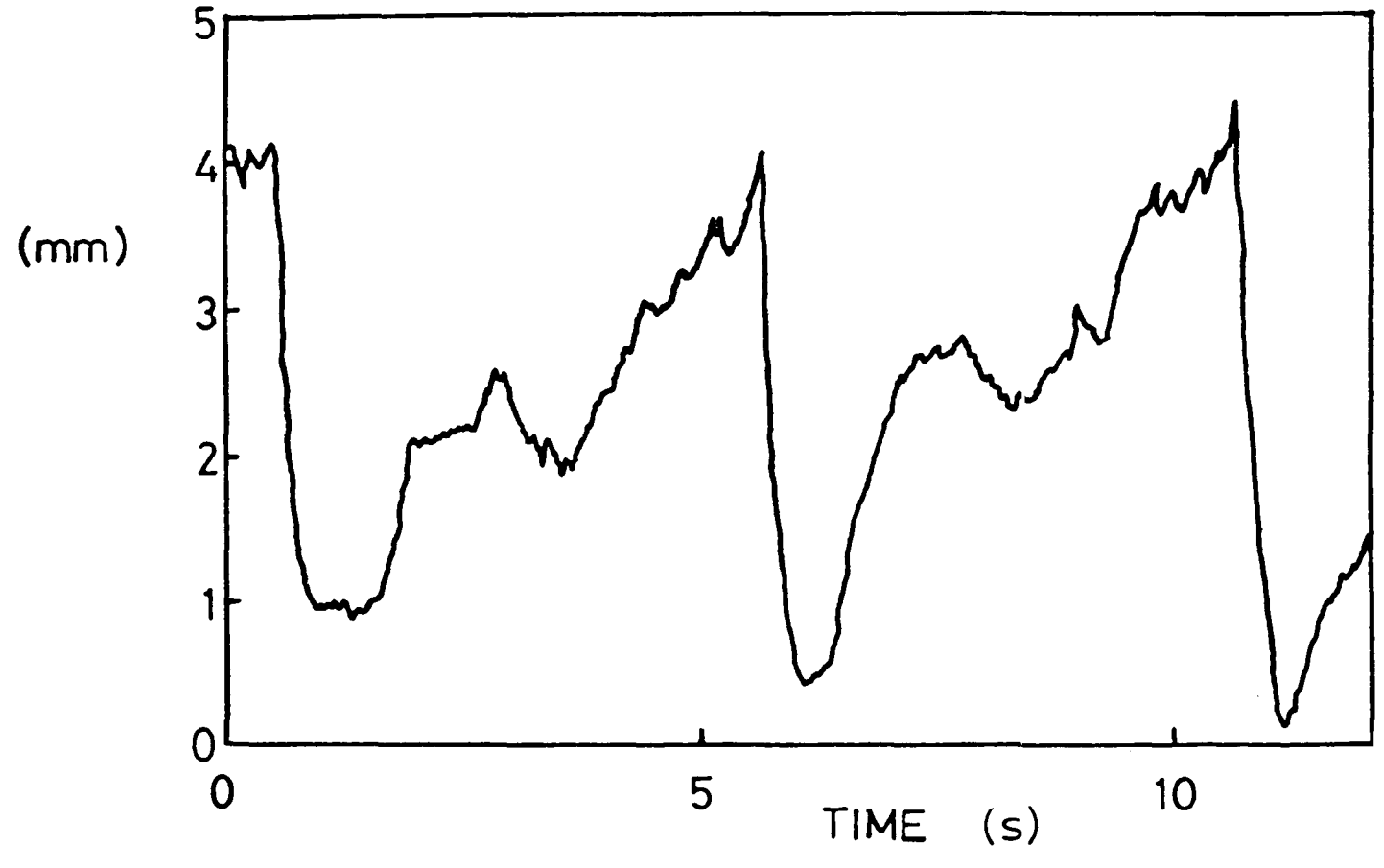


Figure 8.19: Traces showing the variation in bed height over a cycle. h = 201.1mm. (i) $\dot{\gamma} = 0.4\ s^{-1}$, (ii) $\dot{\gamma} = 0.2\ s^{-1}$

Though the material in the cell is not in the critical state for about 25% of the cycle, particles fall from the base plate continually and thus some percolation must be occurring during this period. Scott (1974) proposed a simplified approach to the problem in which he assumed that a fixed strain immediately after reversal γ_d did not cause any percolation. He then deduced that

$$\frac{1}{N_s} = \frac{1}{\gamma_T} (\gamma_s - \gamma_d) \qquad (8.9)$$

where N_s is the measured mean strain for percolation through height h in strokes, γ_T is the 'true' effective mean strain for percolation through this height and γ_s is the strain per stroke. A plot of $1/N_s$ against γ_s gave a straight line corresponding to $\gamma_d = 0.25$. However, though the number of particles leaving the cell is lower at the beginning of a stroke, it is not zero and Scott's model does not provide a complete physical picture of the processes taking place in the cell.

If there is a small variation in the number of particles leaving the cell during a stroke, this would account for the oscillations in figure 8.18 and also for some of the scatter about the regression between mean residence strain and bed height.

Since Scott showed that the movement of bulk balls was virtually the same at different strain rates, the increase in percolation rates for $\dot{\gamma}<0.4\ s^{-1}$ may be due to an increase in the lifetime of gaps below the percolating particle, as it may be that a gap has to have at least a certain duration before a percolating particle can fall into it.

The effect of different strain rates on $D_z t_m$ is shown in figure 8.20. As the cell moves faster, $D_z t_m$ increases, t_m decreases and hence D_z also increases. Values of $D_z/\dot{\gamma}d_b^2$

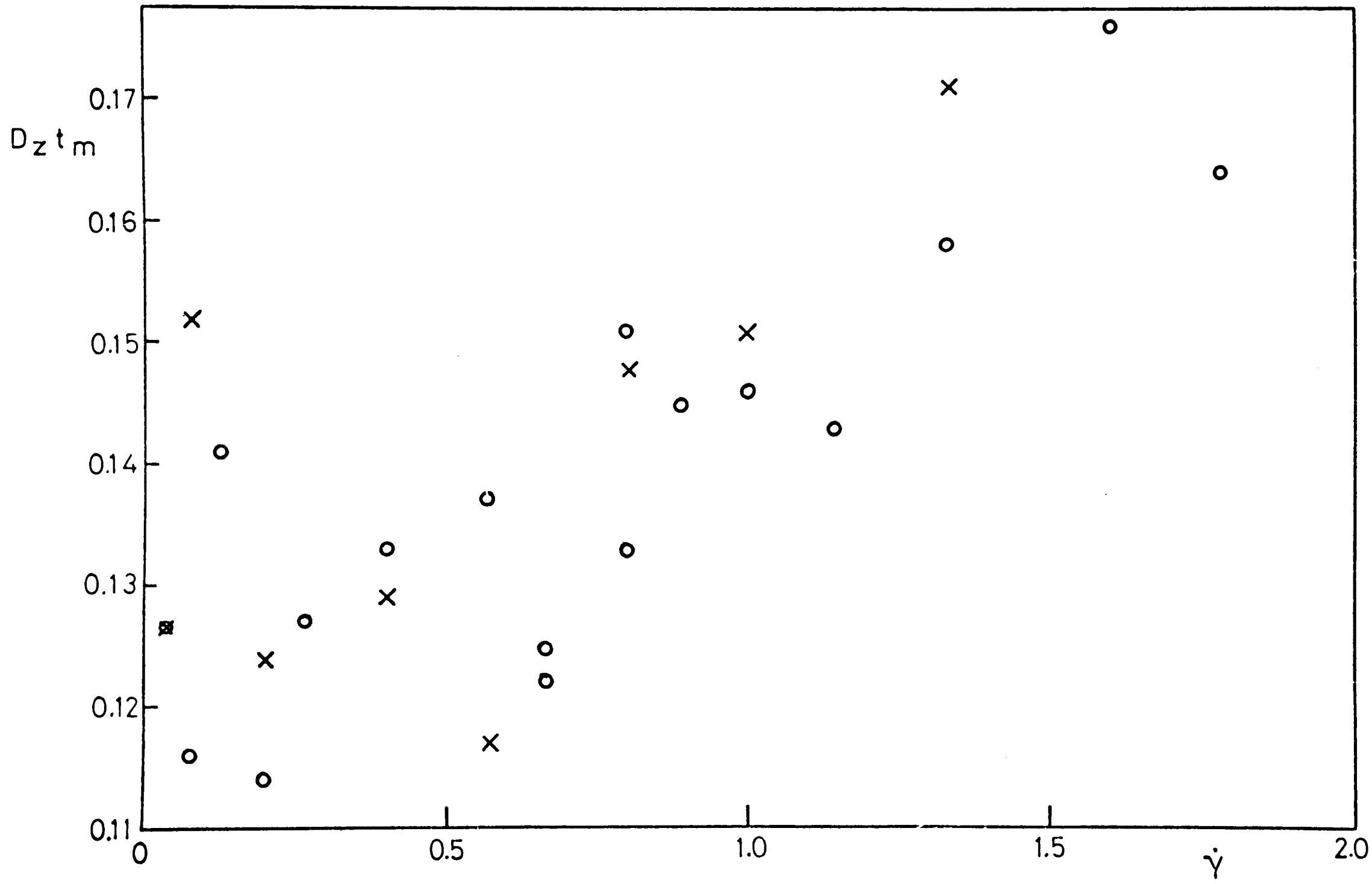


Figure 8.20: Relationship between $D_z t_m$ and strain rate.
Species J, $d_p/d_b = 0.372$, $\sigma_y = 1.40\ kNm^{-2}$.
× expts 48-55, h = 171.5mm
o expts 72-85, 88-93, h = 148.9mm.

from the series of experiments at different strain rates (Table 8.5) are not significantly different, implying that D_z is approximately proportional to $\dot{\gamma}$. The dependence of HPe_y/d_b on strain rate is shown by figure 8.21.

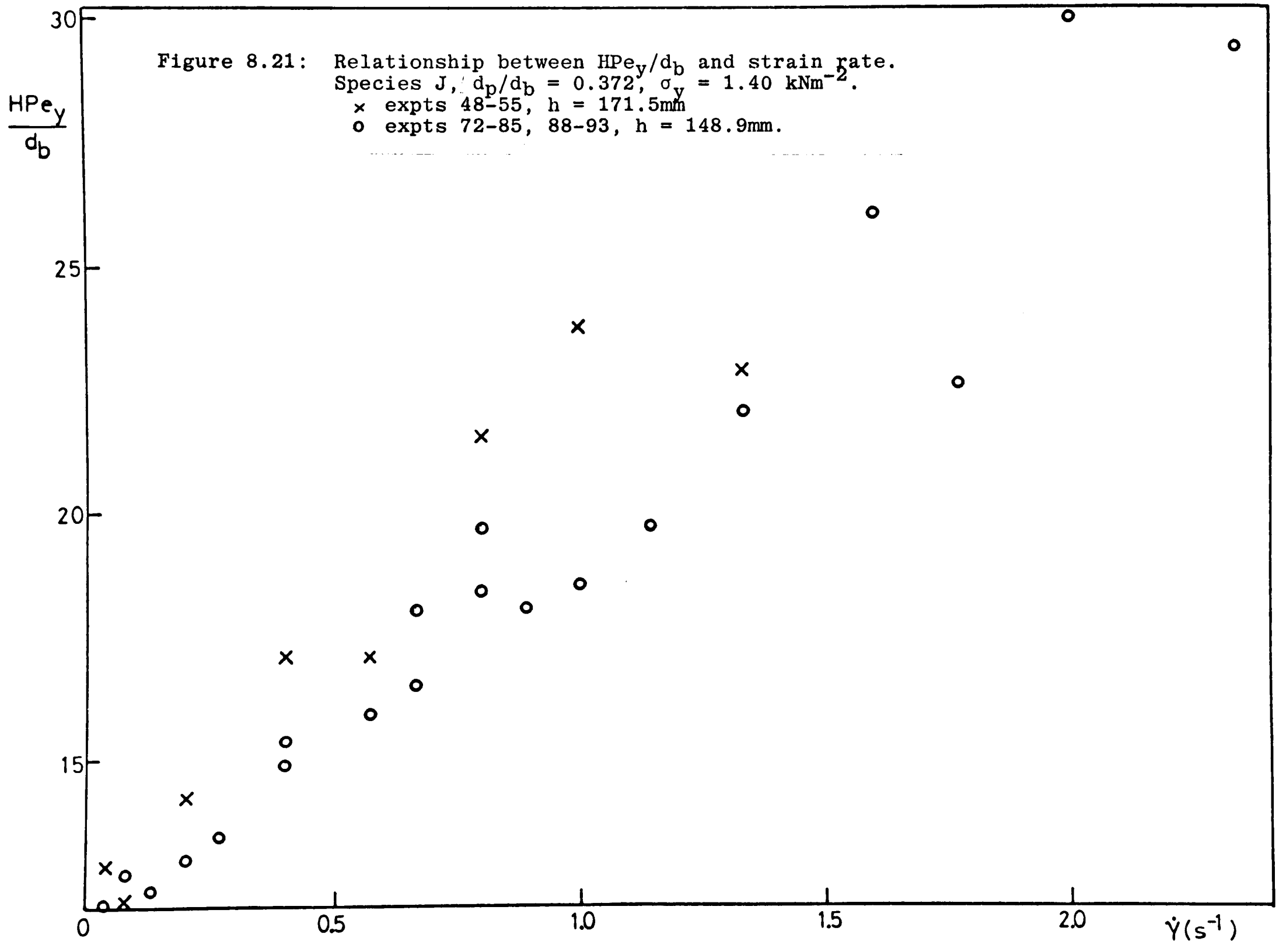
8.3.4.2 Normal stress

Scott's experiments in the SSA Mk. IV led him to conclude that the percolation velocity was reduced by 30% when the normal stress increased from 1.9 kNm^{-2} to 11.8 kNm^{-2}. It was thought that the magnitude of changes in the percolation velocity might depend on the elastic modulus of the percolating particle and thus experiments were performed with two different materials at a constant fill of the cell using a range of normal stresses. The results (figure 8.22) show that the mean residence strain increases by over 20% as σ_y changes from 1.40 kNm^{-2} to 5.21 kNm^{-2}. However the difference between the results with steel particles (E_p = 210 kN mm^{-2}) and 'vulkollan' (E_p = 0.1 kN mm^{-2}) remained constant. The rubber 'vulkollan' particles passed through the cell slower in all experiments.

Variations in the diffusion coefficients are shown in figures 8.23 and 8.24. No trends are discernible because of scatter.

The change in percolation velocity with changes in σ_y has implications for the apparatus used here. If normal stresses in a stationary bed can be found from a force balance on an elemental slice, then, if σ_y is 1.4 kN m^{-2}, the force on a plane at the bottom of a bed 200mm high is about 2.5-3 kNm^{-2}. The average normal stress in a 120mm bed is then about 1.8 kNm^{-2} and that in a 200mm bed about 2.1 kNm^{-2}. The experiments reported

Figure 8.21: Relationship between HPe_y/d_b and strain rate.
Species J, $d_p/d_b = 0.372$, $\sigma_y = 1.40$ kNm^{-2}.
× expts 48-55, h = 171.5mm
o expts 72-85, 88-93, h = 148.9mm.



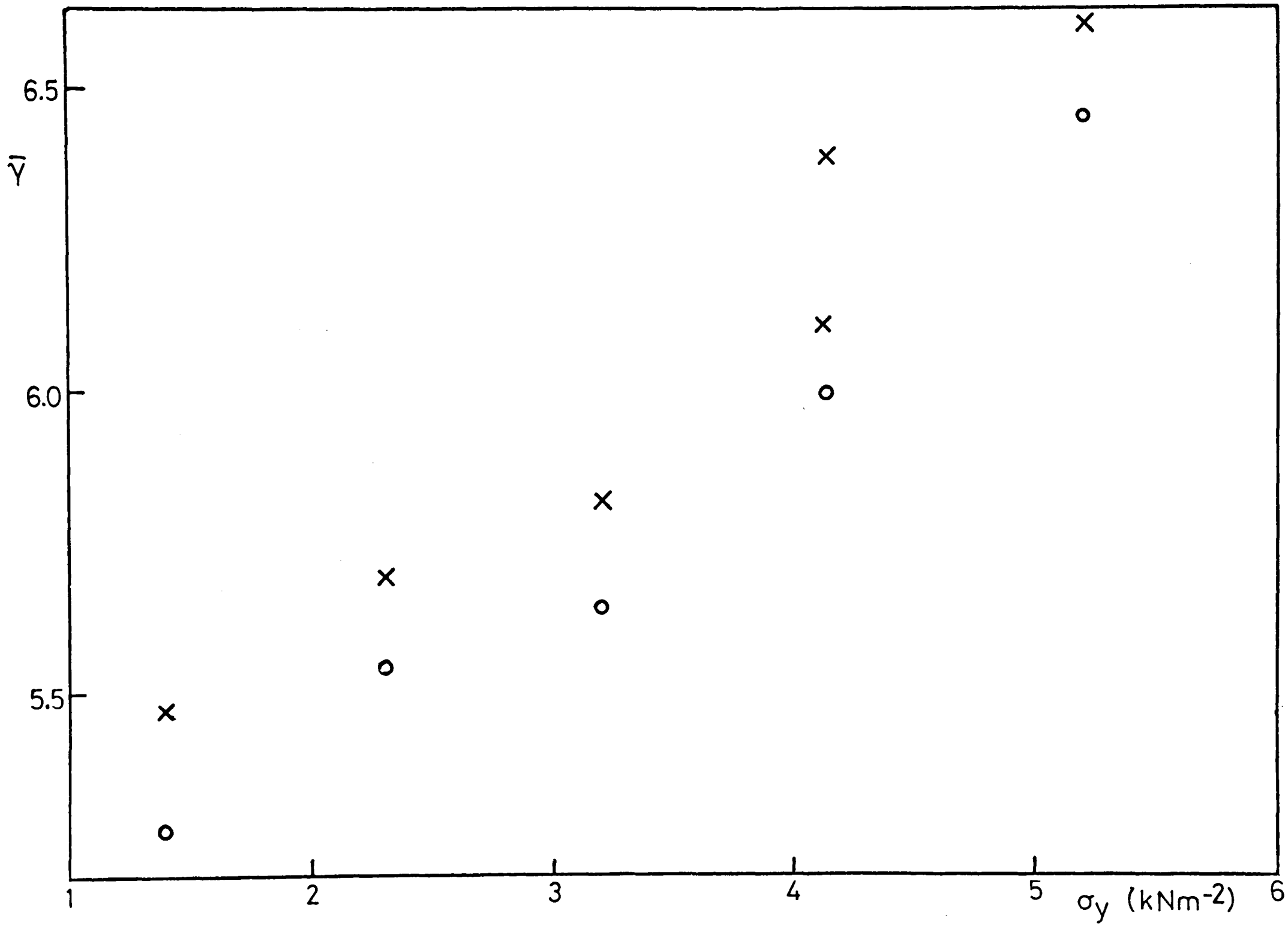


Figure 8.22: Relationship between mean residence strain and normal stress. $\dot{\gamma} = 0.4\ s^{-1}$, expts 146-155, 158.
× Species U, $d_p/d_b = 0.341$, $E_p = 0.1$ kNmm^{-2}
o Species V, $d_p/d_h = 0.341$, $E_p = 210$ kNmm^{-2}

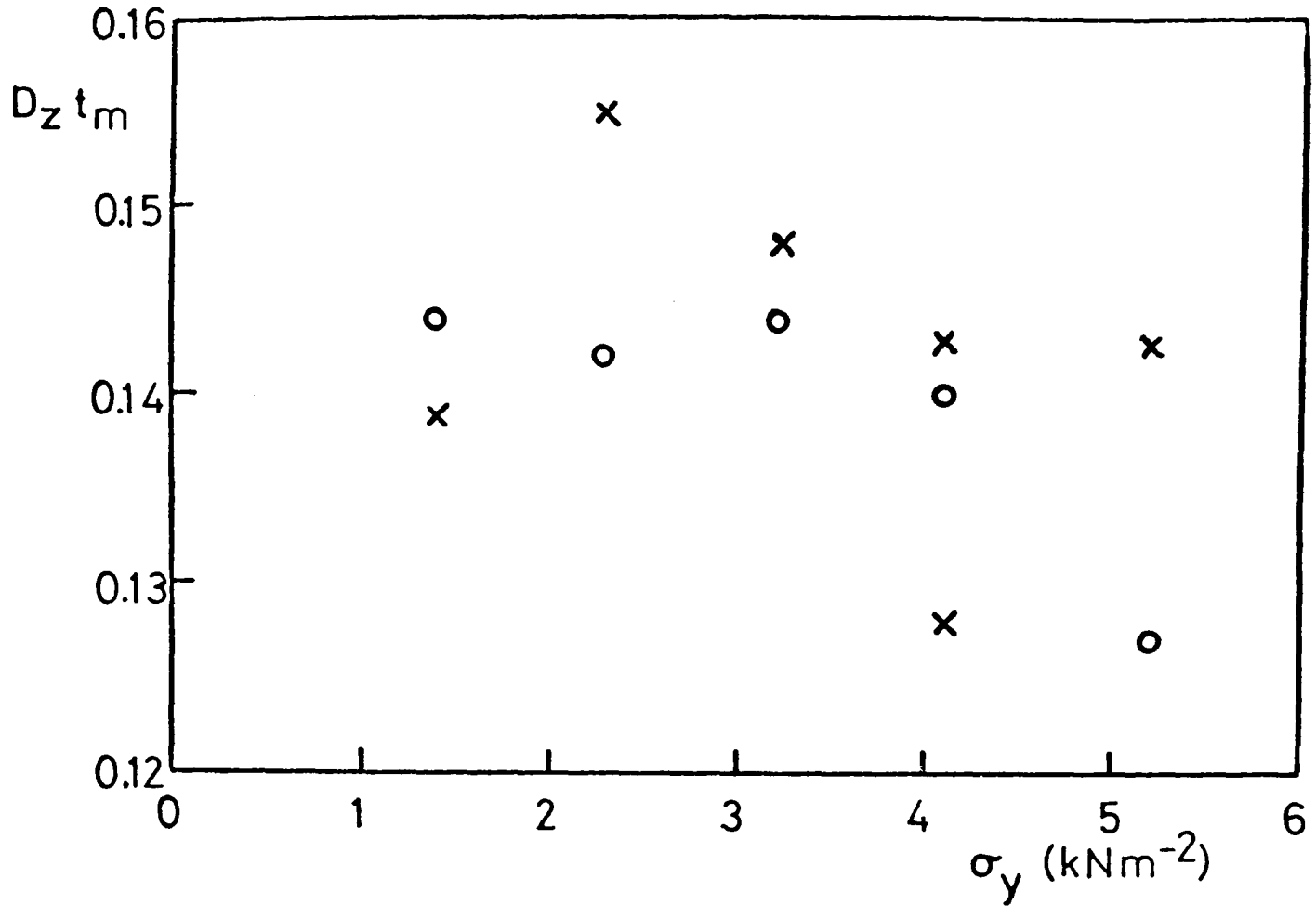


Figure 8.23: Relationship between $D_z t_m$ and normal stress.
$\dot{\gamma}$ = 0.4 s^{-1}, expts 146-155, 158.
× Species U, d_p/d_b = 0.341, E_p = 0.1 kNmm^{-2}
o Species V, d_p/d_b = 0.341, E_p = 210 kNmm^{-2}.

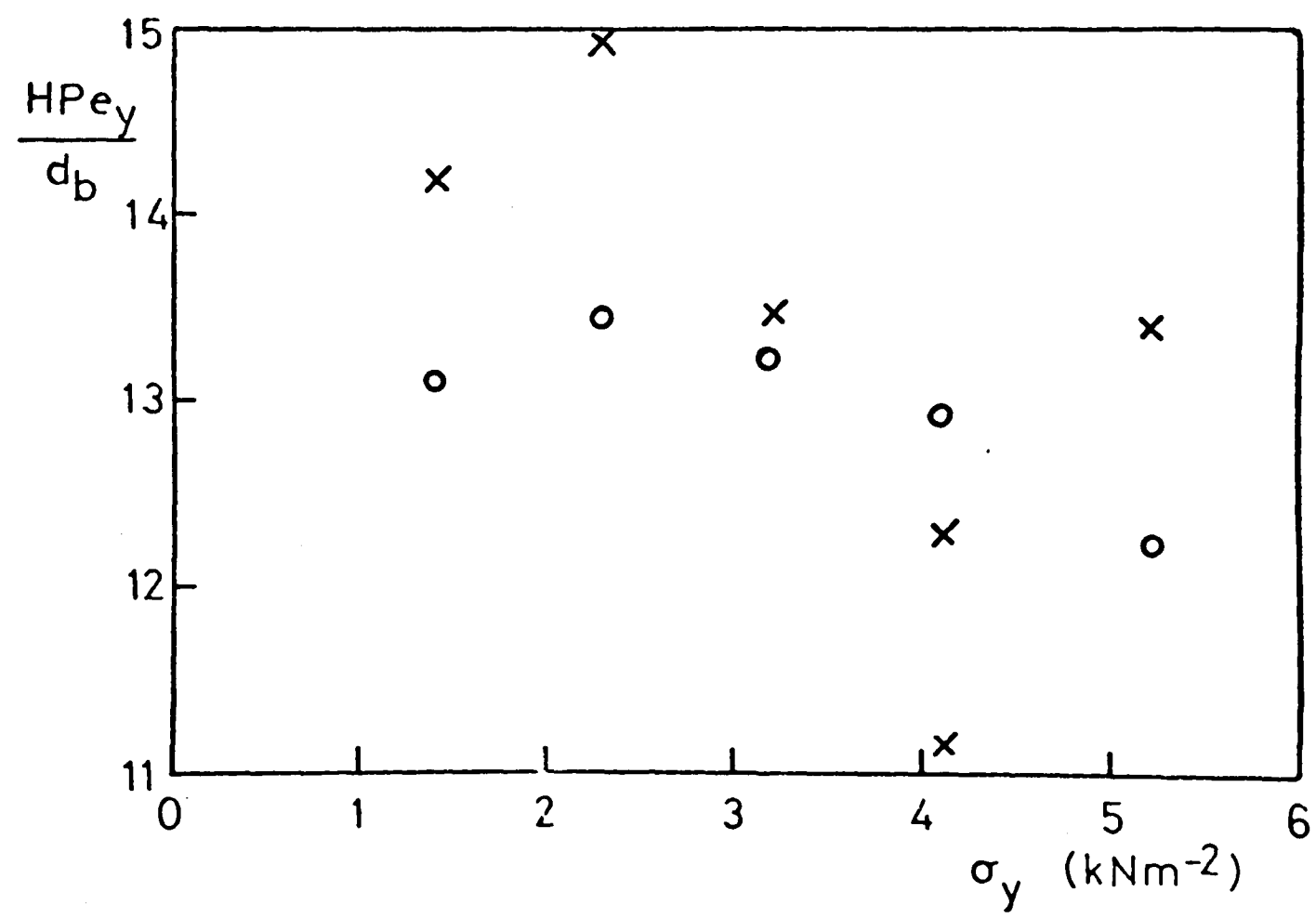


Figure 8.24: Relationship between HPe_y/d_b and normal stress.
$\dot{\gamma}$ = 0.4 s^{-1}, expts 146-155, 158.
× Species U, d_p/d_b = 0.341, E_p = 0.1 kNmm^{-2}
o Species V, d_p/d_b = 0.341, E_p = 210 kNmm^{-2}.

here suggest that such a difference would cause percolation rates to vary by about 2%. This may have contributed to any non-linearity in the regression between $\bar{\gamma}$ and h, but since the effect was small, it was not taken into account.

8.3.4.3 High bed heights

Scott claimed that experiments performed with bed heights >200mm (10.8 d_b) produced anomalous results, in that residence strains were greater than expected. However his results were ambiguous and are largely obscured by scatter. Bed heights up to 247.3mm (13.3 d_b) were used in a series of experiments with species J and L and the mean residence strain plotted against bed height. The results for species J are shown in figure 8.25 together with the regression line for h<198mm. The slopes of the regressions for h>198mm and h<198mm were tested by a t-test and no significant difference was found. The experiments with species L showed more scatter but again there was no significant difference from the earlier experiments.

8.3.4.4 Friction between the particles

The humid air supply to the top of the cell was originally connected to the air main via a Norgren Citation filter, type B02-400-M3MB. However, when a compressor gasket failure occurred during experiment No. 9, the line and bed became noticeably oily. It was suspected that the failure might have occurred gradually and experiments 6-9 were repeated but no significant differences were found between the two series of experiments. After experiment 9 the air lines were replaced, the cell degreased and filled with new bulk particles and a two-stage filter type F40-432-AOMB was installed. This was claimed to remove oil mists to better than 1 part in 10^6 w/w remaining and

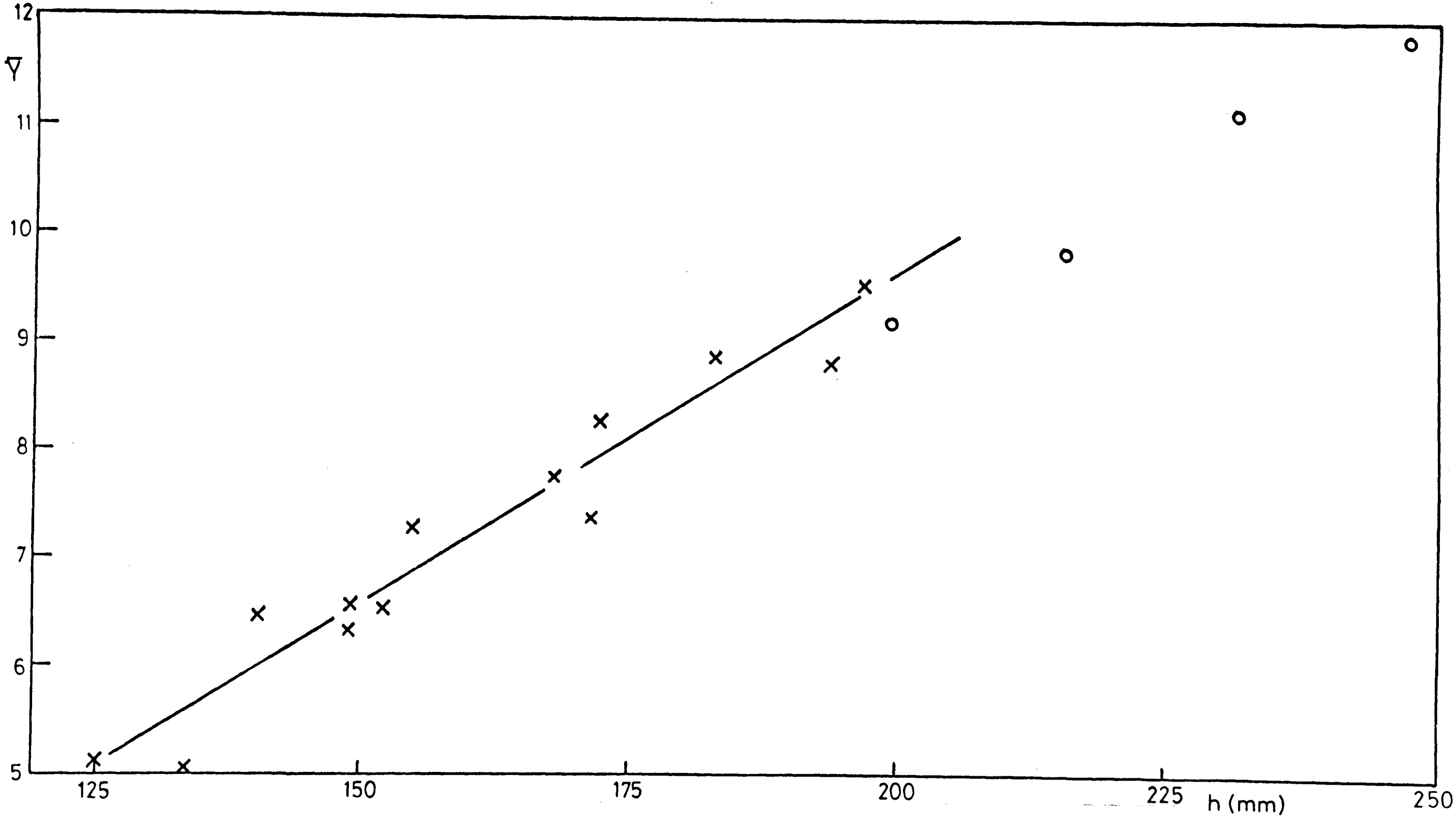


Figure 8.25: Relationship between mean residence strain and bed height at high bed heights. Species J, d_p/d_b = 0.372, σ_y = 1.40 kNm^{-2}, $\dot{\bar{\gamma}}$ = 0.4 s^{-1}.
× h<198mm, expts 113, 115, 117, 119
o h>198mm, expts 2-5, 33-38, 54, 73, 85.

to remove 99.999% of submicron particles. The cell then ran successfully until experiment 42 when the bed began to emit sharp cracking noises which generated spurious readings and the side walls of the cell flexed in an alarming manner. The cell was emptied but no obvious reason for this behaviour was immediately visible, though the bulk particles felt dry. Since it seemed possible that the trouble was due to an increase in the coefficient of friction between the balls, a bulk particle was lightly pressed into a gap between two base plate balls and the base plate rods rotated by hand. The rods were difficult to move and when they were turned the bulk particle shot a foot into the air. It therefore seemed that the original filter had allowed a small quantity of oil to pass and that the installation of a high efficiency filter had resulted in the cell drying out with a consequent increase in the frictional forces between bulk particles. It also appeared likely that the new bulk balls had been supplied with a small quantity of oil or wax on them. A few drops of oil were smeared over the base plate balls, the bulk particles replaced and the equipment restarted; after ten minutes it was again working perfectly, even though the bulk balls did not feel oily. Experiments performed before the breakdown were not significantly different from those done afterwards and it was therefore concluded that if there was a small amount of oil present, the quantity did not significantly affect the percolation rate. However, it was not possible to perform experiments with the cell in a completely dry state. A further few drops of oil were added after experiment 92 when the phenomenon occurred again and the apparatus then ran without mishap for the remainder of the experiments.

8.4 Theories of percolation

The dependence of percolation velocity on particle size ratio has been modelled as follows (Scott and Bridgwater, 1975). For a percolating particle to drop through the bulk material, one of the bulk balls below it must move approximately $d_p - d_s$ in a specified direction where d_s is the diameter of the largest particle which can percolate spontaneously. The time taken for this to occur t is approximately d_b/u. Then, as the mean square lateral displacement in the x direction is $2E_x t$, where E_x is the bulk particle diffusion coefficient in the x direction,

$$2E_x d_b/u \simeq (d_p - d_s)^2 \qquad (8.10)$$

Since for spheres $d_s/d_b = 0.155$,

$$\frac{d_b \bar{\dot{\gamma}}}{u} \simeq \frac{\bar{\dot{\gamma}} d_b^2}{2E_x} (d_p/d_b - 0.155)^2 \qquad (8.11)$$

Scott plotted $(u/\bar{\dot{\gamma}} d_b)^{-1}$ vs. $(d_p/d_b - 0.155)^2$ for his data and found that two straight lines were produced, one for $d_p/d_b < 0.5$ and the other for $d_p/d_b > 0.5$. The results from the Mk. V have been plotted in the same way in figure 8.26; the plot is curved and hence it seems that this analysis is inadequate.

An alternative approach, related to Cohen and Turnbull's (1959) statistical mechanical description of diffusion in liquids is now presented. A percolating particle is assumed to move stepwise through the bulk particles which are undergoing random motion. Eventually this motion produces a hole under the percolating particle into which it can squeeze. Each bulk particle is assumed to lie in a 'cage', the limits of which are the other bulk particles. A characteristic of each is the time-dependent quantity R, the longest distance between the surface of the particle and the extremity of the cage. If this distance is

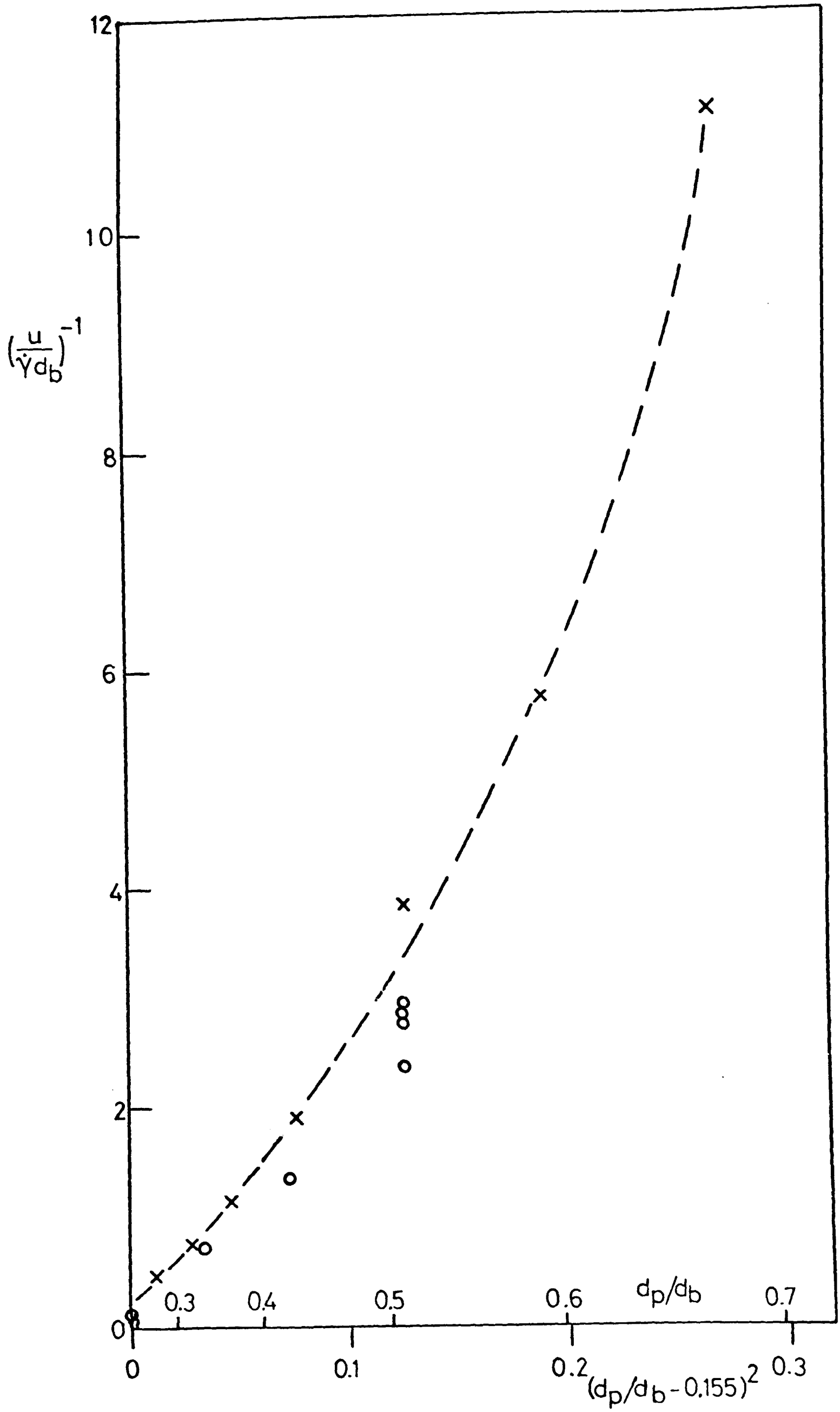


Figure 8.26: Plot of $(u/\dot{\gamma}d_b)^{-1}$ vs. $(d_p/d_b - 0.155)^2$
$\dot{\gamma} = 0.4\ s^{-1}$, $\sigma_y = 1.4\ kN\ mm^{-2}$
× Acrylic resin
o Other materials.

greater than some critical value R*, the percolating particle is able to squeeze past the bulk particle in the cage and thus fall a distance related to the diameter of the bulk particles.

The frequency distribution of R may be divided into regions q, each region having average value R_q. If N_q is the number of separations in region q, then

$$\sum_q N_q R_q = N_b \bar{R} \tag{8.12}$$

where N_b is the number of bulk particles and $\bar{R}$ the average value of R. If d_b is increased, $\bar{R}$ will increase and it will be assumed that these are linearly related,

$$k_r d_b = \bar{R} \tag{8.13}$$

where k_r is a constant. Also

$$\sum_q N_q = N_b \tag{8.14}$$

The number of ways W_R in which the lengths can be redistributed keeping the N_q constant is

$$W_R = \frac{N_b!}{\prod_q N_q!} \tag{8.15}$$

whence

$$\log_e W_R = \log_e N_b! - \sum_q \log_e N_q! \tag{8.16}$$

Using Stirling's approximation and differentiating,

$$d\log_e W_R = \sum_q (\log_e N_q) dN_q \tag{8.17}$$

From the constraints on the system, equations 8.12 and 8.14,

$$\sum_q dN_q = 0 \tag{8.18}$$

$$\sum_q R_q dN_q = 0 \tag{8.19}$$

From equations 8.17-8.19, introducing Lagrangian multipliers α_1 and α_2, at equilibrium,

$$\log_e N_q + \alpha_1 + \alpha_2 R_q = 0$$

or

$$N_q = \exp -(\alpha_1 + \alpha_2 R_q) \tag{8.20}$$

Now $$\sum_q N_q = N_b = e^{-\alpha_1} \sum_q e^{-\alpha_2 R_q}$$

and hence

$$\frac{N_q}{N_b} = \frac{e^{-\alpha_2 R_q}}{\sum_q e^{-\alpha_2 R_q}} = \alpha_2 e^{-\alpha_2 R_q} \tag{8.21}$$

Now, from equations 8.12 and 8.21 , passing to the continuum limit,

$$\sum_q N_q R_q = \int_0^\infty N_b \alpha_2 e^{-\alpha_2 R_q} dR_q = N_b \bar{R}$$

whence $\alpha_2 = 1/\bar{R}$. The probability that a value of R has value R_q is given by

$$p(R = R_q) = \frac{N_q}{N_b} = \frac{1}{\bar{R}} \exp(-R_q/\bar{R}) dR_q \tag{8.22}$$

and thus

$$p(R>R^*) = \int_{R^*}^\infty p(R = R_q)\, dR_q$$

$$= \exp(-R^*/\bar{R}) \tag{8.23}$$

Each time the percolating particle finds a gap greater than R^* it falls a distance $k_f d_b$ where k_f is a constant. The number of times this happens in a given time interval is proportional to $p(R>R^*)$ and $\dot{\gamma}$. Thus, if k_g is another constant,

$$\frac{u}{\dot{\gamma} d_b} = k_g \exp(-R^*/\bar{R})$$

If R^* is proportional to d_p, i.e. $R^* = k_s d_p$ where k_s is a constant then,

$$\frac{u}{\dot{\gamma} d_b} = k_g \exp\left[-(k_s d_p)/(k_r d_b) \right]$$

or $$\log_e (u/\dot{\gamma}d_b) = k_h - (k_s d_p)/(k_r d_b) \qquad (8.24)$$

where k_h is a constant. A graph of $\log_e (u/\dot{\gamma}d_b)$ vs. d_p/d_b should therefore be linear with slope $-k_s d_b/\bar{R}$. The data is plotted in this way in figure 8.27 and agreement between the theory and experimental results is excellent over the range $0.25<d_p/d_b<0.7$ for the acrylic resin particles. The slope of the line is about -8, which if k_s is about 1, implies that the mean separation $\bar{R}$ is about one eighth of the bulk particle diameter, which seems reasonable.

A defect of this model is that it does not take into account the possibility of a percolating particle rising due to it being forced upwards by the movement of the bulk particles. This would be expected to occur at high diameter ratios and the theory should therefore predict that larger particles percolate faster than they in fact do. If $d_p = d_b$ the percolation velocity should be zero, whereas the theory predicts a positive value. Scott's experiments with $d_p/d_b>0.7$ show the opposite trend to that expected. This may be due to truncation of the distribution of residence times due to the timer reaching its limit, or to many of these larger particles reaching the sides of the cell where percolation rates might be faster. The theory would also not apply to smaller particles where the motion is controlled by spontaneous percolation.

8.5 Conclusions

The simple shear apparatus used by Scott has been successfully modified and accurate percolation rates and diffusion coefficients have been found. The major conclusions may be summarised:

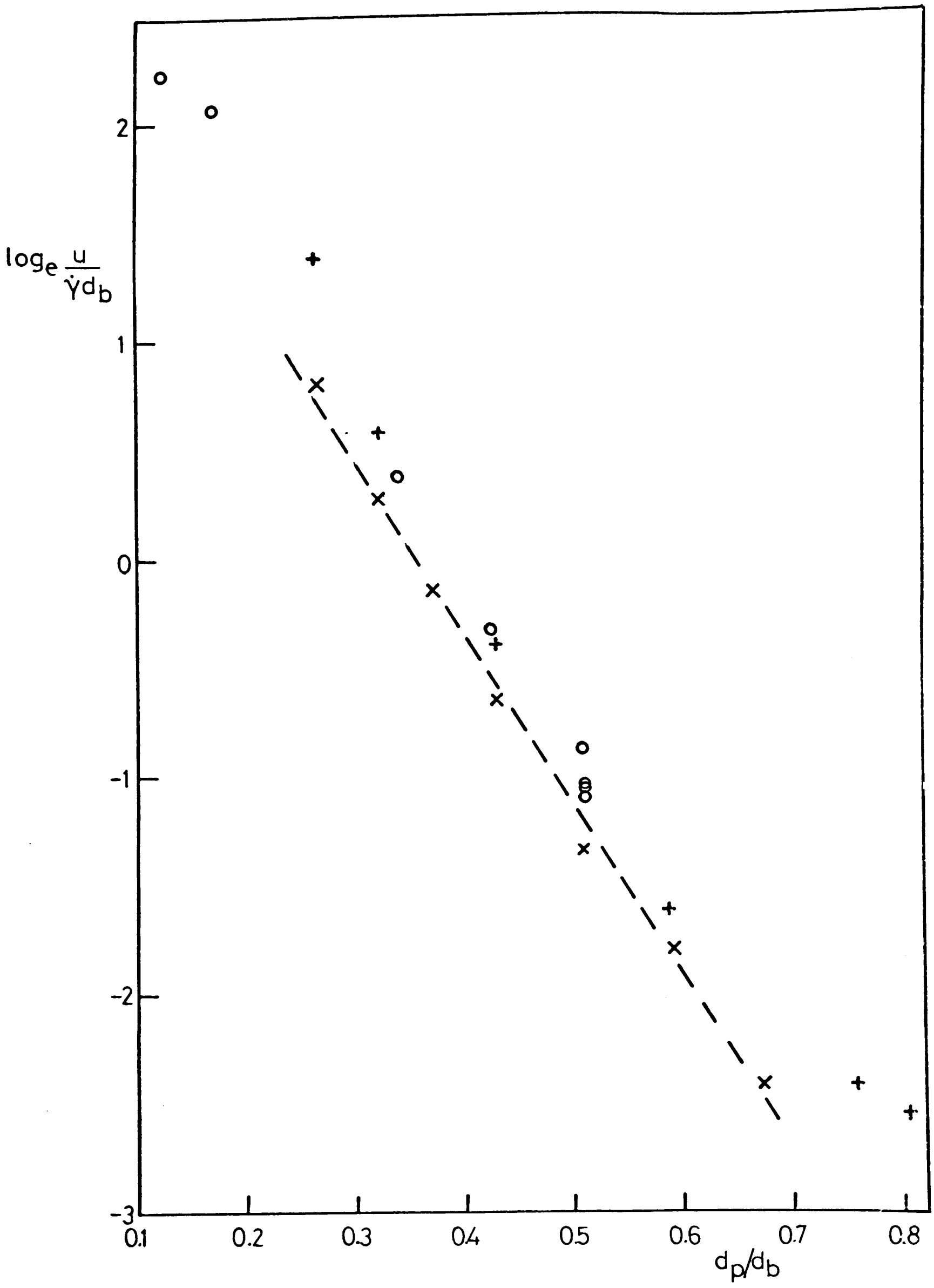


Figure 8.27: Plot of $\log_e(u/\dot{\gamma}d_b)$ vs. d_p/d_b
× Acrylic resin, $\dot{\gamma} = 0.4\ s^{-1}$, $\sigma_y = 1.4\ kNm^{-2}$
o Other materials, $\dot{\gamma} = 0.4\ s^{-1}$. $\sigma_y = 1.4\ kNm^{-2}$
+ Scott's (1974) values, acrylic resin, $\dot{\gamma} = 0.215\ s^{-1}$, $\sigma_y = 1.4\ kNm^{-2}$ or $2.7\ kNm^{-2}$ ($d_p/d_b = 0.430$).

(i) The results from the equipment may be satisfactorily represented by a percolation velocity and by diffusion coefficients but not by modelling the process as a series of ideal stirred tanks. These quantities may be calculated by performing experiments over a range of bed heights.

(ii) Of the particle properties the diameter ratio has the largest effect on percolation velocities and diffusion coefficients. For the range $0.269 \leqslant d_p/d_b \leqslant 0.673$, $u/\dot{\gamma}d_b$ decreased from 2.24 to 0.09 and $D_z/\dot{\gamma}d_b^2$ from 0.088 to 0.029 while the axial Peclet number increased from 1.4 to 2.4. The dependence of $u/\dot{\gamma}d_b$ on d_p/d_b has been successfully modelled by a statistical mechanical method over this range. It has also been found that denser particles percolate faster, as do particles made from materials such as rubber and PTFE, which have a low elastic modulus, though in these cases differences in diffusion coefficients could not be measured.

A particle small enough to undergo spontaneous percolation percolates slower in a moving bed than it does in a stationary one though it has a similar lateral diffusion coefficient. Its axial Peclet number is smaller in the moving bed.

(iii) The bed variables which affect percolation rates include the rate of strain and the normal stress. Reduction of the former below 0.4 s^{-1} leads to an increase in percolation velocity. Increasing it above this value does not appear to affect the velocity but increases the value of the intercept on the bed height axis in the regression between $\bar{\gamma}$ and h. This may be a base plate effect. An increase in the normal stress reduces the percolation velocity. Both strain rates and stresses were only investigated over a limited range of values.

It has also been found that bed heights up to 13.3 d_b

can be used in this equipment and that the presence of a small quantity of interstitial oil does not significantly affect percolation rates.

CHAPTER 9

CONCLUSION

This investigation has demonstrated that certain fundamental powder mixing mechanisms can be rationally explained and that quantitative analyses of the processes are possible.

9.1 Spontaneous percolation and its consequences

The models of spontaneous percolation advanced in Chapter 3 provide a simple physical representation of the process. Though more sophisticated than an earlier model they could probably be developed further, but this is unlikely to prove helpful. One predicts the percolation velocity of an inelastic particle, the other relates the velocity of a partly elastic particle to the diameter of the percolating and bulk particles and the coefficient of restitution between them. Good agreement is observed between numerical values predicted by this model and the existing experimental data.

The principle has been applied to the construction of a new type of static mixer. The simple design procedure used has been shown to work reasonably well and stringent tests have shown that the units produce almost random distributions of most materials in the size range 0.5-3.5mm, though particles with low coefficients of restitution apparently require slightly higher units. The upper size limit could be raised by use of a larger mixer, though the lower one is probably a consequence of material behaviour. Computer-generated design data was obtained from a program which simulates the passage of a spherical particle through a mixer. From this it has been possible to suggest a more efficient bar layout and to show that the quality

of the mixture or distribution is not very sensitive to the vertical bar spacing. By considering changes in the particle diameter and bar thickness as well, it has been shown that in general the performance is improved by increasing the voidage of the system. The next stage in the development of these devices is their application to industrial processes.

The use of different, often poorly defined, indices to characterize mixtures and distributions is one factor which makes comparison of mixers difficult. Introduction of the correlation coefficient between sample compositions has led to the derivation of equations which relate the variance of compositions to the sample size for processes in which two orthogonal mechanisms are in operation. A further finding is that the intercept on the log variance vs. log sample size plot provides a measure of the amount of correlation present in a mixture. These results are applicable to fields other than that of powder mixing. Another method of characterizing distributions is to assume that the probability that a sample has a certain composition is a function of its position only. This is of particular value when the positions of samples have a fixed geometrical relationship to the mixer. In this case it was possible to relate the variance of sample compositions to the number of particles used. The relationship was found to hold in the two-dimensional mixer.

9.2 Strain-induced percolation

Strain-induced percolation has already been studied quite extensively by Scott (1974) whose work was subject to the disadvantage that he was unable to strain material at a constant rate. The installation of a hydraulic system to drive his shear cell removed this restriction and made the operation of the cell more reliable.

In the systems investigated, the most important factor in determining the dimensionless percolation rate $u/\dot{\gamma}d_b$ was the relative diameters of small and large particles d_p/d_b. As this decreased from 0.67 to 0.27 the percolation rate increased twenty-five fold. The density of the percolating particle had an effect, a ten-fold increase in density causing a 25% increase in percolation rate. Other material properties also affected $u/\gamma d_b$. A rubber 'vulkollan' particle with a low elastic modulus (E_p = 0.1kN mm^{-2}) percolated slower than a denser steel particle of the same size (E_p = 210kN mm^{-2}). Among the bed properties investigated were the normal stress σ_y and rate of strain $\dot{\gamma}$. The effect of the former was not investigated in detail though mean residence strains were longer at higher values of σ_y. The strain rate was varied over the range $0.04s^{-1} \leqslant \dot{\gamma} \leqslant 2.34s^{-1}$ and was shown to have no significant effect on $u/\gamma d_b$ for $0.4s^{-1} \leqslant \dot{\gamma} \leqslant 1.0s^{-1}$ though the velocity increased at lower strain rates. This is in contrast to the work of Scott who, using an unsound procedure, deduced that the percolation velocity was inversely proportional to the rate of strain. Axial and lateral diffusion coefficients were also used to characterize the process. Again particle diameter ratio was the major factor, a change in d_p/d_b from 0.67 to 0.27 causing an increase in $D_z/\dot{\gamma}d_b^2$ from 0.029 to 0.088 and a decrease in Pe_y from 2.4 to 1.4.

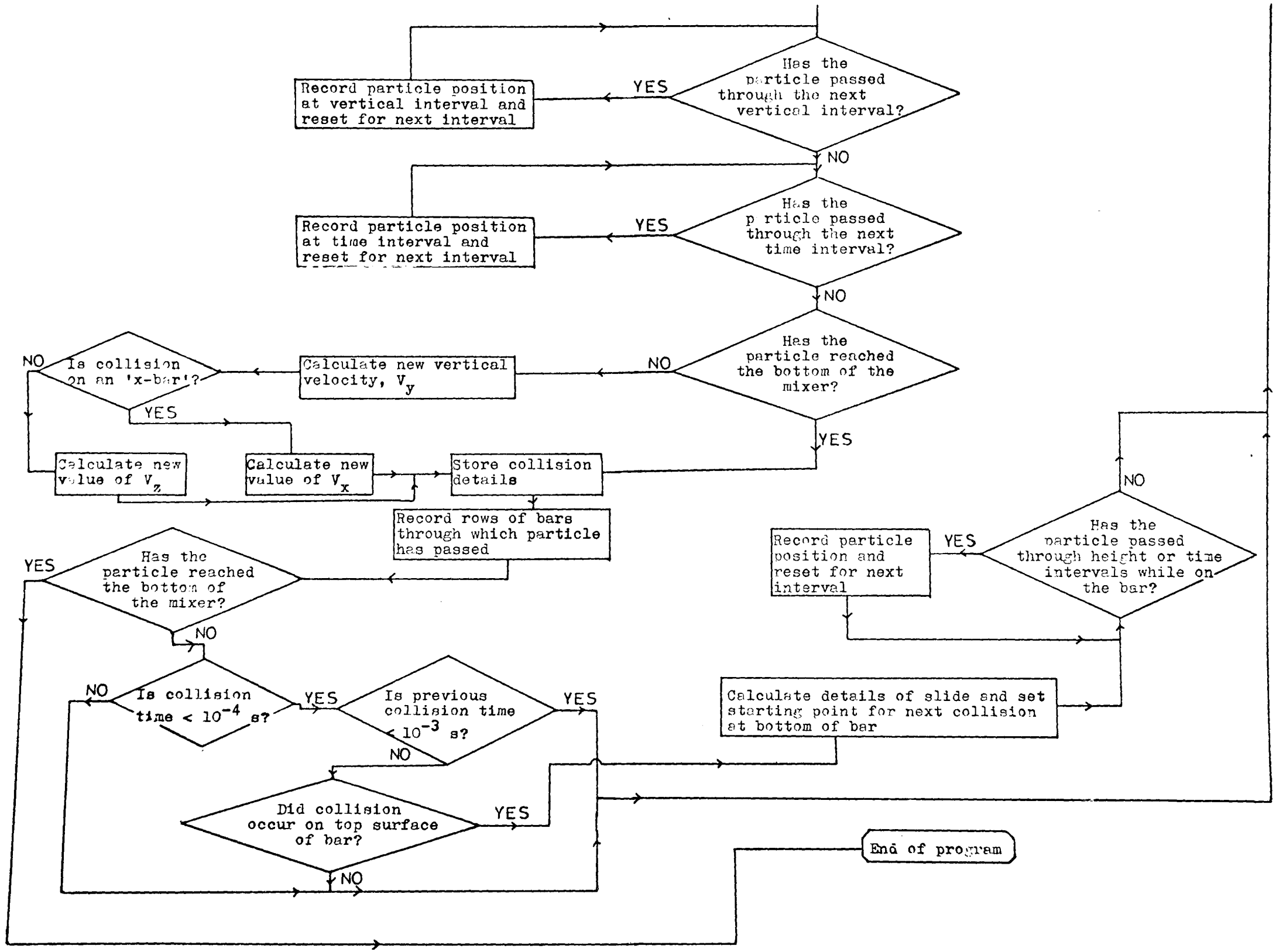
The physical picture of percolation described in Chapter 7 led to a simple model of the process using statistical mechanics. This implied that percolation took place in a stepwise manner, evidence for this coming from West (1976) as well as from Scott. The dependence of percolation velocity on diameter ratio predicted by the model was in good agreement with the experimental data.

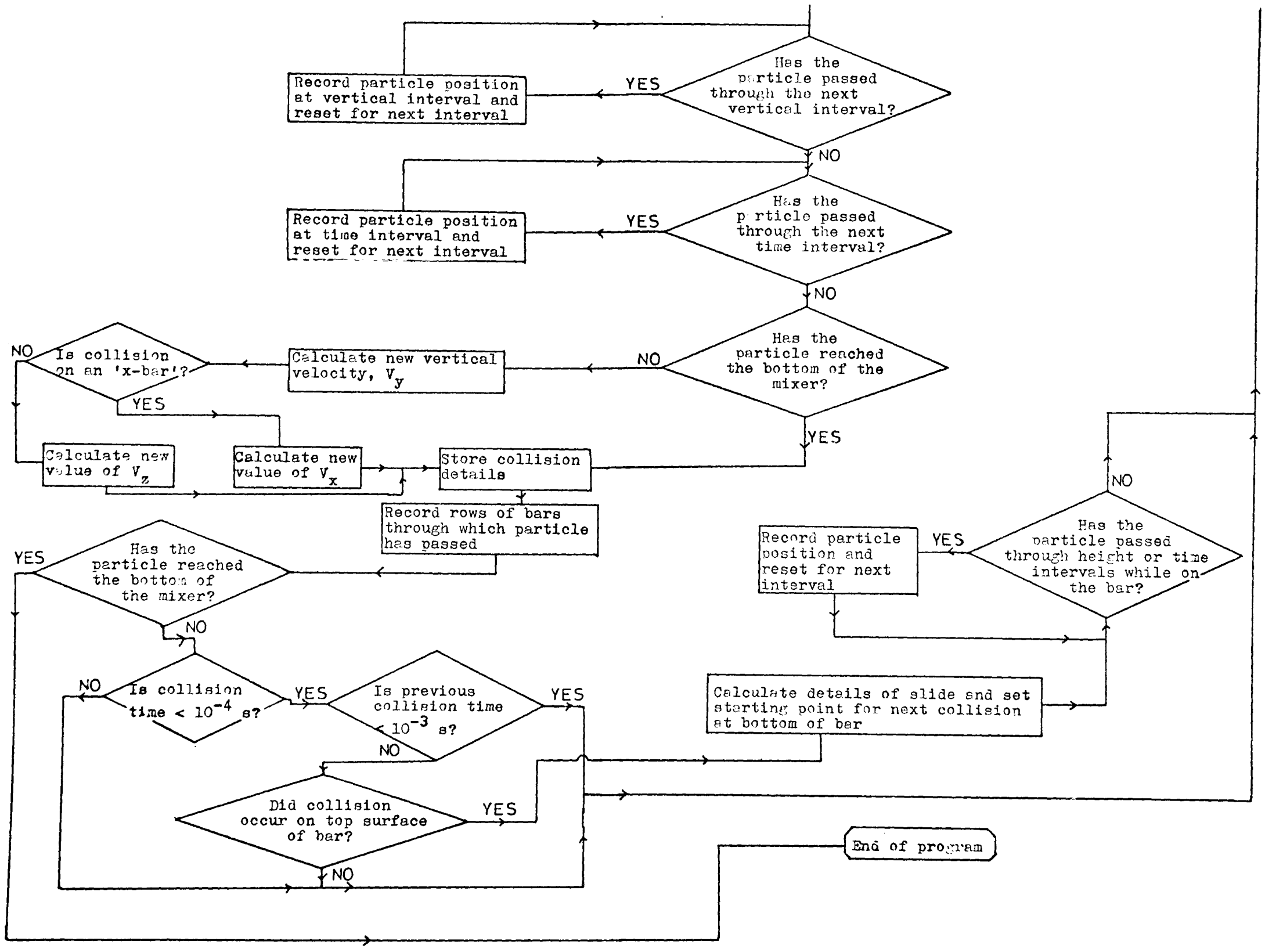
Further work on strain-induced percolation is necessary to extend these results and determine the effect of other important variables. Rates of strain and normal stresses outside the range considered here should be used and the effect of different strains per stroke investigated with a view to determining how much percolation occurs before the critical state is reached. Other bulk particles with different coefficients of friction, materials with a size distribution and more than one percolating particle could all be used. The significance of changes in h_c, the intercept on the bed height axis in the regression between $\bar{\gamma}$ and h, has not been established and this might have important consequences in base plate design. The orientation of the direction of shearing with respect to gravity could also be varied. Finally the general applicability of these results has not been tested and this can only be satisfactorily done by using the results reported here to predict the outcome of experiments performed in other equipment.

APPENDIX I

Main program flowsheet

Subroutine VERTIF flowsheet


Has the particle passed through the next vertical interval?
YES
Record particle position at vertical interval and reset for next interval
NO
Has the particle passed through the next time interval?
YES
Record particle position at time interval and reset for next interval
NO
Has the particle reached the bottom of the mixer?
NO
Calculate new vertical velocity, V_y
Is collision on an 'x-bar'?
NO
YES
Calculate new value of V_z
Calculate new value of V_x
Store collision details
Record rows of bars through which particle has passed
YES
Has the particle reached the bottom of the mixer?
NO
Is collision time < 10^{-4} s?
NO
YES
Is previous collision time < 10^{-3} s?
YES
NO
Did collision occur on top surface of bar?
YES
NO
Has the particle passed through height or time intervals while on the bar?
NO
YES
Record particle position and reset for next interval
Calculate details of slide and set starting point for next collision at bottom of bar
End of program


Has the particle passed through the next vertical interval?
YES
Record particle position at vertical interval and reset for next interval
NO
Has the particle passed through the next time interval?
YES
Record particle position at time interval and reset for next interval
NO
Has the particle reached the bottom of the mixer?
NO
Calculate new vertical velocity, V_y
Is collision on an 'x-bar'?
NO
YES
Calculate new value of V_z
Calculate new value of V_x
Store collision details
Record rows of bars through which particle has passed
YES
Has the particle reached the bottom of the mixer?
NO
Is collision time < 10^{-4} s?
NO
YES
Is previous collision time < 10^{-3} s?
YES
NO
Did collision occur on top surface of bar?
YES
NO
Has the particle passed through height or time intervals while on the bar?
NO
YES
Record particle position and reset for next interval
Calculate details of slide and set starting point for next collision at bottom of bar
YES
End of program

APPENDIX II

II.1 Data fitting

A least squares fit to a set of data points is the determination of the curve which minimises the sum of the squares of the distances between the points and the curve. Thus if a curve is fitted to the points x_i, y_i, i = 1, ...W, and if Y_i is the point on the curve corresponding to x_i, a least squares regression makes $\sum_{i=1}^{W} (y_i - Y_i)^2$ a minimum. If the regression is linear, its slope B is

$$\frac{\sum_{i=1}^{W} (x_i - \bar{x})(y_i - \bar{y})}{\sum_{i=1}^{W} (x_i - \bar{x})^2}$$

and the intercept on the y axis is $\bar{y} - B\,\bar{x}$. The sum of squares about the regression line is associated with W - 2 degrees of freedom and hence the variance about the regression s^2 is

$$\sum_{i=1}^{W} (y_i - Y_i)^2/(W - 2)$$

The variance of the regression coefficient is therefore $s^2 / \sum_{i=1}^{W} (x_i - \bar{x})^2$ (Sprent, 1969).

The regression line may be constrained to pass through a given point. If a linear regression is known to be of the form $y = B\,(x + x_k)$ where x_k is known, then the slope of the line is

$$\frac{\sum_{i=1}^{W} x_i y_i + x_k \sum_{i=1}^{W} y_i}{\sum_{i=1}^{W} (x_i + x_k)^2}$$

Weighted least squares fits are also possible if some of the points are thought to be more accurate than others. If w_i is the weight associated with point i then the general least

squares fit is to minimise $\sum_{i=1}^{W} w_i(y_i - Y_i)^2$.

The gradients of two regression lines may be compared in a t-test. If the parameters of the two lines are denoted by subscripts 1 and 2, the best estimate of the variance about the regression $\hat{s}^2$ is

$$\frac{(W_1 - 2)\, s_1^2 + (W_2 - 2)\, s_2^2}{W_1 + W_2 - 4}$$

and hence t equals

$$\frac{B_1 - B_2}{\hat{s}\left[\frac{1}{\Sigma_1(x_i-\bar{x})^2} + \frac{1}{\Sigma_2(x_i-\bar{x})^2}\right]^{\frac{1}{2}}}$$

based on $W_1 + W_2 - 4$ degrees of freedom.

APPENDIX III.1 Experiments with SSA Mk.IIIA

Run	Perc. ball (a)	$\frac{d_p}{d_b}$	h (mm) (b)	σ_y (kNm^{-2})	$\bar{\dot{\gamma}}$ (s^{-1})	$D_z t_m$ ($mm^2.10^3$)	$D_x t_m$ ($mm^2.10^3$)	n_R
D1	C	0.670	226.6	1.36	0.215	2.23	13.4	50
D2	C	"	"	"	"	2.58	9.16	49
D3	D	0.502	"	"	"	1.04	2.31	220
D4	D	"	179.4	"	"	0.911	1.83	257
D5	D	"	"	"	"	0.657	2.06	168
D6	D	"	"	"	"	0.750	1.96	322
D7	D	"	"	"	"	0.665	1.79	322
D8	D	"	179.6	"	"	0.838	1.97	357
D9	E	0.593	"	"	"	1.48	2.91	348
D10	D	0.502	159.8	"	"	0.630	1.71	356
D11	E	0.593	"	"	"	1.13	2.48	347
D12	D	0.502	139.1	"	"	0.598	1.42	357
D13	E	0.593	"	"	"	0.894	2.02	348
D14	D	0.502	118.7	""	"	0.485	1.10	357
D15	E	0.593	"	"	"	0.685	1.47	348
D16	F	0.759	"	"	"	1.96	4.19	91
D17	F	"	"	"	"	2.47	4.53	92
D18	F	"	139.1	"	"	2.34	7.72	92
D19	F	"	"	"	"	2.60	9.31	92
D20	F	"	159.8	"	"	2.68	11.2	91
D21	F	"	"	"	"	5.33	16.0	92
D22	F	"	179.6	"	"	2.68	31.3	91
D23	F	"	"	"	"	4.37	27.4	92
D24	G	0.626	"	"	"	1.37	3.03	352
D25	G	"	159.8	"	"	1.17	2.25	352
D26	G	"	139.1	"	"	0.815	2.27	351
D27	G	"	118.7	"	"	0.658	1.41	349
D28	H	0.427	"	"	"	0.281	0.846	346
D29	H	"	139.1	"	"	0.363	1.07	347
D30	H	"	159.8	"	"	0.375	1.17	348
D31	H	"	179.6	"	"	0.418	1.24	351
D32	E	0.593	159.8	"	0.613	1.23	3.07	348
D33	E	"	"	"	0.583	0.887	2.61	347
D34	E	"	"	"	0.534	0.863	2.46	348
D35	E	"	"	"	0.472	0.845	2.46	347
D36	E	"	"	"	0.404	1.29	2.51	348
D37	E	"	"	"	0.336	1.11	2.44	348
D38	E	"	"	"	0.274	1.07	2.33	348
D39	E	"	"	"	0.215	0.984	2.32	348
D40	E	"	"	"	0.161	1.03	2.28	349
D41	E	"	"	"	0.108	1.16	2.01	348
D42	E	"	"	"	0.061	0.941	1.96	347
D43	E	"	"	2.27	0.215	1.09	2.08	347
D44	E	"	"	3.18	"	1.20	2.43	347
D45	E	"	"	4.09	"	1.43	2.82	347
D46	E	"	"	5.01	"	1.21	2.49	347
D47	E	"	"	1.36	0.587	1.17	2.33	347
D48	E	"	"	"	0.535	1.07	2.65	347
D49	E	"	"	"	0.473	1.03	2.68	348
D50	E	"	"	"	0.614	1.28	2.61	346

(a) Details of all materials are given in Table 8.1. Bulk balls were species A in all experiments.

(b) Measured at $\sigma_y = 1.36\ kNm^{-2}$.

APPENDIX III.2 Experiments with SSA Mk.V

Run	Perc. Ball (a)	d_p/d_b	ρ_p ($kg.m^{-3}.10^3$)	h (mm) (b)	σ_y (kNm^{-2})	$\dot{\bar{\gamma}}$ (s^{-1})	$\bar{\gamma}$	s_γ^2	$D_z t_m$ ($mm^2.10^3$)	n_R
1	I	0.589	1.19	172.1	1.40	0.402	46.71	294.0	0.407	172
2	J	0.372	"	172.1	"	0.400	8.27	6.62	0.143	677
3	"	"	"	193.7	"	"	8.83	8.19	0.161	744
4	"	"	"	152.2	"	"	6.52	5.73	0.125	691
5	"	"	"	134.0	"	"	5.06	4.19	0.112	906
6	K	0.510	"	134.0	"	"	14.69	27.53	0.255	659
7	"	"	"	154.1	"	"	20.19	52.10	0.272	551
8	"	"	"	174.0	"	"	24.12	61.85	0.304	563
9	"	"	"	195.7	"	0.399	27.70	68.08	0.320	392
10	"	"	"	200.8	"	0.400	28.12	67.89	0.330	604
11	"	"	"	180.2	"	0.399	22.95	51.00	0.252	646
12	"	"	"	159.3	"	0.400	19.10	42.19	0.241	693
13	"	"	"	138.5	"	"	15.80	28.74	0.239	758
14	L	0.431	"	138.5	"	"	9.28	9.08	0.130	677
15	"	"	"	159.3	"	"	10.79	10.94	0.162	570
16	"	"	"	180.2	"	0.401	13.09	14.75	0.204	809
17	"	"	"	200.8	"	0.400	15.33	21.23	0.213	540
18	M	0.591	"	200.8	"	"			0.439	762
19	"	"	"	180.2	"	"	40.76	211.1	0.373	812
20	"	"	"	159.3	"	"	31.97	132.7	0.328	632
21	"	"	"	138.5	"	"	24.67	90.06	0.285	628
22	"	"	"	117.7	"	"	18.35	44.15	0.213	563
23	L	0.431	"	117.7	"	"	6.63	6.20	0.104	712
24	K	0.510	"	117.7	"	0.401	11.06	14.62	0.194	921
25	N	0.673	"	116.7	"	0.400	33.13	212.2	0.380	776
26	"	"	"	139.0	"	"	42.70	340.6	0.365	385
27	"	"	"	139.0	"	"	40.56	240.0	0.309	230
28	"	"	"	139.0	"	"	41.28	295.5	0.458	580
29	"	"	"	160.1	"	"	56.88	568.1	0.476	761
30	"	"	"	180.7	"	"	72.53	809.2	0.485	759
31	"	"	"	200.9	"	"	92.76	1390	0.617	806
32	M	0.591	"	200.9	"	"	43.93	248.0	0.443	418
33	J	0.372	"	196.9	"	"	9.53	8.99	0.201	718
34	"	"	"	182.9	"	"	8.88	7.37	0.138	614
35	"	"	"	168.1	"	"	7.77	6.68	0.139	722
36	"	"	"	155.0	"	"	7.29	5.80	0.126	790
37	"	"	"	140.6	"	"	6.45	5.37	0.116	892
38	"	"	"	126.0	"	"	5.12	4.15	0.116	2364
39	P	0.322	"	126.0	"	"	3.60	2.35	0.115	1070
40	"	"	"	140.6	"	"	4.13	2.62	0.121	701
41	"	"	"	156.8	"	"	4.62	2.88	0.129	927
42	"	"	"	156.8	"	"	4.84	3.48	0.110	771
44	"	"	"	172.2	"	"	5.53	4.62	0.122	748
45	"	"	"	186.9	"	"	6.18	4.83	0.126	348
46	"	"	"	186.9	"	"	6.09	4.80	0.127	818
47	"	"	"	201.6	"	"	6.58	5.73	0.140	827
48	J	0.372	"	171.5	"	0.201	6.64	5.76	0.124	802
49	"	"	"	"	"	0.572	7.82	6.74	0.117	1057
50	"	"	"	"	"	0.040	5.67	4.62	0.127	876
51	"	"	"	"	"	0.800	8.63	6.58	0.148	956
52	"	"	"	"	"	0.079	5.99	5.42	0.152	673
53	"	"	"	"	"	1.000	9.39	7.11	0.151	733
54	"	"	"	"	"	0.400	7.37	5.97	0.129	950
55	"	"	"	"	"	1.333	10.81	9.79	0.171	757
56	P	0.322	"	190.6	"	0.400	6.28	5.18	0.128	1190
57	"	"	"	147.5	"	"	4.35	2.65	0.096	658
58	"	"	"	132.4	"	"	3.86	2.34	0.109	1151

APPENDIX III.2 Continued

Run	Perc. Ball (a)	d_p/d_b	ρ_p ($kg.m^{-3}.10^3$)	h (mm) (b)	σ_y (kNm^{-2})	$\dot{\gamma}_1$ (s^{-1})	$\bar{\gamma}$	s_γ^2	$D_{z_2 t_m}$ ($mm^2.10^3$)	n_R
59	P	0.322	1.19	120.8	1.40	0.400	3.54	2.25	0.079	877
60	J	0.372	"	120.8	"	0.167	4.12	3.22	0.098	1228
61	"	"	"	120.8	"	1.000	6.35	5.29	0.126	781
62	"	"	"	135.2	"	0.167	4.98	3.90	0.101	969
63	"	"	"	135.2	"	1.000	7.39	6.03	0.120	1522
64	"	"	"	149.9	"	0.167	5.48	4.60	0.130	1082
65	"	"	"	149.9	"	1.000	8.05	6.14	0.145	1333
66	"	"	"	164.5	"	0.167	6.19	5.26	0.127	1193
67	"	"	"	164.5	"	1.000	8.79	6.49	0.145	1364
68	"	"	"	179.2	"	0.167	6.89	6.16	0.130	965
69	"	"	"	179.2	"	1.000	10.19	7.90	0.168	1132
70	"	"	"	193.2	"	0.167	7.52	6.50	0.157	943
71	"	"	"	193.2	"	1.000	11.14	9.32	0.179	1214
72	"	"	"	148.9	"	0.080	5.43	4.27	0.116	849
73	"	"	"	"	"	0.400	6.32	4.98	0.133	2058
74	"	"	"	"	"	0.571	6.79	5.44	0.137	1227
75	"	"	"	"	"	1.000	8.24	6.94	0.146	1515
76	"	"	"	"	"	1.333	9.42	7.69	0.158	1003
77	"	"	"	"	"	0.201	6.09	5.28	0.114	1435
78	"	"	"	"	"	1.143	8.92	7.64	0.143	849
79	"	"	"	"	"	0.041	5.03	3.87	0.127	939
80	"	"	"	"	"	1.600	10.56	8.24	0.176	1521
81	"	"	"	"	"	2.000	12.90	10.72	0.236	1497
82	"	"	"	"	"	2.342	13.39	14.24		580
83	"	"	"	"	"	0.267	6.49	5.81	0.127	1595
84	"	"	"	"	"	0.132	5.87	5.12	0.141	1223
85	"	"	"	"	"	0.400	6.53	5.19	0.133	968
86	Q	0.512	7.55	"	"	"	14.7	22.2	0.242	1524
87	R	"	0.74	"	"	"	17.5	31.2	0.268	1597
88	J	0.372	1.19	"	"	0.800	7.15	4.93	0.151	1030
89	"	"	"	"	"	0.667	6.81	5.62	0.122	530
90	"	"	"	"	"	"	6.83	4.89	0.125	531
91	"	"	"	"	"	0.800	7.34	5.54	0.133	790
92	"	"	"	"	"	0.889	7.25	5.51	0.145	973
93	"	"	"	"	"	1.778	9.95	8.35	0.164	790
94	Q	0.512	7.55	137.1	"	0.400	11.2	14.6	0.210	924
95	R	"	0.74	137.1	"	"	13.9	21.3	0.215	1077
96	Q	"	7.55	122.2	"	"	9.90	13.0	0.171	1744
97	R	"	0.74	122.2	"	"	11.6	18.2	0.198	1058
98	Q	"	7.55	165.5	"	"	15.3	23.4	0.248	1547
99	R	"	0.74	165.5	"	"	17.9	32.1		1433
100	Q	"	7.55	181.0	"	"	16.5	24.0		1054
101	R	"	0.74	181.0	"	"	20.8	38.5		822
102	Q	"	7.55	195.0	"	"	19.5	31.9		933
103	R	"	0.74	195.0	"	"	23.5	52.5	0.334	1151
104	Q	"	7.55	195.0	"	"	19.3	31.3	0.285	1017
105	R	"	0.74	176.6	"	"	20.5	43.4	0.301	1316
106	Q	"	7.55	176.6	"	"	16.4	25.3	0.261	1666
107	R	"	0.74	159.5	"	"	17.3	29.9	0.259	823
108	Q	"	7.55	159.5	"	"	14.4	20.3	0.256	897
109	R	"	0.74	141.3	"	"	14.2	22.2	0.227	1008
110	Q	"	7.55	141.3	"	"	11.7	13.4	0.209	1000
111	R	"	0.74	123.5	"	"	11.8	17.4	0.193	1089
112	Q	"	7.55	123.5	"	"	10.1	13.0	0.191	1386
113	J	0.372	1.19	247.3	"	"	11.81	11.15	0.203	741
114	L	0.431	"	247.3	"	"	19.0	28.6	0.255	1333
115	J	0.372	"	231.8	"	"	11.13	11.56	0.183	1935
116	L	0.431	"	231.8	"	"	16.4	21.4	0.226	1090

APPENDIX III.2 Continued

Run	Perc. Ball (a)	d_p/d_b	ρ_p (kg.m^{-3}. 10^3)	h (mm) (b)	σ_y (kNm^{-2})	$\dot{\gamma}$ (s^{-1})	$\bar{\gamma}$	s_γ^2	$D_z t_m$ (mm^2.10^3)	n_R
117	J	0.372	"	215.4	1.40	0.400	9.87	8.55	0.159	1073
118	L	0.431	"	215.4	"	"	15.4	19.3	0.213	840
119	J	0.372	"	199.7	"	"	9.20	9.58	0.156	753
120	L	0.431	"	199.7	"	"	14.9	18.2	0.260	945
121	J	0.372	"	193.5	"	0.667	10.68	10.91	0.174	954
122	"	"	"	179.5	"	"	9.83	10.36	0.179	835
124	"	"	"	150.6	"	"	8.38	9.31	0.153	827
125	"	"	"	136.2	"	"	7.19	7.13	0.133	1068
126	"	"	"	164.3	"	"	8.70	9.16	0.152	1890
127	"	"	"	122.4	"	"	5.96	5.33	0.126	758
128	S	0.269	"	122.4	"	0.400	2.47	1.43	0.121	655
129	"	"	"	137.0	"	"	2.65	1.41	0.129	957
130	"	"	"	151.8	"	"	3.05	1.71	0.125	1270
131	"	"	"	166.1	"	"	3.39	1.81	0.141	854
132	"	"	"	181.9	"	"	3.89	2.46	0.143	635
133	"	"	"	197.3	"	"	4.17	2.74	0.147	807
134	T	0.427	7.77	197.3	"	"	11.22	10.99	0.220	771
135	U	0.341	1.23	197.3	"	"	6.37	4.80	0.162	956
136	T	0.427	7.77	182.5	"	"	9.91	9.34	0.192	1486
137	U	0.341	1.23	182.5	"	"	5.76	4.02	0.165	980
138	T	0.427	7.77	167.4	"	"	8.74	7.60	0.180	1777
139	U	0.341	1.23	167.4	"	"	5.29	3.65	0.161	609
140	"	"	"	152.8	"	"	4.60	2.86	0.145	832
141	T	0.427	7.77	152.8	"	"	7.80	6.75	0.170	1830
142	U	0.341	1.23	138.0	"	"	4.17	2.57	0.144	1342
143	T	0.427	7.77	138.0	"	"	6.71	5.52	0.140	917
144	U	0.341	1.23	123.2	"	"	3.48	2.12	0.113	692
145	T	0.427	7.77	123.2	"	"	5.75	4.47	0.139	2192
146	U	0.341	1.23	170.3	2.31	"	5.70	4.06	0.155	1148
147	V	"	7.77	170.3	"	"	5.55	4.24	0.142	1804
148	U	"	1.23	169.1	3.21	"	5.82	4.66	0.148	991
149	V	"	7.77	169.1	"	"	5.64	4.46	0.144	984
150	"	"	"	168.8	4.12	"	6.02	5.18	0.140	998
151	U	"	1.23	168.8	"	"	6.40	6.68	0.143	1464
152	"	"	"	168.6	5.21	"	6.60	6.03	0.143	856
153	V	"	7.77	168.6	"	"	6.46	6.27	0.127	2071
154	U	"	1.23	171.6	1.40	"	5.47	3.93	0.139	1152
155	V	"	7.77	171.6	"	"	5.28	3.93	0.144	1797
156	W	0.512	2.13	171.1	"	"	20.5	44.2	0.310	768
157	X	0.511	2.52	171.1	"	"	18.8	39.3	0.257	911
158	U	0.341	1.23	168.6	4.12	"	6.12	5.60	0.128	879
159	W	0.512	2.13	185.8	1.40	"	22.2	49.7	0.312	784
160	X	0.511	2.52	185.8	"	"	21.2	45.5	0.331	777
161	W	0.512	2.13	199.7	"	"	24.8	55.6	0.337	1161
162	X	0.511	2.52	199.7	"	"	24.6	56.2	0.388	563
163	W	0.512	2.13	155.6	"	"	17.2	29.2	0.266	1300
164	X	0.511	2.52	155.6	"	"	16.6	30.1	0.280	1657
165	W	0.512	2.13	140.7	"	"	14.5	22.4	0.242	1536
166	X	0.511	2.52	140.7	"	"	13.9	21.5	0.267	651
167	W	0.512	2.13	125.5	"	"	14.2	26.9	0.241	903
168	X	0.511	2.52	125.5	"	"	13.2	22.5	0.233	990
169	Y	0.171	7.77	125.5	"	"	0.751	0.103	0.167	664
170	Z	0.128	"	125.5	"	"	0.562	0.029	0.173	526
171	Y	0.171	"	144.1	"	"	0.854	0.107	0.190	797
172	Z	0.128	"	144.1	"	"	0.632	0.031	0.230	458
173	Y	0.171	"	163.1	"	"	0.929	0.098	0.211	581
174	Z	0.128	"	163.1	"	"	0.702	0.025	0.315	425
175	Y	0.171	"	181.9	"	"	1.097	0.177	0.230	459

Run	Perc. Ball (a)	d_p/d_b	ρ_p ($kg.m^{-3}.10^3$)	h (mm) (b)	σ_y (kNm^{-2})	$\dot{\gamma}$ (s^{-1})	$\bar{\gamma}$	s_γ^2	$D_z t_m$ ($mm^2.10^3$)	n_R
176	Z	0.128	7.77	181.9	1.40	0.400	0.880	0.095	0.300	578
177	Y	0.171	"	201.2	"	"	1.275	0.325	0.254	471
178	Z	0.128	"	201.2	"	"	0.984	0.161	0.271	486

(a) Details of all materials are given in Table 8.4. Bulk balls were species A in all experiments.

(b) Measured at the applied normal stress.

NOTATION

Abbreviations

$C(x_i, x_j)$	Covariance of x_i and x_j	
$E(\quad)$	Expected value of quantity in brackets	
$\binom{N}{M}$	$\frac{N!}{(N-M)!M!}$	
$p(\quad)$	Probability or probability distribution of quantity in brackets	
SCU	System control unit	
SSA	Simple shear apparatus	
$V(\ ), var(\ )$	Variance of quantity in brackets	
$var(\quad)_s$	Variance of quantity in brackets after S bounces	
$var(\quad)_t$	Variance of quantity in brackets at time t	
$\sigma^2(\Delta\ )$	Variance of displacements in direction in brackets	
$\pm$	The figure appearing after this symbol is the standard error in the quantity preceding	
$\overline{\quad}$	Average value of quantity under bar	

English letters

A	Cross-sectional area of mixer	(L^2)
a	Constant in expressions for the correlation coefficient	$(-), (L^{-1})$
B	Slope of regression line	(-)
B_n	log (1 + a)/log 2	(-)
b	Distance between sphere centres in computer simulation of percolation	(L)
C	Concentration	(-)
C_1, C_2, C_3, C_4	Constants used in the equations describing bar surfaces in mixer simulation	(-) or (L)
C_i	Inlet concentration	(-)
C_o	Mean concentration	(-)
C_s	Number of collisions per second between particle and mixer	(T^{-1})

c	Dimensionless concentration, C/C_o	(-)
D	Diffusion coefficient	(L^2T^{-1})
D_s	Number of divisions in a sample tray	(-)
d	Dimensionality of samples (1 for linear sample, 2 for square sample, 3 for cubic sample)	(-)
d(+subscript)	Diameter	(L)
d_s	Diameter of largest particle that can percolate spontaneously	(L)
E	Expected value of an observation	(-)
E(+subscript)	Elastic modulus	$(ML^{-1}T^{-2})$
E_L	Energy lost when a particle collides with a fixed surface averaged over values of the impact angle	(ML^2T^{-2})
E_{Li}	Energy lost when a particle collides with a fixed surface	(ML^2T^{-2})
E_x	Bulk particle diffusion coefficient	(L^2T^{-1})
e	Constant in expressions for the correlation coefficient	$(-),(L^{-1})$
F	Ratio of two variances	(-)
$f_1(x), f_2(x)$	Probability distributions of the particle position in the mixer simulation	(-)
G	Half the horizontal gap between bars	(L)
G'	n-k	(-)
g	Acceleration due tc gravity	(LT^{-2})
H	Vertical distance separating rows of bars in mixer; Effective bed height in simple shear cell, $h-h_c$	(L)
h	Vertical distance travelled by a particle in flight in theory of spontaneous percolation and model of the mixer; measured bed height in simple shear cell	(L)
h_c	Intercept on bed height axis in regression between mean residence strain and bed height	(L)
I	Moment of inertia	(ML^2)
i	Division of sample tray;	(-)
	Distance between two samples in 1 direction in theory of correlation (Chapter 6)	(L)
J	Number of jumps	(-)

J_t	Number of ideal equal-size stirred tanks	(-)
j	Distance between two samples in m direction in theory of correlation (Chapter 6)	(L)
K	$1/(1 + \cos \beta)$	(-)
K_1, K_2	Constants	(L^2)
k	Distance between two samples in n direction in theory of correlation (Chapter 6)	(L)
k_1	In mixer model: 1 for sliding, 1.4 for rolling	(-)
k_2	In mixer model: $0.5 + \sin 4\beta/(4\pi - 8\beta)$	(-)
k_3	In mixer model: $\sin\beta - \mu\cos\beta$ for sliding, $\sin\beta$ for rolling	(-)
k_f, k_g, k_r^f, k_s^g	Constants in model of strain-induced percolation	(-)
L	Height of packed bed	(L)
L_1	$\left[\sum_{i=1}^{D_s} (P_i - 1/D_s)^2\right]/D_s$	(-)
L_2	$\left[\sum_{i=1}^{D_s} P_i(1 - P_i)\right]/D_s$	(-)
L_b	Mixer bar size (see Figure 5.2)	(L)
L_m	Length of one side of the mixer	(L)
l	Distance moved by particle on plane;	(L)
ℓ	Length of one side of a sample in theory of correlation	(L)
l	Distance moved by particle on plane	(L)
l_m	Maximum plane length	(L)
l_u	Distance rolled by particle up a plane	(L)
M	Number of particles in a sample tray division	(-)
m	Mass of particle;	(M)
	length of one side of a sample in theory of correlation	(L)
N	Number of particles; number of unit samples	(-)
$\bar{N}$	Mean number of particles in one half of mixer	(-)
N_1	Number of particles in lower half of mixer	(-)
N(r)	Density function of unit samples distance r apart	(-)
N_b	Number of bulk particles in system	(-)

N_q	Number of particles having separation in region q	(-)
N_s	Measured mean strain for percolation through a height h (in strokes)	(-)
n	Length of one side of a sample in theory of correlation	(L)
n_1	Number of pieces of coal	(-)
n_p	Number of particles passing through a horizontal section per second	(-)
n_r	Density function of unit samples a distance r apart	(-)
n_R	Number of readings in one experiment	(-)
O	Observed frequency of observations	(-)
P_i	Probability that a particle will fall into division i of sample tray	(-)
P_i,M	Probability that M particles will fall into division i of sample tray	(-)
Pe	Peclet number, ud/D , where d is a characteristic length	(-)
p	Proportion of one component in a two-component mixture	(-)
p_c	Probability of particle passing through row of bars without colliding with one	(-)
Q	Mixing index equal to $1 - L_1/\sigma_o^2$	(-)
Q_a	Average value of Q for line samples from three-dimensional mixer	(-)
q	Number of bars; Region of values of R	(-)
R	$\sum_{G'=1}^{n-1} a^{-G'}$;	(-)
	Longest distance between surface of bulk particle and extremity of 'cage' containing bulk particle	(L)
R^*	Critical value of R	(L)
R_1, R_2	Sums of ranks in Mann-Whitney 'U' test	(-)
R_q	Average value of R in region q	(L)
r	Distance between two unit samples	(L)

r_m	Maximum distance over which correlation occurs	(L)
S	Number of surfaces	(-)
S_1	Rectilinear jump fluctuation vector after one jump	(L)
S_a	Sample size	
S_J	Rectilinear jump fluctuation vector after J jumps	(L)
S_y	Mean vertical bar spacing	(L)
s^2	Variance	(-),(L^2)
$\hat{s}^2$	Best estimate of variance about joint regression	(L^2)
s_r	Dummy variable	(L)
s^2_γ	Variance of residence strains	(-)
T	Mean time interval between collisions	(T)
t	Time	(T)
$\bar{t}$	Mean time spent by a particle on a plane	(T)
$\bar{t}'$	Mean time spent by a particle in flight	(T)
t_1, t_2	Number of readings	(-)
t_m	Mean residence time	(T)
t_p	Time spent by particle on plane	(T)
t_u	Mean time taken by particle to roll up a plane to a halt and back to the collision point	(T)
t_{ui}	Time taken by particle to roll up a plane to a halt and back to the collision point	(T)
t_x	Time at which distribution of particles is evaluated	(T)
U	$Pe_a L/2d_b$; quantity in Mann-Whitney statistical test	(-)
u	Vertical velocity of percolating particle	(LT^{-1})
V	Translational velocity	(LT^{-1})
V_1	Vertical velocity of particle leaving plane	(LT^{-1})
V_2	Vertical velocity of particle on collision	(LT^{-1})
V_a	Velocity of particle along plane after impact	(LT^{-1})
V_f	Velocity of particle on impact	(LT^{-1})
V_H	Horizontal velocity of particle leaving plane	(LT^{-1})

V_H'	Horizontal velocity of particle on collision	(LT^{-1})
V_i	Velocity of particle after impact	(LT^{-1})
V_o	Velocity of particle leaving plane	(LT^{-1})
V_{oa}	Average velocity of particle leaving plane	(LT^{-1})
V_p	Volume of single particle	(L^3)
W	Number of points in regression	(-)
W_b	Horizontal bar spacing	(L)
W_R	Number of ways of distributing the lengths R_q	(-)
w	Dummy direction	(L)
w_i	Weight associated with point i in regression	(-)
x	Horizontal co-ordinate; Composition of sample	(L) (-)
$\bar{x}$	Mean number of particles per division	(-)
x_1, x_2	Integration limits	(L)
x_A, x_B	Random values of x	(L)
x_i	Number of particles in division i; composition of sample	(-)
x_j	Composition of sample	(-)
x_k	Known value of x in regression	(L)
x_m	Mean displacement in x direction	(L)
x_o	Co-ordinate of preceding collision	(L)
Y_c	Probability of collision with side wall of mixer	(-)
Y_I	Intercept of straight line portion of graph of $\log \sigma_N^2/\sigma_o^2$ vs. log N on ordinate	(-)
Y_i	Point on regression line corresponding to y_i	(L)
Y_s	Vertical spacing between adjacent parallel rows of bars	(L)
Y_T	Bar thickness	(L)
y	Vertical co-ordinate	(L)
$\bar{y}$	Average vertical distance	(L)
y_m	Mean axial displacement	(L)
$(y^2)_m$	Mean square axial displacement	(L^2)

y_o	Co-ordinate of preceding collision	(L)
Z	y/L	(-)
z	Horizontal co-ordinate	(L)
z_A, z_B	Random values of z	(L)
z_o	Co-ordinate of preceding collision	(L)

Greek letters

α	Coefficient of restitution	(-)
α_1, α_2	Lagrangian multipliers	(-)
β	Angle between collision surface and horizontal	(-)
γ	Strain	(-)
$\bar{\gamma}$	Mean residence strain	(-)
$\dot{\gamma}$	Rate of shear strain	(T^{-1})
γ_d	'Dead' strain per stroke	(-)
γ_s	Strain per stroke	(-)
γ_T	True effective mean strain for percolation	(-)
Δy	Height interval	(L)
$\Delta\bar{y}$	Mean vertical distance between collisions	(L)
$\Delta\bar{r}_r$	Root mean square lateral jump	(L)
δ_x^2	Square of deviations from the mean	(-)
ε	Void fraction	(-)
θ	t/t_m	(-)
θ_f	Impact angle	(-)
θ_i	Rebound angle	(-)
λ	Mean free path	(L)
λ_H	Horizontal displacement	(L)
λ_s	On-surface displacement	(L)
μ	Dynamic coefficient of friction	(-)
μ_n	Roots of equation $\cot\mu_n = (\mu_n/U - U/\mu_n)/2$	(-)
μ_s	Static coefficient of friction between bulk and percolating particles	(-)

ν	Angle between sphere trajectory and x-axis	(-)
ρ	Correlation coefficient; Density	(-) (ML^{-3})
$\bar{\rho}_n$	Mean correlation coefficient averaged over all possible pairs of samples	(-)
σ^2	Variance	(-)
σ_N^2	Variance of samples composed of N unit samples	(-)
σ_n^2	Variance of samples composed of n_1 pieces of coal	(-)
σ_o^2	Variance of unit samples	(-)
σ_R^2	Variance of binomial distribution	(-)
σ_s^2	$(1 - 1/D_s)/D_s$	(-)
σ_t^2	Variance of the residence time distribution	(T^2)
σ_y	Normal stress at top of shear cell	($ML^{-1}T^{-2}$)
τ, τ'	Time interval	(T)
ϕ	Local surface slope	(-)
ϕ_o	Surface slope at point where particle leaves surface	(-)
χ^2	$\Sigma\,(O-E)^2/E$	(-)
ω	Angular velocity	(T^{-1})

Subscripts

The following have been used (unless otherwise defined):

a	Axial
b	Bulk particle property
p	Percolating particle property
r	Radial
w,x,y,z	In the w,x,y or z direction

Computer variables

NPLACE	Quantity used to describe bar surfaces
VERTIF	Subroutine of simulation program used to calculate collision details if V_x or V_z equals 0

XP(I)	Bar co-ordinate (see figure 5.4)
YT(J)	Bar co-ordinate (see figure 5.4)

REFERENCES

AHMAD, K. and SMALLEY, I.J. (1973), Powder Technol., 8, 69.

BELZ, M.H. (1973), 'Statistical methods in the Process Industries'. (London: Macmillan).

BERTHOLF, W.M. (1955), ASTM Special tech. publn., No. 162, 5.

BOURNE, J.R. (1964), Chem. Engr. (London), CE202.

BOURNE, J.R. (1967), Chem. Engng. Sci., 22, 693.

BOURNE, J.R. (1968), Chem. Engng. Sci., 23, 339.

BOWDEN, F.P. and TABOR, D. (1950), 'The Friction and Lubrication of Solids'. (Oxford: Clarendon Press).

BRENNER, H. (1962), Chem. Engng. Sci., 17, 229.

BRIDGWATER, J., SHARPE, N.W. and STOCKER, D.C. (1969a), Trans. Instn. Chem. Engrs., 47, T114.

BRIDGWATER, J., BAGSTER, D.F., CHEN, S.F. and HALLAM, J.M. (1969b), Powder Technol., 2, 198.

BRIDGWATER, J. and INGRAM, N.D. (1971), Trans. Instn. Chem. Engrs., 49, 163.

BRIDGWATER, J. (1972), Powder Technol., 5, 257.

BRIDGWATER, J. and SCOTT, A.M. (1974), Trans. Instn. Chem. Engrs., 52, 317.

BRIDGWATER, J. (1976), Powder Technol., (in press).

BROWN, R.L. (1939), J. Inst. Fuel, 13, 15.

CAHN, D.S. and FUERSTENAU, D.W. (1967), Powder Technol., 1, 174.

CAMPBELL, A.P. and BRIDGWATER, J. (1973), Trans. Instn. Chem. Engrs., 51, 72.

CAMPBELL, A.P. (1975), Birmingham Univ. Chem. Eng., 26, 50.

CHEN, S.J., FAN, L.T. and WATSON, C.A. (1972), A.I.Ch.E.J., 18, 984.

CHEN, S.J., FAN, L.T. and WATSON, C.A. (1973), Ind. Engng. Chem. Process Des. Develop., 12, 42.

CLEMENTS, J.A. (1969), Ph.D. Thesis, Univ. of London.

COCHRAN, W.G. (1946), Ann. Math. Stat., 17, 164.

COHEN, M.H. and TURNBULL, D. (1959), J. Chem. Phys., 31, 1164.

COOKE, M.H., STEPHENS, D.J. and BRIDGWATER, J. (1976), Powder Technol., 15, 1.

CRANK, J. (1956), 'The Mathematics of Diffusion'. (London: Oxford University Press).

CRAVEN, P. (1970), Brit. Chem. Engng., 15, 918.

DALENIUS, T., HAJEK, J. and ZUBRZYCKI, S. (1961), Proc. 4th Berkeley Symp. Math. Prob., 1, 125.

DANCKWERTS, P.V. (1953), Appl. Sci. Res., A3, 279.

DARTON, R.C. (1976), Powder Technol., 13, 241.

DONALD, M.B. and ROSEMAN, B. (1962), Brit. Chem. Engng., 7, 749.

EINSTEIN, A. (1926), 'Investigations on the theory of the Brownian Movement', ed. Fürth, R., tr. Cowper, A.D. (London: Methuen).

EMERY, E.T.G. (1951), Engineering (London), Oct. 12, 452.

FAIMAN, M.D. and RIPPIE, E.G. (1965), J. Pharm. Sci., 54, 719.

FAN, L.T., CHEN, S.J. and WATSON, C.A. (1970), Ind. Engng. Chem., 62, No. 7, 53.

FAN, L.T., CHEN, S.J., ECKHOFF, N.D. and WATSON, C.A. (1971), Powder Technol., 4, 345.

GOLDSMITH, P.L. (1966), The Statistician, 16, 227.

GRANT, J.A. and HITCHINS, G.D. (1971), J.I.M.A., 8, 122.

GUTTMAN, I. and WILKES, S.S. (1965), 'Introductory Engineering Statistics'. (New York: J. Wiley and Sons Inc).

HALL, K.R. and GODFREY, J.C. (1965), Paper 10.7 to joint meeting of A.I.Ch.E. and Instn. Chem. Engrs., London.

HARNBY, N. (1972), Powder Technol., 5, 81.

HARWOOD, C.F., WALANSKI, K., LUEBCKE, E. and SWANSTROM, C. (1975), Powder Technol., 11, 289.

HOGG, R., CAHN, D.S., HEALY, T.W. and FUERSTENAU, D.W. (1966), Chem. Engng. Sci., 21, 1025.

HUDSON, R.B., JANSEN, M.L. and LINKSON, P.B. (1969), Powder Technol., 2, 229.

JENIKE, A.W. (1960), Bull. Univ. Utah, 51, 24.

KRISTENSEN, H.G. (1973a), Powder Technol., 7, 249.

KRISTENSEN, H.G. (1973b), Powder Technol., 8, 149.

KRISTENSEN, H.G. (1973c), Arch. Pharm. Chemi. Sci. Ed., 1, 102.

KRISTENSEN, H.G. (1973d), Arch. Pharm. Chemi. Sci. Ed., 1, 121.

KRISTENSEN, H.G. (1973e), Arch. Pharm. Chemi. Sci. Ed., 1, 145.

KRISTENSEN, H.G. (1976), Powder Technol., 13, 103.

LACEY, P.M.C. (1954), J. Appl. Chem., 4, 257.

LACEY, P.M.C. and MIRZA, F.S.M.A. (1976a), Powder Technol., 14, 17.

LACEY, P.M.C. and MIRZA, F.S.M.A. (1976b), Powder Technol., 14, 25.

LAI, F.S. and FAN, L.T. (1975), Ind. Engng. Chem. Process Des. Develop., 14, 403.

LANDRY, B.A. (1944), 'Fundamentals of Coal Sampling', U.S. Bureau of Mines Bull., 454.

LAWRENCE, L.R. and BEDDOW, J.K. (1969), Powder Technol., 2, 253.

LEVENSPIEL, O. and SMITH, W.K. (1957), Chem. Engng. Sci., 6, 227.

LEVENSPIEL, O. and BISCHOFF, K.B. (1963) in Drew, T.B., Hoopes, J.W. and Vermuelen, T. (eds.) 'Advances in Chemical Engineering', 4, 95. (New York: Academic Press).

MADOW, W.G. and MADOW, L.H. (1944), Ann. Math. Stat., 15, 1.

MANN, H.B. and WHITNEY, D.R. (1947), Ann. Math. Stat., 18, 50.

MASLIYAH, J. and BRIDGWATER, J. (1974), Trans. Instn. Chem. Engrs., 52, 31.

MATTHÉE, H. (1968), Powder Technol., 1, 265.

MITCHELL, D.R. (1938), A.I.M.E., 130, 107.

MOORE, C. and MASLIYAH, J. (1973), Int. J. Num. Meth. Engng., 6, 25.

OLSEN, J.L. and RIPPIE, E.G. (1964), J. Pharm. Sci., 53, 147.

ORR, N.A. and SHOTTON, E. (1973), Chem. Engr., No. 269, 12.

OTAKA, T., KITAOKA, H. and TONE, S. (1961), Kagaku Kogaku, 25, 178.

OYAMA, Y. (1939), Bull. Inst. Phys. Chem. Research (Tokyo), 18, 600.

PARSONS, D.S. (1976), Powder Technol., 13, 269.

QUENOUILLE, M.H. (1949), Ann. Math. Stat., 20, 355.

REYNOLDS, O. (1885), Phil. Mag., 20, 469.

RIPPIE, E.G., OLSEN, J.L. and FAIMAN, M.D. (1964), J. Pharm. Sci., 53, 1360.

RIPPIE, E.G., FAIMAN, M.D. and PRAMODA, M.K. (1967), J. Pharm. Sci., 56, 1523.

ROSCOE, K.H., SCHOFIELD, A.N. and WROTH, C.P. (1958), Géotechnique, 8, 22.

ROSCOE, K.H. (1967), Proc. Geotechnichal Conf., Oslo, 2, 188.

ROSCOE, K.H. (1970), Géotechnique, 20, 129.

SCHOFIELD, C. (1970), Trans. Instn. Chem. Engrs., 48, T28.

SCOTT, A.M. (1974), D.Phil. Thesis, Univ. of Oxford.

SCOTT, A.M. and BRIDGWATER, J. (1974), Chem. Engng. Sci., 29, 1789.

SCOTT, A.M. and BRIDGWATER, J. (1975), Ind. Engng. Chem. Fund., 14, 22.

SCOTT, A.M. and BRIDGWATER, J. (1976), Powder Technol., 14, 177.

SHINOHARA, K., IDEMITSU, Y., GOTOH, K. and TANAKA, T. (1968), Ind. Engng. Chem. Process Des. Develop., 7, 378.

SHINOHARA, K., SHOJI, K. and TANAKA, T. (1970), Ind. Engng. Chem. Process Des. Develop., 9, 174.

SHINOHARA, K., SHOJI, K. and TANAKA, T. (1972), Ind. Engng. Chem. Process Des. Develop., 11, 369.

SPINK, C.D. (1973), Personal communication to J. Bridgwater.

SPRENT, P. (1969), 'Models in Regression and related topics'. (London: Methuen).

STANGE, K. (1967), Chemie-Ingr-Techn., 39, 585.

STEPHENS, D.J. (1976), D.Phil. Thesis, Univ. of Oxford.

SUGIMOTO, M. and YAMOMOTO, K. (1973), J. Soc. Materials Sci., Japan, 22, 684.

TRANTER, I. (1976), Univ. of Oxford, Dept. Engng. Sci., Finals Report.

VALENTIN, F.H.H. (1965), Chem. Process. Engng., 46, 181.

VAN DER LAAN, E. Th. (1958), Chem. Engng. Sci., 7, 187.

WEIDENBAUM, S.S. (1958), in Drew, T.B. and Hoopes, J.W. (eds.) 'Advances in Chemical Engineering', 2, 209. (New York: Academic Press).

WEST, S.P. (1976), University of Oxford, Dept. Engng. Sci., Finals Report.

WEYDANZ, W. (1960), Chemie-Ingr-Techn., 32, 343.

WILLEMSE, Th.W. (1961), Chemisch Weekblad, 57, 377.

WILLIAMS, J.C. (1963), J. Fuel. Soc. Univ. Sheffield, 14, 29.

WILLIAMS, J.C. and SHIELDS, G. (1967), Powder Technol., 1, 134.

WILLIAMS, J.C. (1970), Powder Technol., 3, 189.

WROTH, C.P. (1958), Ph.D. Thesis, Univ. of Cambridge.

YAGI, S. and MIYAUCHI, T. (1953), Chem. Eng. (Tokyo), 17, 382.

ZWEIG, H.J. (1956), J. Opt. Soc. Amer., 46, 805.